Universidade de Brasília – UnB
Instituto de Geociências – IG
Programa de Pós-Graduação em Geologia

CARACTERIZAÇÃO PETROLÓGICA E GEOCRONOLÓGICA DA SUÍTE ALCALINA MONTE SANTO, NA REGIÃO DE PARAÍSO DO TOCANTINS.

Eduardo Valentin dos Santos

Dissertação de Mestrado

Brasília, 2018

Universidade de Brasília – UnB
Instituto de Geociências – IG
Programa de Pós-Graduação em Geologia

CARACTERIZAÇÃO PETROLÓGICA E GEOCRONOLÓGICA DA SUÍTE ALCALINA MONTE SANTO, NA REGIÃO DE PARAÍSO DO TOCANTINS.

Eduardo Valentin dos Santos

Orientador
Prof. Dr. Nilson Francisquini Botelho

Banca Examinadora:

____
Prof. Dr. Nilson Francisquini Botelho

____
Prof. Dr. José Affonso Brod (UFG)

____
Prof. Dr. Herbet Conceição (UFS)

Brasília, 4 de outubro de 2018

Agradecimentos

Gostaria de agradecer primeiramente à minha noiva Gabriela, por me aguentar durante todos esses anos falando de rochas alcalinas, zircões, geoquímica, microssonda eletrônica e tantas outras coisas que para ela não passam de abobrinhas, sem contar com sua imensa paciência com minhas alterações de humor recorrentes, ansiedade e preocupações financeiras nos últimos meses.

Agradeço aos meus pais pela oportunidade de estudar em Brasília, lugar que hoje tanto amo, pois sem eles não teria como sair da megalópole de Pederneiras. Agradeço aos princípios, ensinamentos e exemplos que me deram, os quais carrego para vida.

Agradeço imensamente ao meu orientador, o professor Nilson, por me acolher e orientar desde a graduação. Obrigado por todas as oportunidades valiosas que você proporcionou até aqui. Agradeço também ao professor Elton e toda equipe do projeto de conclusão de curso, TF Paraíso, pelos conhecimentos e por me ensinar a enxergar a geologia como um estilo de vida.

Agradeço aos colegas dos laboratórios da Universidade de Brasília, que me auxiliaram imensamente durante o mestrado.

Por fim agradeço aos amigos de república, com os quais dividi milhares de experiências por longos e memoráveis sete anos, além de todos os amigos que fiz durante minha estadia na Universidade de Brasília, sejam nas aulas, TF, laboratórios, ultimate frisbee, vocês são tantos que nem consigo citá-los.

Obrigado!

Resumo

A Suíte Monte Santo é consituída de dois maciços foliados, variavelmente deformados e metamorfizados (Maciço Estrela e Monte Santo). As intrusões são dominadas por nefelina sienito e feldspato alcalino sienito, mas nefelina monzosienito e nefelina monzodiorito subordinados também estão presentes. Nesse estudo, a química, mineralogia e idade da Suíte Monte Santo foram investigadas. Os cristais de piroxênio variam em composição entre onfacita e aegirina-augita e tem características mistas entre tendências ígneas e metamórficas. Os cristais de biotita variam de flogopita para siderofilita e annita, e apresentam tendências primárias, reequilibradas e neoformadas. Os cristais de anfibólio variam de hastingsita para taramita, e apresentam química muito homogênea. Nefelina apresenta cristais de alta temperatura preservados na paragênese, mas também muitos cristais de baixa temperatura. A maioria das rochas da Suíte Monte Santo não plota nos pontos mínimos no Sistema de Resíduo Petrogenético, além disso, os padrões de elementos terras raras e outros elementos traço demonstram tendências paralelizadas com variações significativas em concentração, sugerindo que a maioria dessas rochas representem cumulados. Os padrões Zr/Hf são similares para todas rochas do maciço, demonstrando que elas evoluíram da mesma fonte. Cristalização fracionada foi o processo principal de diferenciação magmática. A cristalização da Suíte Monte Santo é datada em 545 Ma, onde essas rochas foram geradas em uma fase extensional ou transtensiva na evolução do orógeno e foram subsequentemente deformadas e metamorfizadas em fases compressivas seguintes. Idades T_{DM}, anomalias positivas de Nb e Ta e as formas irregulares encontradas em cristais de zircão Mesoproterozóicos datados nessa suíte sugerem que a Suíte Monte Santo evoluiu de uma fonte mantélica Mesoproterozóica, herdando alguns de seus cristais de zircões.

Palavras-chave: Suíte Monte Santo, Maciço Estrela, Maciço Monte Santo, Rochas Alcalinas Deformadas, Ediacarano-Cambriano, Cinturão Araguaia.

Abstract

The Monte Santo Suite consists of two foliated and variably deformed and metamorphosed massifs (Estrela and Monte Santo). The intrusions are predominantly nepheline syenite and alkali feldspar syenite, but minor nepheline monzosyenite and nepheline monzodiorite are found in the Estrela Massif. In this study, the chemistry, mineralogy and age of the Monte Santo Suite were investigated. Pyroxene crystals vary in composition from omphacite to aegirine-augite to aegirine and have mixed characteristics between igneous and metamorphic trends. Biotite crystals vary from phlogopite to siderophyllite to annite and presents primary, reequilibrated and neoformed trends. Amphibole crystals vary from hastingsite to taramite and have an homogeneous compositions. Nepheline presents high-temperature crystals preserved within the paragenesis but also many low-temperature crystals. The rocks of the Monte Santo Suite mostly do not plot near the minimum in Petrogeny's Residua System. Additionally, REE and trace element patterns depict parallel trends with significant variations in bulk content, suggesting that most of the rocks represent cumulates. Zr/Hf ratios are similar for all the rocks of the massif, showing that they evolved from the same source. Fractional crystallization was the main process that determined the lineage between different rock types. The Monte Santo Suite crystallization age is dated to 545 Ma, when these rocks were generated in an extensional or transtensional phase of orogen evolution and were subsequently deformed and metamorphosed in a compressive phase. T_{DM} ages, positive Nb and Ta anomalies and many irregularly shaped Mesoproterozoic zircon crystals suggest that the Monte Santo Suite evolved from a Mesoproterozoic mantle source, inheriting some of its zircons.

Keywords: Monte Santo Suite, Estrela Massif, Monte Santo Massif, Deformed Alkaline Rocks, Ediacaran-Cambrian, Araguaia Belt.

Sumário

Índice de Figuras

Índice de Tabelas

1. Introdução

1.1. Justificativa e Objetivo

O presente trabalho tem como objetivo aprofundar o conhecimento geológico do segmento sul do Cinturão Araguaia, por meio do estudo do Maciço Monte Santo e Maciço Estrela, constituintes da suíte de rochas alcalinas deformadas denominada Suíte Monte Santo (Hasui et al. 1984b), bem como acrescentar informações e interpretações sobre a gênese e processos evolutivos envolvendo esses tipos de rochas.

Os trabalhos até então realizados nessa suíte, englobaram aspectos predominantemente petrográficos (Iwanuch 1991), ou puramente geocronológicos (Arcanjo e Moura 2000, Arcanjo et al. 2013, Viana e Battilani 2014), por vezes apresentando dados de geoquímica de elementos maiores e traço, entretanto restritos a apenas um dos maciços (Viana e Battilani 2014).

A abordagem adotada neste trabalho é mais ampla, utilizando geoquímica de elementos maiores, traço e isotópica em rocha total, química mineral e geocronologia para se obter melhor detalhamento do significado geológico e das relações entre os maciços Monte Santo e Estrela, bem como seu significado regional.

Especificamente, os objetivos abordados nesse trabalho foram:

- Determinar a idade da Suíte Monte Santo;
- Determinar se os maciços dessa suíte são geneticamente associados;
- Apresentar os primeiros dados de química mineral para essa suíte, e demonstrar seu significado em meio a gênese e evolução da suíte;
- Demonstrar, qualitativamente, processos de evolução magmática na suíte;
- Relacionar sua gênese à rochas alcalinas similares no mundo.

A dissertação foi desenvolvida na forma de artigo, na qual os primeiros três capítulos estão redigidos em português, seguidos pelo artigo, redigido em inglês, a ser submetido a um periódico de circulação internacional, e por fim, a recapitulação das conclusões do artigo, em português. A apresentação completa dos dados obtidos por meio dos métodos analíticos utilizados, é fornecida nos anexos ao final da dissertação.

1.2. Localização e Acesso

A área estudada localiza-se no centro-oeste do Estado do Tocantins, a aproximadamente 70 km da cidade de Palmas e cerca de 770 km de Brasília. O Maciço Monte Santo está a cerca de 15 km a noroeste do município de Paraíso do Tocantins e o Maciço Estrela encontra-se a cerca de 10 km a sudeste do município de Pugmil, na divisa entre este e o município de Porto Nacional (Fig. 1).

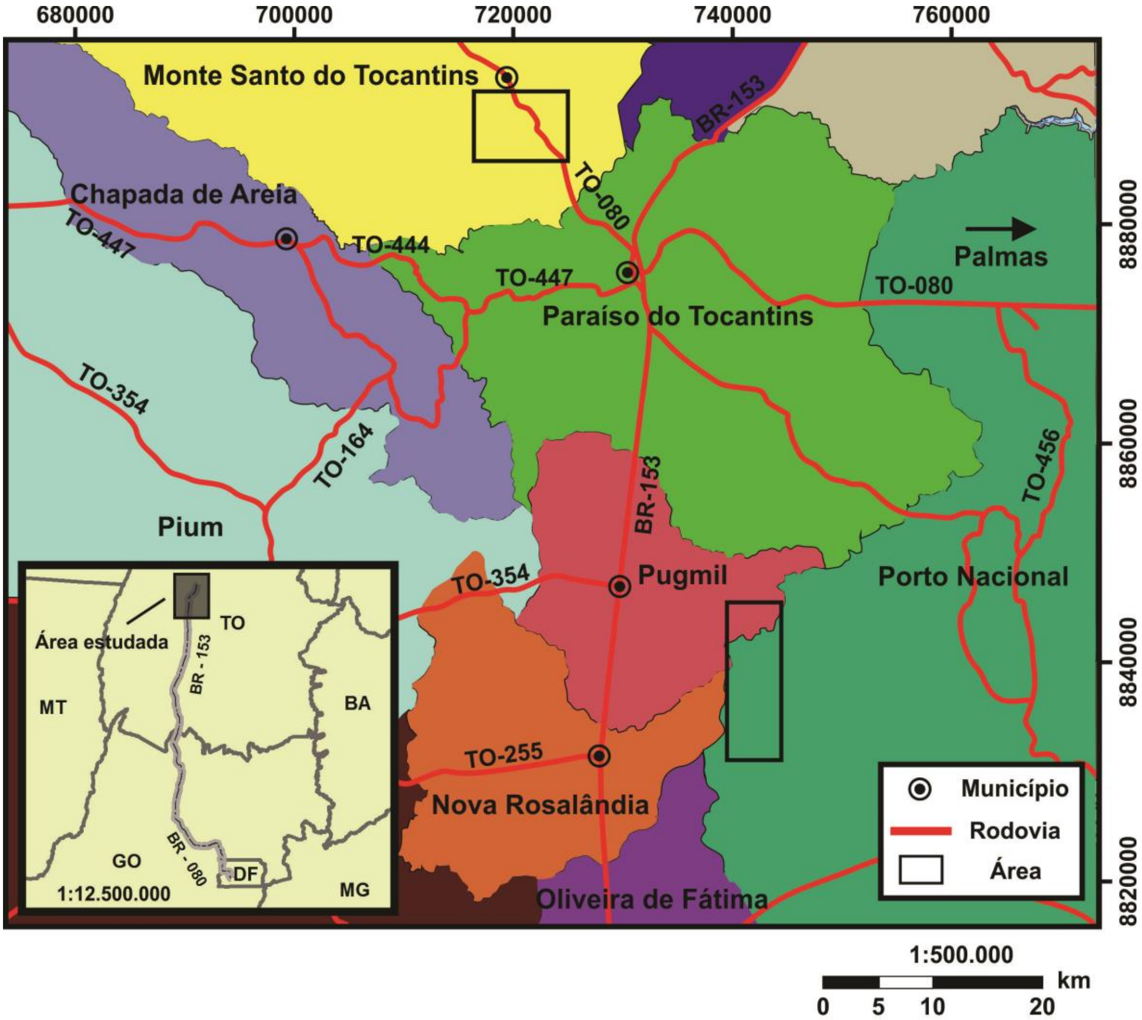

Figura 1. Mapa de localização e rodovias de acesso às áreas estudadas. Os retângulos pretos representam a área de estudo relativa aos maciços Monte Santo (MMS) e Estrela (ME). Os polígonos coloridos representam limites municipais.

Tomando como ponto de partida o Distrito Federal, o acesso se dá pela BR-080 até Uruaçu-GO e depois segue-se pela BR-153. Para acesso ao Maciço Monte Santo, segue-se pela BR-153 até o município de Paraíso do Tocantins, onde toma-se a TO-080 sentido ao município de Monte Santo do Tocantins, por cerca de 20 km, o acesso local é realizado por estradas não pavimentadas. Para acesso ao Maciço Estrela, segue-se pela

BR-153 até o município de Pugmil, onde tomam-se vias não pavimentadas a oeste da cidade, por cerca de 10 km (Fig. 1).

2. Contexto Geológico Regional

A Suíte Monte Santo consiste predominantemente de rochas alcalinas félsicas insaturadas a subsaturadas (feldspato alcalino sienitos e nefelina sienitos) que afloram na porção meridional do Cinturão Araguaia.

Logo, de maneira a situar o leitor no contexto geológico à que pertence a Suíte Monte Santo (SMS), apresenta-se breve introdução sobre o Cinturão Araguaia e posteriormente detalha-se a geologia da região de Paraíso do Tocantins, na qual situa-se a SMS.

2.1. Cinturão Araguaia

O Cinturão Araguaia, em conjunto com os cinturões orogênicos Brasília e Paraguai, constituem o Sistema Orogênico Tocantins (ou Província Tocantins, definida por Almeida et al. 1981), um grande orógeno neoproterozóico que resultou da convergência e colisão dos paleocontinentes Amazônico e São Francisco, no qual a colisão final ocorreu durante a orogenia Brasiliano-Pan Africano (850-480 Ma, Brito Neves e Fuck 2013, Brito Neves et al. 2014) como parte da amalgamação do Gondwana Oeste (Fuck et al. 2017).

O Cinturão Araguaia consiste de uma longa faixa de dobramentos com cerca de 1200 km de comprimento e 100 km de largura, orientado na direção norte-sul, mostrando extensa sucessão de rochas psamíticas e pelíticas metamorfizadas, com menor contribuição de rochas carbonáticas e magmáticas (Alvarenga et al. 2000). Essa unidade é limitada a oeste pelo Cráton Amazônico, por meio de contatos discordantes e empurrões E-W, a sudeste pelo Arco Magmático de Goiás e a norte e leste, o cinturão é encoberto pelas rochas sedimentares da Bacia do Parnaíba.

Arcanjo et al. (2013) subdivide o Cinturão Araguaia em dois domínios com relação à idade predominante do embasamento, o segmento norte e o segmento sul. No segmento norte, o embasamento é representado dominantemente por ortognaisses arqueanos, do tipo TTG (Complexo Colméia - 2,85 Ga, Moura e Gaudette 1999), que afloram na forma de braquianticlinais, com restritos núcleos paleoproterozóicos (Gnaisse Cantão – 1,85 Ga, Moura e Gaudette 1999), acredita-se que o embasamento desse segmento correlaciona-se às rochas da borda sudeste do Cráton Amazônico (Costa 1980, Souza et al. 1985, Dall'Agnol 1988). No segmento sul, o embasamento é predominantemente paleoproterozóico, com ausência da estruturação dômica presente

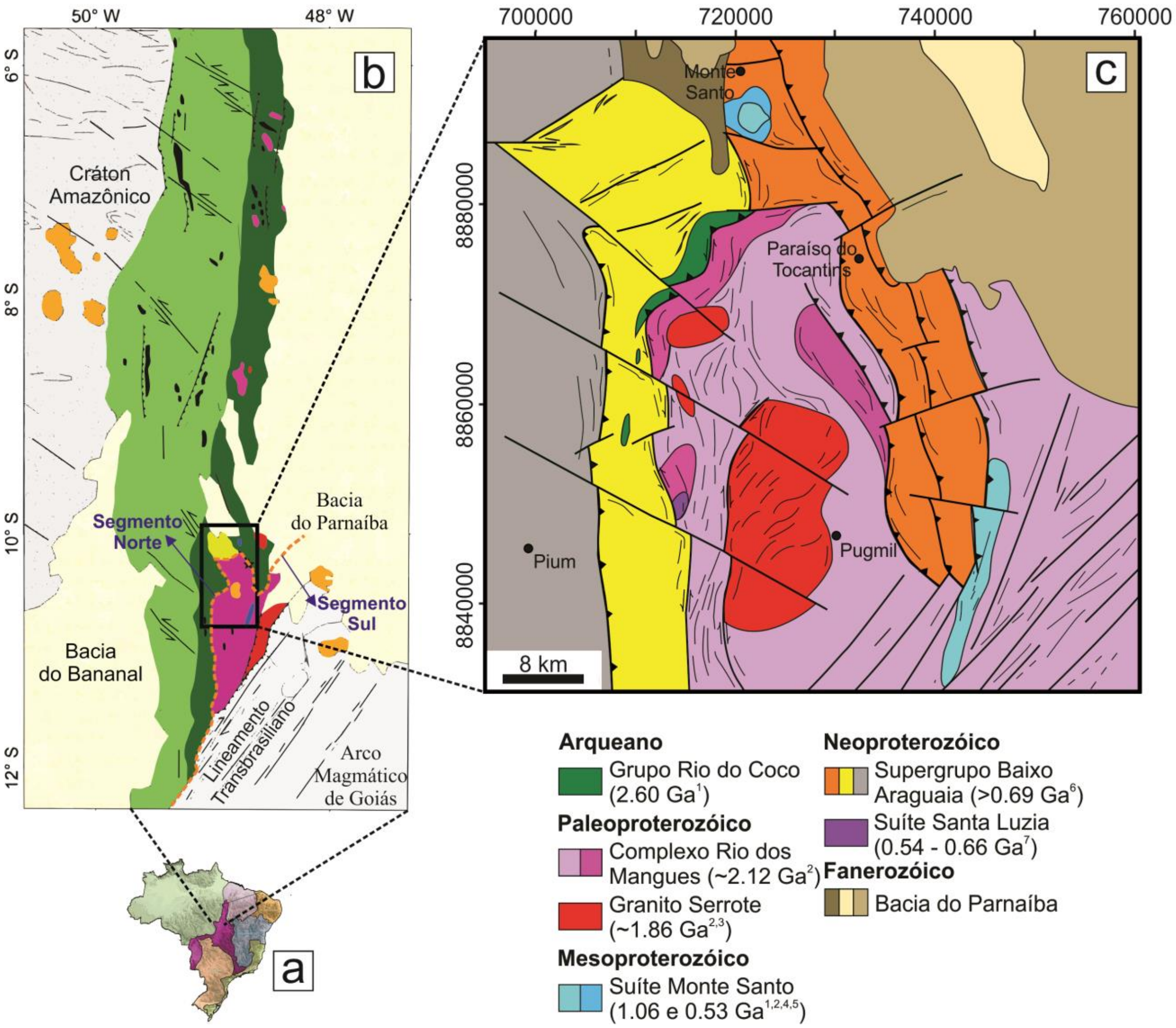

Figura 2A. Localização da área de estudo em relação as províncias estruturais do Brasil, com enfoque no Cinturão Araguaia. 2B. Mapa da geologia regional do Cinturão Araguaia, adaptado de Alvarenga et al. (2000), destacam-se os segmentos norte e sul, por linhas tracejadas alaranjadas e setas azuis. 2C. Enfoque referente a área de etudo, a região de Paraíso do Tocantins, com as unidades geológicas listadas juntamente com suas idades publicadas. 1- Arcanjo 2002, 2-Arcanjo et al. 2013, 3-Souza e Moura 1996, 4-Iwanuch 1991, 5-Viana e Battilani 2014, 6-Pinheiro et al. 2011, 7-Moura e Gaudette 1993. Imagem adaptada de Garcia et al. (2016) e Valentin et al. (2016).

no norte (Complexo Rio dos Mangues 2,05 - 2,12 Ga, Souza 1996, Arcanjo et al. 2013), apresentando apenas vestígios de embasamento arqueano (Grupo Rio do Coco – 2,60 Ga, Arcanjo 2002).

2.2.Geologia da Região de Paraíso do Tocantins

Na região de Paraíso do Tocantins afloram, como embasamento, as unidades Grupo Rio do Coco e Complexo Rio dos Mangues. As unidades mais jovens são representadas pelo Granito Serrote, Suíte Monte Santo, Supergrupo Baixo Araguaia, Suíte Santa Luzia, além de parte da região ser encoberta pela Bacia do Parnaíba. Todas as idades que serão apresentadas, exceto quando especificado, são idades obtidas pelo método de evaporação Pb-Pb.

O Grupo Rio do Coco, que é restritamente aflorante, foi inicialmente descrito por Barreira (1980) e Barreira e Dardenne (1981) como uma sequência metavulcano-sedimentar do tipo *greenstone belt*, com unidade inferior composta de sedimentos pelíticos e químicos e intercalações de xistos magnesianos, e unidade superior com xistos feldspáticos e rochas máficas. Tal conjunto de rochas foi formalmente agrupado e definido por Costa et al. (1983) e posteriormente datada por Arcanjo e Moura (2000) e Arcanjo (2002), apresentando idades arqueanas de 2,60 Ga (Fig. 2C).

O Complexo Rio dos Mangues, que constitui a unidade de embasamento dominante, é uma série de gnaisses tonalíticos, granodioríticos e calcissilicáticos, que se estende desde Paraíso do Tocantins até a região de Gurupi (Costa et al. 1983). Essa unidade apresenta idades de 2,05 a 2,12 Ga, com idades modelo Sm-Nd T_{DM} de 2,21 a 2,25 Ga e ε_{Nd} positivo, com valores de 0,86 à 2,40 (Arcanjo et al. 2013).

Na porção centro-norte do Complexo Rio dos Mangues, está alojado o Granito Serrote (Costa 1985), representado por microclínio granitos e leucogranitos potássicos (Gorayeb 1996), apresentando foliação incipiente, que se torna mais evidente em suas bordas (Souza 1996). O Granito Serrote é datado em 1,84 a 1,86 Ga (Alves 2018), com idades modelo T_{DM} de 2,35 a 2,50 Ga e ε_{Nd} negativo, com valores de -6,01 à -1,04 (Sousa e Moura 1996, Arcanjo et al. 2013).

A Suíte Monte Santo (Hasui et al. 1984b) é formada pelos maciços sieníticos de Monte Santo e Estrela. O Maciço Monte Santo apresenta formato semi-circular, com cerca de 4 km de diâmetro, já o Maciço Estrela apresenta formato elíptico, com eixo maior (16 km) na direção NNE-SSW (Fig. 2C).

Iwanuch (1991) interpreta as rochas da Suíte Monte Santo como gnaisses alcalinos metaígneos insaturados, predominantemente compostos de litchfieldito gnaisses, sódico-persódicos, miasquíticos e subsolvus. Outras variedades descritas pelo autor, além dos litchfielditos gnaisses, são os produtos metamórficos de nefelinólitos, mariupolitos, miaskitos, nefelina sienitos, feldspato alcalino sienitos com nefelina, monzossienito gnaisses com nefelina, sienitos, pegmatitos alcalinos, glimeritos, kersantitos e fenitos. Uma definição para todas as litologias incomuns descritas por Iwanuch (1991), retirada do glossário de termos, nas normas sugeridas para nomenclatura de rochas ígneas da IUGS (*International Union of Geological Sciences*) (Le Maitre et al. 2002) é fornecida na Tabela 1, as referências originais dos termos podem ser encontrada na mesma referência.

Tabela 1. Nomenclatura das rochas descritas por Iwanuch (1991) que não seguem os padrões de classificação de rochas ígneas de Le Maitre et al. (2002).

Rocha	**Definição**
Litchfieldito	Rocha de granulação grossa, variedade foliada de nefelina sienito, contendo K-feldspato, albita, nefelina, cancrinita, sodalita e lepidomelano.
Mariupolito	Variedade leucocrática de nefelina sienito caracterizado pela ausência de K-feldspato e a presença de albita e aegirina.
Miaskito	Variedade leucocrática de biotita nefelina monzosienito com oligoclásio e ortoclásio pertítico.
Glimerito	Rocha ultramáfica que contém quase apenas biotita. O termo foi sugerido como uma alternativa à biotitito, para evitar o som discordante de consecultivos “titos”.
Kersantito	Variedade de lamprófiro que contém fenocristais de Mg-biotita, com ou sem hornblenda, olivina ou piroxênio na matriz, além de plagioclásio e ocasional feldspato alcalino.
Fenito	Rocha metassomática, normalmente associada com carbonatitos ou ijolitos e ocasionalmente com nefelina sienitos e granitos peralcalinos, composta de feldspato alcalino, piroxênio sódico e/ou anfibólio alcalino. Algumas variedades são rochas monominerálicas contendo feldspato alcalino.

As rochas da Suíte Monte Santo foram datadas por Iwanuch (1991), Souza (1996), Arcanjo e Moura (2000), Arcanjo et al. (2013) e Viana e Battilani (2014), utilizando distintos métodos e técnicas analíticas, obtendo diferentes idades, que são sumarizadas na Tabela 2.

Tabela 2. Dados isotópicos U-Pb e Sm-Nd dos maciços Estrela e Monte Santo. 1- Iwanuch (1991), 2-Arcanjo e Moura (2000), 3-Arcanjo et al. (2013) e 4- Viana e Battilani (2014).

Técnica Analítica	Maciço	Idade
ID-TIMS (U-Pb)	Estrela	538 ± 13 Ma[1]
ID-TIMS (Pb-Pb)	Estrela	1050 ± ? Ma[4]
ID-TIMS (Pb-Pb)	Monte Santo	1001 ± 86 Ma[2,3]
MC-LA-ICP-MS (U-Pb)	Monte Santo	1056 ± 21 Ma ~ 1106 ± 10[5]
SHRIMP (U-Pb)	Monte Santo	1048 ± 11 ~ 1051 ± 22 Ma[5]
SHRIMP (U-Pb)	Monte Santo	511 ± 10 ~ 535 ± 8 Ma[5]

Método	Idade T_{DM} Calculada	ε_{Nd} Calculado
Sm-Nd (rocha total)	1,49 - 1,70 Ga[3]	-4,06; -3,74; -2,52[4]

Arcanjo e Moura (2000), Arcanjo et al. (2013) e Viana e Battilani (2014) consideram as idades mesoproterozóicas como idades de cristalização da Suíte Monte Santo. Viana e Battilani (2014) interpretam as idades fanerozóicas como idades de recristalização durante a formação do Orógeno Brasiliano. A interpretação da idade de cristalização da Suíte Monte Santo é especulativamente utilizada para vincular esse evento de magmatismo alcalino com a formação de riftes que permitiram a deposição das rochas sedimentares da Bacia Araguaia, posteriormente metamorfizada, constituindo o Supergrupo Baixo Araguaia (Alvarenga et al. 2000).

O Supergrupo Baixo Araguaia representa as rochas metassedimentares do Cinturão Araguaia, além de ser a unidade geológica com maior área aflorante no mesmo. Essa grande unidade supracrustal representa metamorfismo do tipo barroviano no Cinturão Araguaia, apresentando gradação transicional de fácies ankimetamórficas ao oeste até fácies anfibolito alto à leste. Dessa maneira, o Supergrupo Baixo Araguaia é subdividido em dois grupos, o Grupo Tocantins, representando o topo, contendo rochas de baixo grau metamórfico (ankimetamórfico à xisto verde) e o Grupo Estrondo, representando a base, contendo rochas de mais alto grau metamórfico (anfibolito a anfibolito superior) (Abreu 1978, Costa 1980, Hasui et al. 1984a, Abreu et al. 1994, Moura et al. 2008).

Entremeadas às rochas do Supergrupo Baixo Araguaia ocorrem uma série de rochas metamáficas e metaultramáficas, formando extensos lineamentos ao longo do Cinturão Araguaia (Formação Tucuruí, Morro do Agostinho, Serra do Tapa, Quatipuru). Os membros mais importantes são o Complexo Quatipuru, interpretado como um ofiolito desmembrado, com idade de 0,75 Ga, por isócronas Sm-Nd (Paixão et al. 2008), e a Suíte Xambica, que consiste de metagabros e anfibolitos de 0,81 Ga (Gorayeb et al. 2004).

Na região de Paraíso do Tocantins, as rochas do Supergrupo Baixo Araguaia são representadas pelo Grupo Estrondo, que contém calcixistos, xistos feldspáticos, biotita xistos, granada estaurolita biotita xistos, quartzitos, xistos grafitosos, restritos mármores e ocasionais lentes de rochas metaultramáficas (Fig. 2C).

Predominantemente aflorante nas rochas de mais alto grau metamórfico do Grupo Estrondo, ocorrem os granitos e pegmatitos da Suíte Santa Luzia, esses granitos apresentam idades de cristalização de ~0,54 Ga (Alves 2018) e são considerados como corpos tardi-tectônicos. Alguns trabalhos os consideram como granitos sin-tectônicos e produto de fusão parcial de sequências supracrustais durante o pico do metamorfismo do Cinturão Araguaia (Moura e Gaudette 1993, Alvarenga et al. 2000, Moura et al. 2008).

2.3. Proveniência sedimentar e estimativas de pressão, temperatura e *timing* do metamorfismo (P-T-t)

O único estudo de proveniência de grãos de zircão nas rochas metassedimentares do Supergrupo Baixo Araguaia foi realizado por Pinheiro et al. (2011), que sugere duas fontes sedimentares distintas para os segmentos norte e sul do Cinturão Araguaia, onde idades arqueanas predominam no norte e idades neo-mesoproterozóicas com menor contribuição paleoproterozóica predominam no sul. Os cristais de zircão mais jovens encontrados no estudo de Pinheiro et al. (2011) datam de 697 Ma e foram encontrados no Grupo Estrondo, próximo a Paraíso do Tocantins.

As únicas estimativas de pressão e temperatura (P-T) no Cinturão Araguaia foram realizadas em xistos de protólito pelítico do Grupo Estrondo e anfibolitos da Suíte Xambica, ambos localizados no segmento norte do cinturão, onde as condições de pressão e temperatura variam entre 7-9 kbar e 630-665 ºC, respectivamente (Pinheiro 2016).

O *timing* do metamorfismo no Cinturão Araguaia é ainda mal definido. As primeiras estimativas da idade metamórfica no cinturão foram realizadas por Moura e Gaudette (1993), datando grãos de zircão da Suíte Santa Luzia pelo método de evaporação Pb-Pb, obtendo idades de 655-513 Ma. Moura et al. (2008) reportam idades

U-Pb SHRIMP de 528 ± 4.7 Ma na Suíte Santa Luzia e interpretam-nas como o pico metamórfico no Cinturão Araguaia, entretanto os mesmos autores demonstram grãos de zircão herdados com idades diferentes nos núcleos e bordas, apresentando espalhamento nas idades mais jovens de 500 a 550 Ma. Alves (2018) demonstrou que a Suíte Santa Luzia representa magmatismo tardio a pós-tectônico, ao invés de sin-tectônico, como anteriormente se considerava (Moura e Gaudette 1993, Moura et al. 2008), constatando-se assim, que as idades obtidas anteriormente para esses granitos não representam o metamorfismo do Cinturão Araguaia. Alves (2018) evidenciou a presença de xenocristais do Grupo Estrondo nesses granitos, com grãos com bordas de baixa razão Th/U, com idades em torno de 570 Ma, interpretadas como um possível evento metamórfico no cinturão. Pinheiro (2016) obteve idades U-Th-Pb de 513 ± 14 Ma em monazitas de xistos do Grupo Estrondo.

Para o segmento norte do Cinturão Araguaia estão disponíveis idades de exumação, limitadas entre 489-498 Ma, por termocronologia de traço de fissão em zircão obtidas nos gnaisses do embasamento com estruturas dômicas (Dias et al. 2017), e entre 497-505 Ma, por idades $^{40}Ar/^{39}Ar$ em anfibólio e biotita obtidas por Pinheiro (2016) no Grupo Estrondo.

3. Materiais e métodos

Os métodos aplicados neste trabalho incluem amostragem, petrografia sob microscópio de luz transmitida, análises de química mineral, imageamento de elétrons retroespalhados e catodoluminescência em microssonda eletrônica, geoquímica de elementos maiores e traço, datação U-Pb em zircão utilizando ICP-MS multicoletor com sistema de ablação por laser acoplado e análises de geoquímica isotópica Sm-Nd em ID-TIMS.

Todos os métodos aplicados, assim como preparações dos materiais estudados foram realizados nos laboratórios da Universidade de Brasília, com exceção às análises de geoquímica, que foram realizadas nos laboratórios comerciais ALS e Actlabs.

3.1. Amostragem e Preparações

A coleta de amostras foi realizada em três campanhas de campo. A primeira campanha ocorreu durante a disciplina Trabalho Final de Graduação da Universidade de Brasília, no ano de 2015, denominado Projeto Paraíso do Tocantins, do qual o presente aluno fez parte, onde o Maciço Monte Santo foi mapeado em escala 1:50000. As demais campanhas foram realizadas nos meses de julho de 2016 e março de 2017, com amostragem focada no Maciço Estrela.

Os trabalhos de campo foram guiados pelo mapa em escala 1:50000 do Projeto Paraíso do Tocantins, pela Carta Porto Nacional, em escala 1:250000, do Serviço Geológico do Brasil (CPRM) (http://geobank.cprm.gov.br/pls/publico carta SC.22-Z-B) e por mapas aerogeofísicos de gamaespectrometria e magnetometria.

A amostragem foi realizada de maneira irregular, pois a disposição de afloramentos de rocha em campo não permitiu a confecção de malhas de amostragem regulares. Em cada afloramento, foram coletadas grandes amostras de rocha, para a confecção de lâminas delgadas e eventual preparação para geoquímica. Em alguns pontos foram coletadas amostras de ao menos 10 kg para preparação de separados de zircão e outros minerais pesados.

As amostras utilizadas para análise de geoquímica e petrografia foram cuidadosamente selecionadas, em campo, procurando rochas minimamente intemperizadas nos afloramentos, enquanto na coleta de amostras para geocronologia, o critério mais importante foi o volume e não o estado de preservação das amostras, no entanto esta amostragem foi realizada nos mesmos pontos ou em pontos próximos as amostras de geoquímica. (Anexos)

Do total de 66 amostras coletadas, cerca de 50 foram escolhidas para confecção de lâminas delgadas, dentre as quais, 20 foram selecionadas para geoquímica e 5 para geocronologia. Nas amostras escolhidas para análises de geoquímica, o critério determinante foi petrográfico, tentando abranger a maior variedade possível de diferentes tipos de rocha, com base em variações de tipos de minerais máficos e porcentagem modal, e.g. nefelina sienito com biotita, piroxênio, biotita e anfibólio, feldspato alcalino sienito, nefelina feldspato alcalino sienito. Os critérios de amostragem para geocronologia foram a diferença de litotipos amostrados e seu posicionamento e forma de ocorrência no maciço, e.g. centro, borda.

Para a confecção de lâminas delgadas, foram selecionadas amostras abrangendo variações de feições texturais e estruturais (e.g. granulação fina e média, foliadas ou maciças). Nas amostras foliadas, o corte selecionado para lâmina foi perpendicular à foliação e paralelo à direção do caimento das camadas, para se observar os minerais em sua seção alongada segundo a foliação.

Nas rochas selecionadas para geoquímica foi realizada cominuição em britador de mandíbula, com o quarteamento necessário até atingir pequenas quantidades de amostra, suficientes para a pulverização em panelas de ágata e carbeto de tungtênio, após a pulverização foi realizado o último quarteamento do pó até atingir alíquotas de cerca de 4 g de amostra para análise.

Na preparação de amostras para geocronologia foi realizada cominuição em moinho de mandíbula, peneiramento em frações de 1,2 mm, 600 µm, 200 µm, 125 µm e 90 µm, separação de magnetita, biotita e anfibólio utilizando o separador magnético isodinâmico Frantz, separação gravimétrica por bateamento e catação de grãos em estereomicroscópio Leica EZ4. Os grãos e fragmentos de grãos de zircão obtidos foram selecionados segundo critérios de hábito, tamanho e cor, e montados em fita dupla face, impregnados por resina epóxi em pequenos suportes anelares de plástico de cerca de 9 mm de diâmetro. Por fim foi realizado polimento em feltros com pasta de diamante de 3 µm e 1 µm, de maneira a expor superfícies limpas e não alteradas dos grãos.

3.2.Microssonda Eletrônica

Análises de química mineral e imagens de elétrons retroespalhados (BSE) em minerais essenciais e acessórios e imagens de catodoluminescência em cristais de zircão foram realizadas na microssonda Jeol JXA-8230 Superprobe, equipada com cinco espectrômetros WDS, do Laboratório de Microssonda Eletrônica da Universidade de Brasília.

Os materiais utilizados para análise foram lâminas polidas, seções polidas e *mounts* polidos de grãos impregnados com resina epóxi. Todo o material foi metalizado anteriormente às análises. O controle da espessura adequada de metalização é feito de maneira empírica, colocando-se um disco de latão polido juntamente com o material a ser metalizado, quando o disco adquire cor azulada, a espessura ideal, de cerca de 200 Å é adquirida.

Os minerais essenciais das rochas estudadas foram analisados sob condições de 15 kV de aceleração de voltagem e 10 nA de corrente do feixe, o tempo de contagem para todos os elementos foi de 10 segundos e 5 segundos, no pico e *background*, respectivamente. A lista dos elementos analisados sob essas condições, juntamente com o limite de detecção de cada elemento encontram-se nos Anexos.

Dentre os minerais essenciais analisados estão albita, microclínio, nefelina, biotita, anfibólio, piroxênio e magnetita. A classificação e cálculo de fórmula estrutural das análises de piroxênio foi realizada segundo os critérios de Morimoto *et al*. (1988), as de anfibólio, segundo Leake *et al*. (1997), onde os teores de Fe^{3+} foram estimados por estequiometria, seguindo o método de Schumacher (1997), e a classificação das análises de biotita seguiu os critérios de Tischendorf *et al*. (2007).

Em adição às correções do tipo ZAF, que são realizadas automaticamente e durante o procedimento de análise (*online*), no modelo de microssonda utilizado, uma série de correções empíricas, utilizadas em rotina no laboratório, para a sobreposição das linhas do espectro característico de diversos elementos, principalmente os elementos terras raras, foi realizada nos dados obtidos, seguindo procedimentos similares aos de Åmli & Griffin (1975), Donovan et al. (1993) e Fialin et al. (1997). As correções aplicadas são sumarizadas nos Anexos.

Análises químicas quantitativas com a microssonda podem ser obtidas com o auxílio de padrões, constituídos por elementos puros ou minerais e compostos sintéticos de composição bem conhecida, determinada a partir de diferentes metodologias. Os resultados quantitativos se dão por meio de comparação da intensidade de sinal obtida nos padrões e na amostra, convertidos para valores de porcentagem. Os padrões utilizados nas análises dos minerais da Suíte Monte Santo são sumarizados no Anexos.

3.3. Mapas de Catodoluminescência

Antes de serem realizadas análises isotópicas dos cristais de zircão pelo método U-Pb, usando LA-ICP-MS, os grãos separados nos *mounts* de epoxy, foram imageados em microssonda, tanto por BSE quanto por catodoluminescência (CL).

As varreduras foram realizadas sob aceleração de voltagem de 15 kV, corrente de 10 nA e *dwell time* de 2 microssegundos. O tempo de varredura para cada grão variou entre 1 a 2 horas, onde cerca de 555 grãos foram imageados. A malha de pixels para cada grão analisado foi determinada empiricamente, dependendo do tamanho do grão analisado, visando mapas que demonstrem, com boa qualidade, a distribuição espacial de intensidade de CL nos grãos.

3.4.Geoquímica de Elementos Maiores e Traço

Foram enviadas dez amostras de rocha total para análise química no laboratório Actlabs, no Canadá, e dez amostras para análise no laboratório ALS. As rotinas de análise utilizadas foram a 4B e 4B2, para o laboratório Actlabs, e CCP-PKG01 para o laboratório ALS.

Ambos laboratórios empregam o método de abertura de amostras por fusão com meta/tetraborato de lítio seguido de digestão em ácido nítrico diluído, nas rotinas de análise utilizadas, visto que este é o mais adequado para o ataque de minerais refratários, portadores de elementos terras raras e HFSE (*high field strength elements*), que são de grande importância petrológica, além de que as rochas estudadas são ricas em tais minerais.

Os elementos analisados foram medidos por ICP-AES e por ICP-MS, utilizando o mesmo tipo de preparação de vidro fundido. O pacote de análises do laboratório ALS, também fornece análises de carbono e enxofre total, em forno de combustão. A lista de elementos analisados em cada pacote, assim como seus limites de detecção podem ser encontrados nos sites: www.actlabs.com e www.alsglobal.com.

3.5. Análises isotópicas de U-Pb

As análises isotópicas de U-Pb foram realizadas no Laboratório de Estudos Geocronológicos, Geodinâmicos e Ambientais do Instituto de Geociências da Universidade de Brasília, nos dias 11 de abril de 2016 e 12 de janeiro de 2018. O método analítico utilizado é similar ao descrito por Bühn et al. (2009).

As análises de geocronologia foram realizadas em um espectrômetro de massas do tipo setor magnético, multicoletor e com fonte de plasma indutivamente acoplado, do modelo *Finnigan Neptune*, produzido e comercializado pela *Thermo Fisher Scientific*. Um *laser* de estado sólido (Nd:YAG), com comprimento de onda de saída de 213 nm, da *New Wave Instruments*, é acoplado ao espectrômetro.

A ablação dos grãos foi realizada em *spots* de 30-40 µm, com frequência de 10 Hz e intensidade de 2,64 a 2,77 J/cm^2. O material pulverizado foi carreado por um fluxo de He (~0,70 L/min) e Ar (~0.99 L/min).

Como estratégia de avaliação e correção do fracionamento de massas e o desvio instrumental induzido pelo ICP-MS, utilizou-se o método "*Standard Bracketing*", que consiste na intercalação de padrões de zircão antes e depois das amostras. A sequência de pontos utilizada consiste em ciclos de dez *spots*, iniciando com a análise de um branco, um padrão e oito *spots* em amostras, ocasionalmente encaixando-se um padrão interno entre os *spots* em amostras, para verificação da acurácia das análises.

O padrão utilizado foi o GJ-1, fornecido pelo ARC *National Key Centre for Geochemical Evolution and Metallogeny of Continents* (GEMOC) na Austrália. As idades de referência desse padrão, obtidas por Jackson *et al*. (2004), são 608.6 ± 1.1 Ma (^{207}Pb/^{206}Pb), 600.4 ± 1.8 Ma (^{206}Pb/^{238}U) e 602.1 ± 3.0 Ma (^{207}Pb/^{235}U). Como padrão interno, utilizou-se o zircão 91500 (Wiedenbeck *et al.* 1995, 2004), que apresenta razões certificadas de: ^{207}Pb/^{206}Pb = 0.07488 ± 0.00001, ^{206}Pb/^{238}U = 0.17917 ± 0.00008 e ^{207}Pb/^{235}U = 1.8502 ± 0.0008, com idade estimada de cerca de 1065 Ma. Os resultados obtidos nas análises dos padrões para todas as análises são apresentados no Anexo I.

Os dados foram adquiridos em 40 ciclos de cerca de 1 segundo, onde em cada leitura são determinadas as intensidades das massas ^{202}Hg, ^{204}(Pb+Hg), ^{206}Pb, ^{207}Pb, ^{208}Pb, ^{232}Th e ^{238}U.

A redução dos dados brutos, que inclui as correções para branco, deriva do equipamento e chumbo comum, foi realizada no software Chronus (Oliveira 2015). As razões isotópicas e erros associados obtidos com a redução dos dados foram plotadas em gráficos do tipo Concordia (Wetherill 1956), utilizando o suplemento de Excel, Isoplot (Ludwig 2003), que permitiu o cálculo estatístico das idades.

O critério de seleção para a utilização das razões isotópicas no diagrama de Concordia foi o percentual de discordância nas idades, calculado como:

$$\%\,Discord\hat{a}ncia\ = [1\ -\ \left(\frac{^{206}Pb}{^{238}U}age \div \frac{^{207}Pb}{^{206}Pb}age\right)] * 100$$

Para o cálculo das idades de Concordia, foram selecionados os dados com menor discordância, que se aglomeravam próximos à área das idades mais antigas (*upper intercept*) ou mais jovens (*lower intercept*), no gráfico de Concordia.

Mais detalhes sobre o equipamento utilizado para análises U-Pb, procedimento analítico completo, monitoramento de análises e correções utilizadas no laboratório estão disponíveis em Bühn et al. (2009) e Oliveira (2015).

3.6. Análises isotópicas de Sm-Nd

As análises foram realizadas no Laboratório de Estudos Geocronológicos, Geodinâmicos e Ambientais do Instituto de Geociências da Universidade de Brasília, utilizando espectrômetro de massas do tipo setor magnético, multicoletor, *Thermal Ionization Mass Spectrometer* (TIMS), modelo *Triton Plus™*, produzido e comercializado pela *Thermo Fisher Scientific*. A metodologia utilizada em laboratório segue os critérios de Gioia e Pimentel (2000).

As amostras de rocha total foram pesadas e misturadas com solução *spike* de ^{149}Sm-^{150}Nd e dissolvidas por diversos ataques ácidos, seguido por procedimentos de cromatografia, com separação de Sm e Nd dos outros elementos terras raras em colunas de troca catiônica. Detalhes do procedimento analítico são descritos em Gioia e Pimentel (2000).

4. PETROLOGY AND GEOCHRONOLOGY OF THE MONTE SANTO ALKALINE SUITE, CENTRAL BRAZIL.

Eduardo Valentin dos Santos[a] (corresponding author; Tel: +55-61-981002369; e-mail address: eduardovalentindossantos@gmail.com)

Nilson Francisquini Botelho[a] (nilsonfb@unb.br)

Elton L. Dantas[a] (elton@unb.br)

[a]Instituto de Geociências, Universidade de Brasília, Campos Universitário Darcy Ribeiro, Asa Norte, CEP 70910-900, DF, Brazil

Abstract

The Monte Santo Suite consists of two foliated and variably deformed and metamorphosed massifs (Estrela and Monte Santo). The intrusions are predominantly nepheline syenite and alkali feldspar syenite, but minor nepheline monzosyenite and nepheline monzodiorite are found in the Estrela Massif. In this study, the chemistry, mineralogy and age of the Monte Santo Suite were investigated. Pyroxenes vary in composition from omphacite to aegirine-augite to aegirine and have mixed characteristics between igneous and metamorphic trends. Biotite varies from phlogopite to siderophyllite to annite and presents primary, reequilibrated and neoformed trends. Amphibole varies from hastingsite to taramite. Nepheline presents high-temperature crystals preserved within the paragenesis but also many low-temperature crystals. The rocks of the Monte Santo Suite mostly do not plot near the minimum in the Petrogeny's Residua System. Additionally, REE and trace element patterns show parallel trends with significant variations in bulk content, suggesting that most of the rocks represent cumulates. Zr/Hf ratios are similar for all the rocks of the massif, showing that they evolved from the same source. Fractional crystallization was the main process that determined the lineage between different rock types. The Monte Santo Suite crystallization age is dated to 545 Ma, when these rocks were generated in an extensional or transtensional phase of orogen evolution and were subsequently deformed and metamorphosed in a compressive phase. T_{DM} ages, positive Nb and Ta anomalies and many irregularly shaped Mesoproterozoic zircon crystals suggest that the

Monte Santo Suite evolved from a Mesoproterozoic mantle source, inheriting some of its zircons.

4.1. Introduction

Alkaline rocks and carbonatites occur in almost every known tectonic environment and are distributed from the Archean to the present (Haissen et al. 2017). The most classic examples of alkaline magmatism are associated with intracontinental rifts (e.g., East African Rift, Gardar Province) (Bailey 1974, Bailey 1977, Bailey 1992). These rocks are also typically related to intraplate magmatism, whether continental or oceanic (e.g., Cameroon Line, Monteregian Hills Province, Canary Islands, Hawaiian Islands). Alkaline magmatism associated with subduction or continental collision is less common; these types of rocks are commonly related to potassium-rich magmas and genetically linked to calc-alkaline magmatism, although there are a few examples of carbonatites in China (Western Sichuan, Hou et al. 2006) and Pakistan (Sillai Patti and Loe Shilman, Tilton et al. 1998).

Several mechanisms have been proposed to generate nepheline syenites, among which is fractional crystallization of parent magmas represented by alkaline basalts, nephelinites, basanites or potassic alkaline rocks or by low fractions of partial melts of mantle and/or crustal rocks (Bailey 1974, Sorensen 1974, Price et al. 1985, Fitton and Upton 1987, Leat et al. 1988). Burke et al. (2003) suggested that the generation of younger alkaline rocks and carbonatites (ARCs) is caused by the melting of ancient deformed alkaline rocks and carbonatites (DARCs). This hypothesis came from the observations that DARCs around the world are commonly concentrated along ancient suture zones and that the occurrence of DARCs and ARCs in geographical proximity is very common, showing the recurrence of alkaline magmatism over hundred millions of years. The authors hypothesized that if the subducted DARCs reached adequate depths in the lithospheric mantle, they could be the source material for the later alkaline magmatism. Many authors have suggested similar mechanisms for well-known alkaline provinces in Africa (Ashwal et al. 2016), Canada (Burke et al. 2008), India (Leelanandam et al. 2006), Norway (Roberts et al. 2010) and Russia (Burke et al. 2007).

Other mechanisms for the generation of DARCs have been proposed, such as rifting associated with an intraorogenic extensional or transtensional phase that is terminated by a subsequent compressional phase in the development of the orogen (Attoh et al. 2007, Biswal et al. 2007, Emmanuel et al. 2013). This mechanism is opposed to the hypothesis of Burke et al. (2003), which considers DARCs as indicators of areas that experienced rifting and subsequent collision; therefore, DARCs do not always mark suture zones.

In the Araguaia Belt, Brazil, the occurrence of deformed alkaline rocks, represented by the Monte Santo Suite, is known. Its geological and tectonic significance are still incipient due to the lack of regional and local geological knowledge. The intent of this work is to shed some light on the problems related to the petrology and geochronology of this suite and its regional and global significance, as well as contribute with information about alkaline magmatism.

4.2. Geological Setting

The Monte Santo Suite is dominated by alkaline, silica-undersaturated to subsaturated metaplutonic rocks that crop out in the southern portion of the Araguaia Belt (Iwanuch 1991, Arcanjo et al. 2013) (Fig. 3).

The Araguaia Belt, together with the Brasília and Paraguai belts, constitutes the Tocantins Orogenic System, or Tocantins Province, as defined by Almeida et al. (1981), a large Neoproterozoic orogen that resulted from the convergence and collision of the Amazonian and São Francisco paleocontinents, where the final collision occurred during the Brasiliano – Pan-African orogeny (850-480 Ma, Brito Neves and Fuck 2013, Brito Neves et al. 2014) as part of the West Gondwana amalgamation (Fuck et al. 2017).

The Araguaia Belt consists of extensive successions of metamorphosed psammitic and pelitic rocks, with minor contributions of carbonates and igneous rocks (Alvarenga et al. 2000). This orogen is subdivided into two domains related to the predominant structural framework and basement age (Arcanjo et al. 2013). The basement of the northern domain has domic structure and is dominated by tonaline-trondhjemite-granodiorite (TTG) type Archean orthogneisses (Colméia Complex – 2.85 Ga, Moura and Gaudette 1999) with restricted Paleoproterozoic nuclei (Cantão Gneiss – 1.85 Ga, Moura and Gaudette 1999). In the southern domain, the basement is predominantly Paleoproterozoic rocks represented by the Rio dos Mangues Complex

(2.05-2.12 Ga, Souza 1996, Arcanjo et al. 2013), with an absence of domic structure and vestigial Archean rocks of the Rio do Coco Group (2.60 Ga, Arcanjo 2002). The Rio do Coco Group is a greenstone belt-type, metavolcanosedimentary sequence (Barreira 1980), while the Rio dos Mangues Complex is represented by a series of orthogneisses (tonalites and granodiorites) and paragneisses (calc-silicates) (Arcanjo et al. 2013).

The supracrustal rocks are represented by the Baixo Araguaia Supergroup, which is the most extensive geological unit in the Araguaia Belt. The metamorphic grade increases eastwards, varying between ankimetamorphic to high amphibolite facies (Abreu et al. 1994). The Baixo Araguaia Supergroup is subdivided into the Tocantins Group, which contains low-grade metamorphic rocks, and the Estrondo Group, which contains high-grade rocks. Zircon provenance studies on the metasedimentary rocks of the Baixo Araguaia Supergroup suggest different sedimentary sources from the northern and southern portions of the Araguaia Belt (Pinheiro et al. 2011), where Archean ages predominate in the north and Neo-Mesoproterozoic ages, with minor Paleoproterozoic contributions, predominate in the south. The youngest zircon crystals found in the study of Pinheiro et al. 2011 were dated to 697 Ma and found in the Estrondo Group in the southern Araguaia Belt.

Metamorphosed mafic and ultramafic plutons, as well as dismembered ophiolite complexes, are found interspersed with the Baixo Araguaia Supergroup rocks. The Quatipuru ophiolite is dated to 0.75 Ga by whole-rock Sm-Nd isochrons (Paixão et al. 2008), and the metagabbros of the Xambica Suite are dated to 0.81 Ga in zircon crystals by the Pb-Pb evaporation method (Gorayeb et al. 2004).

Late to post-tectonic granites in the Araguaia Belt are represented by the Santa Luzia Suite with a crystallization age of ~540 Ma (Alves 2018) and the Lajeado Suite from 552-547 Ma (Gorayeb et al. 2013). The Santa Luzia Suite occurs in both the northern and southern portions of the belt and represents I-S hybrid type magmatism, while the Lajeado Suite occurs to the south and represents A type magmatism.

The Monte Santo Suite occurs in the southern portion of the Araguaia Belt and consists of Mesoproterozoic (1.1 Ga) nepheline syenite gneisses that intrude the contact between the Rio dos Mangues Complex and the Estrondo Group. This alkaline magmatism is interpreted to have been generated in the rifting event that allowed the sedimentary deposition of the Baixo Araguaia Supergroup (Alvarenga et al. 2000). Many authors have dated this suite using diverse analytical techniques (LA-ICP-MS, SHRIMP, ID-TIMS, Pb-Pb evaporation), and many of these works have found Cambrian ages (538-402 Ma), interpreted as metamorphic and generated by the recrystallization of zircon grains during the Brasiliano orogeny (Iwanuch 1991, Arcanjo e Moura 2000, Arcanjo et al. 2013, Viana and Battilani 2014).

The only available quantitative P-T condition estimates in the Araguaia Belt were made in schists of the Estrondo Group and amphibolites of the Xambica Suite in the northern portion of the belt, where pressure and temperature conditions varied between 7-9 kbar and 630-665 °C, respectively (Pinheiro 2016).

The timing of the metamorphism in the Araguaia Belt is still loosely constrained. The first estimate of the metamorphic age of the belt was provided by Moura and Gaudette (1993), dating zircon grains from the Santa Luzia Suite by the Pb-Pb evaporation method and yielding ages of 655-513 Ma. Moura et al. (2008) reported a U-Pb SHRIMP age of 528 ± 4.7 Ma in the Santa Luzia Suite and interpreted it as the peak metamorphic age of the Araguaia Belt, despite the authors demonstrated inherited zircon grains with different ages of core and rims and a spread in the younger ages from 500 to 550 Ma. Alves (2018) indicated that the Santa Luzia Suite represents late to post-tectonic instead of syn-tectonic granitic magmatism, as previously thought (Moura and Gaudette 1993, Moura et al. 2008); thus, the ages obtained from these granites do not represent the metamorphism of the Araguaia Belt. Additionally, Alves (2018) presented evidence of xenocrysts from the Estrondo Group in these granites and found low Th/U ratios in the rims of those grains yielding ages of ~570 Ma, interpreted as a possible metamorphic event in the belt. Pinheiro (2016) obtained U-Th-Pb ages of 513 ± 14 Ma in monazites of schists of the Estrondo Group.

Exhumation ages are available for the northern portion of the Araguaia Belt and are constrained between 498 and 489 Ma by zircon fission track thermochronology of the domed basement gneisses (Dias et al. 2017) and between 505 and 497 Ma by the $^{40}Ar/^{39}Ar$ ages in amphibole and biotite obtained by Pinheiro (2016) in the Estrondo Group.

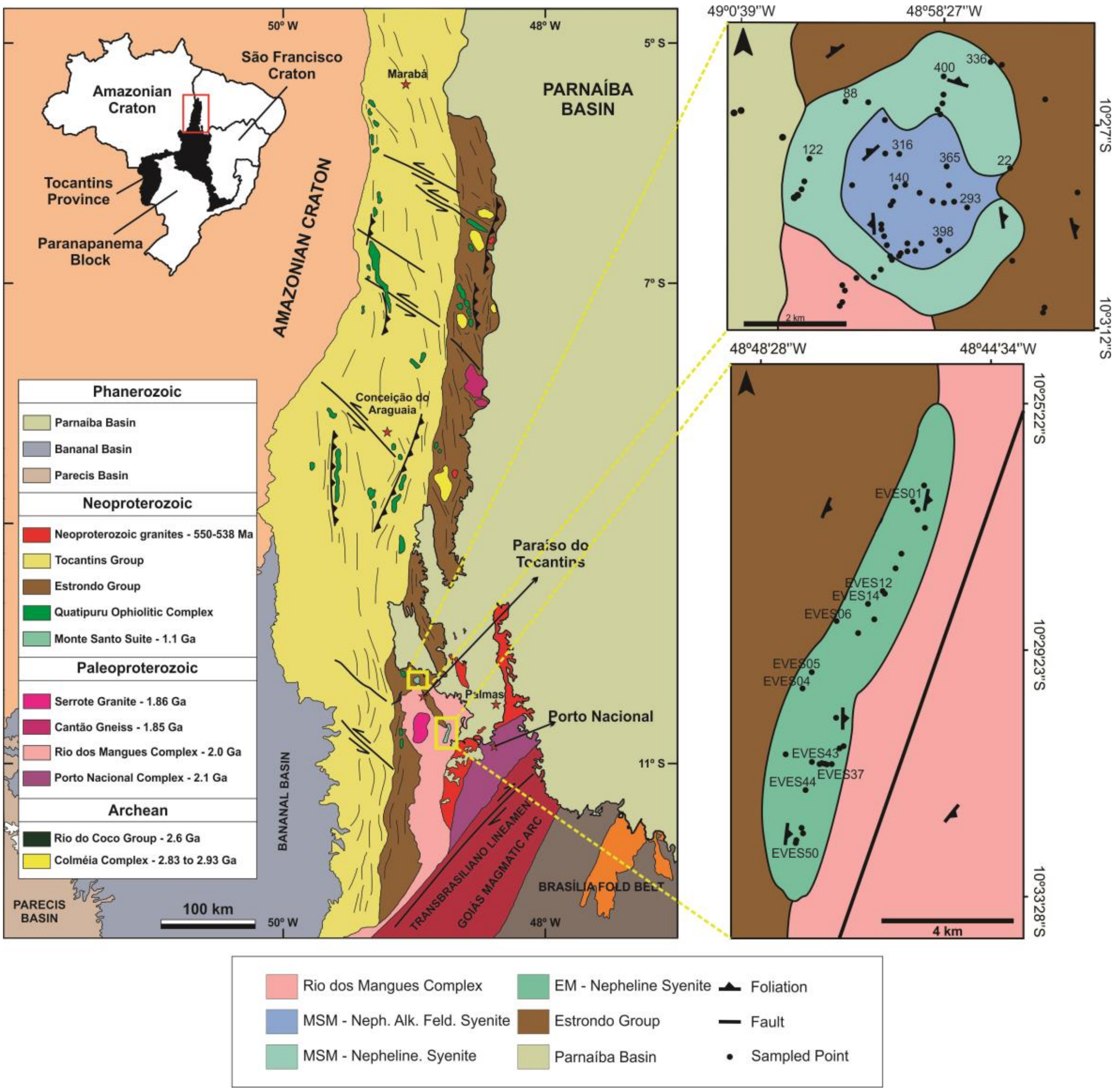

Figura 3. Regional geological map of the Araguaia Belt (AB). Empty red rectangle indicates the position of the AB within the Tocantins Province; yellow rectangles and arrows represent a detailed view of the studied areas, with sampling locations and names indicated by dots. Modified from Alvarenga et al. (2000).

4.3. Method

To evaluate the chemical compositions of the different types of rocks, classified by petrography, whole rock analyses of major and trace elements were performed.

Unweathered central pieces of the rock samples were selected for whole-rock analysis, avoiding cracks and rims affected by alteration. Samples were crushed in a jaw crusher and powdered in agate and tungsten carbide pans.

Major and trace elements were determined at Actlabs and at ALS, by ICP-OES and ICP-MS by standard lithium meta/tetraborate fusion followed by diluted nitric acid digestion methods.

To investigate the variations in chemical composition, as well as to classify and interpret the evolution of the rock-forming minerals of both massifs of the Monte Santo Suite, BSE imaging and EPMA WDS quantitative analysis were carried out on thin sections.

The mineral chemistry analyses were performed using a Jeol JXA-8230 Superprobe equipped with five WDS spectrometers at the EPMA Laboratory of the University of Brasília. Thirteen elements were analyzed, including Ti, Si, Al, Fe, Mn, Mg, Ca, Na, K, Cl, F, Cr and V. The implemented analytical conditions were an acceleration voltage of 15 kV and a beam current of 10 nA. The counting times at peak and background for all elements were 10 and 5 seconds, respectively.

The calibration procedure was carried out using the following natural minerals as standards: albite (NaKα), pyrophanite (TiKα, MnKα), microcline (SiKα, AlKα, KKα), andradite (FeKα), forsterite (MgKα), apatite (CaKα), vanadinite (ClKα, VKα), topaz (FKα) and chromite (CrKα).

The ZAF correction procedure was used to adjust for matrix effects. Interferences caused by peak overlap were corrected using empirical values determined in the laboratory using procedures similar to those of Åmli and Griffin (1975), Donovan et al. (1993) and Fialin et al. (1997).

In situ U-Pb isotopic analyses were carried out on zircon crystals using a Thermo Finnigan Neptune multicollector inductively coupled plasma mass spectrometer coupled with a New Wave Instruments Nd:YAG solid-state laser with an output wavelength of 213 nm at the Geochronology Laboratory of the University of Brasília.

After crushing the rock, zircon crystals were concentrated by panning and individually hand-picked. The selected crystals were set in 9 mm-diameter plastic rings filled with two-compound epoxy that were later polished. Every prepared zircon grain was imaged for back-scattered electrons and cathodoluminescence by EPMA.

The utilized ablation spots were 30 or 40 µm, depending on grain size, with a frequency of 10 Hz, and an intensity of 2.64 – 2.77 J/cm². The pulverized material was carried by a gas flux made up of helium (0.4 L/min) and argonium (0.9 L/min). A standard sample bracketing technique was applied, comprising a cycle of analyzing a blank, a GJ-1 reference zircon (Jackson et al. 2004) and eight samples. Often, between the analyzed samples, an internal standard consisting of the 91500 reference zircon (Wiedenbeck et al. 1995, 2004) was analyzed to evaluate the quality and reproducibility of the analyses. More details about the applied methods, including multicollector setup and data collection procedure, can be found in Bühn et al. (2009).

Data reduction was performed by the Microsoft Excel add-in Chronus (Oliveira 2015), where raw data were corrected offline for background signals, common Pb, elemental fractionation and instrumental drift. The corrected data were plotted in the Wetherill concordia plot (Wetherill 1956) using ISOPLOT (Ludwig 2012).

Whole-rock Sm-Nd analyses were carried out in a multicollector, sector field Thermo Fisher Scientific Triton PlusTM thermal ionization mass spectrometer at the Geochronology Laboratory of the University of Brasília. Sample preparation was the same as for whole-rock geochemistry. Rock powders were mixed with a ^{149}Sm-^{150}Nd spike solution and digested by acid attacks, followed by a procedure of chromatographic separation of Sm and Nd from the other rare earth elements. Details about the applied analytical procedure are described by Gioia and Pimentel (2000).

4.4. Petrography and field relations

A comprehensive characterization of the petrography of the Monte Santo Suite was made by Iwanuch (1991), where metamorphic gneisses of litchfieldite, mariupolite, miaskite, nepheline syenite (with corundum-bearing varieties), syenite, nepheline-bearing monzosyenite (with corundum-bearing varieties), alkaline pegmatites, glimmerite, kersantite and fenite are described in the context of the suite.

Due to the scarce distribution of preserved outcrops and the extensive soil cover on the massifs, the map delineation of all the different lithotypes encountered on a detailed scale could not be performed; therefore, a simplified version of maps and petrography is presented here, describing only the most common and widespread outcrop units in each massif, as well as some localized lithologies with different and important characteristics (mineralogy, geochemistry), using only the IUSGS approved names of Le Maitre et al. (2002).

4.4.1. Field aspects of the Monte Santo Massif and Estrela Massif

The Monte Santo Massif comprises a circular (in plan view) intrusion with radial outward foliation and almost plain terrain. This massif presents two mapped facies with distinct lithologies: a border facies, represented by nepheline syenite, and a central facies, represented by alkali feldspar syenite and nepheline alkali feldspar syenite. The transition between facies is gradual, and modal nepheline increases towards the borders. Around the intrusion is a thin zone of metasomatically altered rocks developed within the host schists and gneisses, comprising rocks of almost pure biotite, muscovite and magnetite.

The Estrela Massif comprises an elongated, fault-controlled intrusion, with its foliations concordant to the host rocks. The Estrela Massif presents three elevations of approximately one hundred meters in height but also crops out in the near lowlands. Within the Estrela Massif, the major outcropping rocks are nepheline syenite; however, there are also alkali feldspar syenite, nepheline monzosyenite and nepheline monzodiorite with restricted areas of occurrence.

In both massifs, planar structures are commonly observed from outcrop to hand sample scales, showing layers of alternating predominance of mafic and felsic minerals (Fig. 4), representing hololeucocratic to leucocratic or mesocratic variations of the same rock.

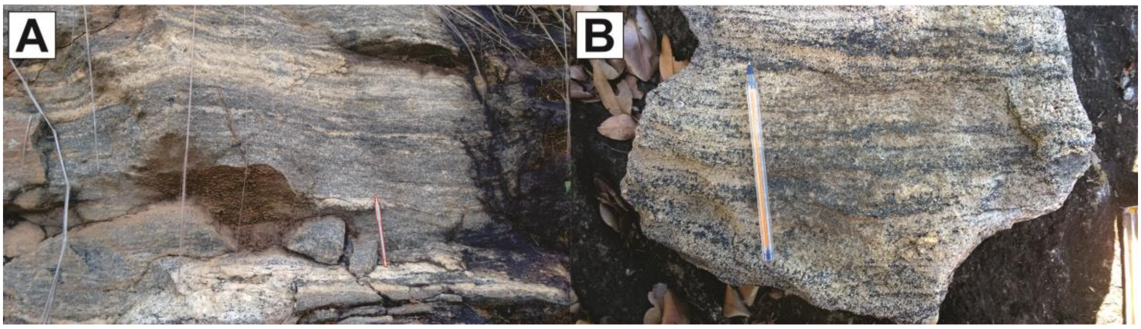

Figura 4. Field aspect of the rocks of the Monte Santo Suite, with evident parallel foliation at the outcrop (A) and hand sample (B) scales.

4.4.2. Nepheline syenite

In the Monte Santo Massif, nepheline syenite are fine- to medium-grained and hololeucocratic to leucocratic and occasionally present gneissic banding.

The predominant texture of the felsic minerals in the Monte Santo Massif is granoblastic, where crystals frequently form 120° triple junctions.

In the Estrela Massif, nepheline syenite commonly has medium-grained domains with well-preserved granular texture, although some rocks present large albite, microcline, nepheline or perthite crystals with undulose extinction, commonly displaying marginal recrystallization, characterized by rims of fine-grained, homogeneous and granoblastic feldspar crystals.

The mafic minerals of these rocks generally occur as oriented agglomerates with cumulate texture, where amphibole and less commonly biotite occur as intercumulus minerals.

The nepheline syenites consist of typical miaskitic mineralogy, comprising albite, microcline, nepheline, amphibole, biotite, magnetite and accessory clinopyroxene, calcite, sodalite, cancrinite, corundum, apatite, allanite, zircon and pyrochlore.

4.4.3. Nepheline monzosyenite

The nepheline monzosyenite occurs in the lowlands between the elevations of the Estrela Massif. These rocks are medium- to coarse-grained and hololeucocratic, consisting of almost only feldspars and nepheline. The most common texture within these rocks is the core-and-mantle (or mortar) microstructure, which is represented by coarse grains of perthite, individual feldspars or nepheline mantled by fine-grained, granoblastic crystals of the same minerals.

4.4.4. Alkali feldspar syenite and nepheline alkali feldspar syenite

In the Monte Santo Massif, alkali feldspar syenites are fine grained, leucocratic and foliated, and their contacts are transitional with nepheline syenite, forming transitional zones of nepheline alkali feldspar syenite. The dominant texture of felsic minerals is granoblastic, whereas for mafic minerals, it is the presence of oriented biotite flakes and interstitial amphiboles.

Nepheline-free rocks contain only biotite and magnetite as mafic minerals, while nepheline-bearing rocks additionally contain amphibole and rare pyroxene.

In the Estrela Massif, alkali feldspar syenites are medium-grained and leucocratic, and their occurrence is restricted to the northern portion of the massif. These rocks shows preserved igneous textures, displaying a hypidiomorphic granular texture.

The mineralogy of the alkali feldspar syenites comprises albite, microcline, biotite, magnetite, zircon and calcite in nepheline-free rocks and a paragenesis similar to that of nepheline syenites, although with smaller amounts of nepheline, in the transitional nepheline alkali feldspar syenites.

4.4.5. Nepheline monzodiorite

The nepheline monzodiorite intrudes the nepheline syenites in the northern portion of the Estrela Massif. This rock is fine-grained and mesocratic, consisting of feldspars, nepheline, clinopyroxene, amphibole, biotite and accessory titanite, fluorite and calcite.

Deformational textures are unusual within this rock, whereas the most commonly observed textures are coarse phenocrysts of amphibole, with flow-oriented flakes of biotite and laths of plagioclase around them (Fig. 5A).

4.5. Mineral Chemistry

4.5.1. Feldspars

Albite and microcline are the predominant felsic minerals in the rocks of the Monte Santo Suite. Albite is volumetrically more abundant than microcline and occurs as fine (0.2 - 0.6 mm) polygonal crystals, as medium to coarse (1 - 6 mm) subhedral to anhedral crystals, usually containing rounded inclusions of nepheline, microcline and biotite, and as flame-texture perthite intergrowths. Microcline occur as medium (1 - 3 mm) subhedral to anhedral granular crystals or as fine (0.2 - 0.6 mm) polygonal crystals.

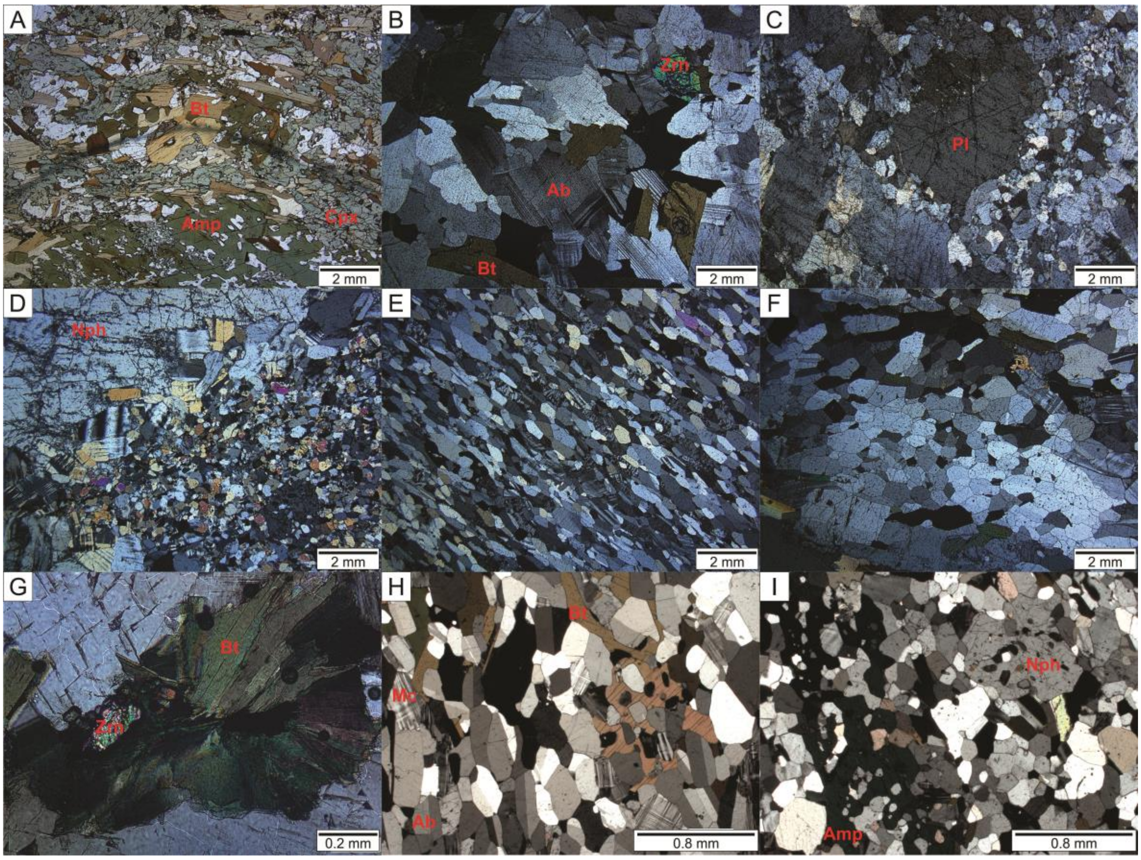

Figura 5. (A) Nepheline monzodiorite sample showing flow bands oriented around amphibole phenocrysts. (B) Well-preserved igneous hypidiomorphic granular texture within a nepheline syenite of the Estrela Massif. (C) Core-and-mantle texture presented in a nepheline monzosyenite sample of the Estrela Massif. (D) Alkaline pegmatite crosscutting a fine-grained, granoblastic alkali feldspar syenite of the Monte Santo Massif. (E) Oriented texture with fine-grained, granoblastic crystals in a border nepheline syenite of the Monte Santo Massif. (F) Fine-grained granoblastic domains within a coarser-grained nepheline syenite of the Monte Santo Suite. (G) Radial biotite presenting zircon inclusions. (H) Interstitial biotite in a nepheline syenite of the Monte Santo Massif, with preserved igneous texture. (I) Poikilitic amphibole and nepheline crystals in a nepheline syenite of the Monte Santo Suite. Mineral abbreviations are defined according to Whitney and Evans (2010).

Plagioclase composition ranges from oligoclase (An18) in nepheline monzosyenites and nepheline monzodiorites to albite reaching almost endmember composition in the other lithologies, whereas microcline ranges from Or90 to almost pure endmember composition in all lithologies (Table 3).

4.5.2. Nepheline

Nepheline structural formula were calculated for thirty-two oxygen per formula; additionally, the Na, K, Ca and appropriate amounts of Al and Si cations were calculated as the endmembers nepheline (Ne – $NaAlSiO_4$), kalsilite (Ks – $KAlSiO_4$) and anorthite (An – $\square_{1/2}Ca_{1/2}AlSiO_4$), and excess Si was calculated as quartz (Qz – $\square Si_2O_4$). The amounts of Ne, Ks and Qz were recalculated to 100%, as proposed in Hamilton and MacKenzie (1960). The normalized endmember percentages were plotted in the ternary diagram of the $NaAlSiO_4$-$KAlSiO_4$-Si_2O_4 system at 1 kb PH_2O using the isotherms defined by Hamilton and MacKenzie (1960) and Hamilton (1961) (Fig. 6). The Barth plane (Barth 1963), which constrains natural nepheline compositions (Dollase and Thomas 1978), was used to control the quality of the analyses.

Tabela 3. Representative compositions of the feldspar group minerals (NS – Nepheline Syenite, AFS – Alkali Feldspar Syenite, NMD – Nepheline Monzodiorite, NMS – Nepheline Monzosyenite).

Massif	MSM	MSM	EM	EM	EM	EM	MSM	MSM	EM	EM	EM
Rock Type	NS	AFS	NMD	NMS	NS	AFS	NS	AFS	NMS	NS	AFS
Sample	MS88	MS140	EVES12	EVES05	EVES14	EVES06A	MS88	MS140	EVES05	EVES37	EVES06A
Spot no.	C2_7	C1_20	C1_9	9	6	6	C2_2	C1_5	6	1	2
Feldspar	Albite	Albite	Albite	Oligoclase	Albite	Albite	Microcli.	Microcli.	Microcli.	Microcli.	Microcli.
SiO_2	69.51	68.37	66.32	64.47	68.94	68.98	64.04	63.25	65.21	64.63	66.38
Al_2O_3	20.05	19.42	20.96	22.56	19.43	19.60	18.37	18.54	18.58	18.58	18.49
Fe_2O_3	0.25	0.00	0.03	0.04	0.00	0.03	0.05	0.05	0.00	0.02	0.02
CaO	0.10	0.13	1.59	3.48	0.13	0.10	0.05	0.02	0.00	0.00	0.02
Na_2O	13.01	11.08	10.89	9.56	12.03	12.28	0.65	0.79	1.16	0.69	0.84
K_2O	0.17	0.16	0.31	0.10	0.07	0.05	15.52	15.97	15.56	15.76	15.64
Total	103.09	99.16	100.10	100.21	100.61	101.05	98.68	98.61	100.50	99.69	101.38
mol.% end-members											
Ab mol %	98.75	98.44	90.95	82.75	99.01	99.29	5.99	6.98	10.18	6.26	7.50
An mol%	0.41	0.61	7.35	16.67	0.59	0.46	0.26	0.10	0.00	0.00	0.08
Or mol%	0.84	0.94	1.69	0.58	0.40	0.25	93.75	92.92	89.82	93.74	92.42

Nepheline occurs in different textural varieties in both massifs, including coarse (5 - 6 mm) subhedral crystals, medium to fine hexagonal crystals and crystals with well-developed faces (0.4 - 2 mm), interstitial anhedral crystals (1 - 1.5 mm) and fine rounded inclusions (0.1 - 0.2 mm) within other minerals, usually feldspars.

There are significant differences between the chemistry of nepheline within the syenites of the Monte Santo Massif and those of the Estrela Massif (Table 4). In the Monte Santo Massif, nepheline composition is constrained in the range of $Ne_{68.6-79.5}Ks_{19.7-23.3}Qz_{0.0-8.3}$, and its temperature is mostly concentrated below 500 ºC, with only one point close to the 775 ºC isotherm.

In the Estrela Massif syenites, nepheline compositions are constrained in the $Ne_{71.2-80.9}Ks_{16.1-21.1}Qz_{0.1-8.7}$ interval, and its temperature is widely spread, with its higher temperatures concentrated between the 775 ºC and 1068 ºC isotherms, well aligned to Barth's joint (an intersection of the Barth plane within the Ne-Ks-Qz-An tetrahedron, projected from the An corner). In the nepheline monzodiorite, compositions are constrained in the $Ne_{75.2\text{-}80.5}Ks_{14.5\text{-}19.0}Qz_{2.8\text{-}9.3}$ interval, presenting higher temperatures than the syenites.

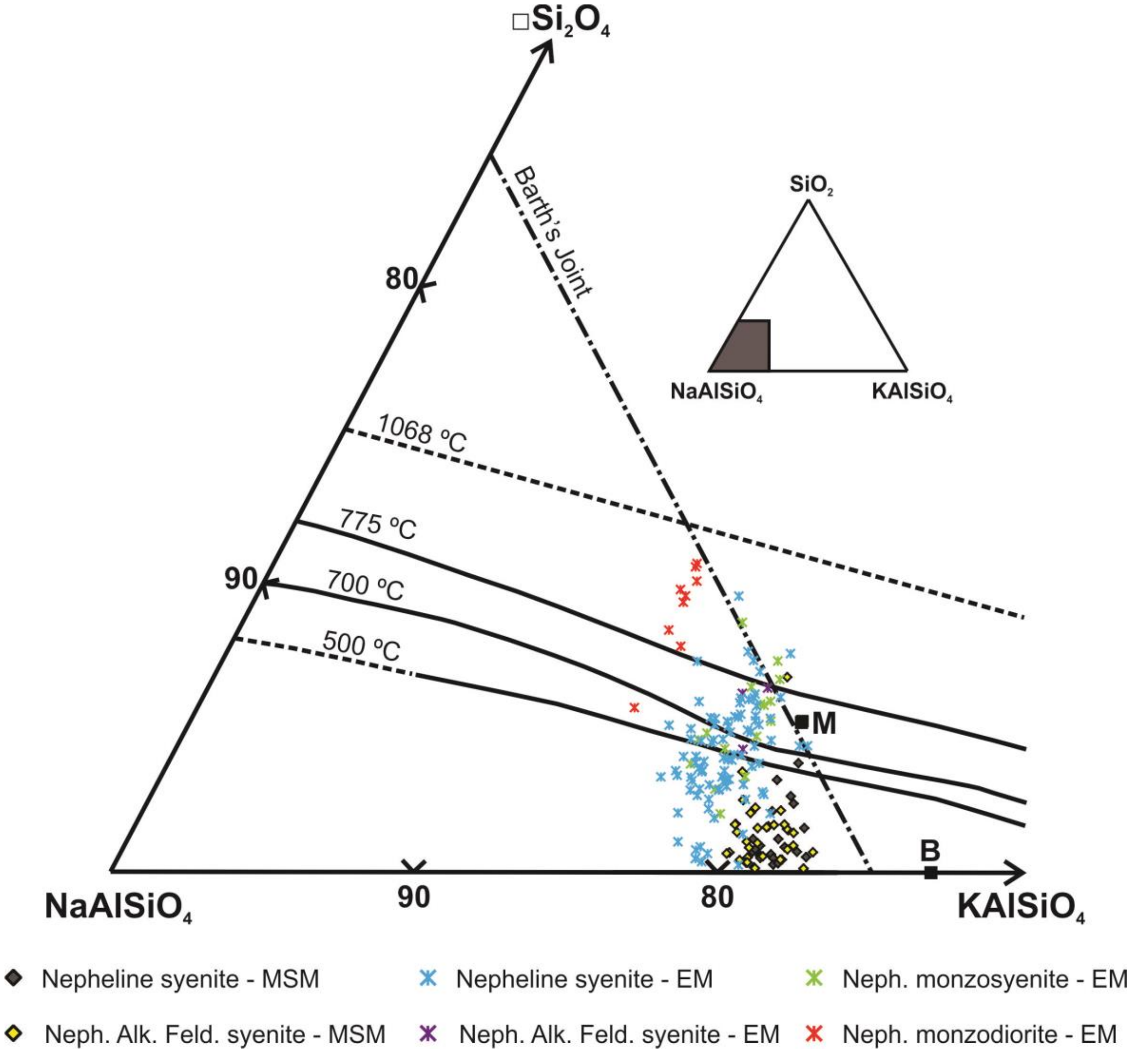

Figura 6. Compositions of Monte Santo (MSM) and Estrela (EM) nephelines in the nepheline-kalsilite-silica diagram, with isotherms defined by Hamilton and MacKenzie (1960) and Hamilton (1961). Morozewicz and Bueger (Tilley 1954) compositions are labeled as filled squares, symbolized by the letters M and B, respectively.

Tabela 4. Representative compositions of nepheline.

Massif	MSM	MSM	EM	EM	EM	EM
Rock Type	NS	AFS	NMD	NMS	NS	AFS
Sample	344A	140	EVES12	EVES05	EVES14	EVES03A
Spot no.	C1_18	C1_3	C3_9	6	5	C10_4
SiO_2	42.01	42.43	42.27	43.09	44.63	43.21
Al_2O_3	33.81	33.88	33.78	34.64	33.53	33.51
Fe_2O_3	0.21	0.08	0.02	0.00	0.13	0.32
CaO	0.13	0.46	1.18	0.77	0.36	0.19
Na_2O	16.02	15.89	16.11	16.22	15.98	16.00
K_2O	6.75	6.24	4.71	6.18	5.80	5.34
Total	98.92	98.97	98.06	100.90	100.43	98.58
Formula based in 32 oxygen atoms						
Si	8.20	8.24	8.24	8.21	8.49	8.38
Al	7.78	7.76	7.76	7.78	7.52	7.66
Fe	0.03	0.01	0.00	0.00	0.02	0.05
Ca	0.03	0.10	0.25	0.16	0.07	0.04
Na	6.06	5.99	6.09	5.99	5.89	6.02
K	1.68	1.55	1.17	1.50	1.41	1.32
mol.% end-members						
Ne	75.77	74.83	76.08	74.90	73.68	75.20
Ks	21.01	19.34	14.64	18.78	17.58	16.51
Qtz	3.22	5.83	9.28	6.32	8.74	8.29

4.5.3. Biotite

Biotite is the most abundant mafic mineral in the nepheline alkali feldspar syenite of the Monte Santo Massif and in all the rocks of the Estrela Massif. It occurs as flakes (Fig. 5B) and rarely as rounded inclusions, interstitial crystals (Fig. 5H) or radial crystals (Fig. 5G). It commonly occurs with other mafic minerals in the paragenesis, such as amphiboles and/or magnetite.

Biotite compositions are classified following the criteria of Tischendorf et al. (2007) as the varieties annite, siderophyllite and phlogopite (Fig. 7A). Structural formulas were calculated for eleven oxygen atoms, considering all the iron atoms as divalent, and no lithium estimation (as proposed by Tischendorf et al. 2004) was made. Representative analyses are listed in Table 5.

In the Monte Santo Massif, biotite is widespread in the nepheline alkali feldspar syenite and rarely occurs in the nepheline syenite. Its composition is annite, its

$Mg/(Mg+Fe^{2+}+Mn)$ ratio ranges from 0.03 to 0.18, and its maximum TiO_2 content is 2.57%.

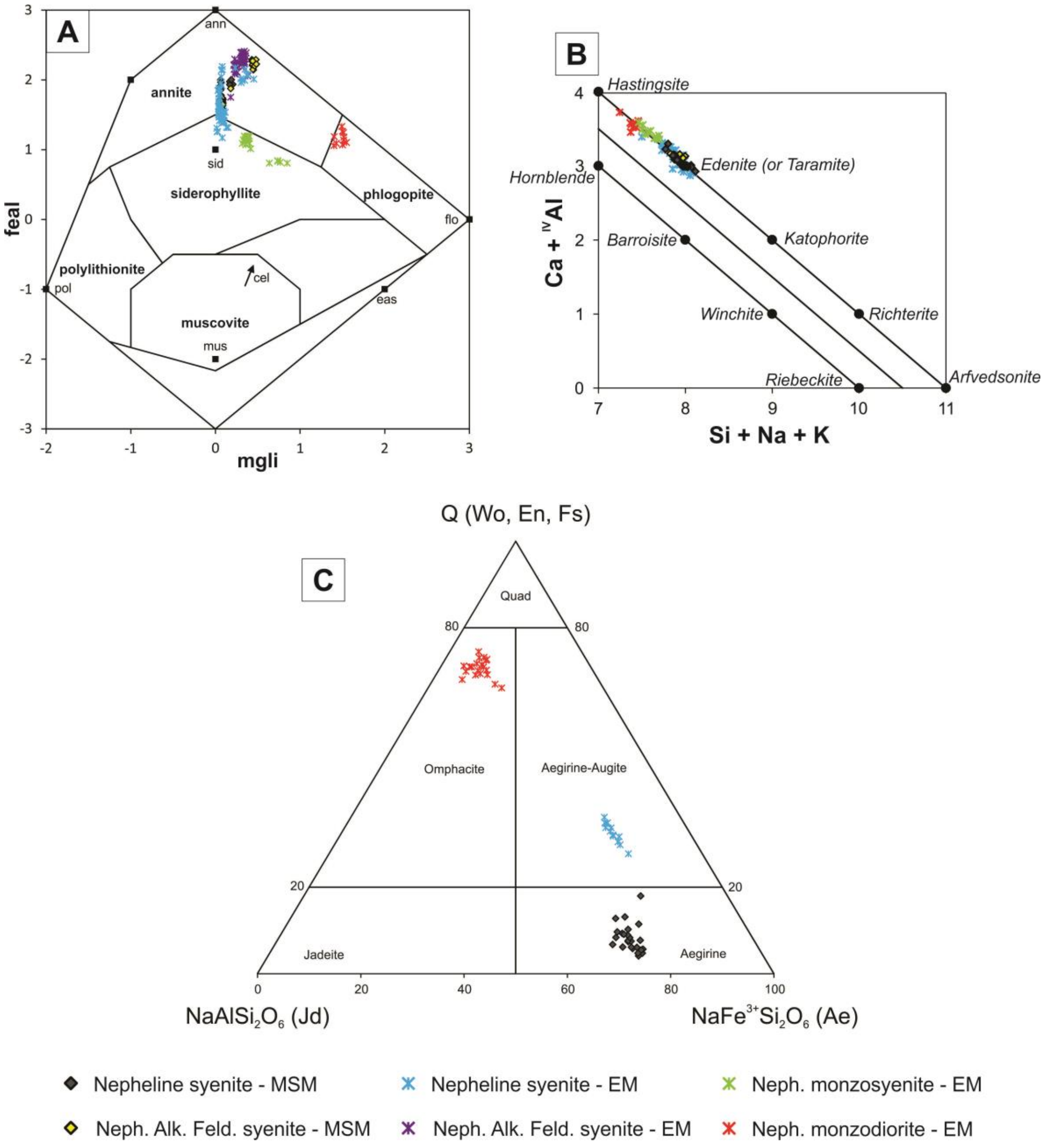

Figura 7. Monte Santo Suite biotite, amphibole and pyroxene analyses plotted in (A) the mgli (Mg – Li) against feal ($^{VI}Fe_{total}$ + Mn + Ti – Al) diagram of Tischendorf et al. (2007) for mica classification. (B) Giret et al. (1980) diagram for amphibole classification and evolution trends. (C) Quadrilateral - jadeite - aegirine ternary diagram of Morimoto et al. (1988).

In the Estrela Massif, biotite occurs in all the lithologies and ranges from phlogopite to siderophyllite to annite, where phlogopite occurs in the nepheline monzodiorite, siderophyllite in the nepheline monzosyenite (and neoformed grains, with radial texture in nepheline syenite) and annite in nepheline syenite and nepheline alkali feldspar syenite. Phlogopite, siderophyllite and annite Mg/(Mg+Fe^{2+}+Mn) ratios range from 0.54-0.56, 0.01-0.38 and 0.01-0.17, with maximum TiO_2 contents of 3.36%, 0.83% and 3.82%, respectively. There is a tendency for the rounded inclusions of biotite to contain the highest amounts of TiO_2, while radial textured grains contain lower amounts.

4.5.4. Amphibole

Amphibole is the most common mineral in the nepheline syenite of the Monte Santo Massif and an usual mafic mineral in the Estrela Massif. It occurs as interstitial (0.8 - 1 mm) crystals or poikilitic phenocrysts (2 - 5 mm) with inclusions of nepheline and feldspars; both textural types are zonation-free (Fig. 5A and I).

Representative amphibole compositions are listed in Table 6. The cation allocation, estimation of ferric iron and nomenclature are in accordance with Leake et al. (1997) and Schumacher (1997).

In the Monte Santo Suite, the amphiboles span a compositional range from calcic to sodic-calcic. In the Monte Santo Massif, the only amphibole phase is the sodic-calcic species taramite. In the Estrela Massif, taramite is present in all the syenites and nepheline monzosyenite, and hastingsite is the species in the nepheline monzodiorite (Fig. 7C).

4.5.5. Clinopyroxene

Representative clinopyroxene compositions are listed in Table 7. The nomenclature and cation allocation are in accordance with Morimoto et al. (1988).

Clinopyroxene is a rare mineral phase within the Monte Santo Suite and occurs as fine rounded crystals or as aggregates of fine anhedral crystals (Fig. 5A). Both types lack zoning.

In the Monte Santo Massif, aegirine occurs in the nepheline syenite, while in the Estrela Massif, aegirine-augite is the main pyroxene in the nepheline syenite, and omphacite occurs in the nepheline monzodiorite (Fig. 7C).

Tabela 5. Representative compositions of biotite.

Massif	MSM	MSM	EM	EM	EM	EM
Rock Type	NS	AFS	NMD	NMS	NS	AFS
Sample	MS88	MS319C	EVES12	EVES06B3	EVES06B1	EVES06A
Spot no.	C2_6	C2_9	C3_6	9	9	30
Classification	Annite	Annite	Phlogopite	Sideroph.	Annite	Annite
SiO_2	31.10	32.88	35.41	32.49	32.97	34.35
TiO_2	1.01	2.57	3.36	0.77	3.82	3.21
Al_2O_3	19.45	14.32	13.29	22.09	19.50	13.79
FeO	31.71	30.56	18.17	26.21	26.13	31.98
MnO	1.77	1.65	0.31	0.75	3.47	0.66
MgO	0.48	3.57	12.43	3.22	0.37	2.62
Na_2O	0.11	0.10	0.15	0.21	0.13	0.16
K_2O	9.40	9.39	9.09	9.57	9.72	9.51
F	0.16	0.44	1.86	1.30	0.42	0.82
Total	95.20	95.48	94.08	96.61	96.51	97.09
Formula based in 11 oxygen atoms						
F	0.04	0.11	0.47	0.33	0.11	0.21
OH	1.96	1.89	1.53	1.67	1.89	1.79
ΣOH	2.00	2.00	2.00	2.00	2.00	2.00
Si	2.58	2.73	2.86	2.61	2.64	2.82
Al^{IV}	1.42	1.27	1.14	1.39	1.36	1.18
ΣT	4.00	4.00	4.00	4.00	4.00	4.00
Al^{VI}	0.48	0.13	0.12	0.71	0.49	0.15
Ti	0.06	0.16	0.20	0.05	0.23	0.20
Mg	0.06	0.44	1.49	0.39	0.04	0.32
Fe	2.20	2.12	1.23	1.76	1.75	2.20
Mn	0.12	0.12	0.02	0.05	0.24	0.05
ΣM	2.92	2.97	3.06	2.95	2.75	2.91
Na	0.02	0.02	0.02	0.03	0.02	0.03
K	0.99	0.99	0.93	0.98	0.99	1.00
ΣI	1.01	1.01	0.96	1.01	1.01	1.02
$Mg/(Mg+Fe^{2+}+Mn)$	0.03	0.16	0.55	0.18	0.02	0.13

Tabela 6. Representative compositions of amphibole.

Massif	MSM	MSM	EM	EM	EM
Rock Type	NS	AFS	NMD	NS	AFS
Sample	MS22	MS319C	EVES12	EVES37	EVES02
Spot no.	C3_12	C2_1	C1_3	C3_2	C5_9
Classification	Taramite	Taramite	Hastingsite	Taramite	Taramite
SiO_2	37.43	37.58	40.08	36.34	37.03
TiO_2	0.54	0.59	1.31	0.23	0.81
Al_2O_3	12.72	12.89	13.11	12.99	10.73
$Fe_2O_3^{calc.}$	14.73	11.70	5.31	9.50	12.85
$FeO^{calc.}$	11.38	17.53	11.73	19.34	18.53
MnO	3.29	1.68	0.21	2.40	1.25
MgO	3.40	1.86	8.76	1.06	1.59
CaO	6.22	6.53	10.53	7.64	6.50
Na_2O	4.58	4.38	2.71	3.69	4.53
K_2O	2.43	2.76	1.93	2.45	2.17
F	0.64	0.51	1.05	0.31	0.55
Total	97.35	98.01	96.72	95.94	96.52
Formula based in 22 oxygen atoms and average estimation of Fe^{3+}					
OH	1.68	1.74	1.48	1.84	1.71
F	0.32	0.26	0.52	0.16	0.29
ΣOH	2.00	2.00	2.00	2.00	2.0
Si	5.99	6.03	6.24	5.99	6.09
ΣT	8.00	8.00	8.00	8.00	8.00
Al	0.39	0.47	0.64	0.51	0.16
Ti	0.06	0.07	0.15	0.03	0.10
Fe3+	1.75	1.49	0.56	1.25	1.67
Mg	0.81	0.44	2.03	0.26	0.39
Fe2+	1.55	2.27	1.59	2.60	2.47
Mn	0.44	0.23	0.01	0.33	0.17
ΣC	5.00	4.98	5.00	4.98	4.98
Mn	0.01	0.00	0.02	0.00	0.00
Fe2+	0.00	0.00	0.00	0.00	0.00
Ca	1.07	1.12	1.76	1.35	1.14
Na	0.93	0.88	0.22	0.65	0.85
ΣB	2.00	2.00	2.00	2.00	2.00
Na	0.50	0.48	0.60	0.53	0.59
K	0.50	0.57	0.38	0.51	0.45
ΣA	0.99	1.05	0.98	1.04	1.05
$Mg/(Mg+Fe^{2+}+Mn)$	0.29	0.15	0.56	0.08	0.13

Tabela 7. Representative compositions of clinopyroxene.

Massif	MSM	MSM	EM	EM
Rock Type	NS	NS	NMD	NS
Sample	MS22	MS336B	EVES12	EVES4C
Spot no.	C3_3	C1_4	C1_1	C3_9
Classification	Aegirine	Aeg.-aug.	Omphacite	Aeg.-aug.
SiO_2	53.35	52.47	51.48	51.47
TiO_2	0.09	0.13	0.34	0.16
Al_2O_3	5.42	4.92	5.14	3.49
Fe_2O_3	22.67	24.54	2.47	19.06
FeO	3.19	2.11	9.02	5.46
MnO	0.52	0.40	0.39	1.18
MgO	0.19	0.10	8.16	1.94
CaO	1.73	2.00	19.00	9.31
Na_2O	12.42	12.43	2.93	8.55
Total	99.58	99.09	98.92	100.62
Formula based in 6 oxygen atoms				
Si	2.01	1.99	1.95	1.96
Al	0.00	0.01	0.05	0.04
ΣT	2.01	2.00	2.00	2.00
Al	0.24	0.21	0.18	0.12
Fe3+	0.64	0.70	0.07	0.55
Ti	0.00	0.00	0.01	0.00
Mg	0.01	0.01	0.46	0. 1
Fe2+	0.10	0.07	0.28	0.17
Mn	0.00	0.01	0.00	0.04
ΣM1	1.00	1.00	1.00	0.99
Fe2+	0.00	0.00	0.00	0.00
Mn	0.01	0.00	0.01	0.00
Ca	0.07	0.08	0.77	0.38
Na	0.91	0.92	0.21	0.63
ΣM2	0.99	1.00	1.00	1.01
%Q	9.29	7.70	71.67	32.09
%Jd	24.71	22.04	21.68	15.14
%Ae	65.99	70.26	6.64	52.77
$Mg/(Mg+Fe^{2+}+Mn)$	0.08	0.06	0.61	0.34

4.6. Geochemistry

Since in the Monte Santo Suite, the majority of outcropping rocks are felsic syenites, our sampling and geochemical data mostly encompass this type of rock, with minor sampling of mafic and intermediate rocks (nepheline monzodiorite and nepheline monzosyenite); therefore, the diagrams shown in this section present our data with the addition of Iwanuch (1991) major element data and Viana and Battilani (2014) major and trace element data in order to improve the presented geochemical trends and interpretations. Care was taken with Iwanuch (1991) data, excluding rocks classified by this author as fenites and metasomatically altered rocks.

The lithotypes of the Monte Santo Suite are classified as metaluminous to peraluminous silica-undersaturated rocks (Frost and Frost 2008), with sodic affinities in terms of Na_2O/K_2O (Table 8), reflecting the modal predominance of albite and nepheline (Fig. 8).

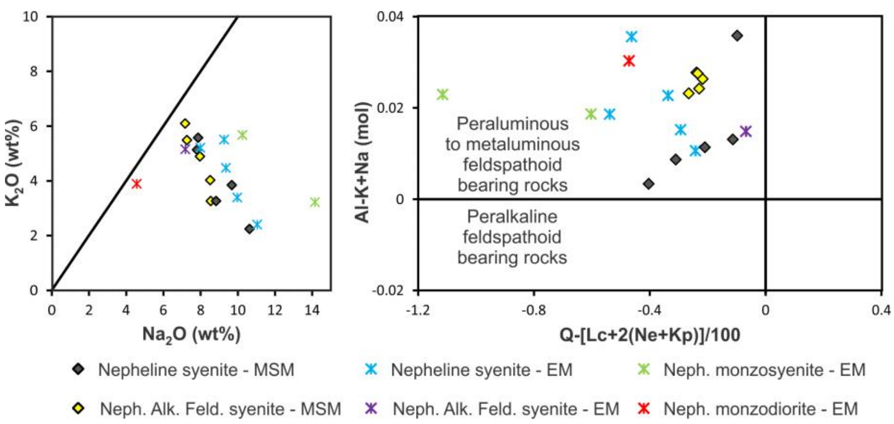

Figura 8. (A) Na_2O against K_2O in weight percent. (B) Feldspathoid silica-saturation index (FSSI), consisting of felsic normative minerals (Q – quartz, Lc – leucite, Ne – nepheline, Kp – kaliophilite) against the alkalinity index (AI) diagram of Frost and Frost (2008) showing the dominant alkali oxide, silica-saturation and aluminum-saturation conditions of the Monte Santo Suite.

In the major element variation diagrams, SiO_2 was chosen as the fractionation index because it presents the highest variation among the evaluated samples (45.2 - 62.7 wt%, Table 8). There are convex trends of depletion in TiO_2, CaO, and MgO and concave trends of enrichment in Na_2O and Al_2O_3 with increasing differentiation (Fig. 9).

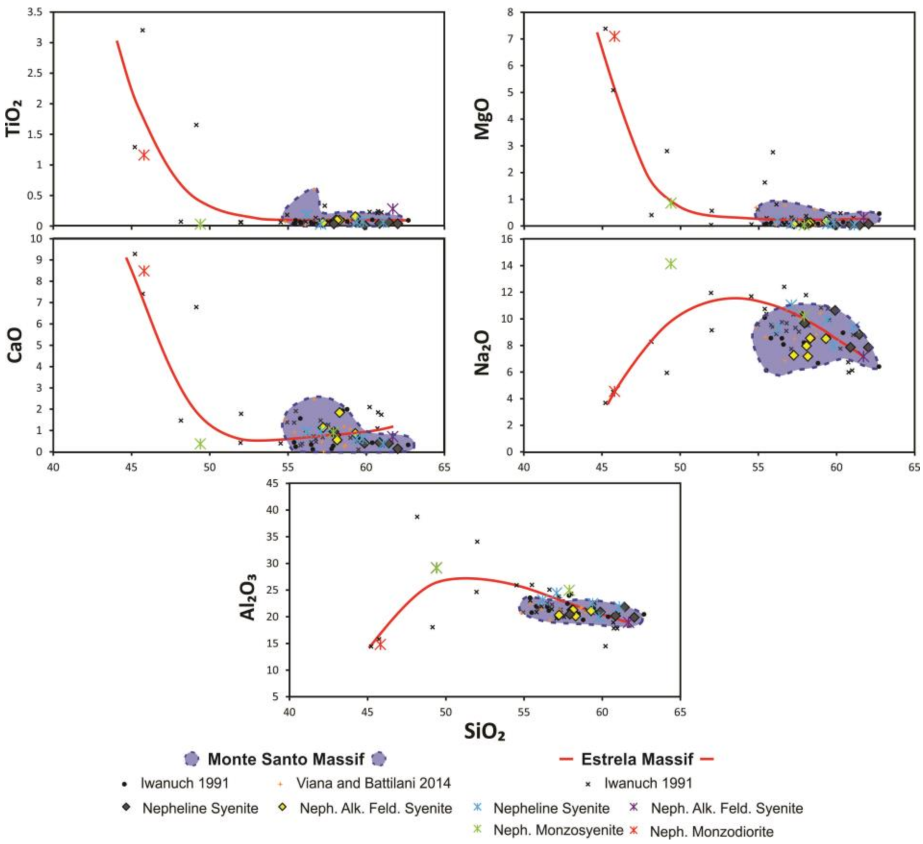

Figura 9. Harker variation diagrams using additional data of Iwanuch (1991) and Viana and Battilani (2014), which are labeled as smaller black and orange symbols. Iwanuch (1991) data encompass both massifs and depicts major variations in terms of SiO_2, while Viana and Battilani (2014) encompass only the Monte Santo Massif and shows the same small variation found in the most felsic studied samples.

The rare earth elements (REEs) present concentrations ranging from 10 to 296 times and 16 to 1450 times the chondritic values for lanthanum in the Monte Santo Massif and Estrela Massif, respectively (Fig. 10, Table 9).

The average La/Sm_N and Gd/Lu_N of the nepheline alkali feldspar syenite and alkali feldspar syenite of the MSM are 12.98 and 1,21, respectively, indicating fractionated LREE behavior and an almost flat HREE pattern. Some of these rocks shows nearly absent Eu anomalies (Eu/Eu* = 0.94) to well-developed anomalies (Eu/Eu* = 0.47). The nepheline syenite present La/Sm_N and Gd/Lu_N ratios of 12.34 and 0.8, respectively, with well-developed Eu anomalies (Eu/Eu* = 0.53 to 0.19).

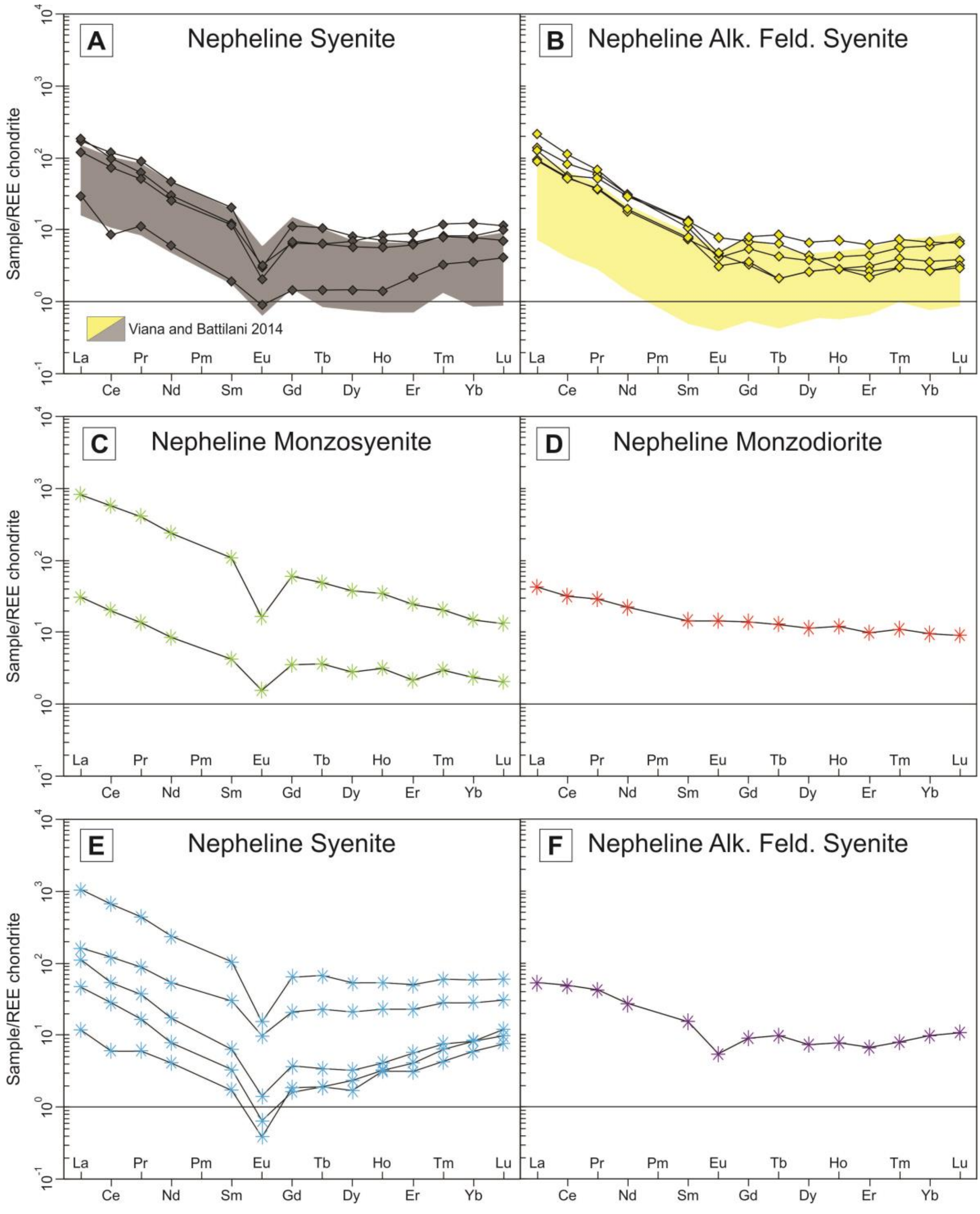

Figura 10. Rare earth element diagrams for the Monte Santo Suite, normalized to the chondritic values of Nakamura (1974) and separated by rock type. The shaded area represents the data of Viana and Battilani (2014).

Tabela 8. Whole-rock major element analyses of the Monte Santo Suite.

Rock type	NS	NS	NS	NS	NS	AFS	AFS	AFS	AFS	AFS
Massif	MSM	MSM	MSM	MSM	MSM	MSM	MSM	MSM	MSM	MSM
Sample no.	MS22B	MS88A	MS122A	MS336	MS400	MS140	MS293	MS316C	MS365	MS398
Major elements (wt%)										
SiO_2	59.9	60.87	61.44	57.94	62.02	59.31	58.31	57.25	58.07	58.15
TiO_2	0.007	0.031	0.053	0.024	0.029	0.143	0.083	0.044	0.09	0.083
Al_2O_3	20.81	20.13	21.72	20.42	19.75	21.05	20.06	20.25	21.23	21.21
$Fe_2O_3^t$	4.45	4.6	2.18	6.26	3.66	4.95	5.65	6.94	4.05	4.73
MnO	0.076	0.095	0.084	0.243	0.082	0.112	0.189	0.152	0.066	0.121
MgO	0.03	0.04	0.02	0.04	0.06	0.17	0.11	0.06	0.11	0.08
CaO	0.4	0.43	0.39	0.94	0.12	0.85	1.83	1.13	0.78	0.55
Na_2O	10.64	7.87	8.84	9.68	7.82	8.52	8.55	7.27	7.97	7.18
K_2O	2.24	5.57	3.26	3.84	5.13	4.02	3.26	5.48	4.89	6.09
P_2O_5	< 0.01	0.02	< 0.01	0.03	< 0.01	0.07	0.06	0.01	0.06	0.02
LOI	0.43	0.69	1.26	0.88	0.65	0.9	1.88	1.35	1.36	1.18
Total	98.98	100.3	99.24	100.3	99.32	100.1	99.99	99.93	98.68	99.39
C	n.a.	n.a.	n.a.	n.a.	n.a.	n.a.	n.a.	n.a.	n.a.	n.a.
S	n.a.	n.a.	n.a.	n.a.	n.a.	n.a.	n.a.	n.a.	n.a.	n.a.
Felsic Normative Minerals (CIPW norm, wt%)										
Orthoclase	13.2	32.9	19.3	22.7	30.3	23.8	19.3	32.4	28.9	36.0
Albite	61.4	47.2	65.8	44.6	55.7	52.0	51.2	37.0	45.4	39.1
Anorthite	2.0	2.0	1.9	0.9	0.6	3.8	6.7	5.5	3.5	2.6
Nepheline	15.5	10.5	4.9	20.2	5.7	10.9	11.5	13.3	11.9	11.7
Leucite	0.0	0.0	0.0	0.0	0.0	0.0	0.0	0.0	0.0	0.0

Tabela 8 - (cont.)

Rock type	NMD	NMS	NMS	NS	NS	NS	NS	NS	AFS
Massif	EM	EM	EM	EM	EM	EM	EM	EM	EM
Sample no.	EVES13	EVES05	EVES06	EVES04	EVES14	EVES37	EVES44	EVES50	EVES01
Major elements (wt%)									
SiO_2	45.8	57.9	49.4	56.2	61.1	59.4	59.8	57.1	61.7
TiO_2	1.15	<0.01	0.02	0.18	0.05	0.05	0.06	0.02	0.27
Al_2O_3	14.8	24.9	29.1	23.1	21.8	22.4	19.85	24.4	18.9
$Fe_2O_3^t$	11.7	0.37	1.51	4.84	2.89	3.25	6	3.05	4.52
MnO	0.2	0.01	0.04	0.15	0.06	0.11	0.15	0.07	0.13
MgO	7.11	0.03	0.86	0.22	0.03	0.08	0.11	0.09	0.32
CaO	8.45	0.91	0.37	0.93	0.37	0.62	0.62	0.93	0.71
Na_2O	4.56	10.25	14.15	9.27	9.37	9.98	7.99	11.05	7.18
K_2O	3.89	5.67	3.22	5.5	4.47	3.39	5.2	2.4	5.15
P_2O_5	0.14	<0.01	0.02	0.06	0.01	0.01	0.02	0.01	0.11
LOI	1.83	0.95	0.91	0.85	0.43	0.91	0.49	1.04	0.61
Total	99.63	100.99	99.6	101.3	100.58	100.2	100.29	100.16	99.6
C	0.44	0.12	0.08	0.05	0.07	0.07	0.04	0.08	0.05
S	0.01	0.01	0.01	0.01	0.01	0.01	0.01	0.03	0.01
Felsic Normative Minerals (CIPW norm, wt%)									
Orthoclase	16.1	33.5	19.0	32.5	26.4	20.0	30.7	14.2	30.4
Albite	0.0	31.1	16.8	28.8	52.3	53.4	45.3	50.8	54.5
Anorthite	8.4	4.5	1.7	4.2	1.8	3.0	2.9	4.5	2.8
Nepheline	20.9	30.1	55.8	26.9	14.6	16.8	12.1	23.1	3.4
Leucite	5.4	0.0	0.0	0.0	0.0	0.0	0.0	0.0	0.0

Tabela 9. Whole-rock trace element analyses of the Monte Santo Suite.

Rock type	NS	NS	NS	NS	NS	AFS	AFS	AFS	AFS	AFS
Massif	MSM	MSM	MSM	MSM	MSM	MSM	MSM	MSM	MSM	MSM
Sample no.	MS22B	MS88A	MS122A	MS336	MS400	MS140	MS293	MS316C	MS365	MS398
Rb	192	269	161	308	319	198	265	291	310	279
Cs	0.6	1	< 0.5	1.9	1.3	1.2	3.5	1.8	1.7	2
Sr	18	41	32	8	18	102	88	92	69	58
Ba	48	213	44	15	74	787	245	70	261	652
Ga	30	21	23	24	27	42	23	17	30	18
Y	2	11	17	14	4	6	7	5	13	4
Zr	412	246	131	318	643	172	380	144	164	69
Hf	10.7	4.7	3.3	7.2	13.2	3.5	6.7	2.7	3	1.3
Nb	39	106	72	62	99	75	74	70	75	62
Ta	4.6	6.3	6.1	4.5	11.9	3.6	5.7	5.6	6.5	2.5
Sn	8	9	8	8	8	51	27	17	21	12
Th	0.5	16.1	18.7	9	1.4	9.8	4.3	1.1	5.5	1.3
U	2	2.9	4.1	2.3	7.5	1.5	1.8	0.6	4.6	0.4
V	< 5	< 5	< 5	< 5	< 5	< 5	< 5	< 5	< 5	< 5
Zn	30	60	50	130	40	50	80	110	60	70
Pb	< 5	< 5	12	8	6	< 5	< 5	15	5	9
Tl	0.2	0.1	0.1	< 0.1	0.1	0.6	0.3	0.3	0.3	0.1
REE (ppm)										
Sc	< 1	< 1	< 1	< 1	< 1	< 1	< 1	< 1	< 1	< 1
La	2.4	56.7	61.4	39.5	9.8	45.7	70.3	30.9	41.6	29.5
Ce	1.3	102	85.3	63.7	7.4	71.3	96.3	46.3	48.8	45
Pr	0.11	10.1	6.97	5.71	1.27	6.65	7.65	4.09	5.81	4.19
Nd	0.3	29.2	18.9	16.2	3.8	19.6	19.4	11.4	18.2	12.2
Sm	< 0.1	4.2	2.5	2.4	0.4	2.7	2.2	1.5	2.6	1.6
Eu	< 0.05	0.23	0.25	0.16	0.07	0.6	0.32	0.36	0.37	0.24
Gd	< 0.1	3.1	1.8	1.9	0.4	1.9	1.5	0.9	2.2	1
Tb	< 0.1	0.5	0.3	0.3	< 0.1	0.3	0.2	0.1	0.4	0.1
Dy	0.2	2.8	2.4	2	0.5	1.5	1.3	0.9	2.3	0.9
Ho	< 0.1	0.5	0.6	0.4	0.1	0.2	0.3	0.2	0.5	0.2
Er	0.3	1.5	2	1.4	0.5	0.7	1	0.6	1.4	0.5
Tm	0.1	0.24	0.36	0.25	0.1	0.12	0.17	0.09	0.22	0.09
Yb	1.1	1.7	2.7	1.8	0.8	0.8	1.3	0.6	1.5	0.6
Lu	0.31	0.24	0.39	0.34	0.14	0.13	0.24	0.11	0.22	0.1
ΣREE	6.02	212.77	185.51	135.81	25.18	152.08	202.01	97.96	125.9	96.13
La/Sm_N	-	8.43	15.34	10.28	15.30	10.57	19.95	12.86	9.99	11.51
Gd/Lu_N	-	1.60	0.57	0.69	0.35	1.81	0.77	1.01	1.24	1.24
Eu/Eu*	-	0.19	0.36	0.23	0.53	0.81	0.54	0.94	0.47	0.58

Tabela 9 - (cont.)

Rock type	NMD	NMS	NMS	NS	NS	NS	NS	NS	AFS
Massif	EM	EM	EM	EM	EM	EM	EM	EM	EM
Sample no.	EVES13	EVES05	EVES06	EVES04	EVES14	EVES37	EVES44	EVES50	EVES01
Rb	512	179	176	207	289	270	480	140	305
Cs	8.43	0.15	1.22	0.43	0.82	0.65	1.05	0.44	2.22
Sr	306	31.9	23	71.3	36.5	83.9	70.5	82.5	137.5
Ba	292	31.3	44.6	123.5	53.1	144.5	52.1	54.5	510
Ga	19.9	37	29.6	42.6	52.5	49.5	50.3	60.4	30.9
Y	21.4	7.1	42.4	44.7	5.1	8.1	5	65.9	10.3
Zr	87	65	259	876	2590	1040	832	2250	865
Hf	2.1	1.4	5.8	18.3	57.5	23.8	18.1	56	21.2
Nb	15.7	4.4	61.7	94.1	448	141	181	445	180
Ta	0.4	0.2	3.2	6.3	33.5	9	10.2	33.9	9.9
Sn	2	<1	3	12	5	7	7	10	6
Th	1.85	0.23	19.8	7.34	1.42	0.75	0.87	8.17	3.96
U	0.82	0.11	2.65	3.81	17.8	2.85	3.01	1.88	6.15
V	255	<5	5	<5	<5	<5	<5	7	6
Zn	101	6	52	100	87	131	149	52	125
Pb	3	6	6	6	7	<2	10	5	4
Tl	0.98	0.23	0.33	0.3	0.28	0.27	0.3	0.13	0.2
REE (ppm)									
Sc	30	<1	<1	<1	<1	<1	<1	<1	2
La	13.9	10	266	52.7	3.9	36.4	15.3	344	17.4
Ce	27.3	17.4	488	104	5.2	46.3	24.1	575	41.8
Pr	3.23	1.52	45.4	9.89	0.68	4.14	1.84	49	4.76
Nd	13.9	5.3	150	33.5	2.6	10.9	4.9	148	17.1
Sm	2.95	0.85	21.6	6.12	0.35	1.3	0.67	21	3.13
Eu	1.11	0.12	1.25	0.75	0.03	0.11	0.05	1.18	0.42
Gd	3.81	0.97	16.35	5.77	0.51	1.03	0.45	17.75	2.5
Tb	0.61	0.17	2.28	1.07	0.09	0.16	0.09	3.15	0.46
Dy	3.88	0.96	12.75	7.24	0.8	1.12	0.58	18.2	2.55
Ho	0.84	0.22	2.41	1.62	0.23	0.29	0.22	3.75	0.55
Er	2.22	0.48	5.54	5.09	0.93	1.29	0.7	11.25	1.5
Tm	0.33	0.09	0.61	0.85	0.19	0.23	0.13	1.78	0.24
Yb	2.08	0.52	3.27	6.23	1.81	1.84	1.31	12.95	2.16
Lu	0.31	0.07	0.45	1.05	0.33	0.41	0.26	2.06	0.37
ΣREE	106.47	38.67	1015.9	235.88	17.65	105.52	50.6	1209.1	96.94
La/Sm_N	2.94	7.35	7.69	5.38	6.96	17.49	14.26	10.23	3.47
Gd/Lu_N	1.52	1.71	4.49	0.68	0.19	0.31	0.21	1.07	0.84
Eu/Eu*	1.01	0.40	0.20	0.38	0.22	0.29	0.28	0.19	0.46

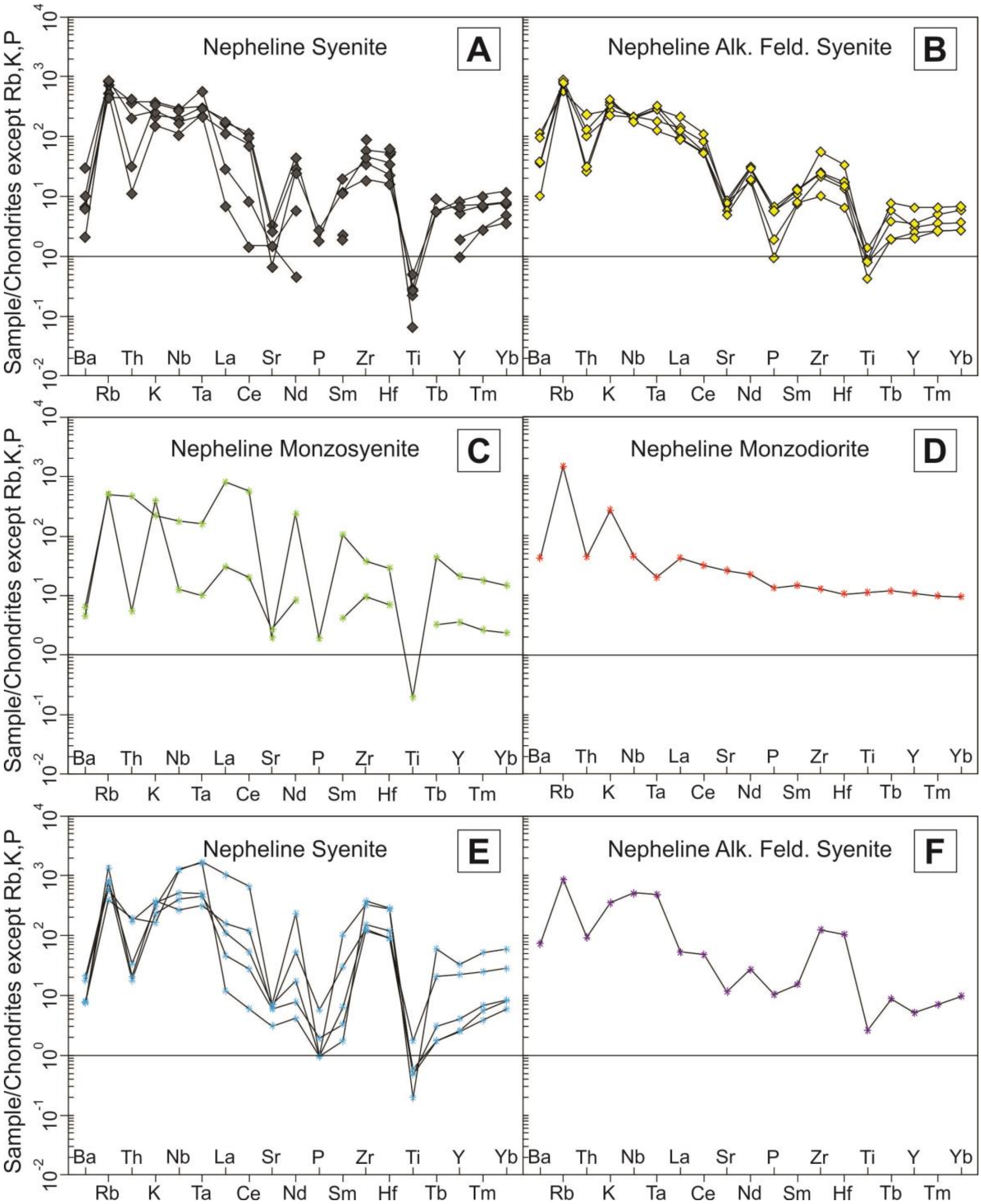

Figura 11. Multielement diagrams of the Monte Santo Suite, normalized following the criteria of Thompson (1982).

The nepheline syenite of the Estrela Massif presents average La/Sm_N and Gd/Lu_N ratios of 10.86 and 0.49, respectively, with well-developed Eu anomalies

(Eu/Eu* = 0.38 to 0.18). The available REE analyses of alkali feldspar syenite, nepheline monzosyenite and nepheline monzodiorite indicate lower LREE enrichment (La/Sm_N of 3.47, 7,34 and 2,94, respectively), almost flat or decreasing HREE patterns (Gd/Lu_N of 0.83, 1,71 and 1.51, respectively) and pronounced Eu anomalies (Eu/Eu* = 0.45 and 0.40), except for the nepheline monzodiorite, which does not present such anomalies.

Throughout both massifs, ascending HREE patterns are commonly observed, depicted by Gd/Lu_N ratios less than one, which sometimes even produce convex REE patterns.

The syenites of the Monte Santo Massif shows well-pronounced negative anomalies for Ba, Sr, P and Ti and positive anomalies for Rb, Nb, Ta, Zr and Hf in the multielement diagrams (Fig. 11, Table 9). Thorium anomalies present weak to well-pronounced troughs.

The nepheline syenite, nepheline monzosyenite and alkali feldspar syenite of the Estrela Massif present anomalies similar to those of the MSM syenites with, however, highly variable bulk concentrations. The nepheline monzodiorite present only positive anomalies for Rb and K and negative anomalies for Ba and Th. Both nepheline monzodiorite and nepheline monzosyenite present negative Nb and Ta anomalies.

4.7. Zircon geochronology

We selected three samples from the Monte Santo Massif and two samples from the Estrela Massif for U-Pb geochronology to date the timing of these intrusions. In the MSM, two samples are distributed in the border facies (MS22 and MS88) and one in the central facies (MS140), while in the EM, the samples are distributed in alkali feldspar syenite and nepheline syenite (EVES01 and EVES12, respectively). The results of the U-Th-Pb isotope analyses on zircons from the Monte Santo Massif and Estrela Massif are presented in the Supplementary Data.

Zircons from the border facies of the MSM are generally anhedral, presenting translucent to pink and brown colors and ranging in size from 0.21 to 0.68 mm. The mineral grains display many textures revealed by cathodoluminescence (CL) patterns. Some crystals preserve oscillatory zoning, with parallel bands with alternating CL intensities, which is typical of igneous crystallization, but are overprinted by patches and overgrowths of light CL; some crystals are featureless, presenting only a light CL fill. Late to postmagmatic recrystallization features are widespread (Corfu et al. 2003), such as convolute zoning or the presence of transgressive zones of rehomogenized zircon, with light CL patches of varied shapes (some appear cauliflower-shaped, others are infills, and still others are overgrowths) (Fig. 12).

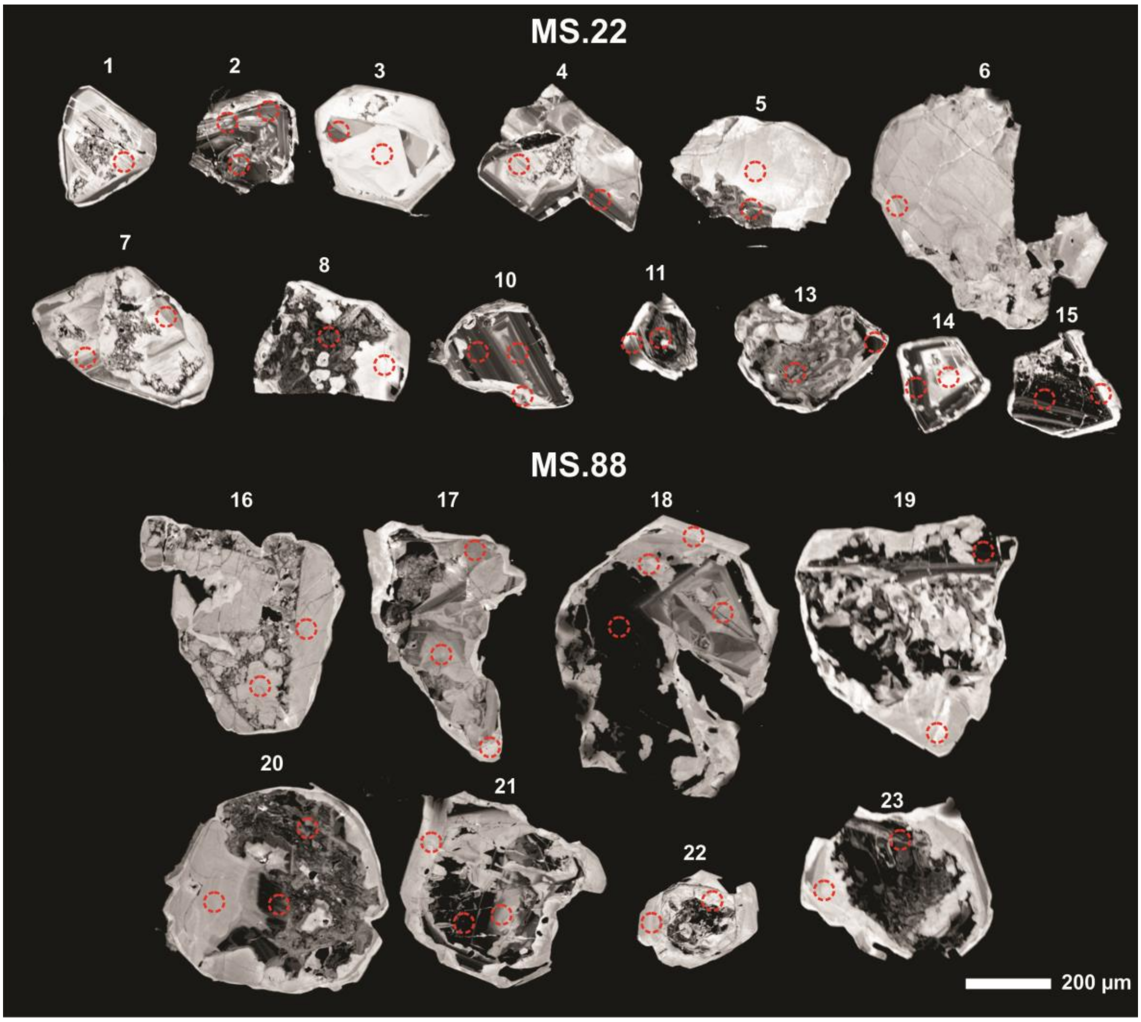

Figura 12. EPMA cathodoluminescence images of the analyzed zircon grains from the border facies of the Monte Santo Massif (samples MS22 and MS88). LA-MC-ICP-MS U-Pb spots are indicated as dashed red circles. Zircon labels are in accord with the enumeration in the Supplementary Data.

In the central facies of the MSM, the zircon grains present the same aspects of colors and shape as those in the border facies and range in size from 0.15 to 0.85 mm. The CL patterns of this facies are darker than those of the border facies, the oscillatory zoning is preserved in more grains, and the overgrowths or patches of light CL are less common or not as well developed as in the border facies. In these crystals, the borders developed on variably altered and/or recrystallized nuclei present oscillatory zoning rather than homogeneous light CL overgrowths (Fig. 13).

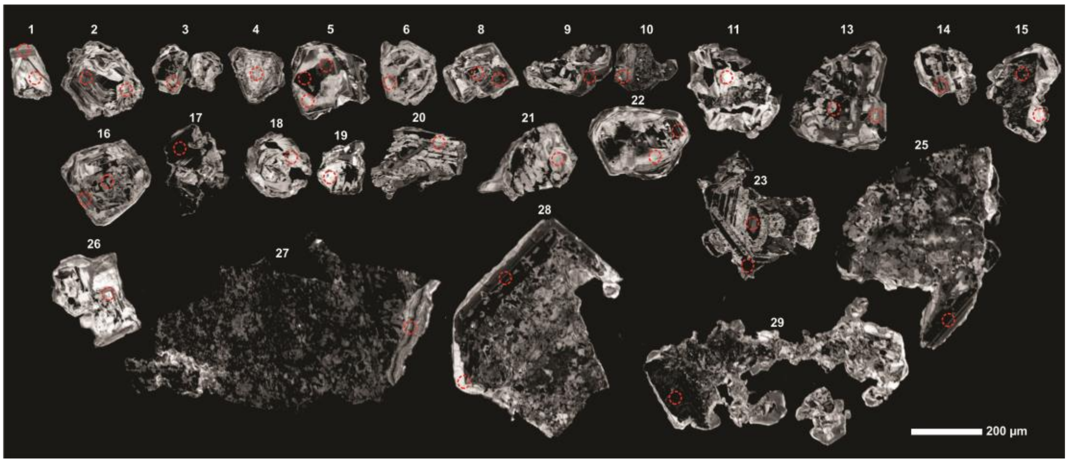

Figura 13. EPMA cathodoluminescence images of the analyzed grains from the central facies of the Monte Santo Massif (sample MS140). LA-MC-ICP-MS U-Pb spots are indicated as dashed red circles. Zircon labels are in accord with the enumeration in the Supplementary Data.

The plot of both concordant and discordant analyses of the border facies (n = 41) delineates a discordia line with an upper intercept of 1114.9 ± 9.5 Ma and a lower intercept of 265 ± 120 Ma, with a MSWD of 1.9 (Fig. 14A). Ten U-Pb measurements on ten different crystals from the border facies are concordant and yield a concordia age of 1108.1 ± 1.9 Ma, with a MSWD of 0.062 (Fig. 14B). These Mesoproterozoic ages are apparently regular regardless of different CL textures within the grains.

In the central facies, in the Wetherill plot of all the measurements, there are three different populations (Fig. 14C). One consists of the older ages, which form a discordia line with an upper intercept of 1142 ± 24 Ma and a lower intercept of 243 ± 130 Ma (Fig. 14D). The second population consists of a single concordant analysis of ca. 780 Ma. The last population is represented by the younger ages found in these rocks, which regardless of the low quantity of analyzed points, yield concordia ages of 530.5 ± 4.3 Ma and 493.4 ± 3.8 Ma, with MSWDs of 0.114 and 5, respectively (Fig. 14E and F). It is noteworthy that the discordia line of the older ages does not intersect the line for the younger ages.

The analyses representing older ages are concentrated in the nuclei of zircon grains with different CL textures and intensities, whereas the younger ages are concentrated in the borders of some of the crystals, especially the borders showing oscillatory zoning with intermediate CL intensity (Fig. 13, crystals 1, 9 and 10).

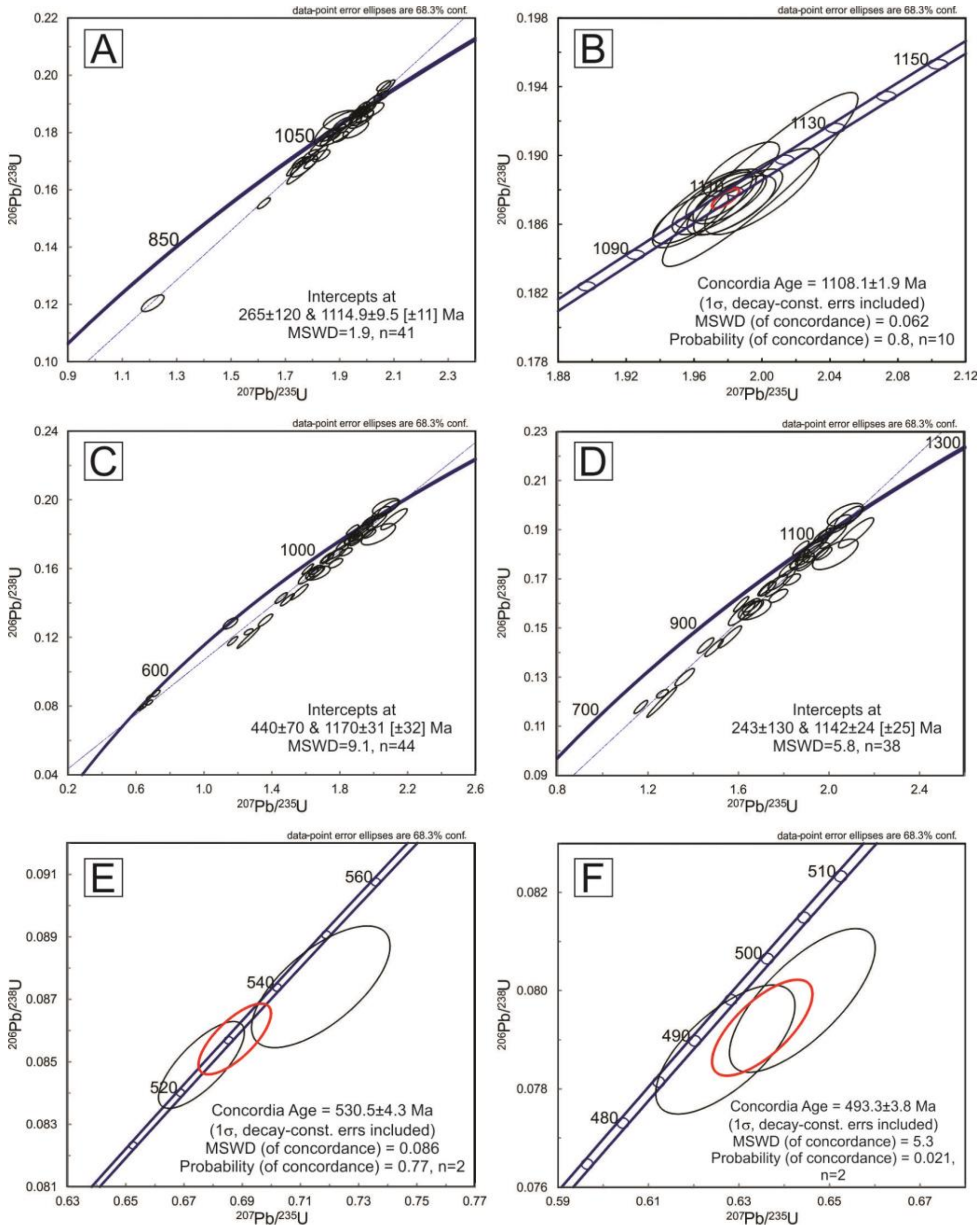

Figura 14. Concordia diagrams of the Monte Santo Massif. (A) All analyses of the border facies. (B) Concordia age of the border facies. (C) All the analyses of the central facies, showing three distinct populations. (D) Mesoproterozoic population of the central facies. (E) Older Cambrian concordant ages of the central facies. (F) Younger Cambrian discordant ages of the central facies.

Zircons from the alkali feldspar syenite of the Estrela Massif are brown with well-developed crystal faces and range from 0.89 to 2.13 mm. Their CL patterns shows well-developed oscillatory zoning, where the nucleus tends to have darker luminescence colors, overgrown by continuous oscillatory zones of intermediate luminescence color, all of which are transgressed by light CL patchy zones or overgrowths (Fig. 15).

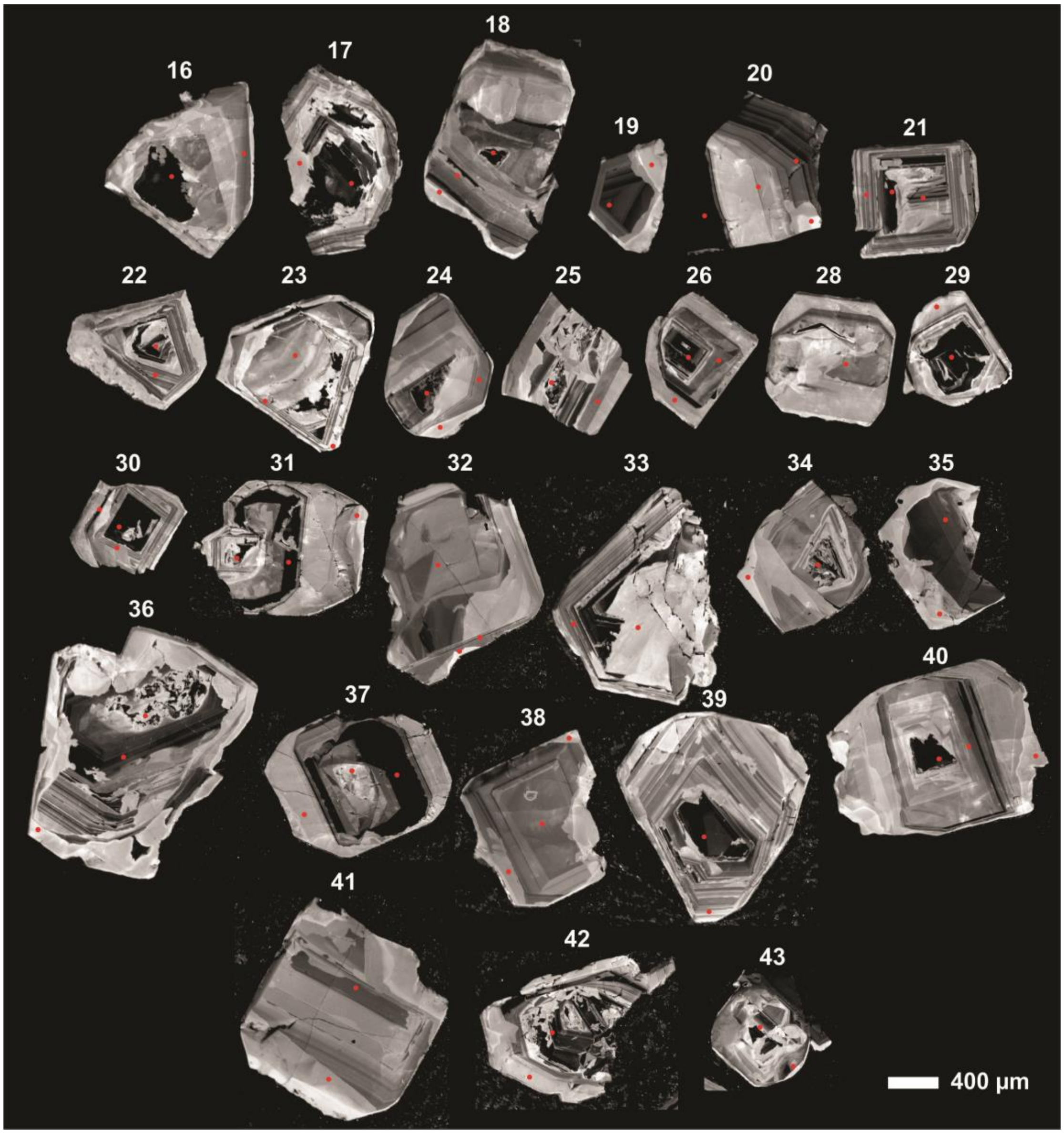

Figura 15. EPMA cathodoluminescence images of the analyzed zircon grains from alkali feldspar syenite (EVES01) of the Estrela Massif. LA-MC-ICP-MS U-Pb spots are indicated by red dots. Zircon labels are in accord with the enumeration in the Supplementary Data.

The zircon crystals from the nepheline syenite are brown, inclusion-rich, anhedral grains, ranging from 0.34 to 2.12 mm. There is a distinction between the CL patterns of the larger and smaller grains. The larger grains are intensely altered, rich in silicate inclusions (feldspars and biotite), with dark nuclei full of patchy, light CL spots, and thin borders with light luminescence color. The smaller grains are more homogeneous, with light to intermediate luminescence colors, often preserving oscillatory zoning but also presenting late to postmagmatic patterns, such as convolute zoning and patchy zoned replacements (Fig. 16).

The analyses of the alkali feldspar syenite, plotted in the Wetherill diagram, show a range of concordant ages from ca. 550 Ma to 510 Ma (Fig. 17A). From this range, the older ages are taken for calculation of the concordia age, where fourteen analyses of eleven different crystals yield an age of 545.7 ± 3.4 with a MSWD of 2.8 (Fig. 17B). None of the analyses yield the older Mesoproterozoic ages observed in the other samples.

Four measurements on four different crystals from the nepheline syenite yield a concordia age of 475.5 ± 4.3 Ma with a MSWD of 1.15 (Fig. 17D), but the majority of the data fall on a discordia line with an upper intercept of 1123 ± 48 Ma and a lower intercept of 453 ± 44 Ma and a MSWD of 3.6 (Fig. 17C). The younger ages obtained from the nepheline syenite tend to concentrate in the smaller, homogeneous and light luminescent crystals and within the light luminescent borders.

4.8. Discussion

4.8.1. Mineral Chemistry

Textural evidence suggests that the rocks of the Monte Santo Massif are finer-grained and present a more recrystallized texture, comprised mainly of granoblastic feldspars and feldspathoids, whereas the Estrela Massif presents coarser-grained rocks and a well-preserved hypidiomorphic granular igneous texture, with minor occurrence of core and mantle textures. A widespread feature in both massifs is the presence of both recrystallized and igneous feldspar assemblages within the same paragenesis, which is a common characteristic of alkaline rock gneisses (Floor 1974).

Nepheline compositions of the two massifs also present some differences. The MSM nepheline compositions are more potassic and less silicic than the EM compositions, which is reflected in the temperatures. In the Estrela Massif, the highest temperatures, in the order of ~1000 °C, are found in rocks of basic composition (nepheline monzodiorites), although the nepheline syenites also contain nepheline crystals that record high temperatures of ~950 °C. The highest temperatures found in the syenites of the MSM are 800 °C.

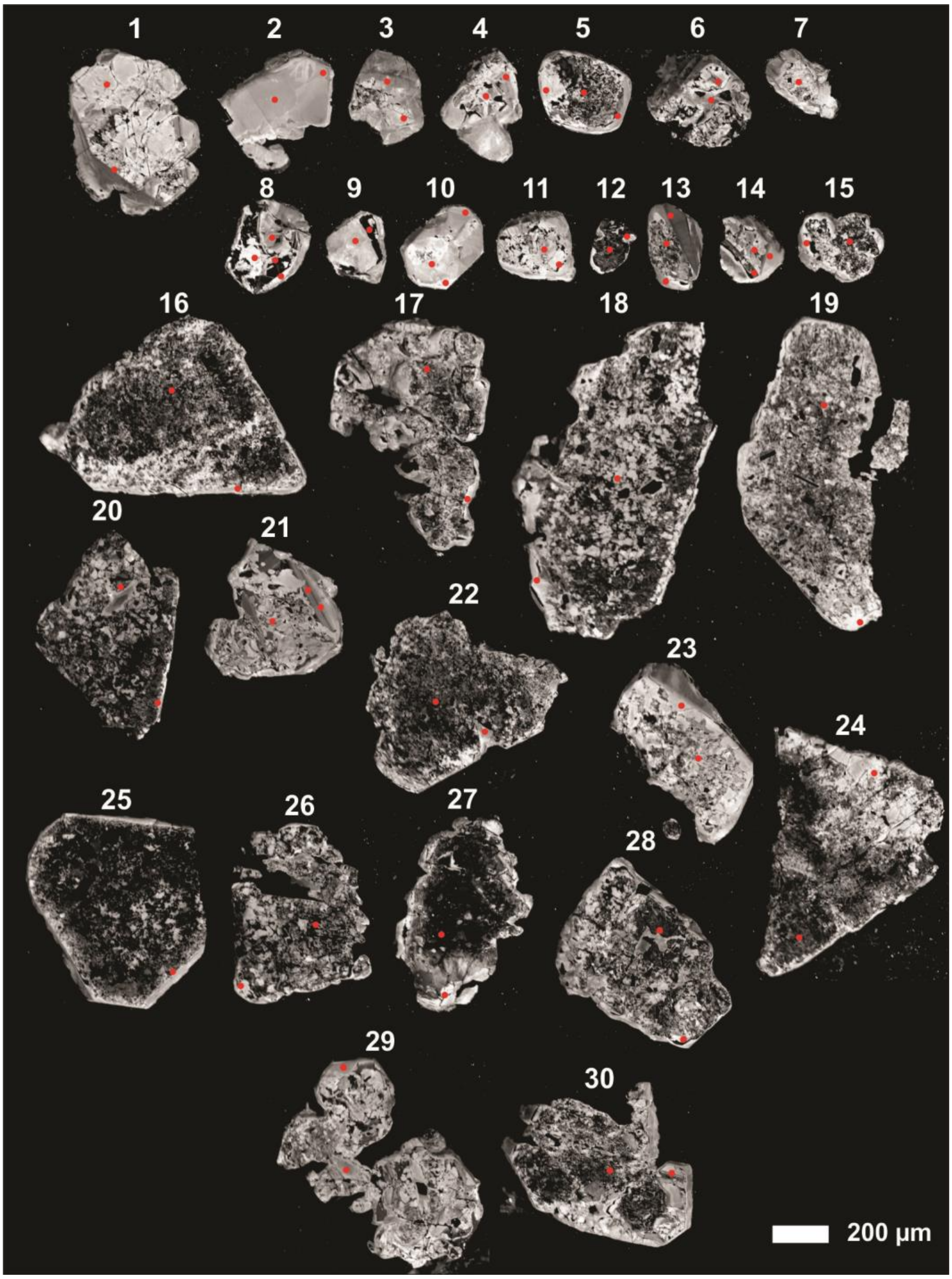

Figura 16. EPMA cathodoluminescence images of the analyzed zircon grains of nepheline syenite (EVES12) of the Estrela Massif. LA-MC-ICP-MS U-Pb spots are

indicated by red dots. Zircon labels are in accord with the enumeration in the Supplementary Data.

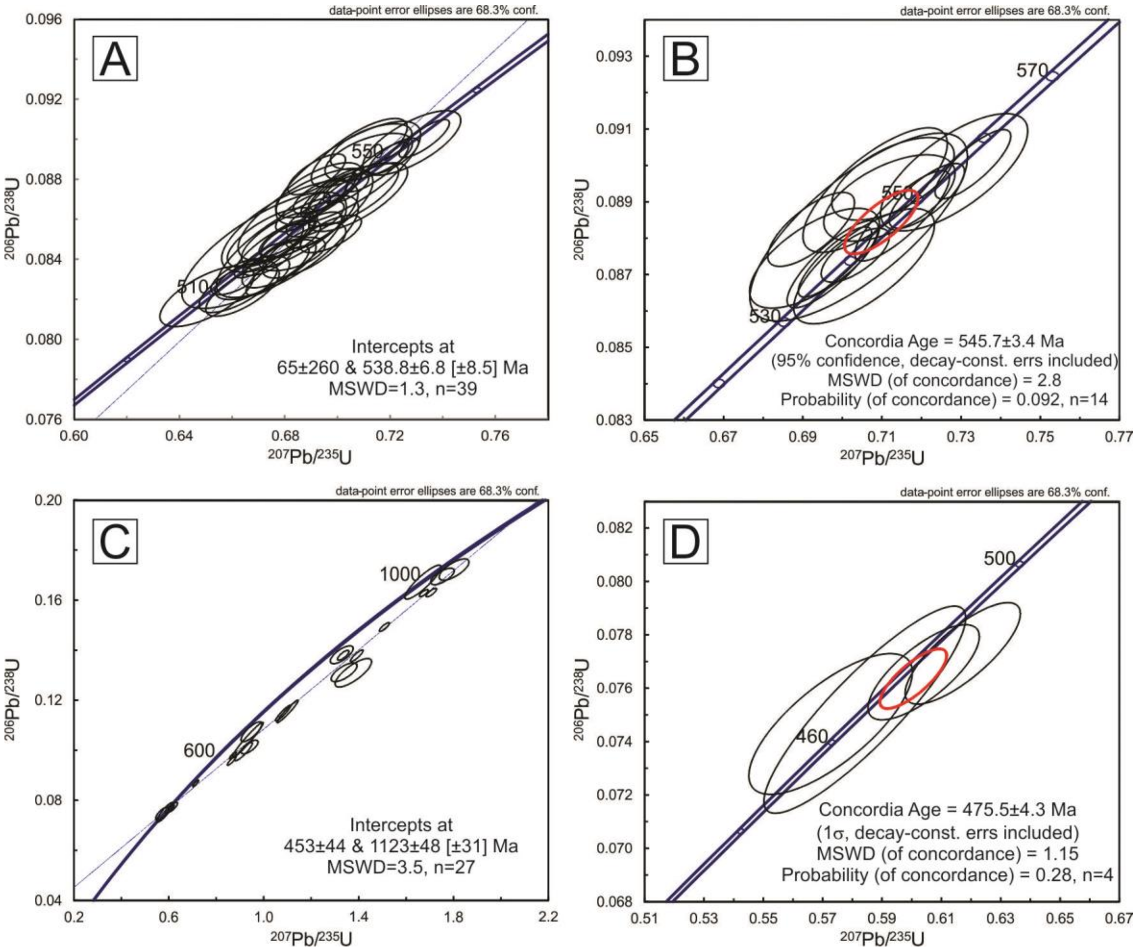

Figura 17. Concordia diagrams of the Estrela Massif. (A) All the analyses of the alkali feldspar syenite. (B) Concordia age of the older apparent ages of the alkali feldspar syenite. (C) All the analyses of the nepheline syenite. (D) Concordia age of the youngest Cambrian ages of the nepheline syenite.

In both massifs, the same types of rocks contain nepheline crystals that preserve higher temperature signatures, as well as crystals with lower temperature signatures, forming a trend from as high as 1000 °C to temperatures lower than 500 °C and indicating reequilibrated crystals (Fig. 6). Tilley (1954) demonstrated that for slowly cooled plutons or recrystallized intrusions, nepheline compositions reequilibrate and concentrate along a line between the Bueger and Morozewicz compositions (Morozewicz-Bueger convergence field); however, this trend is not observed in the Monte Santo Suite.

The diagram of Nachit et al. (2005) is used to discriminate among primary, reequilibrated and neoformed biotites, where the increase in the activity of fluids reequilibrates or promotes new crystallization of biotite grains and shifts their compositions to the base of the diagram. Biotite compositions of the MSS plot in the fields of primary, reequilibrated and neoformed grains (Fig. 18A). Only the compositions of a few annite and phlogopite samples from the EM with the highest TiO_2 contents plot in the primary field, forming a linear array of decreasing TiO_2 towards the reequilibrated field. Siderophyllite samples plots within the neoformed field (radial texture biotite) or in the limit between neoformed and reequilibrated fields. In the MSM, none of the samples plot within the primary field. Interaction with postmagmatic or metamorphic fluids could be responsible for these trends of depletion in TiO_2.

The compositional trends of the biotites from the Monte Santo Suite were compared to those from other well-known alkaline provinces of the world in the Al-Mg-Fe^{2+} diagram (Fig. 18B). Biotite compositions of the Oslo rift, Norway (Andersen and Sorensen 1993); Igdlerfigsalik, South Greenland (Finch 1995); Tenerife, the Canary Islands (Wolff 1987); Chilwa Alkaline Province, Malawi (Woolley and Platt 1988); and Magnet Cove, Arkansas (Flohr and Ross 1990); were used for comparison to preserved igneous complexes, while the North Nyasa Province, Malawi (Eby et al. 1998), was used for comparison to metamorphic complexes.

Biotites with higher amounts of TiO_2 form a trend parallel to magmatic trends (red dashed line), while most of the biotite compositions that plot in the reequilibrated and neoformed fields of Figure 18A define individual trends enriched in aluminum (Fig. 18B). Aluminum-rich biotites are also observed in the trends of the North Nyasa Province, but Eby et al. (1998) interpreted these as the mineral chemistry reflecting its bulk magma composition. In the Monte Santo Suite biotites, there is no clear correlation between aluminum in minerals and its host rock compositions, therefore suggesting postmagmatic compositional modifications.

The clinopyroxene compositions of both massifs range from omphacite to aegirine-augite and aegirine, where all the members are enriched in the jadeite endmember (Jd of Morimoto et al. 1988, Table 7). Woolley et al. (1996) and Curtis and Gittins (1979) demonstrated that through the metamorphism of nepheline-bearing alkaline rocks, igneous clinopyroxene chemistry shifts towards more aluminous compositions. Woolley et al. (1996) stated that the metamorphism of miaskitic rocks generates aluminous aegirine-augite and omphacite, whereas in agpaitic rocks, it generates aluminous aegirine and jadeitic pyroxene.

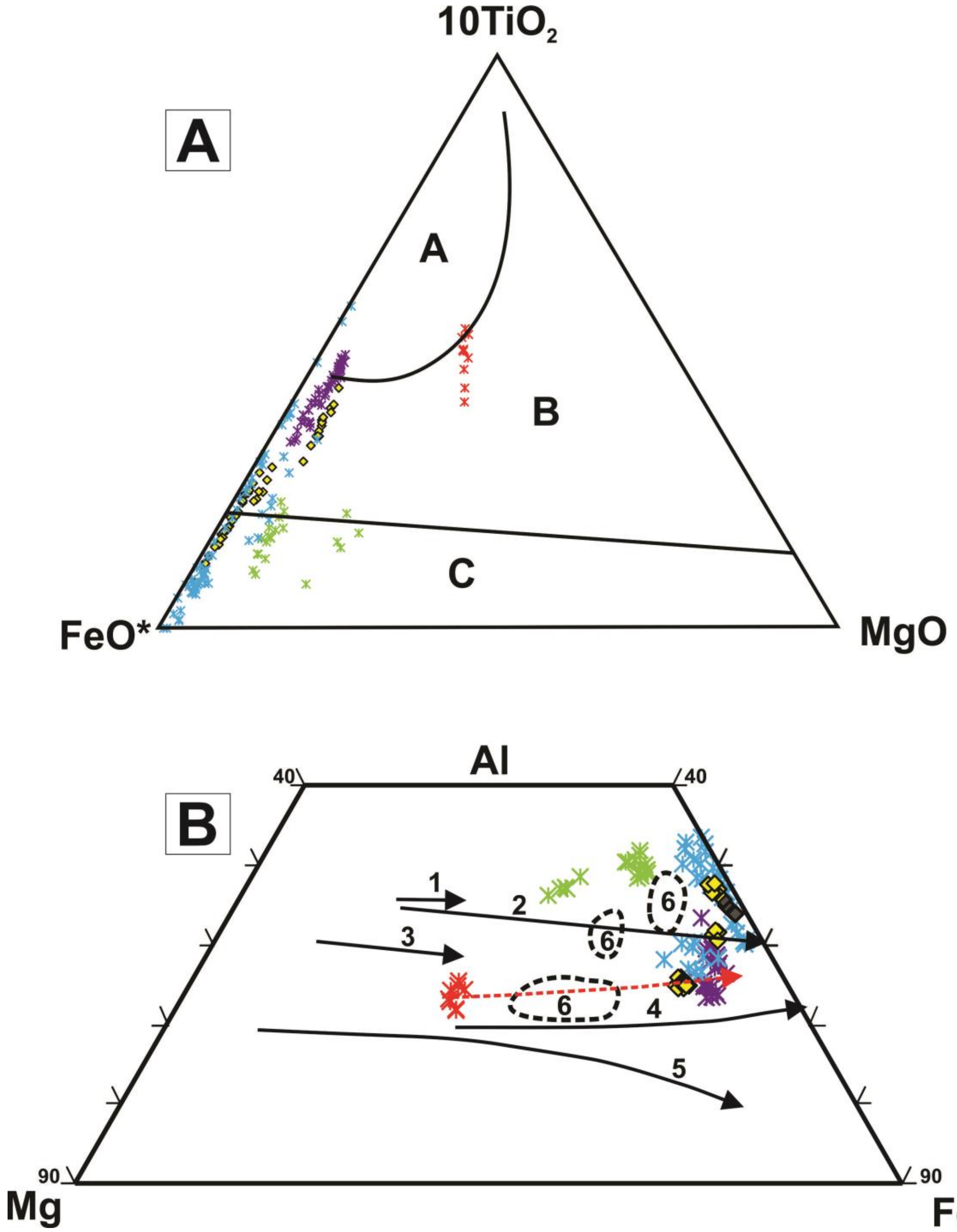

Figura 18. Monte Santo Suite biotite compositional trends. (A) Nachit et al.(2005) diagram, where the A field represents primary compositions, the B field, reequilibrated compositions and the C field, neoformed compositions. (B) Al-Mg-Fe^{2+} ternary diagram. Arrows 1 (Oslo Rift), 2 (Igdlerfigsalik), 3 (Tenerife), 4 (Chilwa Alkaline Province) and 5 (Magnet Cove) represents the evolution trends of igneous complexes and the field 6 (North Nyasa Province) represents metamorphic alkaline complexes. The red arrow represents the high TiO_2 biotites of the Monte Santo Suite, which represents primary compositions.

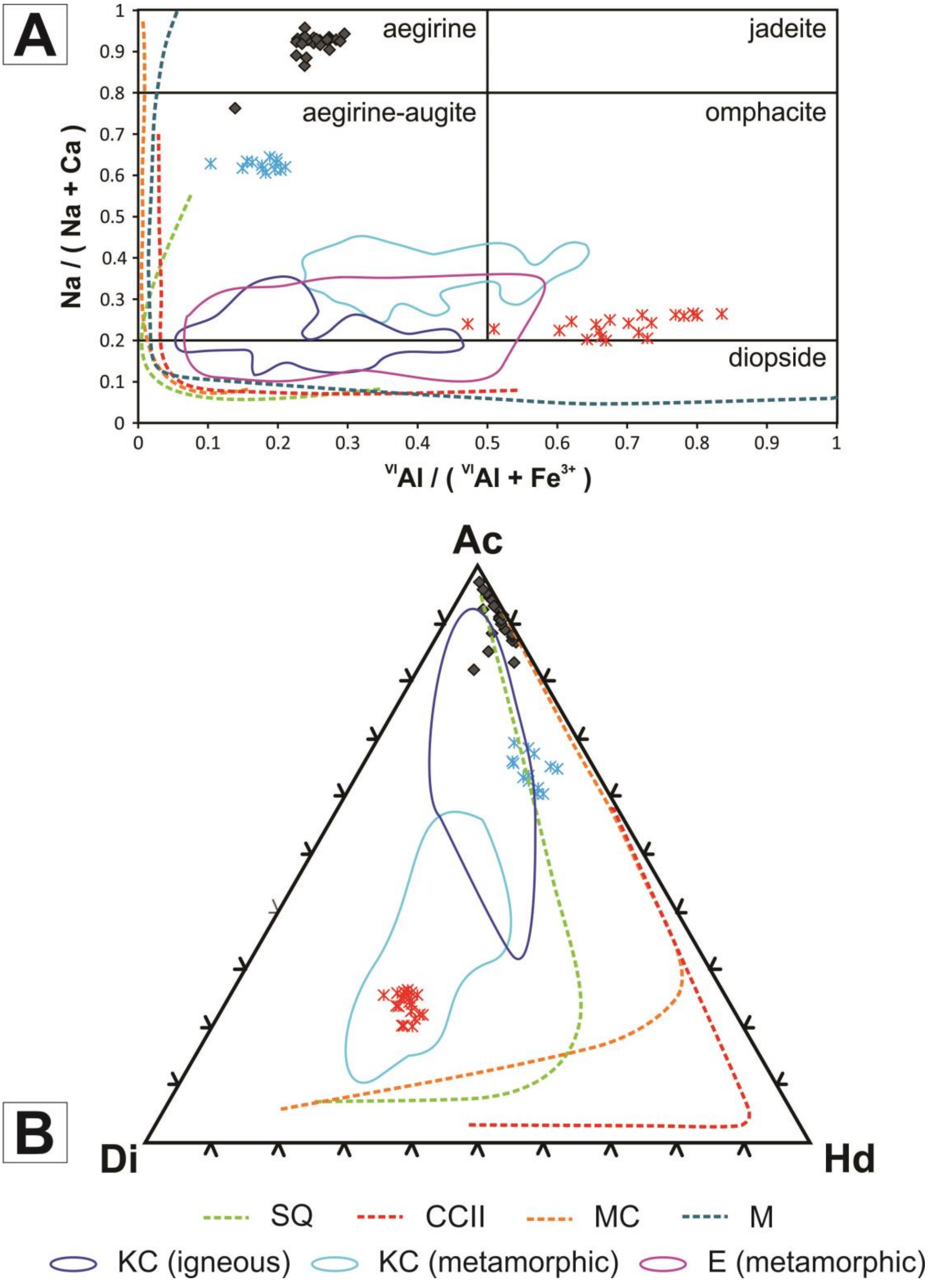

Figura 19. Monte Santo Suite pyroxene compositional trends. (A) Curtis and Gittins (1979) diagram for clinopyroxene compositions. (B) Acmite-diopside-hedenbergite ternary diagram. SQ (South Qoroq), CCII (Coldwell Center II), MC (Magnet Cove) and M (Motzfeldt) are igneous complexes, while KC (Kasungu and Chipala, North Nyasa Province) and E (Elchuru) are metamorphosed complexes.

Despite jadeitic and omphacitic pyroxenes are generally thought to be indicative of high-pressure metamorphism, Curtis and Gittins (1979) described these species as developed within regional amphibolite-facies metamorphism in the agpaitic rocks of the Red Wine alkaline complex and inferred that both jadeite and omphacite crystallize at much lower pressures in a bulk composition or protolith that has low silica activity.

Figure 19A displays the clinopyroxene compositions in the Monte Santo Suite in comparison with primary igneous trends of miaskitic rocks of the Motzfeldt and South Qorôq intrusions of the Gardar Province (Schoenenberger and Markl 2008, Jones 1980, Stephenson 1972), Center II of the Coldwell Complex (Mitchell and Platt 1982) and selected rocks of Magnet Cove (Flohr and Ross 1990), as well as metamorphic trends of the miaskitic Elchuru alkaline complex of the Prakasam Alkaline Province (Upadhyay et al. 2006) and North Nyasa Province (Woolley et al. 1996). Clinopyroxenes of the Monte Santo Suite seem to be too aluminous to represent an igneous trend, but they also do not fit the metamorphic trends of Elchuru and North Nyasa Province, being intermediate between igneous and metamorphic compositions. In the Di-Hd-Ac diagram (Fig. 19B), the Monte Santo Suite pyroxenes depicts trends similar to those of the North Nyasa Province, representing a mixed character with both metamorphic and preserved igneous pyroxenes.

The amphibole compositions of the MSS range from hastingsite in the nepheline monzodiorite to taramite in all the other described rocks (Fig. 7B). This variation is ruled by CaAl↔NaSi substitutions (Giret et al. 1980) with increasing differentiation. It is important to note that the same species of amphibole are found in all the different types of syenites in both massifs. The presence of zoning-free crystals, which are chemically homogeneous, as well as their textural types suggests that the amphiboles of both massifs represent recrystallized crystals. Mitchell (1990) suggested that the presence of taramite amphiboles in paragenesis with jadeitic-rich clinopyroxenes is a feature of metamorphosed assemblages.

From the mineral chemistry and textural information, it is evident that deformation and recrystallization have occurred at P-T conditions high enough to promote feldspar and nepheline grain boundary migration, localized perthite unmixing and compositional reequilibration, but the metamorphism was not pervasive enough to completely reequilibrate high-temperature nepheline crystals. Other features suggestive of recrystallization are clinopyroxene compositional changes, amphibole homogenization and biotite reequilibration.

4.8.2. Evidence for crystal accumulation

The preservation of nepheline crystals (even high-temperature crystals) and the absent evidence of petrographic features of fluid-driven alterations in the sampled rocks are indicative that major element chemistry was not significantly modified by metamorphism.

Important evidence from major and trace elements indicates that crystal accumulation was a significant process in the Monte Santo Massif evolution. To test this hypothesis, the rocks of the Monte Santo Suite are projected in the SiO_2-$NaAlSiO_4$-$KAlSiO_4$ phase diagram (Petrogeny's Residua System, Bowen 1937, Schairer 1950) (Fig. 20). In this diagram, analyses clustered near the minimum represent fractionated liquids. Only analyses in which the sum of modal felsic minerals is higher than 80% were plotted, following the recommendations of Hamilton and MacKenzie (1965).

It is evident that most of the analyses of the MSS do not concentrate near the minimum or in the cotectic lines. Only a few analyses cluster towards the trachytic and phonolitic minimum, and some compositions concentrate in a line between them. This evidence indicates that most of these rocks do not represent the compositions of magmatic liquids but rather solids separated from magma and that the analyses concentrated in the minimum and its joining line could represent liquid compositions.

The three analyses that cluster near the minimum are represented by a nepheline syenite, a nepheline monzosyenite and a nepheline alkali feldspar syenite (EVES01, EVES04 and EVES05). Among them, the syenite analyses occupy the expected position because both are highly fractionated rocks that are poor in mafic minerals and compatible trace elements, e.g., Sc, Co, Ni, and V (Table 9). However, this is not the case for the monzosyenite, which represents an intermediate rock and should at least have a higher abundance of modal mafic minerals and be richer in these compatible elements; therefore, this rock probably does not represent a residual liquid but rather a cumulate.

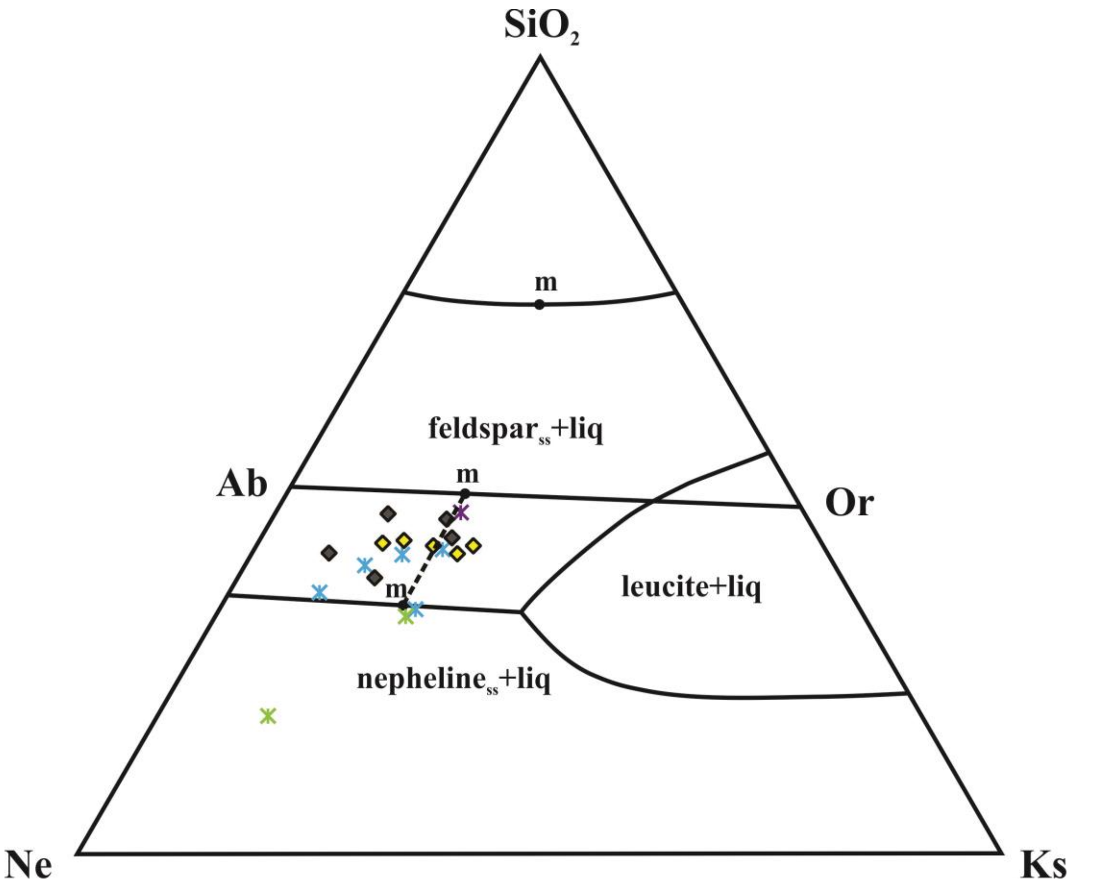

Figura 20. Petrogeny's Residua System ternary diagram, solid lines are the cotetic lines and the dots identified by "m" are the minimum, where the upper dot represents the rhyolite minimum, the intermediate, the trachyte minimum and the lower, the phonolite minimum. Only the samples with more than 80% normative felsic minerals were plotted and a dashed line between the phonolite and trachyte minima were drawn to evaluate a possible petrogenetic evolution path.

The points concentrated along the line between the trachyte and phonolite minima in the Petrogeny Residua diagram (Fig. 20) could represent a magmatic evolution path towards silica-subsaturated rocks, as in Chilwa Province (Woolley 1987), Alto Paraguay Province (Comin-Chiaramonti et al. 2005) and Serra do Mar Province (Enrich et al. 2005). However, some analyses of nepheline syenites occupy positions closer to the trachytic minima than the analyses of alkali feldspar syenites, indicating that these rocks should also not represent liquids.

The Harker diagrams (Fig. 9) show that for the Estrela Massif, with increasing SiO_2, nepheline monzodiorite prograde towards nepheline monzosyenite, nepheline syenite and alkali feldspar syenite, indicating that the evolution accounts for undersaturated rocks reaching subsaturation. For the Monte Santo Massif, on the other hand, these diagrams show that nepheline syenite are richer in silica than nepheline alkali feldspar syenite. This shifted evolution trend can be explained by the accumulation of feldspar in this nepheline syenites, enhancing their silica, alumina and alkali contents and compensating for the accumulation of mafic phases in nepheline alkali feldspar syenites, thereby enhancing their calcium, magnesium and titanium contents, as observed in Table 8.

In the REE diagrams (Fig. 10), different types of rocks present relatively parallel patterns, and the same type of rock commonly presents significant variations in bulk REE content (La varies from 10 to 1450 ppm). However, the lowest REE concentrations observed in the different syenites are too low to represent such a fractionated alkaline rock.

The low concentrations of REE could be explained by some of these rocks being cumulates; however, the variation in only cumulus minerals is insufficient to explain the broad spectrum of REE concentrations. There should be trapped liquid between these cumulates, so in this manner, the REE contents would be enhanced and controlled by both liquid and solids. This situation is evidenced by the europium anomalies of each lithotype, where the highest anomalies are generally found in the samples that contain the highest bulk REE (Fig. 10). As the liquids are mixed with accumulated feldspar and feldspathoid crystals, both the bulk REE content and europium anomalies decrease because the accumulation of feldspars tends to enhance europium concentrations. These features are commonly observed in layered mafic-ultramafic complexes (Charlier et al. 2005, Cawthorn 1996).

In the multielement diagrams (Fig. 11), the highest amounts of zirconium and hafnium are associated with HREE contents, which is a feature interpreted as zircon accumulations that are commonly seen in petrography; therefore, the convex patterns observed in Figure 10 are probably caused by this mechanism. Niobium and tantalum, similar to zirconium and hafnium, present parallel patterns with wide variations. In the zircon-enriched zones, pyrochlore is present, and its accumulation could explain the variations observed in Nb and Ta contents.

4.8.3. Source and evolution processes

The distribution of the Zr/Hf ratios found in rocks of the Monte Santo Suite is regular, both in the most primitive rocks found in the suite and in the more fractionated ones, and concentrates along a straight line of 43.1 and $R^2 = 0.9928$ (Fig. 21A).

Zirconium and hafnium are elements with the same charge and very similar ionic ratios; therefore, it is expected that in the same magmatic series, these ratios remain constant (Linnen and Keppler 2002), as observed in the Monte Santo Suite. The presence of positive niobium and tantalum anomalies in the multielement diagrams indicates that the rocks of the MSS have their evolution connected to mantle-sourced rocks (Thompson et al. 1984). The negative Nb and Ta anomalies found in the nepheline monzodiorite and nepheline monzosyenite are different from the anomalies found in syenites, this could be evidence of different sources or processes involved in the evolution of the magmatic series, however due to the small sampling, only speculative interpretations can be made.

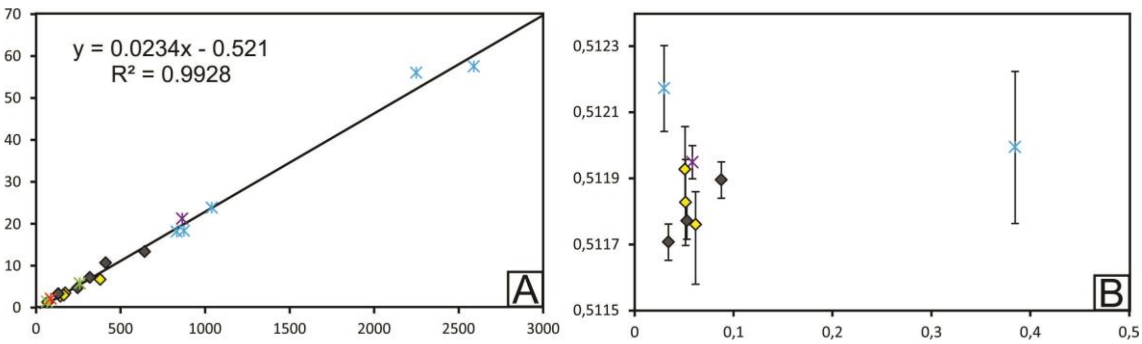

Figura 21. (A) Zr (ppm) versus Hf (ppm) diagram for the different rock types of the Monte Santo Suite. (B) Whole rock initial $^{143}Nd/^{144}Nd$ data are ploted against 1/Nd to evaluate the role of magmatic processes that may have acted in the Monte Santo Suite, the 2σ values are ploted as vertical bars.

The Harker diagrams (Fig. 9) shows curved patterns and expressive depletion in CaO, MgO and TiO_2 and enrichment in Na_2O and Al_2O_3 towards the more fractionated rocks. Curved patterns in variation diagrams are indicative of fractional crystallization with changing cumulate composition (Janousek et al. 2016). From the trends of depletion and enrichment, the extensive extraction of mafic minerals and possibly calcic plagioclase can be qualitatively inferred, generating fractionated magmas enriched in alkali-rich feldspars and nepheline, although it is impractical to model evolution processes, since most of the rocks of the Monte Santo Massif represent mixtures of cumulates and magmatic liquids.

The relatively parallel REE trends (Fig. 10) observed within the different types of rocks of the Monte Santo Suite, not considering the anomalous patterns generated by the effect of accumulations of REE-bearing phases, which can either increase or decrease La/Sm$_N$ and Gd/Lu$_N$ ratios, also suggest that fractional crystallization was the main evolution process acting in the suite.

In the diagram of Figure 21B, all the plotted values (Table 10) are within the 2σ errors, indicating that no significant vertical ^{143}Nd/^{144}Nd variations are found and that fractional crystallization was the dominant differentiation mechanism in the suite (Faure 2004, Janousek et al. 2016).

Tabela 10. Sm-Nd isotope data. Errors in the last two digits of ^{143}Nd/^{144}Nd are 2σ. Present-day ^{143}Nd/^{144}Nd$_{CHUR}$ and ^{147}Sm/^{144}Nd$_{CHUR}$ values used in calculations were 0.512638 and 0.1966, respectively (Jacobsen and Wasserburg 1980, 1984). T$_{DM}$ ages according to the depleted mantle model of DePaolo (1981).

Sample	Rock Type	Sm (ppm)	Nd (ppm)	^{143}Nd/^{144}Nd	^{147}Sm/^{144}Nd	ε_{Nd} (T)	T$_{DM}$ (Ga)	T (Ga)
MS88A	NS	4.502	33.477	0.511707 (±11)	0.0812	-10.1	1.53	0.545
MS122A	NS	2.780	21.260	0.511771 (±18)	0.0790	-8.7	1.43	0.545
MS336	NS	2.259	18.024	0.51176 (±18)	0.0757	-8.7	1.41	0.545
MS140	AFS	3.183	22.730	0.511927 (±10)	0.0846	-6.1	1.31	0.545
MS293	AFS	3.380	21.764	0.511827 (±13)	0.0938	-8.7	1.54	0.545
MS316C	AFS	1.470	11.974	0.511895 (±13)	0.0742	-6.0	1.25	0.545
EVES04	NS	6.231	34.329	0.512172 (±13)	0.1097	-3.0	1.27	0.545
EVES14	NS	0.400	2.411	0.511994 (±23)	0.1002	-5.9	1.40	0.545
EVES01	AFS	3.101	17.949	0.511949 (±5)	0.1044	-7.0	1.52	0.545

4.8.4. Age and significance of the Monte Santo Suite

As pointed out by the geochemical data, the different rock types and massifs of the Monte Santo Suite belong to the same evolution series and probably have the same source. Furthermore, the observed textures and mineral chemistry compositions suggest that these rocks were at some point variably deformed and recrystallized.

The internal features and oscillatory zoning of the zircon found in the alkali feldspar syenite of the Estrela Massif (Fig. 15) strongly suggest that 545.7±3.4 Ma represents the crystallization age of these rocks. The younger ages obtained in the same zircon crystals are mostly concentrated in overgrowths and transgressive zones of brighter CL, suggesting that the spread down to 510 Ma found in these samples could be explained by processes involving zircon rejuvenation. An episodic protracted growth history is unlikely to explain such a spread along the concordia line, because a period of crystallization of 35 Ma is too large, especially for such a small pluton. Long-lived crystallization ages are reported for the timespans of 8-10 Ma found in nepheline syenite pegmatites (Schaltegger et al. 2015), 20 Ma in carbonatite-nepheline syenite systems (Nedosekova et al. 2016), and 7-8 Ma in large composite granitic plutons (Miller et al. 2007), all of which are much narrower in range.

The 475.5±4.3 Ma age shown in the nepheline syenite of this massif were obtained both in the borders of crystals with older nuclei and as individual smaller, light CL crystals (Fig. 16). The fact that Mesoproterozoic ages found in the same samples exhibit a discordia line towards the Cambrian ages is probably indicative that these Cambrian ages could represent an event responsible for Pb loss. The Mesoproterozoic ages are similar to those found in the Monte Santo Massif, and its crystals show many postmagmatic alteration features, most likely due to interaction with the alkaline magma.

Most of the data obtained in the Monte Santo Massif have populations of 1.1 Ga, which exhibit discordia lines towards imprecise young ages (243±130 Ma and 265±120 Ma). Additionally, the central facies of this massif presents Cambrian ages (530.5±4.3 Ma and 493.3±3.8 Ma), which, despite the low statistical sampling, depicts important geological meaning, since they are very similar to both populations of Cambrian ages obtained in the Estrela Massif. Viana and Battilani (2014) also obtained a similar population of ages for the Monte Santo Massif, and some of the crystals presented by the authors resemble in size, shape and CL characteristics the igneous crystals found in the Estrela Massif.

The nepheline syenite and alkali feldspar syenite of both massifs are very similar in terms of their geochemical anomalies, ratios and patterns. They also present great overlap in terms of the chemistry of their mineral paragenesis, where both contain minerals indicative of metamorphism, in addition to both being foliated massifs and intruding the contact between the same geologic units. We believe that the geochemical and mineralogical resemblance are sufficient indications to suggest that the crystallization age of the Monte Santo Massif is similar to that of the Estrela Massif and therefore is approximately 545 Ma and that both are cogenetic.

The alkaline rocks of Monte Santo Suite are depicted to have concordant or near-concordant ages ranging from ca. 545 Ma to 475 Ma. Many mechanisms have been proposed to elucidate zircon rejuvenation processes, which involve isotopic disturbance occasioned by solid-state recrystallization and precipitation during high-grade metamorphism (Hoskin and Black 2000) or fluid-driven disturbances (diffusion, leaching and/or recrystallization) caused by lower-grade metamorphism in previously metamict zircon crystals (Geisler et al. 2003, Mezger and Krogstad 1997); therefore involving the action of metamorphic, late-magmatic, hydrothermal or meteoric fluids (Geisler et al. 2004, Geisler et al. 2003, Vavra et al. 1999, Pidgeon 1992).

In the zircon population found in the alkali feldspar syenite of the Estrela Massif, there is CL textural evidence of postmagmatic processes that are slightly younger than the magmatic crystallization, which possibly could suggest the effect of a fluid phase disturbing the isotopic system of the previous igneous zircon. Additionally, all the Mesoproterozoic zircon grains in both of the Monte Santo Suite massifs define different Pb loss discordia lines that eventually reach a concordant lower intercept age (near 475 Ma) that according to Mezger and Krogstad 1997 may or may not have geological significance. The younger Cambrian ages found in the central facies of the Monte Santo Massif are different because they do not represent lower intercept ages; instead, they occur in areas of the zircon grains that are texturally different from the Mesoproterozoic portions (Fig. 13) and do not form a discordant Pb loss trend from the older ages. Additionally, the youngest Cambrian population in this sample (493 Ma) is slightly discordant, while the older Cambrian population (530 Ma) is concordant, suggesting that 530 Ma is more akin to a crystallization age and 498 Ma defines a Pb loss path.

Another important fact is that the regional timing of metamorphism is not well constrained, but there is evidence of regional U-Pb disturbances ca. 570 Ma, 528 Ma and 513 Ma (Alves 2018, Pinheiro 2016, Moura et al. 2008, Moura and Gaudette 1993), with cooling of the orogen occurring ca. 505-489 Ma (Dias et al. 2017, Pinheiro 2016). The internal features observed in the studied samples, together with the regional background of the Araguaia Belt, allow us to interpret that the alkaline rocks of the Monte Santo Suite crystallized slightly prior or during a relaxation extensional phase of the orogen construction and were then metamorphosed in its subsequent compressional evolution. This same process has been proposed for other Gondwana-related alkaline intrusions in Africa (Attoh et al. 2007, Emmanuel et al. 2013) and India (Biswal et al. 2007).

Due to the lack of a wide background of local and regional geochronological information and to the lack of additional geochronometer minerals in the paragenesis (e.g., monazite, titanite) of the investigated syenites, it is difficult to estimate whether the youngest Cambrian ages (498 and 475 Ma) and the age spread found in the dated igneous zircon (EVES01) have geological meaning.

The Mesoproterozoic crystals, and a single 780 Ma crystal found in the Monte Santo Massif can be interpreted, using the terminology of Miller et al. (2007), as inherited crystals from the source or xenocrysts from buried geological units in the emplacement path of these magmas. The metamafic and ultramafic rocks of the Araguaia Belt are dated from 750-810 Ma (Paixão e al. 2008, Gorayeb et al. 2004) and could be a source of contamination for the 780 Ma population. However, no known geological unit of the Araguaia Belt has an age of 1.1 Ga, although these ages are found in provenance studies of the metasedimentary rocks of the Estrondo Group (Pinheiro et al. 2011).

The shapes of the Mesoproterozoic zircon crystals are consistently irregular, well-developed crystal faces are rarely observed, and magma interaction features on CL images are relatively frequent. These facts indicate that these crystals are most likely inherited from their source.

As indicated by the absence of vertical or sloped trends in the $^{143}Nd/^{144}Nd$ against 1/Nd diagram, contamination processes or significant differences between the sources of the two massifs were not found in the analyzed samples. The T_{DM} ages for the Monte Santo Suite range from 1.25 Ga to 1.54 Ga (Table 10), which, within the associated errors, points to the existence of a Mesoproterozoic source. Additionally, the ε(Nd) values calculated to 545 Ma indicate that this source is enriched in radiogenic ^{143}Nd, ranging from –10.1 to -3.0 (Table 10).

4.9.Summary

The textural, petrographic and field relations, as well as mineralogical, geochemical and isotopic data of the Monte Santo Suite, suggest that the Estrela and Monte Santo massifs are cogenetic and intruded into the Araguaia Belt near 545-530 Ma.

This alkaline magmatism is mantle-sourced and presents mafic-intermediate to felsic, highly fractionated magmas that are related by fractional crystallization, involving changing cumulate compositions. The Monte Santo and Estrela massifs are composed of foliated rocks that represent a mixture between cumulates and magmatic liquids.

Textural evidence and mineral trends and compositions point out that these massifs were, at some point, recrystallized and metamorphosed, although there is significant evidence of preserved igneous compositions in nepheline, biotite and pyroxene.

The Monte Santo Suite represents Cambrian alkaline magmatism in the Araguaia Belt, emplaced in an intraorogenic extensional or transtensional tectonic setting and subsequently deformed and metamorphosed during the final evolution of the orogen. The timing of metamorphism is not well constrained due to the lack of other geochronometer pairs in the paragenesis. These magmas were probably generated from a Mesoproterozoic source with mantle affinity that was enriched in radiogenic ^{143}Nd.

The interpretation of the age, emplacement mechanism and deformation of the Monte Santo Suite contradicts the idea that this set of rocks is part of a Mesoproterozoic rift responsible for the sedimentation of the Baixo Araguaia Supergroup (Alvarenga et al. 2000), contributing with significant changes in the tectonic evolution of the Araguaia Belt.

5. Conclusões

- As estruturas encontradas em campo e texturas descritas em lâminas petrográficas, assim como as tendências nos dados de química mineral, sugerem que as rochas da Suíte Monte Santo foram submetidas a eventos que, além de deformá-las, alteraram e homogeneizaram a química de seus minerais, entretanto, também é muito comum a presença tendências primárias preservadas, principalmente na química de nefelina, biotita e piroxênio.

- As semelhanças entre as razões e padrões geoquímicos, assim como similaridade na química da maioria dos minerais do Maciço Monte Santo e Maciço Estrela, sugerem que ambos são cogenéticos.

-O magmatismo da Suíte Monte Santo tem afinidade mantélica, onde na mesma suíte, são encontradas predominantemente rochas altamente fracionadas, com pequenas ocorrências de rochas menos diferenciadas, incluindo rochas máficas.

-A diferenciação magmática é associada a processos de cristalização fracionada, com cumulados apresentando mudanças em sua composição à medida que o líquido evolui. Processos de contaminação não são evidentes nos dados apresentados.

-Os nefelina sienitos e nefelina feldspato alcalino sienitos representam uma mistura entre líquidos magmáticos e cumulados.

-As idades de cristalização interpretadas para a Suíte Monte Santo, embasadas em cristais de zircão com texturas ígneas preservadas, sugerem que essa suíte intrudiu o Cinturão Araguaia durante o período Cambriano, em um intervalo de tempo contido entre 545 a 530 Ma. As idades mesoproterozóicas obtidas nesse trabalho e em outros da literatura, provavelmente indicam heranças da fonte desses magmas, o que é corroborado pelas idades modelo T_{DM} obtidas.

- As rochas da Suíte Monte Santo provavelmente foram alojadas em período de extensão e relaxamento tectônico na evolução do orógeno, ou em um contexto transtensional, sendo subsequentemente variadamente deformadas e metamorfizadas

- A Suíte Monte Santo não representa magmas remanescentes de um rifte Mesoproterozóico no Cinturão Araguaia.

6. Referências Bibliográficas

Abreu, F.A.M., 1978. Estratigrafia e evolução estrutural do segmento setentrional da Faixa de Dobramentos Paraguai-Araguaia. Unpublised M.Sc. Thesis, Universidade Federal do Pará, Belém, Pará, Brazil.

Abreu, F.A.M., Gorayeb, P.S.S., Hasui, Y., 1994. Tectônica e inversão metamórfica no Cinturão Araguaia (abstract). Simpósio de Geologia da Amazônia, 4, Belém, Pará, Brazil.

Almeida, F.F.M., Hasui, Y., Brito Neves, B.B., Fuck, R.A., 1981. Brazilian Structural Provinces: an introduction. Earth Science Review, 17, 1-19.

Alvarenga, C.J.S., Moura, C.A.V., Gorayeb, P.S.S., Abreu, F.A.M., 2000. Paraguay and Araguaia Belts. In: Cordani, U.G., Milani, E.J., Thomaz Filho, A., Campos, D.A., 2000. Tectonic Evolution of South America (eds). International Geological Congress, 31, Rio de Janeiro, Brazil.

Alves, P.V.F.S., 2018. Caracterização Petrológica dos Granitos das Suítes Serrote e Santa Luzia, na região de Paraíso do Tocantins-Pugmil. Unpublished M.Sc. Thesis, Universidade de Brasília, Brasília, Brazil.

Åmli, R., Griffin, W.L., 1975. Microprobe Analysis of REE Minerals Using Empirical Correction Factors. American Mineralogist, 60, 599-606.

Andersen, T., Sorensen, H., 1993. Crystallization and metasomatism of nepheline syenite xenoliths in quartz-bearing intrusive rocks in the Permian Oslo rift, SE Norway. Norsk Geologisk Tifsskrift, 73, 250-266.

Arcanjo, S.H.S., 2002. Evolução Geológica das Sequências do Embasamento na Porção Sul do Cinturão Araguaia – Região de Paraíso do Tocantins. Unpublished Ph.D. Thesis, Universidade Federal do Pará, Belém, Pará, Brazil.

Arcanjo, S.H.S., Abreu, F.A.M., Moura, C.A.V., 2013. Evolução Geológica das Sequências do Embasamento do Cinturão Araguaia na Região de Paraíso do Tocantins (TO). Brazilian Journal of Geology, 43(3), 501-514.

Arcanjo, S.H.S., Moura, C.A.V., 2000. Geocronologia Pb-Pb em zicão (método de evaporação) das rochas do embasamento do setor meridional do Cinturão Araguaia – Região de Paraíso do Tocantins (TO). Revista Brasileira de Geociências, 30(4), 665-670.

Ashwal, L.D., Patzelt, M., Schmitz, M.D., Burke, K., 2016. Isotopic evidence for a lithospheric origin of alkaline rocks and carbonatites: an example from southern Africa. Canadian Journal of Earth Sciences, 53(11), 1216-1226.

Attoh, K., Corfu, F., Nude, P.M., 2007. U-Pb zircon age of deformed carbonatite and alkaline rocks in the Pan-African Dahomeyide suture zone, West Africa. Precambrian Research, 155, 251-260.

Bailey, D.K., 1974. Melting in the deep crust. In: Sorensen, H., 1974. The Alkaline Rocks. John Wiley and Sons, 436-442.

Bailey, D.K., 1977. Lithosphere control of continental rift magmatism. Journal of the Geological Society of London, 133, 103-106.

Bailey, D.K., 1992. Episodic alkaline igneous activity across Africa: implications for the causes of continental break-up. In: Storey, B.C., Alabaster, T., Pankhurst, R.J., 1992. Magmatism and the Causes of Continental Break-up. Geological Society Special Publication, 68, 91-98.

Barreira, C.F., 1980. Geologia, prospecção geoquímica e geofísica da área de Rio do Coco, Paraíso do Norte-GO. Unpublished M.Sc. thesis. Universidade de Brasília, Brasília, Distrito Federal, Brazil.

Barreira, C.F., Dardenne, M.A., 1981. Sequência vulcano-sedimentar do Rio do Coco (abstract). Simpósio de Geologia do Centro-Oeste, 1, Atas, p. 241-264.

Barth, T.F., 1963. The composition of nepheline. Schweiz. Mineral. Petrog. Mitt., 43, 153-164.

Biswal, T.K., Waele, B.D., Ahuja, H., 2007. Timing and dynamics of the juxtaposition of the Eastern Ghats Mobile Belt against the Bhandara Craton, India: A structural and zircon U-Pb SHRIMP study of the fold-thrust belt and associated nepheline syenite plutons. Tectonics, 26, TC4006.

Bowen, N.L., 1928. The Evolution of Igneous Rocks. Princeton University Press, Princeton, New Jersey.

Brito Neves, B.B., Fuck, R.A., 2013. Neoproterozoic evolution of the basement of the South-American platform. Journal of South American Earth Sciences, 47, 72-89.

Brito Neves, B.B., Fuck, R.A., Pimentel, M.M., 2014. The Brasiliano collagein South America: a review. Brazilian Journal of Geology, 44(3), 493-518.

Bühn, B., Pimentel, M.M., Matteini, M., Dantas, E.L., 2009. High spatial resolution analysis of Pb and U isotopes for geochronology by laser ablation multi-collector inductively coupled plasma mass spectrometry (LA-MC-ICP-MS). Annals of the Brazilian Academy of Sciences, 81(1), 99-114.

Burke, K., Ashwal, L.D., Webb, S.J., 2003. New way to map old sutures using deformed alkaline rocks and carbonatites. Geology, 31(5), 391-394.

Burke, K., Khan, S.D., Mart, R.W., 2008. Grenville Province and Monteregian carbonatite and nepheline syenite distribution related to rifting, collision, and plume passage. Geology, 36(12), 983-986.

Burke, K., Roberts, D., Ashwal, L.D., 2007. Alkaline rocks and carbonatites of northwestern Russia and northern Norway: Linker Wilson cycle records extending over two billion years. Tectonics, 26, TC4015.

Cawthorn, R.G., 1996. Models for incompatible trace-element abundances in cumulus minerals and their application to plagioclase and pyroxenes in the Bushveld Complex. Contributions to Mineralogy and Petrology, 123, 109-115.

Charlier, B., Auwera, J.V., Duchesne, J.C., 2005. Geochemistry of cumulates from the Bjerkreim-Sokndal layered intrusion (S. Norway) Part II. REE and the trapped liquid fraction. Lithos, 83, 255-276.

Comin-Chiaramonti, P., Gomes, C.B., Censi, P., Gasparon, M., Velázquez, V.F., 2005. Alkaline complexes from the Alto Paraguay Province at the border of Brazil (Mato Grosso do Sul state) and Paraguay. In: Comin-Chiaramonti, P., Gomes, C.B., 2005. Mesozoic to Cenozoic Alkaline Magmatism in the Brazilian Platform. Editora da Universidade de São Paulo, 71-149.

Corfu, F., Hanchar, J.M., Hoskin, P.W.O., Kinny, P., 2003. Atlas of Zircon Textures. In: Hanchar, J.M., Hoskin, P.W.O., 2003. (eds) Reviews in Mineralogy and Geochemistry, Volume 53:Zircon.

Costa J.B.S., 1980. Estratigrafia da região de Colméia (abstract). Congresso Brasileiro de Geologia, 31, annals, 2, 720-728.

Costa, J.B.S., 1985. Aspectos lito-estruturais e evolução crustal da região centro norte de Goiás. Upublished Ph.D. Thesis. Universidade Federal do Pará, Belém, Pará, Brazil.

Costa, J.B.S., Gorayeb, P.S.S., Bermeguy, R.L., Gama Jr., T., Kotschoubey, B., Lemos, R.L., 1983. Projeto Paraíso do Norte. Belém, UFPA, Conv. CVRD. 125 p.

Curtis, L.W., Gittins, J., 1979. Aluminous and Titaniferous Clinopyroxenes from Regionally Metamorphosed Agpaitic Rocks in Central Labrador. Journal of Petrology, 20(1), 165-186.

Dall'Agnol, R., Teixeira, N.P., Macambira, J.B., Kotschoubey, B., Gorayeb, P.S.S., Santos, M.D., 1988. Petrologia dos gnaisses e micaxistos da porção norte da faixa de dobramentos Araguaia, Goiás-Brasil (abstract). Congresso Latino-Americano de Geologia, 7, atas, 1, 1-19.

DePaolo, D.J., 1981. A neodymium and strontium isotopic study of the Mesozoic calc-alkaline granitic batholiths of the Sierra Nevada and Peninsular Ranges, California. Journal of Geophysical Research, 86(B11), 10470-10488.

Dias, A.N.C., Moura, C.A.V., Milhomem Neto, J.M., Chemale Jr., F., Girelli, T.J., Masuyama, K.M., 2017. Geochronology and thermochronology of the gneisses of the Brasiliano/Pan-African Araguaia Belt: Records of exhumation of West Gondwana and Pangea break up. Journal of South American Earth Sciences, 80, 174-191.

Dollase, W.A., Thomas, W.M., 1978. The Crystal Chemistry of Silica-Rich, Alkali-Deficient Nepheline. Contributions to Mineralogy and Petrology, 66, 311-318.

Donovan, J.J., Snyder, D.A., Rivers, M.L., 1993. An Improved Interference Correction for Trace Element Analysis. Microbeam Analysis, 2, 23-28.

Eby, G.N., Woolley, A.R., Din, V., Platt, G., 1998. Geochemistry and Petrogenesis of Nepheline Syenites: Kasungu-Chipala, Ilomba, and Ulindi Nepheline Syenite Intrusions, North Nyasa Alkaline Province, Malawi. Journal of Petrology, 39(8), 1405-1424.

Emmanuel, N.N., Rigobert, T., Nédélec, A., Siqueira, R., Pouclet, A., Bascou, J., 2013. Structure and petrology of Pan-African nepheline syenites from the South West

Cameroon; Implications for their emplacement mode, petrogenesis and geodynamic significance. Journal of African Earth Sciences, 87, 44-58.

Enrich, G.E.R., Azzone, R.G., Ruberti, E., Gomes, C.B., Comin-Chiaramonti, P., 2005. Itatiaia, Passa Quatro and São Sebastião island, the major alkaline syenitic complexes from the Serra do Mar region. In: Comin-Chiaramonti, P., Gomes, C.B., 2005. Mesozoic to Cenozoic Alkaline Magmatism in the Brazilian Platform. Editora da Universidade de São Paulo, 419-443.

Faure, G., Mensing, T.M., 2004. Isotopes Principles and Applications (3rd edition). John Wiley & Sons. 928 p.

Fialin, M., Outrequin, M., Staub, P.F., 1997. A new tool to treat peak overlaps in electron-probe microanalysis of rare-earth-element L-series X-rays. European Journal of Mineralogy, 9, 965-968.

Finch, A., 1995. Metasomatic overprinting by juvenile igneous fluids, Igdlerfigsalik, South Greenland. Contributions to Mineralogy and Petrology, 122, 11-24.

Fitton, J.G., Upton, B.G.J., 1987. Alkaline Igneous Rocks. Geological Society of London Special Publication, vol. 30.

Flohr, M.J.K., Ross, M., 1990. Alkaline igneous rocks of Magnet Cove, Arkansas: mineralogy and geochemistry of syenites. Lithos, 26, 67-98.

Floor, P., 1974. Alkaline gneisses. In: Sorensen, H., 1974. The Alkaline Rocks. John Wiley and Sons, 124-145.

Frost, B.R., Frost, C.D., 2008. A Geocemical Classification for Feldspathic Igneous Rocks. Journal of Petrology, 49(11), 1955-1969.

Fuck, R.A., Pimentel, M.M., Alvarenga, C.J.S., Dantas, E.L., 2017. The Northern Brasília Belt. In: Heilbron, M., Cordani, U.G., Alkmin, F.F., 2017. São Francisco Craton, Eastern Brazil – Tectonic Genealogy of a Miniature Continent. Regional Geology Reviews, Springer, 205-220.

Garcia, V.B., Dantas, E.L., Yokoyama, E., Vidotti, R.M., Hauser, N., Alves, P.V.F.S., Reis, M.A., Teles, L.S.B., Queiroz, S.O., Oliveira, G.N.R., 2016. Novas Evidências da Tectônica Tipo Thick Skin na Porção Sul da Faixa Araguaia (abstract). Congresso Brasileiro de Geologia, 48, annals 6739, Porto Alegre, Rio Grande do Sul, Brazil.

Geisler, T., Rashwan, A.A., Rahn, M.K.W., Poller, U., Zwingmann, H., Pidgeon, R.T., Schleicher, H., Tomaschek, F., 2003. Low-temperature hydrothermal alteration of natural metamict zircons from the Eastern Desert, Egypt. Mineralogical Magazine, 67(3), 485-508.

Geisler, T., Seydoux-Guillaume, A.M., Wiedenbeck, M., Wirth, R., Berndt, J., Zhang, M., Mihailova, B., Putnis, A., Salje, E.K.H., Schluter, J., 2004. Periodic precipitation patter formation in hydrothermally treated metamict zircon. American Mineralogist, 89(8-9), 1341-1347.

Gioia, S.M.C.L., Pimentel, M.M., 2000. The Sm-Nd isotopic method in the geochronology laboratory of the University of Brasília. Annals of the Brazilian Academy of Sciences, 72(2), 219-245.

Giret, A., Bonin, B., Leger, J.M., 1980. Amphibole compositional trends in oversaturated and undersaturated alkaline plutonic ring-complexes. Canadian Mineralogist, 18, 481-195.

Gorayeb, P.S.S., 1996. Petrologia e evolução estrutural das rochas de alto grau de Porto nacional - TO. Unpublished Ph.D. thesis. Universidade Federal do Pará, Belém, Pará, Brazil.

Gorayeb, P.S.S., Chaves, C.L., Moura, C.A.V., Lobo, L.R.S., 2013. Neoproterozoic granites of the Lajeado intrusive suite, north-center Brazil: A late Ediacaran remelting of a Paleoproterozoic crust. Journal of South American Earth Sciences, 45, 278-292.

Gorayeb, P.S.S., Moura, C.A.V., Calado, W.M., 2004. Suíte Intrusiva Xambica: um magmatismo toleítico neoproterozóico pré-tectônico no Cinturão Araguaia (abstract). Congresso Brasileiro de Geologia, 42, Araxá, Minas Gerais, Brazil.

Haissen, F., Cambeses, A., Montero, P., Bea, F., Dilek, Y., Mouttaqi, A., 2017. The Archean kalsilite-nepheline syenites of the Awsard intrusive massif (Reguibat Shield, West African Craton, Morocco) and its relationship to the alkaline magmatism of Africa. Journal of African Earth Sciences, 127, 16-50.

Hamilton, D.L., 1961. Nephelines as crystallization temperature indicators. The Journal of Geology, 69(3), 321-329.

Hamilton, D.L., MacKenzie, W.S., 1960. Nepheline Solid Solution in the System NaAlSiO4-KalSiO4-SiO2. Journal of Petrology, 1(1), 56-72.

Hamilton, D.L., MacKenzie, W.S., 1965. Phase-equilibrium studies in the system NaAlSiO4 (nepheline) – KalSiO4 (kalsilite) – SiO2 – H2O. Mineralogical Magazine, 34, 214-231.

Hasui, Y., Costa, J.B.S., Abreu, F.A.M., 1984a. Província Tocantins: Setor Setentrional. In: Almeida, F.F.M., Hasui, Y., 1984. O Pré-Cambriano do Brasil (eds.). São Paulo, Editora Edgar Blücher, 137-204.

Hasui, Y., Costa, J.B.S., Gorayeb, P.S.S., Lemos, R.L., Gama Jr., T., Bemerguy, E.L., 1984b. Geologia do Pré-Cambriano da região de Paraíso do Norte de Goiás-GO (abstract). Congresso Brasileiro de Geologia, 33, annals, 2220-2230.

Hoskin, P.W.O., Black, L.P., 2000. Metamorphic zircon formation by solid-state recrystallization of protolith igneous zircon. Journal of Metamorphic Geology, 18, 423-439.

Hou, Z., Tian, S., Yuan, Z., Xie, Y., Yin, S., Yi, L., Fei, H., Yang, Z., 2006. The Himalayan collision zone carbonatites in western Sichuan, SW China: Petrogenesis, mantle source and tectonic implication. Earth and Planetary Science Letters, 244, 234-250.

Iwanuch, W., 1991. Geologia dos Complexos Alcalinos Proterozóicos do Centro do Estado do Tocantins. Unpublished Ph.D thesis. Universidade de São Paulo, São Paulo, Brazil.

Jackson, S.E., Pearson, N.J., Griffina, W.L., Belousova, E.A., 2004. The application of laser ablation-inductively coupled plasma-mass spectrometry to in situ U-Pb zircon geochronology. Chemical Geology, 211, 47-69.

Jacobsen, S.B., Wasserburg, G.J., 1980. Sm-Nd isotopic evolution of chondrites. Earth and Planetary Science Letters, 50, 139-155.

Jacobsen, S.B., Wasserburg, G.J., 1984. Sm-Nd isotopic evolution of chondrites and achondrites, II. Earth and Planetary Science Letters, 67, 137-150.

Janousek, V., Moyen, J.F., Martin, H., Erban, V., Farrow, C., 2016. Geochemical Modelling of Igneous Processes – Principles And Recipes in R Language –

Bringing the Power of R to a Geochemical Community. Springer Geochemistry. 354p.

Jones, A.P. 1980. The petrology and structure of the Motzfeldt centre, Igaliko, south Greenland. Unpublished Ph.D . thesis. Durham University, United Kingdom.

Le Maitre, R.W., Streckeisen, A., Zanettin, B., Le Bas, M.J., Bonin, B., Bateman, P., Bellieni, G., Dudek, A., Efremova, S., Keller, J., Lameyre, J., Sabine, P.A., Schmid, R., Sorensen, H., Woolley, A.R., 2002. Igneous Rocks – A Classification and Glossary of Terms (2nd edition) Recommendations of the International Union of Geological Sciences Subcommission on the Systematics of Igneous Rocks. Cambridge University Press. 252p.

Leake, B.E., Woolley, A.R., Arps, C.E.S., Birch, W.D., Gilbert, M.C., Grice, J.D., Hawthorne, F.C., Kato, A., Kisch, H.J., Krivovichev, V.G., Linthout, K., Laird, J., Mandarino, J.A., Maresch, W.V., Nickel, E.H., Rock, N.M.S., Schumacher, J.C., Smith, D.C., Stephenson, N.C.N., Ungaretti, L., Whittaker, E.J.W., Youzhi, G., 1997. Nomenclature of amphiboles: report of the subcommittee on amphiboles of the international mineralogical association, commission on new minerals and mineral names. The Canadian mineralogist, 35, 219-246.

Leat, P.T., Thomson, R.N., Morrison, M.A., Hendry, G.L., Dickin, A.P., 1988. Silicic magmas derived by fractional crystallization of Miocene minette, Elkhead Mountains, Colorado. Mineralogical Magazine, 52, 577-585.

Leelanandam, C., Burke, K., Ashwal, L.D., Webb, S.J., 2006. Proterozoic mountaain building in Peninsular India: an analysis based primarily on alkaline rock distribution. Geological Magazine, 143(2), 195-212.

Linnen, R.L., Keppler, H., 2002. Melt composition control of Zr/Hf fractionation in magmatic processes. Geochimica et Cosmochimica Acta, 66(18), 3293-3301.

Ludwig, K.R., 2003. User's Manual for Isoplot/Ex version 3.00 – A Geochronology Toolkit for Microsoft Excel. Berkeley Geochronological Center, Special Publications, vol 4.

Mezger, K., Krogstad, E.J., 1997. Interpretation of discordant U-Pb zircon ages: An evaluation. Journal of Metamorphic Geology, 15, 127-140.

Miller, J.S., Matzel, J.E.P., Miller, C.F., Burgess, S.D., Miller, R.B., 2007. Zircon growth and recycling during the assembly of large, composite arc plutons. Journal of Volcanology and Geothermal Research, 167, 282-299.

Mitchell, R.H., 1990. A review of the compositional variation of amphiboles in alkaline plutonic complexes, Lithos, 26, 135-156.

Mitchell, R.H., Platt, R.G., 1982. Mineralogy and Petrology of Nepheline Syenites from the Coldwell Alkaline Complex, Ontario, Canada. Journal of Petrology, 23(2), 186-214.

Morimoto, N., Fabries, J., Ferguson, A.K., Ginzburg, I.V., Ross, M., Seifert, F.A., Zussman, J., Aoki, K., Gottardi, G., 1988. American Mineralogist, 73, 1123-1133.

Moura, C.A.V., Gaudette, H.E., 1993. Evidence of Brasiliano/Panafrican deformation in the Araguaia Belt: implication for Gondwana evolution. Revista Brasileira de Geociências, 23(2), 117-123.

Moura, C.A.V., Gaudette, H.E., 1999. Zircon Ages of Basement Orthogneisses from the Northern Segment of the Araguaia Belt, Brazil. In: Sinha, A.K., 1999. Basement Tectonics 13, 155-179.

Moura, C.A.V., Macambira, M.J.B., Armstrong, R.A., 2008. U-Pb SHRIMP zircon age of the Santa Luzia Granite: Constraints on the age of metamorphism of the Araguaia Belt, Brazil (abstract). South American Symposium on Isotope Geology, 6, San Carlos de Bariloche, Argentina.

Moura, C.A.V., Pinheiro, B.L.S., Nogueira, A.C.R., Gorayeb, P.S.S., Galarza, M.A., 2008. Sedimentary provenance and palaenvironment of the Baixo Araguaia Supergroup: constraints on the palaeogeographical evolution of the Araguaia Belt and assembly of West Gondwana. In: Pankhurst, R.J., Trouw, R.A.J, Brito Neves, B.B & De Wit, M.J. (eds) West Gondwana: Pre Cenozoic Correlations Across the South Atlantic Region. Geological Society, London, Special Publications, 294, 173-196.

Nachit, H., Ibhi, A., Abia, E.H., Ohoud, M.B., 2005. Discrimination between primary magmatic biotites, reequilibrated biotites and neoformed biotites. Geomaterials (Mineralogy), 337, 1415-1420.

Nakamura, N., 1974. Determination of REE, Ba, Fe, Mg, Na and K in carbonaceous and ordinary chondrites. Geochimica et Cosmochimica Acta, 38, 757-775.

Nedosekova, I.L., Belyatsky, B.V., Belousova, E.A., 2016. Trace elements and Hf isotope composition as indicators of zircon genesis due to the evolution of alkaline-carbonatite magmatic system (Ilmeny-Vishnevogorsky complex, Urals, Russia). Russian Geology and Geophysics, 57, 891-906.

Oliveira, F.V., 2015. Chronus: um novo suplemento para a redução de dados U-Pb obtidos por LA-MC-ICPMS. Unpublished M.Sc thesis, Universidade de Brasília, Brasília, Distrito Federal, Brazil.

Paixão, M.A.P., Nilson, A.A., Dantas, E.L., 2008. The Neoproterozoic Quatipuru ophiolite and the Araguaia fold belt, central-northern Brazil, compared with correlatives in NW Africa. Geological Society of London Special Publications, 294, 297-318.

Pidgeon, R.T., 1992. Recrystallisation of oscillatory zoned zircon: some geochronological and petrological implications. Contributions to Mineralogy and Petrology, 110, 463-472.

Pinheiro, B.L.S., 2016. Petrologia e geotermobarometria das rochas metamórficas do Cinturão Araguaia: Região de Xambioá-Araguanã (TO). Unpublished Ph.D. thesis, Universidade Federal do Pará, Belém, Pará, Brazil.

Pinheiro, B.L.S., Moura, C.A.V., Gorayeb, P.S.S., 2011. Proveniência das rochas metassedimentares do Cinturão Araguaia com base em datações Pb-Pb em zircão e idades-modelo Sm-Nd. Revista Brasileira de Geociências, 41(2), 304-318.

Price, R.C., Johnson, R.W., Gray, C.M., Frey, F.A., 1985. Geochemistry of phonolites and trachytes from the summit region of Mount Kenya. Contributions to Mineralogy and Petrology, 89, 394-409.

Roberts, R.J., Corfu, F., Torsvik, T.H., Hetherington, C.J., Ashwal, L.D., 2010. Age of alkaline rocks in the Seiland Igneous Province, Northern Norway. Journal of the Geological Society of London, 167, 71-81.

Schairer, J.F., 1950. The alkali feldspar join in the system NaAlSiO4-KAlSiO4-SiO2. Journal of Geology, 58, 512-517.

Schaltegger, U., Ulianov, A., Muntener, O., Ovtcharova, M., Peytcheva, I., Vonlanthen, P., Vennemann, T., Antognini, M., Girlanda, F., 2015. Megacrystic zircon with planar fractures in miaskite-type nepheline pegmatites formed at high pressures in the lower crust (Ivrea Zone, southern Alps, Switzerland). American Mineralogist, 100, 83-94.

Schoenenberger, J., Markl, G., 2008. The Magmatic and Fluid Evolution of the Motzfeldt Intrusion in South Greenland: Insights into the Formation of Agpaitic and Miaskitic Rocks. Journal of Petrology, 49(9), 1549-1577.

Schumacher, J.C., 1997. Appendix 2. The Estimation of the Proportion of Ferric Iron in the Electron-Microprobe Analysis of Amphiboles. In: Leake et al. 1997. Nomenclature of Amphiboles: Report of the Subcommittee on Amphiboles of the International Mineralogical Association, Commission on New Minerals and Mineral Names. The Canadian Mineralogist, 238-246.

Sorensen, H., 1974. Origin of the alkaline rocks – a summary and retrospect. In: Sorensen, H., 1974. The Alkaline Rocks. John Wiley and Sons, 535-543.

Souza, A.C.C., Dall' Agnol, R., Teixeira, N.P., 1985. Petrologia do gnaisse Cantão: implicações na evolução da faixa de dobramentos Araguaia, Serra do Estrondo (GO). Revista Brasileira de Geociências, 15, 300-310.

Souza, D.J.L., Moura, C.A.V., 1996. Estudo Geocronológico do Granito Serrote, Paraíso do Tocantins. Congresso Brasileiro de Geoquímica, 5.

Souza, S.H.P., 1996. Geologia e geocronologia da região sul de Paraíso do Tocantins. Unpublished M.Sc. thesis, Universidade Federal do Pará, Belém, Pará, Brazil.

Stephenson, D., 1972. Alkali clinopyroxenes from nepheline syenites of the South Qoroq Centre, south Greenland. Lithos, 5, 187-201.

Thompson, R.N., 1982. Magmatism of the British Tertiary Volcanic Province. Scottish Journal of Geology, 18, 49-107.

Thompson, R.N., Morrison, M.A., Hendry, G.L., Parry, S.J., 1984. An assessment of the relative roles of crust and mantle in magma genesis: an elemental approach. Philosophical Transactions of the Royal Society of London A, 310, 549-590.

Tilley, C.E., 1954. Nepheline-alkali feldspar parageneses. American Journal of Science, 252, 65-75.

Tilton, G.R., Bryce, J.G., Mateen, A., 1998. Pb-Sr-Nd Isotope Data from 30 and 300 Ma Collision Zone Carbonatites in Northwest Pakistan. Journal of Petrology, 39(11-12), 1865-1874.

Tischendorf, G., Forster, H.J., Gottesmann, B., Rieder, M., 2007. True and brittle micas: composition and solid-solution series. Mineralogical Magazine, 71(3), 285-320.

Tischendorf, G., Rieder, M., Forster, H.J., Gottesmann, B., Guidotti, C.V., 2004. A new graphical presentation and subdivision of potassium micas. Mineralogical Magazine, 68(4), 649-667.

Upadhyay, D., Raith, M.M., Mezger, K., Hammerschmidt, K., 2006. Mesoproterozoic rift-related alkaline magmatism at Elchuru, Prakasam Alkaline Province, SE India. Lithos, 89, 447-477.

Valentin, E., Caixeta, G.M., Botelho, N.F., 2016. Aspectos Texturais, Geotectônicos e Geofísicos Aplicados à Interpretação da Idade do Maciço Alcalino Monte Santo –TO. Congresso Brasileiro de Geologia, 48, annals 6596, Porto Alegre, Rio Grande do Sul, Brazil.

Vavra, G., Schmid, R., Gebauer, D., 1999. Internal morphology, habit and U-Th-Pb microanalysis of amphibolite-to-granulite facies zircons: geochronology of the Ivrea Zone (Southern Alps). Contributions to Mineralogy and Petrology, 134, 380-404.

Viana, R.R., Battilani, G.A., 2014. Geochemistry and Petrography of Alkaline rocks from Monte Santo Alkaline Intrusive Suite, Western Araguaia Belt, Tocantins State, Brazil. Journal of Geoscience and Environment Protection, 2, 72-79.

Viana, R.R., Battilani, G.A., 2014. SHRIMP U-Pb and U-Pb Laser Ablation Geochronological on Zircons from Monte Santo Alkaline Intrusive Suite, Westhern Araguaia Belt, Tocantins State, Brazil. Journal of Geoscience and Environment Protection, 2, 170-180.

Wetherill, G.W., 1956. Discordant Uranium-Lead Ages, I. Transactions, American Geophysical Union, 37(3), 320-326.

Whitney, D.L., Evans, B.W., 2010. Abbreviations for names of rock-forming minerals. American Mineralogist, 95, 185-187.

Wiedenbeck, M., Allé, P., Corfu, F., Griffin, W.L., Meier, M., Oberli, F., Von Quadt, A., Roddick, J.C., Spiegel. W., 1995. Three Natural Zircon Standards for U-Th-Pb, Lu-Hf, Trace Element and REE Analyses. Geostandards Newsletter, 19(1), 1-23.

Wiedenbeck, M., Hanchar, J.M., Peck, W.H., Sylvester, P., Valley, J., Whitehouse, M., Kronz, A., Morishita, Y., Nasdala, L., Fiebig, ., Franchi, M., Girard, J.P., Greenwood, R.C., Hinton, R., Kita, N., Mason, P.R.D., Norman, M., Ogasawara, M., Piccoli, P.M., Rhede, D., Satoh, H., Schulz-Dobrick, B., Skar, O., Spicuzza, M.J., Terada, K., Tindle, A., Togashi, S., Vennemann, T., Xie, Q., Zheng, Y.F., 2004. Further Characterisation of the 91500 Zircon Crystal. Geostandards and Geoanalytical Research, 28(1), 9-39.

Wolff, J.A., 1987. Crystallisation of nepheline syenite in a subvolcanic magma system: Tenerife, Canary Islands. Lithos, 20, 207-223.

Woolley, A.R., 1987. Lithosphere metasomatism and the petrogenesis of the Chilwa Province of alkaline igneous rocks and carbonatites, Malawi. Journal of African Earth Sciences, 6(6), 891-898.

Woolley, A.R., Platt, R.G., 1988. The peralkaline nepheline syenites of the Junguni intrusion, Chilwa province, Malawi. Mineralogical Magazine, 52, 425-433.

Woolley, A.R., Platt, R.G., Eby, G.N., 1996. Relatively aluminous alkali pyroxene in nepheline syenites from Malawi: mineralogical response to metamorphism in alkaline rocks. The Canadian Mineralogist, 34, 423-434.

ANEXOS

Coordenadas dos pontos amostrados durante os campos realizados, com amostras analisadas indicadas.

Ponto	E	N	Análises			Ponto	E	N	Análises			Ponto	E	N	Análises		
EV-ES-01	744611	8844003	Lâmina	Geoq	U-Pb	EV-ES-40	742143	8835927	Lâmina			TF15II300	721226	8888831			
EV-ES-02	742504	8836477	Lâmina			EV-ES-43	741543	8836046	Lâmina	Geoq		TF15II303	720985	8888502			
EV-ES-03	742385	8836411	Lâmina			EV-ES-44	741350	8835139	Lâmina	Geoq		TF15II307	720180	8888822			
EV-ES-04	741255	8838245	Lâmina	Geoq		EV-ES-47	746642	8842441				TF15II316	721108	8889436	Lâmina	Geoq	
EV-ES-05	741487	8838795	Lâmina	Geoq		EV-ES-48	741270	8833864	Lâmina			TF15II319	722090	8888818	Lâmina		
EV-ES-06	742213	8840363	Lâmina	Geoq		EV-ES-49	741119	8833656	Lâmina			TF15II335	723131	8891194			
EV-ES-07	741226	8834032				EV-ES-50	741101	8833571	Lâmina	Geoq		TF15II336	722912	8891248	Lâmina	Geoq	
EV-ES-08	741775	8835978				TF15II6	721990	8888473				TF15II344	721960	8890431	Lâmina		
EV-ES-09	742329	8837397	Lâmina			TF15II9	721864	8890312				TF15II365	722041	8889190	Lâmina	Geoq	
EV-ES-11	743481	8840405				TF15II10	721920	8890218				TF15II366	720833	8889443			
EV-ES-12	743778	8841219	Lâmina	Geoq	U-Pb	TF15II16	720825	8890106				TF15II392	720932	8887423	Lâmina		
EV-ES-13	743693	8841271				TF15II20	720499	8890455				TF15II398	721906	8887732	Lâmina	Geoq	
EV-ES-14	743298	8840880	Lâmina	Geoq		TF15II22	720052	8890470	Lâmina	Geoq	U-Pb	TF15II399	721982	8890607			
EV-ES-15	744264	8842360	Lâmina			TF15II88	723295	8889157	Lâmina	Geoq	U-Pb	TF15II400	721985	8890963	Lâmina	Geoq	
EV-ES-16	744976	8843154	Lâmina			TF15II112	719240	8888896				TF15IV144	721137	8887479	Lâmina		
EV-ES-19	744954	8844500	Lâmina			TF15II113	719183	8888740				TF15IV145	721105	8887425			
EV-ES-22	745660	8843735	Lâmina			TF15II114	719108	8888624				TF15IV146	721423	8887528			
EV-ES-24	746254	8842726	Lâmina			TF15II122	719341	8889341	Lâmina	Geoq		TF15IV148	720964	8887347	Lâmina		
EV-ES-26	744757	8843707	Lâmina			TF15II135	719040	8888572				TV15IV150	720864	8887640			
EV-ES-27	744087	8841964	Lâmina			TF15II140	721034	8888787	Lâmina	Geoq	U-Pb	TV15IV151	720810	8887816	Lâmina		
EV-ES-28	745443	8839858	Lâmina			TF15II143	720939	8888426	Lâmina			TV15IV152	720758	8887949			
EV-ES-31	742947	8839936	Lâmina			TF15II146	719040	8888574	Lâmina			TV15IV153	720755	8888046	Lâmina		
EV-ES-36	740795	8836279	Lâmina			TF15II293	722447	8888382	Lâmina	Geoq		TV15IV154	721270	8887519			
EV-ES-37	741846	8836010	Lâmina	Geoq		TF15II294	722190	8888496				TV15IV155	721270	8887673			
EV-ES-38	741932	8835991	Lâmina			TF15II297	721763	8888510				TV15IV156	721545	8887673			
EV-ES-39	742000	8835972	Lâmina			TF15II299	721510	8888669				TV15IV157	722077	8887531			

Limites de detecção médio, máximo e mínimo, para cada elemento analisado nos minerais essenciais presentes nas rochas da Suíte Monte Santo (n=433), com indicação das linhas do espectro característico analisado.

	Média (ppm)	Máximo (ppm)	Mínimo (ppm)
Ti (Kα)	920	1555	328
Si (Kα)	194	272	122
Al (Kα)	163	213	76
Fe (Kα)	331	455	198
Mn (Kα)	481	832	148
Mg (Kα)	158	193	82
Ca (Kα)	190	246	122
Na (Kα)	196	279	81
K (Kα)	161	214	93
Cl (Kα)	126	170	72
F (Kα)	377	1097	149
Cr (Kα)	540	841	267
V (Kα)	264	455	168

Esquema de correção para sobreposição de linhas do espectro característico aplicadas nas análises na Suíte Monte Santo. *(soma das contagens interferentes)/(pico das contagens nas linhas de interesse)*100, calculado referente ao equipamento do laboratório.

Elemento	Interferência	Razão de sobreposição* (%)
V (Kα)	Ti (Kβ)	0.00500
P (Kα)	Y (Lβ)	0.00640
Nb (Lβ)	Ti (Kβ)	0.16010
Er (Lα)	Tb (Lβ)	0.05480
Gd (Lα)	La (Lγ)	0.02560
Gd (Lα)	Ce (Lγ)	0.05468
Nd (Lα)	Pb (Lα)	0.01410
Eu (Lα)	Nd ($L\beta_3$)	0.00290
Tm (Lα)	Sm (Lγ)	0.14540
Gd (Lα)	Nd ($L\beta_2$)	0.00240
Lu (Lα)	Ho ($L\beta_3$)	0.14620
Lu (Lα)	Dy (Lβ)	0.09510
Na (Kα)	Ho (Mζ)	0.20630
K (Kα)	U (Mβ)	0.00490
U (Mβ)	K (Kα)	0.10240
Ce (Lα)	Ba (Lα)	0.11094

Padrões utilizados nas análises de microssonda eletrônica nos minerais da Suíte Monte Santo.

Elemento	Padrão	Elemento	Padrão
V	Vanadinita	La	REE-3
Ta	$LiTaO_3$	Ce	CeO_2
Nb	$LiNbO_3$	Pr	REE-3
Ti	$MnTiO_3$	Nd	REE-2
Si	Microclínio	Sm	REE-2
P	Apatita Gaspox	Eu	REE-1
Y	YFe_2O_{12}	Gd	REE-1
Zr	Badeleíta	Tb	REE-1
Hf	HfO_2	Dy	REE-4
Al	Microclínio	Ho	REE-4
Fe	Andradita Gaspox	Er	REE-4
Mn	$MnTiO_3$	Tm	REE-1
Cr	Cromita	Yb	REE-2
Ca	Apatita Gaspox	Lu	REE-2
Mg	Forsterita	U	UO_2
Sr	$SrSO_4$	Th	ThO_2
Ba	Barita Gaspox	Pb	Vanadinita
K	Microclínio	F	Topázio
Na	Albita Gaspox	Cl	Vanadinita

Dados Isotópicos U-Pb

Sample MS 22	f206 (%)	Th/U	$^{206}Pb/^{204}Pb$ ratio	$^{207}Pb/^{206}Pb$ ratio	1σ (%)	$^{207}Pb/^{235}U$ ratio	1σ (%)	$^{206}Pb/^{238}U$ ratio	1σ (%)	Error corr. (ρ)	$^{207}Pb/^{206}Pb$ age (Ma)	2σ (Ma)	$^{207}Pb/^{235}U$ age (Ma)	2σ (Ma)	$^{206}Pb/^{238}U$ age (Ma)	2σ (Ma)	Disc. (%)
ZR1R	0.02	0.408	64418	0.07784	0.64	1.992	1.07	0.1856	0.78	0.72	1143	25	1098	16	1113	14	3.96
ZR1C	**0.03**	**1.199**	**50564**	**0.07718**	**0.57**	**2.000**	**1.11**	**0.1879**	**0.88**	**0.79**	**1126**	**23**	**1110**	**18**	**1116**	**15**	**1.38**
ZR2R	0.01	0.413	182161	0.07513	0.36	1.737	1.21	0.1677	1.10	0.90	1072	14	999	20	1022	16	6.78
ZR2C	0.01	0.513	236629	0.07552	0.31	1.772	0.73	0.1702	0.55	0.75	1082	12	1013	10	1035	9	6.39
ZR2O	0.01	0.384	172956	0.07487	0.41	1.750	0.94	0.1695	0.76	0.81	1065	16	1009	14	1027	12	5.22
ZR3R	**0.01**	**1.505**	**266948**	**0.07685**	**0.50**	**1.982**	**0.87**	**0.1871**	**0.61**	**0.70**	**1117**	**20**	**1105**	**12**	**1109**	**12**	**1.06**
ZR3C	0.08	0.315	20605	0.07574	2.05	1.895	3.06	0.1814	2.23	0.73	1088	81	1075	44	1079	40	1.23
ZR4R	**0.00**	**0.759**	**461218**	**0.07661**	**0.34**	**1.981**	**0.72**	**0.1875**	**0.52**	**0.72**	**1111**	**13**	**1108**	**11**	**1109**	**10**	**0.30**
ZR4C	0.03	0.696	57256	0.07756	0.70	1.972	1.07	0.1844	0.71	0.67	1136	28	1091	14	1106	14	3.94
ZR5R	0.03	1.675	44287	0.07579	0.77	1.912	1.20	0.1830	0.84	0.70	1090	31	1083	17	1085	16	0.59
ZR5C	0.02	0.674	85158	0.07576	0.32	1.853	0.87	0.1774	0.72	0.83	1089	13	1053	14	1065	11	3.32
ZR6	0.04	3.110	34888	0.07624	1.06	1.769	1.86	0.1682	1.48	0.80	1101	42	1002	27	1034	24	8.99
ZR7C	0.04	1.205	38160	0.07495	1.89	1.906	2.26	0.1844	1.17	0.52	1067	75	1091	24	1083	30	-2.21
ZR7R	0.01	0.541	220730	0.07526	0.64	1.858	1.08	0.1790	0.79	0.73	1075	26	1062	16	1066	14	1.26
ZR8C	0.01	0.365	247829	0.07627	0.38	1.880	0.76	0.1788	0.55	0.72	1102	15	1060	11	1074	10	3.78
ZR8R	0.13	0.562	11482	0.07443	1.59	2.341	3.65	0.2281	3.26	0.89	1053	64	1325	78	1225	51	-25.79
ZR9C	0.01	0.616	131762	0.07551	0.27	1.874	0.76	0.1800	0.60	0.79	1082	11	1067	12	1072	10	1.37
ZR9R	0.03	0.665	55642	0.07311	0.69	1.647	1.27	0.1634	1.00	0.79	1017	28	975	18	988	16	4.08
ZR10R	**0.00**	**0.952**	**324350**	**0.07641**	**0.31**	**1.976**	**0.69**	**0.1876**	**0.50**	**0.72**	**1106**	**12**	**1108**	**10**	**1107**	**9**	**-0.20**
ZR10O	0.03	0.816	52708	0.07738	0.58	1.905	0.97	0.1785	0.69	0.71	1131	23	1059	13	1083	13	6.39
ZR10C	0.68	2.475	2266	0.08462	0.95	2.216	1.29	0.1899	0.79	0.61	1307	37	1121	16	1186	18	14.21
ZR11C	0.12	0.603	12704	0.07547	0.50	1.825	1.35	0.1754	1.20	0.89	1081	20	1042	23	1055	18	3.64
ZR12C	0.91	1.829	1704	0.08355	0.68	2.372	2.88	0.2059	2.77	0.96	1282	26	1207	61	1234	41	5.87
ZR12R	0.18	2.697	8629	0.07853	1.80	1.441	4.15	0.1331	3.72	0.90	1160	71	805	56	906	49	30.59
ZR13C	0.01	1.003	149253	0.07624	0.35	1.922	0.86	0.1828	0.70	0.81	1101	14	1082	14	1089	12	1.72

Sample MS 22 (cont.)	f206 (%)	Th/U	$^{206}Pb/^{204}Pb$ ratio	$^{207}Pb/^{206}Pb$ ratio	1σ (%)	$^{207}Pb/^{235}U$ ratio	1σ (%)	$^{206}Pb/^{238}U$ ratio	1σ (%)	Error corr. (ρ)	$^{207}Pb/^{206}Pb$ age (Ma)	2σ (Ma)	$^{207}Pb/^{235}U$ age (Ma)	2σ (Ma)	$^{206}Pb/^{238}U$ age (Ma)	2σ (Ma)	Disc. (%)
ZR13R	0.01	1.862	298457	0.07640	0.30	2.036	0.81	0.1932	0.65	0.81	1106	12	1139	14	1128	11	-3.00
ZR14R	**0.01**	**0.956**	**164623**	**0.07688**	**0.42**	**1.986**	**0.87**	**0.1873**	**0.67**	**0.77**	**1118**	**17**	**1107**	**14**	**1111**	**12**	**1.02**
ZR14C	0.04	1.960	38046	0.07846	1.08	1.959	1.58	0.1811	1.10	0.70	1159	42	1073	22	1102	21	7.39
ZR15O	2.73	2.963	569	0.08873	3.61	2.205	4.76	0.1802	3.08	0.65	1398	135	1068	60	1183	65	23.62

Sample MS 88	f206 (%)	Th/U	$^{206}Pb/^{204}Pb$ ratio	$^{207}Pb/^{206}Pb$ ratio	1σ (%)	$^{207}Pb/^{235}U$ ratio	1σ (%)	$^{206}Pb/^{238}U$ ratio	1σ (%)	Error corr. (ρ)	$^{207}Pb/^{206}Pb$ age (Ma)	2σ (Ma)	$^{207}Pb/^{235}U$ age (Ma)	2σ (Ma)	$^{206}Pb/^{238}U$ age (Ma)	2σ (Ma)	Disc. (%)
ZR16R	0.02	1.056	65696	0.07564	0.66	1.792	1.14	0.1718	0.85	0.74	1086	26	1022	16	1043	15	5.85
ZR16C	0.02	1.129	95146	0.07572	0.39	1.621	0.96	0.1553	0.80	0.83	1088	16	930	14	978	12	14.46
ZR17R	0.71	1.455	2176	0.09597	1.00	2.573	1.31	0.1944	0.77	0.59	1547	37	1145	16	1293	19	25.98
ZR17C	**0.02**	**1.580**	**76885**	**0.07685**	**0.59**	**1.999**	**1.90**	**0.1886**	**1.77**	**0.93**	**1117**	**23**	**1114**	**36**	**1115**	**26**	**0.31**
ZR18C	0.02	2.009	89378	0.07730	0.49	2.054	0.89	0.1927	0.64	0.72	1129	19	1136	13	1134	12	-0.63
ZR18R	0.00	2.846	519287	0.07620	0.43	2.063	0.82	0.1963	0.60	0.73	1100	17	1155	13	1136	11	-5.00
ZR18O1	0.01	1.208	122599	0.07698	0.56	2.029	0.94	0.1911	0.65	0.70	1121	22	1127	13	1125	13	-0.59
ZR18O2	0.06	1.668	26078	0.08011	1.08	1.877	1.61	0.1699	1.14	0.71	1200	42	1012	21	1073	21	15.68
ZR19C	**0.01**	**2.286**	**185239**	**0.07616**	**0.36**	**1.958**	**0.75**	**0.1864**	**0.54**	**0.72**	**1099**	**14**	**1102**	**11**	**1101**	**10**	**-0.25**
ZR19R	0.03	1.215	52432	0.07730	0.75	1.832	1.15	0.1719	0.79	0.69	1129	30	1023	15	1057	15	9.42
ZR20O	0.07	1.239	21663	0.07771	1.00	1.978	1.55	0.1846	1.13	0.73	1140	39	1092	23	1108	21	4.16
ZR20R	0.00	0.181	411500	0.07617	0.38	1.915	0.90	0.1824	0.73	0.81	1099	15	1080	14	1086	12	1.79
ZR20C	0.13	0.837	12394	0.07651	0.69	1.781	2.78	0.1688	2.67	0.96	1108	27	1006	50	1039	36	9.29
ZR21O	0.07	2.271	23579	0.07300	1.56	1.212	2.26	0.1204	1.59	0.70	1014	63	733	22	806	25	27.72
ZR21R	**0.01**	**2.654**	**236807**	**0.07624**	**0.44**	**1.965**	**0.99**	**0.1869**	**0.80**	**0.81**	**1101**	**17**	**1104**	**16**	**1103**	**13**	**-0.29**
ZR21C	0.49	2.480	3145	0.07898	1.18	2.009	1.55	0.1845	0.92	0.60	1172	46	1091	19	1119	21	6.84
ZR23C	0.02	0.955	75316	0.07603	0.34	1.899	0.82	0.1811	0.65	0.79	1096	14	1073	13	1081	11	2.08

Sample MS 88 (cont.)	f206 (%)	Th/U	$^{206}Pb/^{204}Pb$ ratio	$^{207}Pb/^{206}Pb$ ratio	1σ (%)	$^{207}Pb/^{235}U$ ratio	1σ (%)	$^{206}Pb/^{238}U$ ratio	1σ (%)	Error corr. (ρ)	$^{207}Pb/^{206}Pb$ age (Ma)	2σ (Ma)	$^{207}Pb/^{235}U$ age (Ma)	2σ (Ma)	$^{206}Pb/^{238}U$ age (Ma)	2σ (Ma)	Disc. (%)
ZR23R	0.03	1.571	46124	0.07815	0.80	2.025	1.24	0.1879	0.87	0.70	1151	32	1110	18	1124	17	3.52
ZR24	1.64	0.190	942	0.09703	0.79	2.519	1.05	0.1882	0.59	0.56	1568	29	1112	12	1277	15	29.08
ZR25C	0.09	1.503	17948	0.07678	0.29	2.070	1.06	0.1955	0.95	0.90	1116	11	1151	20	1139	14	-3.20
ZR25R	**0.02**	**1.375**	**83171**	**0.07621**	**0.32**	**1.988**	**0.74**	**0.1892**	**0.55**	**0.75**	**1101**	**13**	**1117**	**11**	**1111**	**10**	**-1.47**
ZR26C	0.01	0.554	104742	0.07797	0.44	2.006	0.83	0.1866	0.59	0.72	1146	18	1103	12	1118	11	3.77
ZR27R	0.08	2.286	19396	0.07783	1.02	1.558	1.31	0.1452	0.74	0.57	1142	40	874	12	954	16	23.50
ZR27C	0.29	4.082	5319	0.07621	0.51	1.291	1.09	0.1228	0.89	0.81	1101	20	747	12	842	12	32.13
ZR28O	0.05	1.979	34220	0.08047	0.53	2.124	2.43	0.1914	2.34	0.96	1208	21	1129	48	1157	33	6.57
ZR28C	0.33	1.149	4736	0.08418	1.14	2.161	1.42	0.1862	0.75	0.53	1297	44	1101	15	1169	20	15.12
ZR28R	0.04	2.315	43641	0.07487	0.52	1.701	0.84	0.1648	0.55	0.65	1065	21	983	10	1009	11	7.66
ZR29R	0.04	0.421	35488	0.07688	0.40	1.792	0.84	0.1691	0.64	0.76	1118	16	1007	12	1043	11	9.94
ZR29C	0.00	0.427	319676	0.07564	0.31	1.860	0.79	0.1783	0.63	0.79	1085	13	1058	12	1067	10	2.55
ZR30C	0.10	1.091	15922	0.07974	1.03	1.740	1.40	0.1582	0.88	0.63	1191	40	947	15	1023	18	20.47
ZR30R	**0.01**	**2.261**	**196531**	**0.07644**	**0.47**	**1.974**	**0.90**	**0.1873**	**0.67**	**0.74**	**1107**	**19**	**1107**	**14**	**1107**	**12**	**0.00**

Sample MS 140	f206 (%)	Th/U	$^{206}Pb/^{204}Pb$ ratio	$^{207}Pb/^{206}Pb$ ratio	1σ (%)	$^{207}Pb/^{235}U$ ratio	1σ (%)	$^{206}Pb/^{238}U$ ratio	1σ (%)	Error corr. (ρ)	$^{207}Pb/^{206}Pb$ age (Ma)	2σ (Ma)	$^{207}Pb/^{235}U$ age (Ma)	2σ (Ma)	$^{206}Pb/^{238}U$ age (Ma)	2σ (Ma)	Disc. (%)
ZR1R	**0.08**	**0.158**	**19931**	**0.05945**	**1.59**	**0.717**	**2.19**	**0.0874**	**1.47**	**0.67**	**584**	**68**	**540**	**15**	**549**	**19**	**7.44**
ZR1C	0.03	0.486	60987	0.08146	1.07	2.120	2.42	0.1887	2.14	0.88	1233	42	1114	44	1155	33	9.58
ZR2R	0.02	2.095	70578	0.07697	0.70	1.884	1.11	0.1775	0.77	0.70	1120	28	1053	15	1075	15	5.98
ZR2C	0.03	2.072	49279	0.07629	0.93	1.773	1.60	0.1686	1.25	0.78	1103	37	1004	23	1036	21	8.93
ZR3	0.05	1.176	28363	0.07644	1.09	1.667	1.73	0.1581	1.29	0.75	1107	43	946	23	996	22	14.47
ZR4	0.03	0.740	47103	0.07686	0.93	1.785	2.44	0.1685	2.22	0.91	1118	37	1004	41	1040	31	10.19
ZR5C	0.03	0.488	52446	0.07627	0.52	1.858	1.07	0.1767	0.86	0.80	1102	21	1049	17	1066	14	4.82

Sample MS 140 (cont.)	f206 (%)	Th/U	$^{206}Pb/^{204}Pb$ ratio	$^{207}Pb/^{206}Pb$ ratio	1σ (%)	$^{207}Pb/^{235}U$ ratio	1σ (%)	$^{206}Pb/^{238}U$ ratio	1σ (%)	Error corr. (ρ)	$^{207}Pb/^{206}Pb$ age (Ma)	2σ (Ma)	$^{207}Pb/^{235}U$ age (Ma)	2σ (Ma)	$^{206}Pb/^{238}U$ age (Ma)	2σ (Ma)	Disc. (%)
ZR5R	0.03	1.583	44263	0.07819	0.77	2.019	1.92	0.1872	1.72	0.89	1152	31	1106	35	1122	26	3.94
ZR6	0.04	0.244	41767	0.07546	0.97	1.656	1.54	0.1592	1.15	0.74	1081	38	952	20	992	19	11.88
ZR7R	**0.05**	**1.165**	**33387**	**0.06545**	**1.76**	**1.156**	**2.44**	**0.1281**	**1.66**	**0.68**	**789**	**73**	**777**	**24**	**780**	**26**	**1.50**
ZR7C	0.02	0.445	85436	0.07616	0.52	1.886	1.04	0.1796	0.83	0.79	1099	21	1065	16	1076	14	3.14
ZR8R	0.01	1.795	132660	0.07557	0.70	1.729	1.42	0.1659	1.17	0.83	1084	28	989	22	1019	18	8.69
ZR8C	0.03	0.591	45225	0.07807	0.74	1.897	1.38	0.1762	1.10	0.80	1149	29	1046	21	1080	18	8.91
ZR9	**0.02**	**0.127**	**86332**	**0.05779**	**0.87**	**0.676**	**1.44**	**0.0849**	**1.08**	**0.75**	**522**	**38**	**525**	**11**	**525**	**12**	**-0.66**
ZR9A	0.01	1.576	42666	0.07147	2.61	0.751	3.97	0.0762	2.98	0.75	971	105	474	27	569	34	51.20
ZR9B	**0.03**	**0.097**	**69332**	**0.05849**	**1.06**	**0.644**	**1.65**	**0.0798**	**1.21**	**0.73**	**548**	**46**	**495**	**12**	**505**	**13**	**9.70**
ZR9C	**0.02**	**0.064**	**40147**	**0.05768**	**1.14**	**0.627**	**1.62**	**0.0788**	**1.10**	**0.68**	**518**	**49**	**489**	**10**	**494**	**13**	**5.49**
ZR10	0.05	2.767	32049	0.06440	1.45	0.871	1.92	0.0981	1.20	0.62	755	61	603	14	636	18	20.09
ZR10A	**0.06**	**2.593**	**22037**	**0.06005**	**1.20**	**0.680**	**1.69**	**0.0821**	**1.13**	**0.67**	**605**	**52**	**509**	**11**	**527**	**14**	**15.94**
ZR10B	0.04	3.080	38805	0.06277	1.40	0.690	1.81	0.0797	1.08	0.60	700	59	494	10	533	15	29.44
ZR11	0.03	0.805	46925	0.07678	0.83	1.943	1.95	0.1835	1.72	0.88	1116	33	1086	34	1096	26	2.65
ZR13R	0.04	3.698	41116	0.07666	1.99	2.073	2.54	0.1961	1.54	0.61	1112	78	1154	33	1140	35	-3.79
ZR13C	0.01	0.359	138998	0.07660	0.71	1.987	1.24	0.1881	0.94	0.76	1111	28	1111	19	1111	17	-0.04
ZR14	0.04	0.632	37185	0.07590	0.77	1.821	1.48	0.1740	1.21	0.82	1092	30	1034	23	1053	19	5.33
ZR15R	0.09	0.782	16603	0.08171	2.31	2.028	3.27	0.1800	2.28	0.70	1239	89	1067	45	1125	44	13.87
ZR15C	0.13	0.459	12109	0.07848	0.95	1.836	1.35	0.1697	0.89	0.66	1159	37	1010	17	1059	18	12.82
ZR16R	0.04	1.693	42794	0.07695	1.36	1.881	1.89	0.1772	1.26	0.67	1120	54	1052	24	1074	25	6.08
ZR17R	0.01	0.607	162606	0.07619	0.64	1.969	1.27	0.1875	1.02	0.81	1100	26	1108	21	1105	17	-0.69
ZR19	0.08	0.776	18389	0.07703	2.27	1.672	2.85	0.1574	1.69	0.59	1122	89	942	30	998	36	16.03
ZR20	0.17	1.470	9225	0.07002	0.87	0.788	2.30	0.0817	2.10	0.91	929	35	506	20	590	21	45.52
ZR20B	0.02	0.663	30003	0.07387	0.73	1.455	1.66	0.1428	1.44	0.87	1038	29	861	23	912	20	17.08
ZR21	0.04	0.895	43124	0.07754	1.14	2.086	1.94	0.1951	1.52	0.79	1135	45	1149	32	1144	26	-1.19

Sample MS 140 (cont.)	f206 (%)	Th/U	$^{206}Pb/^{204}Pb$ ratio	$^{207}Pb/^{206}Pb$ ratio	1σ (%)	$^{207}Pb/^{235}U$ ratio	1σ (%)	$^{206}Pb/^{238}U$ ratio	1σ (%)	Error corr. (ρ)	$^{207}Pb/^{206}Pb$ age (Ma)	2σ (Ma)	$^{207}Pb/^{235}U$ age (Ma)	2σ (Ma)	$^{206}Pb/^{238}U$ age (Ma)	2σ (Ma)	Disc. (%)
ZR22R	0.03	1.720	44903	0.07947	0.77	1.975	1.27	0.1802	0.94	0.74	1184	30	1068	18	1107	17	9.77
ZR22C	0.05	0.244	32943	0.07802	1.34	1.944	2.01	0.1807	1.45	0.72	1147	53	1071	29	1096	27	6.66
ZR23C	0.02	0.443	93928	0.07454	0.57	1.876	1.26	0.1825	1.05	0.84	1056	23	1081	21	1073	17	-2.33
ZR23R	0.41	1.174	3834	0.07194	0.72	1.169	1.70	0.1178	1.49	0.88	984	29	718	20	786	18	27.06
ZR24	0.05	0.501	28409	0.07706	1.20	2.043	1.81	0.1923	1.30	0.72	1123	48	1134	27	1130	24	-0.99
ZR25	0.02	0.982	65316	0.07320	0.38	1.612	1.38	0.1597	1.27	0.92	1020	15	955	23	975	17	6.35
ZR26	0.03	1.142	60783	0.07634	0.68	1.931	1.37	0.1834	1.13	0.83	1104	27	1086	23	1092	18	1.67
ZR26B	0.07	1.043	29872	0.07605	0.95	1.362	2.07	0.1299	1.81	0.87	1096	38	787	27	873	24	28.17
ZR28R	0.02	1.386	101636	0.07511	0.48	1.721	1.34	0.1661	1.20	0.89	1071	19	991	22	1016	17	7.52
ZR28O	0.02	0.688	87728	0.07510	1.16	1.615	2.43	0.1560	2.11	0.87	1071	46	934	37	976	30	12.76
ZR29	0.73	1.820	2125	0.07440	0.94	1.264	1.36	0.1232	0.91	0.67	1052	38	749	13	830	15	28.85
ZR31A	0.10	1.657	6777	0.07640	0.59	1.261	3.46	0.1197	3.39	0.98	1106	24	729	47	828	39	34.07
ZR31B	0.11	0.258	8880	0.06685	1.86	0.817	2.57	0.0886	1.74	0.68	833	76	547	18	606	23	34.31
ZR32A	0.02	1.881	60301	0.07899	1.00	1.776	1.52	0.1631	1.09	0.71	1172	39	974	20	1037	20	16.91
ZR33A	0.14	1.819	11801	0.07742	0.77	1.562	2.20	0.1463	2.02	0.92	1132	31	880	33	955	27	22.24
ZR33B	0.06	1.555	8558	0.07629	0.65	1.492	1.80	0.1419	1.64	0.91	1103	26	855	26	927	22	22.45
ZR34	0.09	0.548	3020	0.06824	2.26	1.876	3.79	0.1993	3.02	0.80	876	92	1172	65	1073	50	-33.77
ZR35	0.08	1.382	4067	0.07641	1.00	1.655	1.91	0.1571	1.58	0.83	1106	40	941	28	991	24	14.95

Sample EVES01	f206 (%)	Th/U	$^{206}Pb/^{204}Pb$ ratio	$^{207}Pb/^{206}Pb$ ratio	1σ (%)	$^{207}Pb/^{235}U$ ratio	1σ (%)	$^{206}Pb/^{238}U$ ratio	1σ (%)	Error corr. (ρ)	$^{207}Pb/^{206}Pb$ age (Ma)	2σ (Ma)	$^{207}Pb/^{235}U$ age (Ma)	2σ (Ma)	$^{206}Pb/^{238}U$ age (Ma)	2σ (Ma)	Disc. (%)
ZR15C	**0.03**	**0.193**	**44547**	**0.05796**	**0.48**	**0.698**	**1.09**	**0.0873**	**0.91**	**0.83**	**528**	**21**	**539**	**9**	**537**	**9**	**-2.12**
ZR15R	0.04	0.101	37511	0.05785	1.67	0.688	2.46	0.0862	1.77	0.72	524	72	533	18	532	20	-1.71
ZR16C	**0.01**	**2.757**	**128265**	**0.05688**	**0.61**	**0.692**	**1.05**	**0.0882**	**0.76**	**0.73**	**487**	**27**	**545**	**8**	**534**	**9**	**-11.93**

Sample EVES01 (cont.)	f206 (%)	Th/U	$^{206}Pb/^{204}Pb$ ratio	$^{207}Pb/^{206}Pb$ ratio	1σ (%)	$^{207}Pb/^{235}U$ ratio	1σ (%)	$^{206}Pb/^{238}U$ ratio	1σ (%)	Error corr. (ρ)	$^{207}Pb/^{206}Pb$ age (Ma)	2σ (Ma)	$^{207}Pb/^{235}U$ age (Ma)	2σ (Ma)	$^{206}Pb/^{238}U$ age (Ma)	2σ (Ma)	Disc. (%)
ZR16R2	0.02	0.116	89834	0.05770	0.56	0.687	1.00	0.0863	0.74	0.74	518	24	534	8	531	8	-2.99
ZR17C	0.05	1.123	28750	0.06120	0.94	0.761	1.21	0.0902	0.66	0.55	646	40	556	7	575	11	13.89
ZR17O1	0.05	0.250	33280	0.05836	1.66	0.681	2.62	0.0846	1.99	0.76	543	72	524	20	527	21	3.58
ZR18O2	0.01	0.173	125212	0.05933	0.74	0.698	1.10	0.0853	0.73	0.66	579	32	527	7	537	9	8.92
ZR18R1	0.02	0.153	72464	0.05790	0.64	0.674	1.29	0.0844	1.06	0.82	526	28	522	11	523	10	0.65
ZR19C	**0.01**	**0.136**	**169937**	**0.05827**	**0.46**	**0.703**	**0.81**	**0.0875**	**0.56**	**0.69**	**540**	**20**	**541**	**6**	**541**	**7**	**-0.20**
ZR20R2	**0.03**	**0.130**	**55915**	**0.05866**	**1.09**	**0.706**	**1.66**	**0.0872**	**1.20**	**0.72**	**554**	**47**	**539**	**12**	**542**	**14**	**2.74**
ZR20O1	0.03	0.138	62056	0.05985	1.00	0.694	1.68	0.0841	1.30	0.77	598	43	520	13	535	14	13.00
ZR21C	**0.01**	**0.584**	**165363**	**0.05768**	**1.10**	**0.713**	**1.43**	**0.0896**	**0.83**	**0.58**	**517**	**48**	**553**	**9**	**546**	**12**	**-6.93**
ZR21R1	**0.01**	**0.395**	**123609**	**0.05853**	**0.47**	**0.715**	**1.10**	**0.0886**	**0.92**	**0.84**	**549**	**21**	**547**	**10**	**548**	**9**	**0.39**
ZR21O1	**0.05**	**0.362**	**30722**	**0.05747**	**1.12**	**0.693**	**1.57**	**0.0874**	**1.04**	**0.66**	**510**	**49**	**540**	**11**	**535**	**13**	**-6.03**
ZR22C	0.03	0.441	57122	0.05844	0.89	0.664	1.39	0.0824	1.00	0.72	546	39	510	10	517	11	6.60
ZR22R1	0.02	0.473	86124	0.05822	0.73	0.682	1.09	0.0850	0.73	0.66	538	32	526	7	528	9	2.24
ZR23C	0.01	0.493	111052	0.05830	0.69	0.692	1.05	0.0860	0.69	0.66	541	30	532	7	534	9	1.71
ZR23O1	0.05	0.495	31560	0.05773	2.03	0.672	3.07	0.0844	2.28	0.74	519	88	523	23	522	25	-0.62
ZR23R1	0.04	0.440	35881	0.05998	0.92	0.691	1.48	0.0835	1.10	0.74	603	40	517	11	533	12	14.19
ZR24R2	0.03	0.122	59702	0.05868	0.91	0.678	1.37	0.0838	0.95	0.69	555	40	519	9	525	11	6.59
ZR25R2	0.03	0.211	53911	0.05829	1.04	0.668	1.40	0.0831	0.86	0.62	541	45	514	9	519	11	4.88
ZR25C	0.12	1.749	13059	0.06373	0.62	0.715	1.13	0.0814	0.87	0.77	733	26	504	8	548	10	31.14
ZR29C	**0.01**	**0.696**	**131204**	**0.05904**	**0.34**	**0.733**	**0.86**	**0.0900**	**0.70**	**0.81**	**569**	**15**	**556**	**7**	**558**	**7**	**2.28**
ZR29O2	**0.02**	**0.146**	**75629**	**0.05751**	**1.07**	**0.708**	**1.70**	**0.0893**	**1.26**	**0.74**	**511**	**47**	**552**	**13**	**544**	**14**	**-7.91**
ZR30C	**0.00**	**0.157**	**325658**	**0.05797**	**0.32**	**0.698**	**0.88**	**0.0873**	**0.73**	**0.83**	**529**	**14**	**540**	**8**	**538**	**7**	**-2.14**
ZR30O2	0.19	0.529	8190	0.07304	2.60	1.031	3.20	0.1023	1.83	0.57	1015	104	628	22	719	33	38.13
ZR30O1	0.03	0.248	56923	0.05778	0.83	0.678	1.36	0.0850	1.01	0.74	521	36	526	10	525	11	-0.91
ZR31C	1.89	1.081	824	0.10805	2.19	1.347	2.68	0.0904	1.50	0.56	1767	79	558	16	866	31	68.43

Sample EVES01 (cont.)	f206 (%)	Th/U	$^{206}Pb/^{204}Pb$ ratio	$^{207}Pb/^{206}Pb$ ratio	1σ (%)	$^{207}Pb/^{235}U$ ratio	1σ (%)	$^{206}Pb/^{238}U$ ratio	1σ (%)	Error corr. (ρ)	$^{207}Pb/^{206}Pb$ age (Ma)	2σ (Ma)	$^{207}Pb/^{235}U$ age (Ma)	2σ (Ma)	$^{206}Pb/^{238}U$ age (Ma)	2σ (Ma)	Disc. (%)
ZR31O1	0.03	0.103	55882	0.05756	1.15	0.675	1.67	0.0851	1.16	0.69	513	50	526	12	524	14	-2.58
ZR31R1	**0.93**	**0.263**	**1680**	**0.05794**	**1.21**	**0.712**	**1.54**	**0.0891**	**0.88**	**0.57**	**528**	**52**	**550**	**9**	**546**	**13**	**-4.30**
ZR32C	0.03	0.335	60479	0.05894	1.12	0.708	1.76	0.0871	1.30	0.74	565	49	538	13	543	15	4.67
ZR32O1	**0.04**	**0.489**	**36561**	**0.05783**	**1.67**	**0.704**	**2.58**	**0.0883**	**1.93**	**0.75**	**523**	**72**	**546**	**20**	**541**	**22**	**-4.25**
ZR32R1	0.02	0.216	97708	0.05797	0.49	0.680	0.93	0.0851	0.70	0.75	529	21	526	7	527	8	0.45
ZR33R1	0.02	0.426	84772	0.05865	0.63	0.691	1.01	0.0854	0.70	0.69	554	27	529	7	533	8	4.64
ZR33O1	0.01	0.519	120810	0.05888	0.54	0.677	1.17	0.0834	0.97	0.83	563	23	517	10	525	10	8.20
ZR35C	0.02	0.258	90035	0.05972	0.47	0.691	0.82	0.0839	0.56	0.68	593	20	519	6	533	7	12.44
ZR36R1	0.03	7.497	52343	0.06846	1.52	0.859	1.86	0.0910	1.02	0.55	883	62	562	11	630	17	36.38
ZR37O1	0.04	0.127	37761	0.05942	1.32	0.674	1.89	0.0823	1.30	0.69	582	57	510	13	523	15	12.46
ZR38C	0.03	0.165	61253	0.05779	0.66	0.662	1.04	0.0831	0.72	0.68	522	29	515	7	516	8	1.37
ZR38O1	0.03	0.098	58630	0.05742	1.29	0.650	1.81	0.0821	1.22	0.67	508	56	509	12	509	14	-0.21
ZR38R1	0.03	0.099	55170	0.05814	1.00	0.662	1.48	0.0826	1.02	0.69	535	44	512	10	516	12	4.37
ZR39C	0.01	1.173	210454	0.05816	0.58	0.674	0.95	0.0840	0.65	0.69	536	25	520	7	523	8	2.94
ZR39R	**0.03**	**0.700**	**54182**	**0.05881**	**1.14**	**0.728**	**1.68**	**0.0898**	**1.18**	**0.70**	**560**	**49**	**554**	**13**	**556**	**14**	**0.98**
ZR40C	**0.00**	**0.510**	**415461**	**0.05867**	**0.43**	**0.721**	**0.87**	**0.0892**	**0.66**	**0.76**	**555**	**19**	**551**	**7**	**551**	**7**	**0.80**
ZR41C	0.01	0.278	120444	0.05771	0.61	0.694	0.98	0.0871	0.67	0.68	519	27	539	7	535	8	-3.81
ZR41	0.03	0.132	60955	0.05904	1.02	0.687	1.52	0.0844	1.07	0.70	569	44	523	11	531	13	8.11
ZR42R	0.04	0.134	36744	0.05774	1.74	0.682	2.51	0.0856	1.76	0.70	520	76	530	18	528	21	-1.86
ZR43C	0.01	0.671	188213	0.06264	0.63	0.715	1.07	0.0828	0.78	0.73	696	27	513	8	548	9	26.29
ZR43R	0.02	0.293	72431	0.05878	0.95	0.683	1.21	0.0843	0.65	0.54	559	41	521	7	529	10	6.68

Sample EVES12	f206 (%)	Th/U	$^{206}Pb/^{204}Pb$ ratio	$^{207}Pb/^{206}Pb$ ratio	1σ (%)	$^{207}Pb/^{235}U$ ratio	1σ (%)	$^{206}Pb/^{238}U$ ratio	1σ (%)	Error corr. (ρ)	$^{207}Pb/^{206}Pb$ age (Ma)	2σ (Ma)	$^{207}Pb/^{235}U$ age (Ma)	2σ (Ma)	$^{206}Pb/^{238}U$ age (Ma)	2σ (Ma)	Disc. (%)
ZR1C	0.15	0.828	10638	0.07404	1.88	1.339	2.69	0.1311	1.89	0.70	1043	75	794	28	863	31	23.81
ZR2R1	0.11	0.120	13962	0.06765	3.37	0.566	4.71	0.0607	3.27	0.69	858	137	380	24	456	34	55.73
ZR2C	0.07	0.170	23327	0.05390	2.37	0.616	4.39	0.0828	3.67	0.84	367	105	513	36	487	34	-39.75
ZR301	0.66	0.102	2356	0.06326	1.17	0.681	1.99	0.0781	1.56	0.79	717	49	485	15	527	16	32.39
ZR3C	0.51	0.095	3071	0.06924	1.72	0.904	2.48	0.0946	1.75	0.70	906	70	583	19	654	24	35.65
ZR4C	0.03	0.748	62026	0.08046	1.24	1.742	2.98	0.1571	2.69	0.90	1208	48	940	47	1024	38	22.17
ZR4O1	0.08	0.379	19029	0.07417	0.64	1.259	1.55	0.1231	1.36	0.88	1046	26	748	19	827	17	28.45
ZR5C	0.02	0.416	92153	0.07332	0.32	1.509	0.92	0.1492	0.78	0.84	1023	13	897	13	934	11	12.34
ZR5R1	0.04	0.742	42577	0.06672	1.09	0.915	2.70	0.0995	2.44	0.90	829	45	611	28	660	26	26.27
ZR6C	0.01	0.172	137109	0.06536	1.03	0.367	3.49	0.0407	3.31	0.95	786	43	257	17	318	19	67.25
ZR6R1	0.03	0.891	51850	0.07505	1.32	1.753	1.88	0.1694	1.28	0.68	1070	53	1009	24	1028	24	5.69
ZR7C	1.08	1.556	1440	0.07771	1.80	1.097	3.49	0.1024	2.96	0.85	1139	71	628	35	752	37	44.87
ZR8C	0.03	0.918	56134	0.06977	1.64	1.329	2.39	0.1381	1.70	0.71	922	67	834	27	858	28	9.49
ZR8R1	0.12	5.558	13245	0.07750	1.31	1.575	2.42	0.1473	2.00	0.83	1134	52	886	33	960	30	21.86
ZR8O2	0.08	2.870	20660	0.07633	2.28	1.378	3.68	0.1309	2.87	0.78	1104	90	793	43	880	43	28.13
ZR9C	**0.01**	**0.158**	**152923**	**0.05563**	**2.12**	**0.573**	**3.17**	**0.0747**	**2.33**	**0.73**	**438**	**93**	**464**	**21**	**460**	**23**	**-6.05**
ZR9R1	0.03	0.817	56195	0.06408	1.81	0.949	3.06	0.1074	2.44	0.80	744	76	657	30	677	30	11.66
ZR10R	0.11	0.209	14128	0.06715	1.12	0.730	1.65	0.0788	1.15	0.70	842	46	489	11	556	14	41.96
ZR11R2	**0.02**	**0.139**	**81386**	**0.05719**	**1.31**	**0.604**	**2.05**	**0.0766**	**1.54**	**0.75**	**499**	**57**	**476**	**14**	**480**	**16**	**4.67**
ZR12C	0.33	0.368	4717	0.08534	1.89	1.244	2.54	0.1058	1.65	0.65	1323	72	648	20	821	28	51.03
ZR12O1	0.02	0.144	100616	0.06450	0.43	0.870	1.04	0.0979	0.88	0.84	758	18	602	10	636	10	20.59
ZR13	0.60	0.368	2612	0.06306	1.42	0.598	3.59	0.0688	3.28	0.91	710	60	429	27	476	27	39.58
ZR13R1	**0.02**	**0.361**	**71019**	**0.05635**	**1.74**	**0.584**	**3.84**	**0.0752**	**3.41**	**0.89**	**466**	**76**	**467**	**31**	**467**	**29**	**-0.27**
ZR13O1	**0.04**	**0.184**	**39922**	**0.05833**	**1.45**	**0.611**	**2.03**	**0.0759**	**1.38**	**0.68**	**542**	**63**	**472**	**13**	**484**	**16**	**12.99**

Sample EVES12 (cont.)	f206 (%)	Th/U	$^{206}Pb/^{204}Pb$ ratio	$^{207}Pb/^{206}Pb$ ratio	1σ (%)	$^{207}Pb/^{235}U$ ratio	1σ (%)	$^{206}Pb/^{238}U$ ratio	1σ (%)	Error corr. (ρ)	$^{207}Pb/^{206}Pb$ age (Ma)	2σ (Ma)	$^{207}Pb/^{235}U$ age (Ma)	2σ (Ma)	$^{206}Pb/^{238}U$ age (Ma)	2σ (Ma)	Disc. (%)
ZR14C	0.10	0.598	16037	0.07799	2.36	1.370	3.54	0.1274	2.62	0.74	1147	92	773	38	876	41	32.59
ZR15C	0.20	0.200	7733	0.06549	0.52	0.865	1.41	0.0958	1.26	0.89	790	22	590	14	633	13	25.37
ZR15R1	0.11	0.040	14641	0.05964	0.38	0.713	1.12	0.0867	0.99	0.88	591	16	536	10	547	9	9.19
ZR16C	0.17	0.232	9317	0.06834	0.57	1.082	1.93	0.1148	1.81	0.94	879	24	701	24	745	20	20.27
ZR16O2	0.02	0.239	62753	0.05864	0.86	0.566	2.97	0.0700	2.82	0.95	554	37	436	24	455	22	21.20
ZR17O1	0.08	0.412	18454	0.06500	1.11	0.933	4.63	0.1041	4.48	0.97	774	46	638	54	669	45	17.56
ZR17O2	0.57	1.339	2754	0.06737	1.70	0.941	2.49	0.1013	1.78	0.71	849	70	622	21	673	24	26.75
ZR18C	0.05	0.641	31739	0.07250	1.33	1.671	3.02	0.1672	2.68	0.89	1000	54	996	49	998	38	0.35
ZR19C	0.17	0.899	9291	0.07991	2.62	1.890	3.28	0.1715	1.93	0.59	1195	102	1021	36	1078	43	14.59
ZR19O2	0.06	1.084	27046	0.07080	0.89	1.197	2.01	0.1226	1.76	0.88	952	36	746	25	799	22	21.64
ZR20C	0.08	0.300	19308	0.07021	0.66	1.335	1.20	0.1379	0.93	0.77	934	27	833	14	861	14	10.86
ZR21O1	0.02	1.149	69797	0.07592	1.58	1.803	2.31	0.1722	1.63	0.71	1093	63	1024	31	1046	30	6.29
ZR21R1	0.04	0.633	38502	0.06980	1.78	1.625	2.52	0.1688	1.73	0.69	923	72	1005	32	980	31	-8.99
ZR22C	1.79	0.645	864	0.14890	2.10	3.480	2.47	0.1695	1.25	0.51	2333	71	1009	23	1523	39	56.75
ZR23C	0.02	0.792	72202	0.07686	0.66	1.675	1.36	0.1580	1.13	0.83	1118	26	946	20	999	17	15.37
ZR24C	0.01	0.613	246103	0.07462	0.26	1.675	0.73	0.1628	0.57	0.78	1058	11	972	10	999	9	8.12
ZR25R1	0.05	0.610	32660	0.07331	0.44	1.392	1.26	0.1377	1.12	0.89	1023	18	832	18	886	15	18.66
ZR26R1	0.02	0.319	74375	0.06913	0.63	1.101	2.66	0.1155	2.56	0.96	903	26	705	34	754	28	21.94
ZR26C	0.38	0.625	4099	0.07949	0.58	1.317	1.93	0.1202	1.81	0.93	1184	23	732	25	853	22	38.23
ZR28C	0.01	0.350	154505	0.07594	0.33	1.707	0.85	0.1630	0.69	0.81	1093	13	973	12	1011	11	10.97
ZR28R	0.12	0.790	13385	0.07903	1.40	1.508	2.10	0.1384	1.52	0.72	1173	55	835	24	933	25	28.77
ZR29R	**0.02**	**0.230**	**69699**	**0.05790**	**1.24**	**0.617**	**2.08**	**0.0773**	**1.62**	**0.78**	**526**	**54**	**480**	**15**	**488**	**16**	**8.77**
ZR30O2	0.11	0.512	13885	0.10484	3.39	1.528	4.81	0.1057	3.39	0.71	1712	122	648	42	942	58	62.16

Sample	f206 (%)	Th/U	$^{206}Pb/^{204}Pb$ ratio	$^{207}Pb/^{206}Pb$ ratio	1σ (%)	$^{207}Pb/^{235}U$ ratio	1σ (%)	$^{206}Pb/^{238}U$ ratio	1σ (%)	Error corr. (ρ)	$^{207}Pb/^{206}Pb$ age (Ma)	2σ (Ma)	$^{207}Pb/^{235}U$ age (Ma)	2σ (Ma)	$^{206}Pb/^{238}U$ age (Ma)	2σ (Ma)	Disc. (%)
91500	0.01	0.222	186883	0.07510	0.47	1.823	0.90	0.1761	0.67	0.74	1071	19	1045	13	1054	12	2.41
91500	0.01	0.223	276310	0.07445	0.51	1.795	0.95	0.1748	0.71	0.75	1054	20	1039	14	1044	12	1.42
91500	0.01	0.220	158271	0.07470	0.55	1.844	0.95	0.1790	0.68	0.72	1060	22	1062	13	1061	12	-0.12
91500	0.01	0.222	154540	0.07512	0.47	1.829	0.85	0.1765	0.60	0.70	1072	19	1048	12	1056	11	2.21
91500	0.01	0.223	129822	0.07503	0.56	1.823	1.08	0.1762	0.84	0.78	1069	23	1046	16	1054	14	2.18
91500	0.01	0.230	220325	0.07474	0.47	1.797	0.90	0.1744	0.68	0.75	1061	19	1036	13	1044	12	2.38
91500	0.04	0.235	40235	0.07545	0.90	1.792	1.44	0.1723	1.06	0.74	1081	36	1025	20	1043	19	5.18
91500	0.03	0.234	53354	0.07628	1.00	1.802	1.53	0.1713	1.11	0.72	1103	40	1020	21	1046	20	7.53
91500	0.03	0.230	56604	0.07421	1.02	1.768	1.46	0.1727	0.98	0.67	1047	41	1027	19	1034	19	1.93

Análises de química mineral em feldspatos

Massif	MSM	MSM	MSM	MSM	MSM	MSM	MSM	MSM	MSM	MSM	MSM	MSM
Rock Type	NS	NS	NS	NS	NS	NS	NS	NS	NS	NS	NS	NS
Sample	MS22	MS22	MS22	MS22	MS22	MS22	MS22	MS22	MS22	MS22	MS22	MS22
Spot no.	C3_1	C3_2	C3_4	C3_5	C3_5	C3_9	C4_11	C3_12	C3_13	C3_18	C3_25	C3_26
Feldspar	Albite	Albite	Albite	Albite	Albite	Albite	Albite	Albite	Albite	Albite	Albite	Albite
SiO_2	68.89	68.30	67.61	68.48	70.22	67.95	67.90	67.97	68.32	68.48	67.91	68.51
Al_2O_3	19.46	19.68	19.31	20.09	19.69	19.38	19.44	19.33	19.18	19.43	19.29	19.04
Fe_2O_3	0.14	0.06	0.40	0.07	0.40	0.01	0.51	0.44	0.38	0.30	0.29	0.14
CaO	0.10	0.06	0.11	0.13	0.14	0.08	0.12	0.16	0.13	0.12	0.05	0.10
Na_2O	11.99	10.85	11.91	10.86	8.51	11.36	11.70	10.63	11.44	10.96	10.97	10.66
K_2O	0.23	0.15	0.10	0.28	0.08	0.26	0.20	0.17	0.15	0.16	0.21	0.24
Total	100.80	99.11	99.44	99.90	99.03	99.04	99.87	98.69	99.59	99.45	98.72	98.68
mol.% end-members												
Ab mol %	98.30	98.78	98.95	97.73	98.50	98.12	98.34	98.19	98.51	98.46	98.50	98.06
An mol%	0.43	0.30	0.50	0.63	0.90	0.39	0.55	0.80	0.64	0.62	0.24	0.49
Or mol%	1.26	0.92	0.56	1.65	0.61	1.49	1.11	1.01	0.85	0.93	1.26	1.45

Análises de química mineral em feldspatos (cont.)

MSM	MSM	MSM	MSM	MSM	MSM	MSM	MSM	MSM	MSM	MSM	MSM	MSM
NS	NS	NS	NS	NS	NS	NS	NS	NS	NS	NS	NS	NS
MS88	MS88	MS88	MS122A	MS122A	MS122A	MS336B	MS336B	MS336B	MS336B	MS336B	MS336B	MS344A
C2_7	C2_9	C2_10	C4_3	C4_4	C4_20	C1_1	C1_2	C1_5	C1_5	C1_6	C1_6	C1_1
Albite	Albite	Albite	Albite	Albite	Albite	Albite	Albite	Albite	Albite	Albite	Albite	Albite
69.51	68.29	67.87	68.56	68.92	68.26	68.70	67.82	68.86	68.25	66.66	68.71	66.48
20.05	19.77	19.38	19.28	19.47	19.48	19.43	19.33	19.41	19.47	19.20	19.59	19.24
0.25	0.03	0.00	0.01	0.03	0.00	0.05	0.00	0.08	0.05	0.00	0.07	0.05
0.10	0.26	0.20	0.08	0.08	0.23	0.10	0.04	0.04	0.12	0.04	0.07	0.04
13.01	11.73	11.48	12.13	11.12	11.81	11.35	11.20	11.49	11.16	10.96	11.69	11.48
0.17	0.14	0.17	0.20	0.21	0.12	0.27	0.23	0.26	0.25	0.25	0.13	0.22
103.09	100.21	99.09	100.26	99.83	99.89	99.89	98.61	100.13	99.29	97.11	100.26	97.50
98.75	98.04	98.13	98.56	98.40	98.28	98.02	98.49	98.34	98.02	98.33	98.97	98.56
0.41	1.18	0.94	0.36	0.37	1.04	0.46	0.21	0.20	0.56	0.20	0.31	0.18
0.84	0.78	0.93	1.09	1.23	0.68	1.52	1.30	1.46	1.42	1.48	0.72	1.27

Análises de química mineral em feldspatos (cont.)

MSM NS MS344A C1_1 Albite	MSM NS MS344A C1_31 Albite	MSM AFS MS140 C1_20 Albite	MSM AFS MS319C C2_4 Albite	MSM AFS MS398 1 Albite	MSM AFS MS398 7 Albite	MSM AFS MS398 13 Albite	MSM AFS MS398 19 Albite	MSM AFS MS398 30 Albite	EM NMD EVES12 C1_5 Albite	EM NMD EVES12 C1_7 Albite	EM NMD EVES12 C1_9 Albite	EM NMD EVES12 C2_3(inc) Albite
71.01	67.11	68.37	69.27	68.95	69.21	69.83	68.88	69.26	66.12	65.58	66.32	65.73
19.98	19.32	19.42	19.60	19.17	19.48	19.41	19.31	19.30	20.91	20.80	20.96	20.83
0.08	0.06	0.00	0.07	0.03	0.02	0.02	0.00	0.03	0.02	0.02	0.03	0.08
0.05	0.05	0.13	0.08	0.06	0.04	0.01	0.05	0.07	1.63	1.58	1.59	1.65
11.91	11.73	11.08	11.66	11.54	11.49	11.60	11.47	11.34	10.76	10.76	10.89	11.17
0.28	0.29	0.16	0.15	0.18	0.29	0.22	0.20	0.25	0.34	0.15	0.31	0.24
103.30	98.56	99.16	100.84	99.93	100.52	101.11	99.91	100.24	99.77	98.89	100.10	99.69
98.28	98.17	98.44	98.76	98.74	98.20	98.69	98.63	98.27	90.53	91.69	90.95	91.26
0.23	0.23	0.61	0.39	0.27	0.18	0.07	0.25	0.32	7.57	7.46	7.35	7.44
1.49	1.60	0.94	0.85	0.99	1.62	1.25	1.12	1.41	1.89	0.85	1.69	1.30

Análises de química mineral em feldspatos (cont.)

EM	EM	EM	EM	EM	EM	EM	EM	EM	EM	EM	EM
NMD	NMD	NMD	NMD	NMS	NMS	NMS	NMS	NMS	NMS	NMS	NMS
EVES12	EVES12	EVES12	EVES12	EVES05	EVES05	EVES05	EVES05	EVES05	EVES05	EVES05	EVES05
C2_7(inc)	C3_11(inc)	C3_12	C3_12(inc)	2	4	5	7	8	9	11	15
Albite	Albite	Albite	Albite	Oligoclase	Oligoclase	Oligoclase	Oligoclase	Albite	Oligoclase	Oligoclase	Oligoclase
65.43	64.99	65.09	65.46	65.37	64.29	65.38	63.95	68.48	64.47	65.10	64.89
20.94	20.64	20.77	20.57	22.67	23.08	22.46	22.59	19.94	22.56	22.94	22.95
0.28	0.07	0.03	0.20	0.06	0.01	0.04	0.02	0.02	0.04	0.00	0.00
1.75	1.57	1.63	1.62	3.47	3.79	3.21	3.68	0.41	3.48	3.36	3.40
10.52	10.40	11.07	10.76	10.24	9.71	10.06	9.63	11.66	9.56	9.95	9.73
0.68	0.39	0.38	0.18	0.11	0.13	0.09	0.09	0.06	0.10	0.10	0.12
99.60	98.06	98.96	98.78	101.91	101.02	101.24	99.96	100.56	100.21	101.45	101.09
88.17	90.22	90.61	91.40	83.76	81.65	84.56	82.15	97.79	82.75	83.78	83.23
8.09	7.54	7.36	7.62	15.67	17.61	14.94	17.33	1.90	16.67	15.65	16.08
3.74	2.24	2.03	0.98	0.58	0.74	0.50	0.52	0.31	0.58	0.57	0.69

Análises de química mineral em feldspatos (cont.)

EM	EM	EM	EM	EM	EM	EM	EM	EM	EM	EM	EM
NMS	NMS	NMS	NMS	NMS	NMS	NMS	NS	NS	NS	NS	NS
EVES05	EVES063	EVES063	EVES063	EVES063	EVES063	EVES06B3	EVES06B1	EVES06B1	EVES06B2	EVES14	EVES14
17	1	2	5	4	10	14	2	3	2	2	4
Oligoclase	Oligoclase	Oligoclase	Oligoclase	Oligoclase	Albite	Oligoclase	Albite	Albite	Albite	Albite	Albite
64.28	63.06	64.22	63.89	65.09	64.80	65.78	69.10	67.56	66.75	67.32	67.37
23.13	22.02	22.56	22.14	21.73	21.47	21.95	19.52	19.95	19.60	19.29	19.15
0.00	0.00	0.01	0.00	0.00	0.00	0.00	0.02	0.00	0.02	0.01	0.09
3.70	2.81	3.04	2.96	2.41	2.19	2.38	0.16	0.43	0.49	0.25	0.25
10.09	10.33	10.39	9.91	10.57	10.91	10.26	12.07	12.13	11.61	11.48	11.53
0.16	0.12	0.34	0.36	0.16	0.19	0.12	0.09	0.10	0.09	0.23	0.18
101.35	98.35	100.56	99.26	99.96	99.54	100.49	100.95	100.17	98.56	98.57	98.58
82.46	86.36	84.53	84.09	88.06	89.11	88.04	98.82	97.55	97.24	97.54	97.81
16.71	12.97	13.66	13.88	11.08	9.88	11.31	0.72	1.92	2.28	1.16	1.16
0.84	0.67	1.81	2.03	0.85	1.01	0.65	0.46	0.53	0.47	1.30	1.03

Análises de química mineral em feldspatos (cont.)

EM NS EVES146 Albite	EM NS EVES373 Albite	EM NS EVES374 Albite	EM NS EVES392 Albite	EM NS EVES393 Albite	EM NS EVES442 Albite	EM NS EVES443 Albite	EM NS EVES445 Albite	EM NS EVES501 (inc) Albite	EM NS EVES502 (inc) Albite	EM NS EVES503 (inc) Albite	EM NS EVES504 (inc) Albite	EM NS EVES501 Albite
68.94	68.41	68.88	66.60	67.92	66.45	68.81	68.68	65.86	66.72	67.02	67.51	67.20
19.43	19.79	19.50	20.88	20.97	20.19	19.84	19.94	20.82	21.01	20.83	21.10	21.00
0.00	0.06	0.05	0.06	0.02	0.05	0.02	0.00	0.00	0.01	0.05	0.07	0.00
0.13	0.36	0.44	1.43	1.25	0.69	0.36	0.62	1.35	1.31	1.42	1.48	1.34
12.03	12.11	11.52	10.99	11.28	11.85	11.89	11.98	11.13	11.16	10.97	11.29	11.54
0.07	0.05	0.10	0.23	0.24	0.22	0.11	0.22	0.17	0.21	0.09	0.11	0.16
100.61	100.79	100.48	100.19	101.67	99.46	101.04	101.44	99.33	100.41	100.37	101.56	101.25
99.01	98.12	97.39	92.11	93.03	95.72	97.74	96.07	92.85	92.86	92.89	92.69	93.15
0.59	1.59	2.03	6.62	5.68	3.10	1.64	2.75	6.24	6.01	6.63	6.71	5.98
0.40	0.29	0.58	1.27	1.29	1.18	0.62	1.18	0.91	1.13	0.48	0.60	0.87

Análises de química mineral em feldspatos (cont.)

EM NS EVES50 2 Albite	EM NS EVES50 3 Albite	EM NS EVES50 5 Albite	EM AFS EVES02 C1_3 Albite	EM AFS EVES03A C10_2 Albite	EM AFS EVES4C C1_2 Albite	EM AFS EVES4C C2_3 Albite	EM AFS EVES4C C2_6 Albite	EM AFS EVES4C C3_7 Albite	EM AFS EVES4C C3_8 Albite	EM AFS EVES06A 1 Albite	EM AFS EVES06A 3 Albite	EM AFS EVES06A 6 Albite
66.22	65.79	67.09	66.89	67.08	66.84	68.51	69.42	67.74	68.22	69.62	69.52	68.98
20.70	20.76	21.27	19.55	19.31	19.83	19.81	19.78	19.25	19.70	19.63	19.89	19.60
0.00	0.05	0.01	0.03	0.11	0.07	0.05	0.07	0.07	0.07	0.01	0.01	0.03
0.79	0.88	1.24	0.23	0.28	0.56	0.64	0.49	0.20	0.25	0.13	0.38	0.10
11.84	11.40	11.48	11.39	11.38	11.65	11.37	11.58	11.85	12.07	12.24	12.08	12.28
0.09	0.52	0.11	0.14	0.14	0.14	0.19	0.21	0.09	0.13	0.06	0.11	0.05
99.65	99.40	101.20	98.23	98.31	99.10	100.56	101.56	99.21	100.44	101.68	102.00	101.05
95.97	93.23	93.83	98.12	97.87	96.64	95.98	96.57	98.57	98.17	99.10	97.70	99.29
3.56	3.97	5.58	1.10	1.34	2.58	2.97	2.27	0.94	1.13	0.58	1.70	0.46
0.47	2.80	0.59	0.78	0.79	0.78	1.05	1.16	0.49	0.70	0.31	0.60	0.25

Análises de química mineral em feldspatos (cont.)

Massif	MSM	MSM	MSM	MSM	MSM	MSM	MSM	MSM	MSM	MSM
Rock Type	NS	NS	NS	NS	NS	NS	NS	NS	NS	NS
Sample	MS22	MS22	MS22	MS22	MS22	MS22	MS22	MS22	MS22	MS88
Spot no.	C3_2	C3_3	C3_6	C3_8	C3_8	C3_10	C3_11	C3_14	C3_18	C2_2
Feldspar	Microcline	Microcline	Microcline	Microcline	Microcline	Microcline	Microcline	Microcline	Microcline	Microcline
SiO_2	63.49	63.91	64.44	64.42	64.85	65.02	66.07	64.70	64.90	64.04
Al_2O_3	18.02	18.11	18.31	18.24	18.55	18.26	18.84	18.21	18.12	18.37
Fe_2O_3	0.00	0.23	0.05	0.07	0.02	0.09	0.07	0.02	0.04	0.05
CaO	0.01	0.00	0.01	0.01	0.02	0.00	0.00	0.00	0.00	0.05
Na_2O	0.50	0.37	0.71	0.93	0.70	0.84	0.86	0.90	0.72	0.65
K_2O	16.14	16.23	15.38	15.49	15.67	15.45	13.85	15.24	15.57	15.52
Total	98.16	98.86	98.90	99.16	99.81	99.65	99.70	99.07	99.36	98.68
mol.% end-members										
Ab mol %	4.53	3.35	6.59	8.39	6.35	7.61	8.66	8.19	6.59	5.99
An mol%	0.03	0.01	0.06	0.05	0.11	0.00	0.00	0.01	0.00	0.26
Or mol%	95.44	96.64	93.35	91.56	93.54	92.39	91.34	91.80	93.41	93.75

Análises de química mineral em feldspatos (cont.)

MSM NS MS88 C2_7 Microcline	MSM NS MS88 C2_7 Microcline	MSM NS MS88 C2_9 Microcline	MSM NS MS88 C2_9 Microcline	MSM NS MS88 C2_11 Microcline	MSM NS MS88 C2_12 Microcline	MSM NS MS88 C2_13 Microcline	MSM NS MS122A C4_5 Microcline	MSM NS MS122A C4_8 Microcline	MSM NS MS122A C4_9 Microcline	MSM NS MS122A C4_10 Microcline
64.52	64.61	64.88	63.54	63.91	64.86	65.09	64.21	65.32	64.50	64.53
18.72	18.59	18.53	18.26	18.35	18.44	18.46	18.19	18.64	18.55	18.37
0.03	0.03	0.02	0.02	0.00	0.00	0.02	0.00	0.04	0.02	0.00
0.00	0.00	0.06	0.03	0.04	0.00	0.03	0.01	0.03	0.00	0.00
1.03	0.75	1.05	0.76	0.83	0.79	1.08	0.85	0.93	0.96	1.17
15.41	15.51	15.49	15.64	15.45	15.78	15.31	15.49	15.49	15.59	15.07
99.71	99.50	100.04	98.25	98.57	99.88	99.99	98.74	100.44	99.61	99.13
9.21	6.88	9.34	6.89	7.52	7.10	9.64	7.65	8.32	8.58	10.52
0.00	0.00	0.31	0.14	0.18	0.00	0.15	0.04	0.14	0.00	0.00
90.79	93.12	90.35	92.96	92.30	92.90	90.21	92.31	91.55	91.42	89.48

Análises de química mineral em feldspatos (cont.)

MSM NS MS122A C4_11 Microcline	MSM NS MS122A C4_12 Microcline	MSM NS MS122A C4_13 Microcline	MSM NS MS336B C1_1 Microcline	MSM NS MS336B C1_2 Microcline	MSM NS MS336B C1_3 Microcline	MSM NS MS336B C1_4 Microcline	MSM NS MS336B C1_5 Microcline	MSM NS MS336B C1_10 Microcline	MSM NS MS344A C1_1 Microcline	MSM NS MS344A C1_1 Microcline
64.89	64.34	64.83	64.12	64.64	64.74	64.07	64.64	64.74	64.35	63.98
18.57	18.30	18.57	18.14	18.52	18.52	18.33	18.39	18.31	18.45	18.32
0.00	0.08	0.00	0.09	0.12	0.11	0.09	0.12	0.11	0.04	0.19
0.00	0.03	0.04	0.00	0.00	0.01	0.00	0.04	0.01	0.00	0.00
0.66	0.93	1.30	1.27	0.85	0.74	0.83	0.75	0.85	0.84	1.04
15.82	15.72	15.21	14.66	15.68	15.39	15.53	15.94	15.46	15.57	15.15
99.93	99.38	99.95	98.28	99.81	99.51	98.85	99.88	99.46	99.26	98.69
5.93	8.22	11.50	11.61	7.65	6.84	7.54	6.68	7.70	7.55	9.45
0.00	0.12	0.21	0.00	0.00	0.05	0.01	0.19	0.03	0.00	0.00
94.07	91.66	88.29	88.39	92.35	93.11	92.45	93.13	92.27	92.45	90.55

Análises de química mineral em feldspatos (cont.)

MSM	MSM	MSM	MSM	MSM	MSM	MSM	MSM	MSM	MSM	MSM
NS	NS	NS	NS	NS	NS	NS	AFS	AFS	AFS	AFS
MS344A	MS344A	MS344A	MS344A	MS344A	MS344A	MS344A	MS140	MS140	MS319C	MS398
C1_3	C1_5	C1_7	C1_10	C1_18	C1_32	C1_34	C1_4	C1_5	C2_1	3
Microcline	Microcline	Microcline	Microcline	Microcline	Microcline	Microcline	Microcline	Microcline	Microcline	Microcline
63.82	63.51	64.72	63.11	64.48	64.06	63.96	63.97	63.25	64.18	64.93
18.57	19.07	18.43	18.17	18.16	18.04	18.33	18.59	18.54	18.82	18.52
0.02	0.55	0.01	0.16	0.13	0.07	0.04	0.13	0.05	0.20	0.05
0.00	0.17	0.00	0.00	0.01	0.00	0.00	0.01	0.02	0.01	0.00
1.48	1.87	1.03	1.25	1.07	0.66	1.12	0.99	0.79	1.16	0.99
14.40	14.77	15.06	15.34	15.25	15.99	15.33	15.00	15.97	15.17	15.11
98.29	99.93	99.25	98.03	99.09	98.82	98.77	98.69	98.61	99.53	99.60
13.48	16.03	9.44	11.05	9.66	5.94	9.98	9.07	6.98	10.41	9.02
0.00	0.79	0.02	0.00	0.04	0.00	0.00	0.06	0.10	0.04	0.00
86.52	83.17	90.54	88.95	90.30	94.06	90.02	90.88	92.92	89.55	90.98

Análises de química mineral em feldspatos (cont.)

MSM AFS MS398 8 Microcline	MSM AFS MS398 14 Microcline	MSM AFS MS398 18 Microcline	MSM AFS MS398 31 Microcline	EM NMD EVES12 C1_1 Microcline	EM NMD EVES12 C1_6 Microcline	EM NMD EVES12 C1_8 Microcline	EM NMS EVES05 3 Microcline	EM NMS EVES05 6 Microcline	EM NMS EVES05 10 Microcline	EM NMS EVES05 12 Microcline
64.41	64.87	65.04	64.11	64.26	64.24	64.44	65.29	65.21	66.20	66.54
18.60	18.64	18.77	18.53	19.54	18.88	18.72	18.67	18.58	19.10	19.22
0.00	0.02	0.00	0.01	0.00	0.05	0.00	0.00	0.00	0.05	0.00
0.02	0.00	0.03	0.00	0.15	0.11	0.11	0.09	0.00	0.30	0.05
1.28	1.13	1.19	0.99	2.12	2.10	2.18	2.88	1.16	3.57	2.99
15.15	15.38	15.43	15.07	12.80	12.66	12.95	12.96	15.56	10.89	11.96
99.47	100.04	100.45	98.71	98.86	98.05	98.39	99.88	100.50	100.11	100.76
11.39	10.03	10.45	9.04	19.97	20.02	20.22	25.13	10.18	32.76	27.46
0.09	0.00	0.16	0.00	0.75	0.57	0.55	0.43	0.00	1.52	0.26
88.51	89.97	89.39	90.96	79.27	79.41	79.22	74.44	89.82	65.71	72.27

Análises de química mineral em feldspatos (cont.)

EM NMS EVES06B3 3 Microcline	EM NMS EVES06B3 4 Microcline	EM NMS EVES06B3 7 Microcline	EM NMS EVES06B3 11 Microcline	EM NMS EVES06B3 13 Microcline	EM NS EVES06B1 1 Microcline	EM NS EVES06B1 4 Microcline	EM NS EVES06B2 1 Microcline	EM NS EVES06B2 3 Microcline	EM NS EVES14 1 Microcline	EM NS EVES14 5 Microcline	EM NS EVES37 1 Microcline
65.03	63.97	65.79	64.69	63.51	66.16	66.20	64.99	64.71	65.23	66.48	64.63
18.58	18.69	18.90	18.74	18.71	18.60	18.63	18.81	18.35	18.39	18.62	18.58
0.04	0.07	0.00	0.00	0.04	0.02	0.00	0.02	0.03	0.01	0.12	0.02
0.03	0.06	0.02	0.05	0.03	0.00	0.01	0.04	0.00	0.02	0.00	0.00
2.06	1.39	1.84	1.13	1.29	1.09	1.19	0.74	0.81	1.32	2.07	0.69
14.05	14.67	14.70	15.02	14.89	15.55	15.39	15.99	15.80	15.15	14.46	15.76
99.79	98.85	101.24	99.63	98.47	101.41	101.42	100.58	99.69	100.12	101.74	99.69
18.19	12.55	15.97	10.20	11.62	9.60	10.52	6.54	7.23	11.71	17.83	6.26
0.14	0.29	0.09	0.25	0.16	0.00	0.03	0.18	0.00	0.11	0.00	0.00
81.66	87.16	83.94	89.55	88.22	90.40	89.45	93.28	92.77	88.17	82.17	93.74

Análises de química mineral em feldspatos (cont.)

EM NS EVES39 1 Microcline	EM NS EVES39 5 Microcline	EM NS EVES44 1 Microcline	EM NS EVES44 4 Microcline	EM NS EVES44 6 Microcline	EM AFS EVES4C C1_1 Microcline	EM AFS EVES4C C2_4 Microcline	EM AFS EVES4C C2_5 Microcline	EM AFS EVES4C C3_9 Microcline	EM AFS EVES4C C3_10 Microcline	EM AFS EVES06A 2 Microcline	EM AFS EVES06A 5 Microcline
64.34	64.70	64.35	65.46	65.88	64.50	66.02	65.84	66.52	65.67	66.38	65.21
18.75	18.84	18.36	18.42	18.48	18.47	18.34	18.66	18.51	18.57	18.49	18.76
0.09	0.03	0.04	0.02	0.00	0.15	0.00	0.02	0.05	0.13	0.02	0.02
0.04	0.02	0.00	0.00	0.02	0.02	0.00	0.00	0.00	0.01	0.02	0.00
1.40	1.81	1.12	1.75	1.76	0.95	0.73	1.01	0.72	0.89	0.84	0.78
14.20	13.57	15.48	14.69	14.83	15.51	16.13	15.54	16.15	15.69	15.64	15.68
98.82	98.96	99.36	100.34	100.96	99.59	101.22	101.08	101.95	100.96	101.38	100.45
13.01	16.84	9.90	15.31	15.25	8.51	6.40	9.02	6.36	7.89	7.50	7.06
0.21	0.09	0.00	0.00	0.08	0.09	0.00	0.00	0.00	0.05	0.08	0.00
86.78	83.07	90.10	84.69	84.67	91.40	93.60	90.98	93.64	92.06	92.42	92.94

Análises de química mineral em nefelina

Massif	MSM	MSM	MSM	MSM	MSM	MSM	MSM	MSM	MSM	MSM	MSM
Rock Type	NS	NS	NS	NS	NS	NS	NS	NS	NS	NS	NS
Sample	22	22	22	22	88	88	88	88	336B	336B	336B
Spot no.	C3_3	C3_7	C3_10	C3_17	C2_1	C2_5	C2_11	C2_12	C1_1	C1_2	C1_4
SiO_2	41.58	42.07	42.95	41.45	42.41	41.26	42.35	42.18	41.70	42.14	40.90
Al_2O_3	34.42	33.87	34.30	33.84	34.35	34.20	34.16	34.34	34.14	34.18	34.00
Fe_2O_3	0.06	0.19	0.21	0.20	0.08	0.11	0.11	0.12	0.11	0.16	0.14
CaO	0.29	0.29	0.30	0.28	0.24	0.17	0.20	0.21	0.05	0.12	0.12
Na_2O	16.26	16.27	17.03	16.52	16.90	16.80	16.53	17.01	16.17	16.55	16.15
K_2O	7.16	6.63	6.53	6.62	6.84	6.88	6.78	6.85	6.83	6.97	7.10
Total	99.77	99.31	101.32	98.92	100.81	99.43	100.13	100.72	99.00	100.12	98.40
Formula based in 32 oxygen atoms											
Si	8.08	8.19	8.20	8.12	8.15	8.05	8.18	8.12	8.14	8.15	8.06
Al	7.88	7.77	7.71	7.81	7.78	7.87	7.77	7.79	7.85	7.79	7.90
Fe	0.01	0.03	0.03	0.03	0.01	0.01	0.02	0.02	0.02	0.03	0.02
Ca	0.06	0.06	0.06	0.06	0.05	0.03	0.04	0.04	0.01	0.02	0.02
Na	6.12	6.14	6.30	6.27	6.29	6.36	6.19	6.35	6.12	6.21	6.17
K	1.78	1.64	1.59	1.65	1.67	1.71	1.67	1.68	1.70	1.72	1.78
mol.% end-members											
Ne	76.55	76.73	78.76	78.41	78.50	78.43	77.36	78.62	76.52	77.58	77.16
Ks	22.19	20.56	19.86	20.66	20.89	21.14	20.88	20.84	21.26	21.50	22.31
Qtz	1.25	2.71	1.38	0.92	0.61	0.43	1.76	0.54	2.22	0.92	0.53

Análises de química mineral em nefelina (cont.)

MSM NS 336B C1_9	MSM NS 344A C1_10	MSM NS 344A C1_16	MSM NS 344A C1_18	MSM NS 344A C1_33	MSM NS MS400 2	MSM NS MS400 3	MSM NS MS400 4	MSM NS MS400 5	MSM NS MS400 6	MSM NS MS400 7	MSM NS MS400 8	MSM NS MS400 9
41.83	40.86	41.20	42.01	40.98	41.79	42.04	42.13	42.03	41.76	41.79	42.29	42.81
34.01	34.12	33.58	33.81	33.59	33.80	33.61	33.61	33.81	33.47	33.84	34.18	33.74
0.13	0.19	0.10	0.21	0.10	0.09	0.00	0.05	0.09	0.06	0.07	0.07	0.26
0.12	0.14	0.17	0.13	0.16	0.13	0.12	0.06	0.11	0.07	0.08	0.04	0.07
16.60	16.33	16.35	16.02	16.48	16.92	16.15	16.65	16.78	16.59	16.29	16.55	14.98
6.76	7.32	6.84	6.75	6.90	7.12	6.88	7.03	7.19	7.07	6.96	7.09	6.78
99.44	98.95	98.24	98.92	98.20	99.85	98.81	99.54	100.01	99.01	99.03	100.23	98.64
8.14	8.03	8.13	8.20	8.10	8.13	8.22	8.20	8.16	8.18	8.17	8.17	8.33
7.80	7.90	7.81	7.78	7.82	7.75	7.74	7.71	7.73	7.72	7.79	7.78	7.74
0.02	0.02	0.02	0.03	0.01	0.01	0.00	0.01	0.01	0.01	0.01	0.01	0.04
0.02	0.03	0.04	0.03	0.03	0.03	0.02	0.01	0.02	0.02	0.02	0.01	0.01
6.26	6.22	6.25	6.06	6.31	6.38	6.12	6.28	6.31	6.30	6.17	6.20	5.65
1.68	1.83	1.72	1.68	1.74	1.77	1.72	1.75	1.78	1.77	1.74	1.75	1.68
78.29	76.94	78.06	75.77	78.08	78.04	76.54	78.13	77.78	77.95	77.11	77.49	70.66
20.99	22.69	21.48	21.01	21.49	21.62	21.46	21.71	21.93	21.86	21.69	21.83	21.04
0.72	0.37	0.46	3.22	0.42	0.34	2.00	0.16	0.29	0.19	1.19	0.68	8.30

Análises de química mineral em nefelina (cont.)

MSM NS MS400 10	MSM NS MS400 12	MSM AFS MS293 C1_2	MSM AFS 140 C1_3	MSM AFS MS293 C2_4	MSM AFS MS293 C3_8	MSM AFS MS293 C3_9	MSM AFS MS293 C3_10	MSM AFS MS293 11	MSM AFS MS293 12	MSM AFS MS293 13	MSM AFS MS293 14	MSM AFS MS293 16
42.66	42.24	42.88	42.43	42.11	41.68	41.72	41.64	43.14	42.33	43.37	42.89	43.11
33.23	34.07	34.33	33.88	33.57	33.53	33.14	33.76	33.54	34.05	34.11	34.25	34.05
0.12	0.10	0.02	0.08	0.01	0.02	0.02	0.00	0.03	0.06	0.04	0.05	0.02
1.51	0.14	0.07	0.46	0.02	0.02	0.03	0.08	0.02	0.05	0.06	0.10	0.05
14.58	17.13	16.75	15.89	16.79	16.64	16.73	16.93	16.87	16.71	16.89	16.82	16.61
7.52	7.03	6.87	6.24	6.46	6.56	6.81	6.77	6.46	6.77	6.64	6.46	6.66
99.62	100.70	100.91	98.97	98.96	98.45	98.44	99.17	100.07	99.97	101.11	100.56	100.49
8.29	8.14	8.21	8.24	8.22	8.18	8.21	8.14	8.31	8.19	8.27	8.22	8.27
7.61	7.74	7.74	7.76	7.72	7.76	7.68	7.77	7.61	7.76	7.67	7.74	7.70
0.02	0.01	0.00	0.01	0.00	0.00	0.00	0.00	0.01	0.01	0.01	0.01	0.00
0.32	0.03	0.01	0.10	0.00	0.00	0.01	0.02	0.00	0.01	0.01	0.02	0.01
5.49	6.40	6.22	5.99	6.35	6.33	6.38	6.41	6.30	6.27	6.25	6.25	6.18
1.86	1.73	1.68	1.55	1.61	1.64	1.71	1.69	1.59	1.67	1.62	1.58	1.63
68.63	78.46	77.72	74.83	79.40	79.18	78.82	79.01	78.79	78.33	78.10	78.15	77.20
23.31	21.19	20.97	19.34	20.08	20.54	21.11	20.78	19.85	20.87	20.19	19.75	20.37
8.06	0.35	1.31	5.83	0.51	0.28	0.07	0.21	1.37	0.80	1.71	2.10	2.43

Análises de química mineral em nefelina (cont.)

MSM AFS MS293 17	MSM AFS MS316C C1_2	MSM AFS MS316C C1_3	MSM AFS MS316C C1_4	MSM AFS MS316C 7	MSM AFS MS316C 8	MSM AFS MS316C 9	MSM AFS MS316C 10	MSM AFS 319C C2_2	MSM AFS 319C C2_3	MSM AFS MS365 2	MSM AFS MS365 3	MSM AFS MS365 4
41.52	41.97	42.44	42.79	41.95	41.85	42.37	42.21	41.92	42.14	42.67	42.38	42.30
33.58	33.73	33.91	34.30	33.60	34.10	33.70	33.63	34.19	34.17	33.91	33.94	33.97
0.01	0.05	0.04	0.09	0.08	0.01	0.00	0.09	0.15	0.28	0.05	0.03	0.05
0.10	0.10	0.00	0.03	0.01	0.00	0.03	0.00	0.08	0.10	0.02	0.02	0.04
16.93	16.28	16.44	16.63	16.41	16.34	16.55	16.24	16.73	16.54	16.70	16.85	16.50
6.71	7.04	7.01	7.23	7.36	6.91	7.07	7.36	6.62	6.24	6.71	6.75	6.84
98.84	99.17	99.83	101.06	99.41	99.22	99.72	99.53	99.69	99.48	100.06	99.98	99.69
8.14	8.19	8.22	8.20	8.19	8.15	8.22	8.22	8.13	8.17	8.24	8.20	8.20
7.76	7.76	7.74	7.74	7.73	7.83	7.71	7.72	7.82	7.81	7.71	7.74	7.76
0.00	0.01	0.01	0.01	0.01	0.00	0.00	0.01	0.03	0.05	0.01	0.00	0.01
0.02	0.02	0.00	0.01	0.00	0.00	0.01	0.00	0.02	0.02	0.00	0.00	0.01
6.44	6.16	6.17	6.17	6.21	6.17	6.23	6.13	6.29	6.22	6.25	6.32	6.20
1.68	1.75	1.73	1.77	1.83	1.72	1.75	1.83	1.64	1.54	1.65	1.67	1.69
79.12	76.98	77.14	77.18	77.19	77.16	77.82	76.64	78.67	77.75	78.09	78.96	77.51
20.63	21.91	21.64	22.10	22.78	21.48	21.88	22.84	20.50	19.29	20.65	20.83	21.14
0.25	1.11	1.22	0.72	0.03	1.36	0.30	0.52	0.84	2.96	1.26	0.21	1.34

Análises de química mineral em nefelina (cont.)

MSM AFS MS365 6	MSM AFS MS365 7	MSM AFS MS365 8	MSM AFS MS365 11	MSM AFS MS365 12	MSM AFS MS365 13	MSM AFS MS365 14	MSM AFS MS365 15	MSM AFS 398 4	MSM AFS 398 29	EM NMD EVES12 37	EM NMD EVES12 C1_2	EM NMD EVES12 C1_3
42.13	42.61	42.32	42.22	42.50	41.79	42.81	42.20	42.79	42.48	42.95	42.06	42.55
34.25	34.27	34.39	33.95	33.60	33.95	33.95	33.95	34.24	33.80	34.65	34.18	34.26
0.00	0.01	0.00	0.04	0.00	0.00	0.05	0.03	0.02	0.00	0.11	0.02	0.05
0.03	0.04	0.02	0.03	0.06	0.03	0.01	0.01	0.04	0.03	1.35	1.14	1.24
16.71	16.69	16.59	16.37	16.73	16.82	16.90	16.89	16.98	16.56	17.48	16.57	16.52
6.89	6.83	7.15	6.83	6.68	6.43	6.53	6.90	6.80	6.55	4.88	4.97	4.81
100.01	100.46	100.46	99.44	99.57	99.02	100.24	99.97	100.86	99.43	101.43	98.94	99.42
8.15	8.19	8.15	8.20	8.24	8.15	8.24	8.17	8.20	8.24	8.14	8.16	8.20
7.81	7.77	7.81	7.77	7.68	7.80	7.70	7.75	7.73	7.73	7.74	7.81	7.78
0.00	0.00	0.00	0.01	0.00	0.00	0.01	0.00	0.00	0.00	0.02	0.00	0.01
0.01	0.01	0.00	0.01	0.01	0.01	0.00	0.00	0.01	0.01	0.27	0.24	0.26
6.27	6.22	6.20	6.17	6.29	6.36	6.31	6.34	6.31	6.23	6.43	6.23	6.17
1.70	1.67	1.76	1.69	1.65	1.60	1.60	1.70	1.66	1.62	1.18	1.23	1.18
78.35	77.79	77.44	77.07	78.68	79.51	78.84	78.80	78.88	77.86	80.34	77.88	77.12
21.25	20.93	21.96	21.15	20.66	20.01	20.04	21.17	20.77	20.27	14.75	15.36	14.77
0.40	1.28	0.60	1.78	0.66	0.48	1.13	0.03	0.36	1.87	4.90	6.77	8.10

Análises de química mineral em nefelina (cont.)

EM NMD EVES12 C1_11	EM NMD EVES12 C2_1(inc)	EM NMD EVES12 C2_2(inc)	EM NMD EVES12 C2_5(inc)	EM NMD EVES12 C3_9(inc)	EM NMD EVES12 C3_14(inc)	EM NMS EVES05 1	EM NMS EVES05 2	EM NMS EVES05 3	EM NMS EVES05 4	EM NMS EVES05 5	EM NMS EVES05 6	EM NMS EVES05 7
42.59	42.37	42.33	41.97	42.27	41.96	42.87	42.48	42.67	42.82	43.15	43.09	42.84
34.26	34.09	34.35	33.56	33.78	33.88	34.23	33.88	34.18	34.37	34.35	34.64	34.21
0.09	0.15	0.08	0.18	0.02	0.19	0.05	0.02	0.00	0.02	0.00	0.00	0.00
1.17	1.27	1.35	1.18	1.18	1.22	0.72	0.66	0.85	0.91	0.82	0.77	0.83
16.35	16.43	16.46	16.46	16.11	16.10	16.37	16.13	16.34	16.85	16.63	16.22	16.36
4.85	4.69	4.80	4.72	4.71	4.70	6.37	6.20	6.15	6.03	6.33	6.18	6.21
99.31	99.00	99.37	98.06	98.06	98.04	100.61	99.37	100.19	101.00	101.28	100.90	100.44
8.21	8.20	8.16	8.21	8.24	8.19	8.22	8.23	8.20	8.18	8.22	8.21	8.22
7.78	7.77	7.81	7.73	7.76	7.80	7.73	7.73	7.74	7.74	7.71	7.78	7.73
0.01	0.03	0.01	0.03	0.00	0.03	0.01	0.00	0.00	0.00	0.00	0.00	0.00
0.24	0.26	0.28	0.25	0.25	0.26	0.15	0.14	0.18	0.19	0.17	0.16	0.17
6.11	6.16	6.16	6.24	6.09	6.10	6.08	6.06	6.09	6.24	6.14	5.99	6.08
1.19	1.16	1.18	1.18	1.17	1.17	1.56	1.53	1.51	1.47	1.54	1.50	1.52
76.36	77.03	76.95	78.02	76.08	76.19	76.03	75.75	76.13	77.97	76.74	74.90	76.03
14.90	14.48	14.75	14.71	14.64	14.63	19.47	19.16	18.86	18.36	19.23	18.78	19.00
8.74	8.49	8.30	7.26	9.28	9.18	4.50	5.10	5.01	3.67	4.03	6.32	4.98

Análises de química mineral em nefelina (cont.)

EM NMS EVES05 8	EM NMS EVES05 11	EM NMS EVES05 12	EM NMS EVES063 1	EM NMS EVES063 6	EM NMS EVES063 5	EM NMS EVES06B3 9	EM NMS EVES06B3 12	EM NMS EVES06B3 18	EM NS EVES06B1 C2_2(big)	EM NS EVES06B1 C2_3(big)	EM NS EVES06B1 C2_4(big)
42.88	43.24	42.88	42.33	43.84	43.01	42.02	42.78	41.58	43.42	44.10	42.90
34.57	34.01	33.69	33.95	34.70	33.70	34.12	34.29	33.96	33.97	33.72	33.98
0.09	0.00	0.04	0.00	0.01	0.00	0.05	0.01	0.08	0.00	0.02	0.00
0.80	0.69	0.87	0.48	0.65	0.59	0.63	0.52	0.56	0.16	0.20	0.14
16.23	16.41	17.03	16.57	16.48	16.78	16.73	17.01	16.73	16.58	17.29	16.60
6.28	5.99	5.69	6.30	5.65	5.71	5.61	6.11	6.17	6.16	5.87	6.63
100.84	100.33	100.20	99.63	101.34	99.78	99.15	100.71	99.08	100.29	101.19	100.25
8.19	8.28	8.25	8.20	8.29	8.28	8.16	8.19	8.11	8.32	8.37	8.25
7.78	7.68	7.64	7.75	7.73	7.65	7.80	7.74	7.81	7.67	7.54	7.70
0.01	0.00	0.01	0.00	0.00	0.00	0.01	0.00	0.01	0.00	0.00	0.00
0.16	0.14	0.18	0.10	0.13	0.12	0.13	0.11	0.12	0.03	0.04	0.03
6.01	6.09	6.35	6.22	6.04	6.27	6.30	6.31	6.33	6.16	6.36	6.19
1.53	1.46	1.40	1.56	1.36	1.40	1.39	1.49	1.54	1.51	1.42	1.63
75.11	76.17	79.35	77.72	75.48	78.33	78.72	78.91	79.11	76.95	79.55	77.38
19.12	18.30	17.45	19.46	17.03	17.54	17.35	18.65	19.20	18.83	17.76	20.34
5.76	5.53	3.20	2.82	7.50	4.13	3.93	2.44	1.69	4.23	2.69	2.27

Análises de química mineral em nefelina (cont.)

EM NS EVES061 C2_6(big)	EM NS EVES061 C1_1	EM NS EVES061 C1_2	EM NS EVES06B1 6	EM NS EVES06B1 7	EM NS EVES06B1 10	EM NS EVES6B2 1	EM NS EVES6B2 2	EM NS EVES6B2 3	EM NS EVES6B2 4	EM NS EVES6B2 6	EM NS EVES6B2 7
43.76	43.56	43.02	42.86	42.98	43.67	42.85	41.93	43.12	42.30	43.60	42.05
33.89	34.03	34.22	34.14	33.50	33.76	33.74	33.50	33.98	34.27	33.93	34.06
0.02	0.00	0.11	0.00	0.00	0.00	0.04	0.00	0.09	0.09	0.00	0.02
0.16	0.14	0.20	0.23	0.84	0.11	0.14	0.10	0.14	0.19	0.11	0.13
17.26	17.56	17.35	17.34	16.57	16.64	16.65	16.42	17.09	17.17	17.19	15.98
5.99	6.01	6.26	6.20	5.86	6.47	6.34	6.34	5.93	6.31	6.28	6.69
101.08	101.31	101.16	100.77	99.76	100.66	99.76	98.29	100.34	100.31	101.12	98.94
8.33	8.28	8.21	8.21	8.29	8.35	8.28	8.22	8.27	8.15	8.31	8.19
7.60	7.63	7.70	7.71	7.62	7.61	7.68	7.74	7.68	7.78	7.62	7.82
0.00	0.00	0.02	0.00	0.00	0.00	0.01	0.00	0.01	0.01	0.00	0.00
0.03	0.03	0.04	0.05	0.17	0.02	0.03	0.02	0.03	0.04	0.02	0.03
6.37	6.47	6.42	6.44	6.20	6.17	6.23	6.25	6.35	6.41	6.35	6.04
1.45	1.46	1.52	1.52	1.44	1.58	1.56	1.59	1.45	1.55	1.53	1.66
79.59	80.93	80.28	80.47	77.48	77.06	77.91	78.06	79.42	80.14	79.38	75.48
18.17	18.23	19.04	18.94	18.03	19.72	19.52	19.82	18.14	19.38	19.06	20.79
2.24	0.83	0.68	0.59	4.49	3.21	2.57	2.12	2.44	0.48	1.56	3.74

Análises de química mineral em nefelina (cont.)

EM NS EVES6B2 8	EM NS EVES6B2 10	EM NS EVES6B2 11	EM NS EVES14 C3_1	EM NS EVES14 C3_7	EM NS EVES14 1	EM NS EVES14 4	EM NS EVES14 5	EM NS EVES14 6	EM NS EVES14 7	EM NS EVES14 8	EM NS EVES14 9	EM NS EVES14 10
42.64	43.26	42.59	42.54	42.66	42.78	42.90	44.63	43.88	43.14	43.10	43.18	41.66
33.70	33.87	33.85	34.01	34.20	33.51	33.74	33.53	33.93	33.13	33.36	33.99	33.86
0.06	0.00	0.02	0.06	0.12	0.07	0.11	0.13	0.05	0.13	0.16	0.12	0.04
0.15	0.09	0.05	0.05	0.05	0.13	0.15	0.36	0.20	0.09	0.27	0.22	0.13
16.99	17.39	16.52	17.05	16.79	17.37	16.86	15.98	16.91	16.83	16.09	16.98	16.60
5.78	6.34	6.76	6.72	6.15	6.24	6.11	5.80	6.19	5.96	5.93	6.16	6.49
99.32	100.96	99.79	100.43	99.97	100.10	99.88	100.43	101.17	99.28	98.91	100.64	98.78
8.26	8.27	8.24	8.19	8.22	8.26	8.27	8.49	8.34	8.36	8.36	8.27	8.15
7.69	7.63	7.72	7.72	7.76	7.62	7.67	7.52	7.60	7.57	7.63	7.67	7.81
0.01	0.00	0.00	0.01	0.02	0.01	0.02	0.02	0.01	0.02	0.03	0.02	0.01
0.03	0.02	0.01	0.01	0.01	0.03	0.03	0.07	0.04	0.02	0.06	0.05	0.03
6.38	6.44	6.20	6.37	6.27	6.50	6.30	5.89	6.23	6.32	6.05	6.30	6.29
1.43	1.55	1.67	1.65	1.51	1.54	1.50	1.41	1.50	1.47	1.47	1.50	1.62
79.75	80.45	77.46	79.30	78.37	80.62	78.80	73.68	77.92	79.03	75.65	78.78	78.68
17.84	19.31	20.84	20.57	18.90	19.06	18.79	17.58	18.77	18.40	18.36	18.79	20.25
2.41	0.24	1.70	0.13	2.72	0.33	2.41	8.74	3.31	2.57	5.99	2.43	1.07

Análises de química mineral em nefelina (cont.)

EM NS EVES37 1	EM NS EVES37 2	EM NS EVES37 3	EM NS EVES37 4	EM NS EVES37 7	EM NS EVES37 8	EM NS EVES37 9	EM NS EVES39 1	EM NS EVES39 2	EM NS EVES44 1	EM NS EVES44 2	EM NS EVES44 3	EM NS EVES44 4
43.36	42.60	43.85	43.47	42.06	43.18	43.31	43.74	43.62	43.80	43.01	42.56	42.68
33.37	33.83	33.63	33.62	33.99	32.92	33.44	33.93	34.06	33.73	33.80	32.79	33.65
0.13	0.19	0.04	0.10	0.12	0.11	0.00	0.19	0.05	0.10	0.19	0.09	0.26
0.63	0.31	0.27	0.37	0.36	0.16	0.14	0.51	0.52	0.32	0.27	0.28	0.35
16.20	16.94	17.00	16.75	16.45	15.96	16.56	17.10	16.77	17.08	16.80	16.64	16.65
5.74	6.04	6.25	6.14	6.54	6.26	6.35	5.59	5.30	5.62	6.19	5.74	6.04
99.41	99.90	101.03	100.44	99.51	98.60	99.81	101.06	100.32	100.66	100.25	98.11	99.62
8.37	8.22	8.36	8.33	8.17	8.41	8.35	8.32	8.33	8.35	8.27	8.34	8.26
7.59	7.70	7.55	7.59	7.78	7.56	7.60	7.60	7.66	7.58	7.66	7.57	7.67
0.02	0.03	0.01	0.02	0.02	0.02	0.00	0.03	0.01	0.02	0.03	0.02	0.04
0.13	0.06	0.06	0.08	0.08	0.03	0.03	0.10	0.11	0.06	0.06	0.06	0.07
6.06	6.34	6.28	6.22	6.19	6.03	6.19	6.30	6.20	6.32	6.26	6.32	6.24
1.41	1.49	1.52	1.50	1.62	1.55	1.56	1.36	1.29	1.37	1.52	1.44	1.49
75.74	79.28	78.49	77.77	77.39	75.35	77.36	78.80	77.56	78.95	78.30	79.04	78.04
17.65	18.60	18.99	18.75	20.26	19.43	19.52	16.94	16.13	17.10	18.97	17.95	18.62
6.61	2.13	2.52	3.48	2.35	5.22	3.12	4.26	6.31	3.95	2.74	3.01	3.33

Análises de química mineral em nefelina (cont.)

EM NS EVES44 5	EM NS EVES44 6	EM NS EVES44 7	EM NS EVES44 8	EM NS EVES44 9	EM NS EVES44 10	EM NS EVES44 11	EM NS EVES50 1	EM NS EVES50 2	EM NS EVES50 3	EM NS EVES50 5	EM NS EVES50 6	EM NS EVES50 1(big)
42.63	43.21	44.07	43.75	43.94	42.61	43.45	43.64	43.40	43.14	43.78	44.00	42.63
33.92	33.78	33.74	32.88	33.95	33.64	33.21	33.91	34.01	34.07	34.24	34.18	34.21
0.10	0.10	0.16	0.13	0.11	0.10	0.00	0.01	0.02	0.01	0.07	0.00	0.01
0.31	0.30	0.27	0.26	0.28	0.26	0.30	0.37	0.36	0.38	0.26	0.40	0.32
16.91	17.01	17.01	16.64	17.00	16.93	16.66	17.02	16.29	16.78	16.71	17.01	16.83
5.78	5.75	5.89	5.72	5.90	6.07	5.74	5.74	5.88	5.70	6.07	5.56	6.10
99.64	100.15	101.15	99.37	101.17	99.61	99.36	100.69	99.95	100.08	101.13	101.14	100.10
8.23	8.30	8.37	8.45	8.34	8.25	8.39	8.32	8.32	8.28	8.32	8.34	8.20
7.72	7.64	7.55	7.48	7.60	7.67	7.56	7.62	7.69	7.70	7.66	7.63	7.76
0.02	0.02	0.03	0.02	0.02	0.02	0.00	0.00	0.00	0.00	0.01	0.00	0.00
0.06	0.06	0.06	0.05	0.06	0.05	0.06	0.07	0.07	0.08	0.05	0.08	0.07
6.33	6.33	6.27	6.23	6.26	6.35	6.24	6.29	6.06	6.24	6.15	6.25	6.28
1.42	1.41	1.43	1.41	1.43	1.50	1.41	1.40	1.44	1.39	1.47	1.34	1.50
79.13	79.15	78.32	77.83	78.22	79.42	77.95	78.64	75.69	77.97	76.92	78.12	78.49
17.81	17.61	17.84	17.59	17.86	18.74	17.66	17.46	17.97	17.42	18.37	16.79	18.70
3.06	3.23	3.85	4.58	3.93	1.84	4.39	3.90	6.34	4.61	4.70	5.09	2.80

Análises de química mineral em nefelina (cont.)

EM NS EVES50 2(big)	EM NS EVES50 3(big)	EM NS EVES50 5(big)	EM NS EVES50 6(big)	EM NS EVES50 7(big)	EM NS EVES50 1(inc)	EM NS EVES50 2(inc)	EM NS EVES50 3(inc)	EM NS EVES50 4(inc)	EM AFS EVES02 C1_5	EM AFS EVES02 C1_6	EM AFS EVES02 C4_hex	EM AFS EVES03A C10_4
42.23	42.79	43.11	43.16	43.16	42.89	42.74	43.69	42.62	42.84	42.51	43.55	43.21
34.05	33.71	34.24	34.09	34.22	33.74	33.65	34.27	33.30	32.89	33.27	33.62	33.51
0.03	0.00	0.01	0.00	0.00	0.03	0.05	0.00	0.09	0.28	0.25	0.31	0.32
0.37	0.36	0.36	0.31	0.30	0.32	0.27	0.27	0.24	0.15	0.14	0.13	0.19
17.03	16.44	16.91	17.12	17.18	17.25	16.84	17.15	16.76	17.04	16.91	17.10	16.00
5.56	5.90	6.13	5.61	5.80	5.79	5.67	5.90	5.78	5.37	5.49	5.29	5.34
99.27	99.20	100.76	100.28	100.66	100.03	99.22	101.28	98.79	98.57	98.56	99.99	98.58
8.18	8.29	8.24	8.27	8.25	8.26	8.28	8.29	8.30	8.35	8.29	8.35	8.38
7.78	7.69	7.71	7.69	7.71	7.65	7.68	7.66	7.64	7.56	7.65	7.60	7.66
0.01	0.00	0.00	0.00	0.00	0.01	0.01	0.00	0.01	0.05	0.04	0.05	0.05
0.08	0.07	0.07	0.06	0.06	0.07	0.05	0.05	0.05	0.03	0.03	0.03	0.04
6.40	6.17	6.27	6.36	6.36	6.44	6.32	6.31	6.33	6.44	6.39	6.36	6.02
1.38	1.46	1.49	1.37	1.41	1.42	1.40	1.43	1.44	1.33	1.37	1.29	1.32
79.95	77.15	78.33	79.46	79.53	80.50	79.04	78.86	79.09	80.51	79.93	79.46	75.20
17.19	18.21	18.68	17.12	17.67	17.78	17.52	17.86	17.95	16.68	17.07	16.16	16.51
2.85	4.63	2.99	3.42	2.80	1.72	3.43	3.28	2.96	2.81	2.99	4.37	8.29

Análises de química mineral em nefelina (cont.)

EM AFS EVES4B C1_5	EM AFS EVES4B C1_6	EM AFS EVES4B C2_8	EM AFS EVES4C C1_1(b)	EM AFS EVES4C C1_2(b)	EM AFS EVES4C C1_3(b)	EM AFS EVES4C C1_4(b)	EM AFS EVES4C C1_5(b)	EM AFS EVES4C C2_1(h)	EM AFS EVES4C C2_2(h)	EM AFS EVES4C C2_3(h)	EM AFS EVES4C C2_1	EM AFS EVES4C C2_2
43.48	42.65	42.09	43.74	43.38	43.44	43.40	43.32	42.42	42.56	42.58	44.12	43.98
33.64	33.33	34.16	33.10	33.04	33.92	34.29	33.53	33.13	33.34	33.50	33.49	33.98
0.07	0.01	0.02	0.26	0.33	0.10	0.15	0.15	0.27	0.29	0.24	0.15	0.12
0.19	0.12	0.14	0.69	0.41	0.26	0.29	0.35	0.34	0.35	0.33	0.40	0.35
16.43	15.97	16.42	15.18	16.24	16.48	16.30	16.40	16.03	16.21	16.35	16.07	16.72
5.90	6.05	6.12	5.73	6.01	6.18	6.93	6.23	6.22	6.10	6.23	6.27	6.27
99.71	98.14	98.95	98.69	99.41	100.38	101.35	99.98	98.41	98.85	99.24	100.50	101.41
8.36	8.34	8.19	8.47	8.39	8.32	8.26	8.34	8.30	8.29	8.27	8.43	8.34
7.63	7.68	7.83	7.55	7.53	7.65	7.69	7.61	7.64	7.65	7.67	7.54	7.60
0.01	0.00	0.00	0.04	0.05	0.02	0.02	0.02	0.05	0.05	0.04	0.02	0.02
0.04	0.02	0.03	0.14	0.09	0.05	0.06	0.07	0.07	0.07	0.07	0.08	0.07
6.12	6.05	6.19	5.70	6.09	6.12	6.02	6.12	6.08	6.12	6.16	5.95	6.15
1.45	1.51	1.52	1.41	1.48	1.51	1.68	1.53	1.55	1.52	1.54	1.53	1.52
76.56	75.64	77.39	71.22	76.15	76.46	75.20	76.49	76.01	76.54	76.96	74.36	76.87
18.10	18.86	18.97	17.69	18.53	18.88	21.05	19.13	19.40	18.95	19.30	19.09	18.97
5.34	5.50	3.64	11.10	5.32	4.66	3.75	4.39	4.58	4.51	3.74	6.54	4.16

Análises de química mineral em nefelina (cont.)

EM AFS EVES4C C2_3	EM AFS EVES4C C4_5(h)	EM AFS EVES4C C4_6(h)	EM AFS EVES4C C4_8(h)	EM AFS EVES4C C4_9(h)	EM AFS EVES4C C4_11(h)	EM AFS EVES4C C7_2(t)	EM AFS EVES4C C7_3(t)	EM AFS EVES4C C7_4(t)	EM AFS EVES4C C8_1(t)	EM AFS EVES4C C8_2(t)	EM AFS EVES4C C8_3(t)	EM AFS EVES4C C8_4(t)
44.02	44.08	43.62	43.62	43.72	43.78	44.18	44.82	43.76	43.02	44.04	43.89	43.46
33.32	33.89	34.15	33.90	33.40	33.53	33.36	33.40	34.01	33.40	33.51	33.46	33.77
0.25	0.21	0.06	0.25	0.29	0.25	0.28	0.25	0.22	0.25	0.28	0.08	0.25
0.33	0.36	0.39	0.36	0.40	0.37	0.34	0.29	0.34	0.35	0.38	0.39	0.37
16.49	16.57	16.56	16.94	16.60	16.46	16.80	16.76	16.85	16.79	16.59	16.74	16.80
6.03	6.13	6.52	6.08	6.00	6.15	6.03	6.03	6.28	6.12	5.96	5.95	5.95
100.44	101.23	101.30	101.14	100.41	100.55	100.99	101.54	101.45	99.93	100.76	100.51	100.61
8.42	8.37	8.29	8.31	8.38	8.37	8.41	8.47	8.31	8.30	8.40	8.39	8.31
7.51	7.58	7.65	7.61	7.54	7.56	7.49	7.44	7.61	7.60	7.53	7.54	7.61
0.04	0.03	0.01	0.04	0.05	0.04	0.05	0.04	0.04	0.04	0.05	0.01	0.04
0.07	0.07	0.08	0.07	0.08	0.07	0.07	0.06	0.07	0.07	0.08	0.08	0.08
6.12	6.10	6.11	6.25	6.16	6.10	6.20	6.14	6.20	6.28	6.13	6.20	6.23
1.47	1.48	1.58	1.48	1.47	1.50	1.46	1.45	1.52	1.51	1.45	1.45	1.45
76.44	76.24	76.32	78.16	77.05	76.28	77.54	76.78	77.53	78.51	76.68	77.52	77.89
18.40	18.56	19.77	18.46	18.33	18.77	18.30	18.16	19.01	18.83	18.12	18.14	18.16
5.15	5.21	3.91	3.38	4.61	4.95	4.17	5.05	3.46	2.67	5.20	4.34	3.95

Análises de química mineral em biotita

Massif	MSM	MSM	MSM	MSM	MSM	MSM	MSM	MSM
Rock Type	NS	NS	NS	NS	NS	NS	NS	AFS
Sample	MS88	MS88	MS88	MS88	MS88	MS336B	MS344	MS140
Spot no.	C2_3	C2_4	C2_6	C2_7	C2_8	C1_5	C1_1	C1_13
Classification	Annite	Annite	Annite	Annite	Annite	Annite	Annite	Annite
SiO_2	31.88	30.98	31.10	31.22	32.12	32.84	33.27	32.43
TiO_2	0.44	0.68	1.01	0.50	1.00	0.20	0.37	1.06
Al_2O_3	19.20	18.95	19.45	18.85	19.71	17.72	17.47	17.35
FeO	32.07	32.68	31.71	32.58	30.48	29.22	31.32	31.77
MnO	1.59	1.74	1.77	1.65	2.23	4.00	1.83	0.70
MgO	0.52	0.51	0.48	0.52	0.56	1.47	0.47	1.67
Na_2O	0.09	0.11	0.11	0.06	0.10	0.14	2.18	0.08
K_2O	9.55	9.28	9.40	9.48	9.39	9.46	8.49	9.53
F	0.00	0.07	0.16	0.12	0.12	0.13	0.07	0.13
Total	95.32	95.01	95.20	94.98	95.72	95.17	95.48	94.72
Formula based in 11 oxygen atoms								
F	0.00	0.02	0.04	0.03	0.03	0.03	0.02	0.03
OH	2.00	1.98	1.96	1.97	1.97	1.97	1.98	1.97
ΣOH	2.00	2.00	2.00	2.00	2.00	2.00	2.00	2.00
Si	2.63	2.58	2.58	2.60	2.62	2.71	2.73	2.69
Al^{IV}	1.37	1.42	1.42	1.40	1.38	1.29	1.27	1.31
ΣT	4.00	4.00	4.00	4.00	4.00	4.00	4.00	4.00
Al^{VI}	0.49	0.44	0.48	0.46	0.52	0.43	0.43	0.38
Ti	0.03	0.04	0.06	0.03	0.06	0.01	0.02	0.07
Mg	0.06	0.06	0.06	0.06	0.07	0.18	0.06	0.21
Fe	2.21	2.28	2.20	2.27	2.08	2.02	2.15	2.20
Mn	0.11	0.12	0.12	0.12	0.15	0.28	0.13	0.05
ΣM	2.90	2.95	2.92	2.94	2.89	2.92	2.79	2.91
Na	0.01	0.02	0.02	0.01	0.02	0.02	0.35	0.01
K	1.00	0.99	0.99	1.01	0.98	1.00	0.89	1.01
ΣI	1.02	1.00	1.01	1.02	0.99	1.02	1.24	1.02
$Mg/(Mg+Fe^{2+}+Mn)$	0.03	0.03	0.03	0.03	0.03	0.07	0.02	0.08

Análises de química mineral em biotita (cont.)

MSM AFS MS140 C1_15 Annite	MSM AFS MS140 C1_16 Annite	MSM AFS MS140 C2_21 Annite	MSM AFS MS140 C2_22 Annite	MSM AFS MS140 C2_23 Annite	MSM AFS MS319C C2_1 Annite	MSM AFS MS319C C2_4 Annite	MSM AFS MS319C C2_5 Annite	MSM AFS MS319C C2_5 Annite	MSM AFS MS319C C2_6 Annite
32.48	32.56	32.62	32.60	32.24	32.94	33.61	32.92	33.12	33.04
1.01	1.08	1.34	0.97	1.20	1.81	2.21	1.83	2.07	1.99
17.14	17.89	17.69	17.46	17.26	14.09	14.77	14.22	14.13	14.39
32.38	32.18	32.29	31.93	32.16	30.61	30.54	31.42	31.00	30.71
0.86	0.88	0.81	0.83	0.78	1.58	1.38	1.41	1.98	1.49
1.53	1.41	1.39	1.39	1.53	3.86	3.67	3.70	3.50	3.54
0.10	0.14	0.17	0.15	0.10	0.11	0.14	0.08	0.08	0.18
9.32	9.10	9.59	9.51	9.55	9.39	9.38	9.19	9.38	9.37
0.14	0.06	0.14	0.17	0.06	0.49	0.54	0.45	0.44	0.48
94.95	95.30	96.05	95.00	94.88	94.88	96.22	95.22	95.70	95.19
0.04	0.02	0.04	0.04	0.02	0.13	0.14	0.12	0.12	0.13
1.96	1.98	1.96	1.96	1.98	1.87	1.86	1.88	1.88	1.87
2.00	2.00	2.00	2.00	2.00	2.00	2.00	2.00	2.00	2.00
2.69	2.67	2.67	2.70	2.67	2.76	2.76	2.74	2.75	2.75
1.31	1.33	1.33	1.30	1.33	1.24	1.24	1.26	1.25	1.25
4.00	4.00	4.00	4.00	4.00	4.00	4.00	4.00	4.00	4.00
0.37	0.40	0.38	0.40	0.36	0.14	0.18	0.14	0.13	0.16
0.06	0.07	0.08	0.06	0.07	0.11	0.14	0.11	0.13	0.12
0.19	0.17	0.17	0.17	0.19	0.48	0.45	0.46	0.43	0.44
2.24	2.21	2.21	2.21	2.23	2.14	2.09	2.19	2.15	2.14
0.06	0.06	0.06	0.06	0.05	0.11	0.10	0.10	0.14	0.11
2.92	2.91	2.90	2.90	2.91	2.99	2.96	3.01	2.98	2.97
0.02	0.02	0.03	0.02	0.02	0.02	0.02	0.01	0.01	0.03
0.99	0.95	1.00	1.00	1.01	1.00	0.98	0.98	0.99	0.99
1.00	0.98	1.03	1.03	1.03	1.02	1.00	0.99	1.01	1.02
0.08	0.07	0.07	0.07	0.08	0.18	0.17	0.17	0.16	0.16

Análises de química mineral em biotita (cont.)

MSM AFS MS319C C2_6 Annite	MSM AFS MS319C C2_7 Annite	MSM AFS MS319C C2_8 Annite	MSM AFS MS319C C2_9 Annite	MSM AFS MS319C C2_9 Annite	MSM AFS MS319C C2_10 Annite	MSM AFS MS319C C2_11 Annite	MSM AFS MS319C C2_11 Annite	MSM AFS MS319C C2_13 Annite	MSM AFS MS319C C2_19 Annite
33.25	33.16	33.09	32.88	33.26	33.03	33.37	32.99	33.09	33.10
2.33	1.96	1.82	2.57	1.49	1.83	1.87	2.16	2.11	1.69
14.15	14.26	14.51	14.32	14.40	14.22	14.78	14.22	14.38	14.40
30.89	30.91	30.95	30.56	31.16	31.27	30.58	30.31	31.37	31.00
1.82	1.48	1.43	1.65	1.74	1.48	1.64	1.66	1.51	1.65
3.91	3.68	3.76	3.57	3.60	3.69	3.63	3.91	3.50	3.57
0.13	0.15	0.13	0.10	0.15	0.11	0.08	0.15	0.14	0.12
9.26	9.25	9.39	9.39	9.36	9.33	9.40	9.32	9.26	9.36
0.43	0.45	0.50	0.44	0.46	0.44	0.58	0.47	0.50	0.37
96.16	95.28	95.57	95.48	95.62	95.39	95.93	95.18	95.86	95.25
0.11	0.12	0.13	0.11	0.12	0.11	0.15	0.12	0.13	0.10
1.89	1.88	1.87	1.89	1.88	1.89	1.85	1.88	1.87	1.90
2.00	2.00	2.00	2.00	2.00	2.00	2.00	2.00	2.00	2.00
2.74	2.76	2.74	2.73	2.76	2.75	2.76	2.74	2.74	2.75
1.26	1.24	1.26	1.27	1.24	1.25	1.24	1.26	1.26	1.25
4.00	4.00	4.00	4.00	4.00	4.00	4.00	4.00	4.00	4.00
0.11	0.15	0.16	0.13	0.17	0.14	0.19	0.14	0.15	0.16
0.14	0.12	0.11	0.16	0.09	0.11	0.12	0.13	0.13	0.11
0.48	0.46	0.47	0.44	0.45	0.46	0.45	0.48	0.43	0.44
2.13	2.15	2.15	2.12	2.16	2.18	2.11	2.11	2.17	2.15
0.13	0.10	0.10	0.12	0.12	0.10	0.11	0.12	0.11	0.12
2.99	2.98	2.99	2.97	2.99	2.99	2.98	2.98	2.99	2.98
0.02	0.02	0.02	0.02	0.02	0.02	0.01	0.02	0.02	0.02
0.97	0.98	0.99	0.99	0.99	0.99	0.99	0.99	0.98	0.99
0.99	1.00	1.01	1.01	1.01	1.01	1.00	1.01	1.00	1.01
0.18	0.17	0.17	0.16	0.16	0.17	0.17	0.18	0.16	0.16

Análises de química mineral em biotita (cont.)

MSM AFS MS398 6 Annite	MSM AFS MS398 9 Annite	MSM AFS MS398 12 Annite	MSM AFS MS398 15 Annite	MSM AFS MS398 16 Annite	MSM AFS MS398 20 Annite	MSM AFS MS398 21 Annite	MSM AFS MS398 22 Annite	MSM AFS MS398 23 Annite	MSM AFS MS398 24 Annite
31.50	31.07	31.47	32.29	31.44	31.81	31.47	31.24	31.58	31.34
1.22	1.00	0.62	0.55	1.01	0.70	0.84	0.70	0.78	0.92
20.35	20.16	20.55	20.66	20.36	20.55	20.29	20.21	20.24	20.27
31.35	31.04	31.19	30.99	30.51	31.07	31.38	31.30	30.90	31.27
0.80	0.94	0.85	0.78	0.68	0.76	0.89	0.85	0.77	0.82
0.70	0.70	0.69	0.68	0.67	0.71	0.72	0.68	0.73	0.69
0.16	0.24	0.15	0.18	0.15	0.12	0.10	0.17	0.13	0.14
9.59	9.43	9.52	9.60	9.64	9.65	9.51	9.41	9.64	9.58
0.44	0.52	0.50	0.49	0.55	0.55	0.47	0.45	0.41	0.50
96.11	95.09	95.54	96.22	95.01	95.92	95.65	95.02	95.18	95.53
0.11	0.14	0.13	0.13	0.14	0.14	0.12	0.12	0.11	0.13
1.89	1.86	1.87	1.87	1.86	1.86	1.88	1.88	1.89	1.87
2.00	2.00	2.00	2.00	2.00	2.00	2.00	2.00	2.00	2.00
2.58	2.58	2.59	2.63	2.60	2.61	2.59	2.59	2.61	2.59
1.42	1.42	1.41	1.37	1.40	1.39	1.41	1.41	1.39	1.41
4.00	4.00	4.00	4.00	4.00	4.00	4.00	4.00	4.00	4.00
0.54	0.55	0.59	0.61	0.59	0.60	0.56	0.57	0.57	0.56
0.08	0.06	0.04	0.03	0.06	0.04	0.05	0.04	0.05	0.06
0.09	0.09	0.08	0.08	0.08	0.09	0.09	0.08	0.09	0.09
2.15	2.16	2.15	2.11	2.11	2.13	2.16	2.17	2.13	2.16
0.06	0.07	0.06	0.05	0.05	0.05	0.06	0.06	0.05	0.06
2.91	2.92	2.92	2.89	2.89	2.91	2.93	2.92	2.90	2.92
0.03	0.04	0.02	0.03	0.02	0.02	0.02	0.03	0.02	0.02
1.00	1.00	1.00	1.00	1.02	1.01	1.00	1.00	1.01	1.01
1.03	1.04	1.03	1.03	1.04	1.03	1.01	1.02	1.04	1.03
0.04	0.04	0.04	0.04	0.04	0.04	0.04	0.04	0.04	0.04

Análises de química mineral em biotita (cont.)

MSM AFS MS398 26 Annite	MSM AFS MS398 28 Annite	MSM AFS MS398 33 Annite	MSM AFS MS398 34 Annite	MSM AFS MS398 36 Annite	MSM AFS MS398 38 Annite	MSM AFS MS398 39 Annite	MSM AFS MS398 40 Annite	MSM AFS MS398 41 Annite	MSM AFS MS398 42 Annite
31.61	31.56	31.66	31.60	31.07	31.84	31.42	31.64	31.40	30.87
0.56	0.67	0.38	1.12	0.28	0.55	0.42	0.61	0.79	0.93
20.19	20.16	20.63	20.61	20.65	20.67	20.43	20.19	20.61	20.54
31.28	31.19	31.90	31.64	31.33	32.23	31.70	31.83	31.87	30.93
0.90	0.75	0.94	0.83	0.78	0.83	1.00	0.97	0.77	0.92
0.70	0.69	0.68	0.67	0.57	0.55	0.56	0.64	0.48	0.64
0.11	0.15	0.17	0.14	0.19	0.14	0.18	0.13	0.18	0.17
9.51	9.37	9.70	9.37	9.67	9.58	9.56	9.56	9.43	9.43
0.48	0.62	0.54	0.49	0.43	0.30	0.41	0.47	0.56	0.58
95.33	95.16	96.59	96.46	94.97	96.70	95.69	96.06	96.09	95.00
0.13	0.16	0.14	0.13	0.11	0.08	0.11	0.12	0.15	0.15
1.87	1.84	1.86	1.87	1.89	1.92	1.89	1.88	1.85	1.85
2.00	2.00	2.00	2.00	2.00	2.00	2.00	2.00	2.00	2.00
2.61	2.62	2.59	2.58	2.58	2.59	2.59	2.60	2.58	2.57
1.39	1.38	1.41	1.42	1.42	1.41	1.41	1.40	1.42	1.43
4.00	4.00	4.00	4.00	4.00	4.00	4.00	4.00	4.00	4.00
0.58	0.59	0.58	0.56	0.60	0.57	0.58	0.56	0.58	0.58
0.03	0.04	0.02	0.07	0.02	0.03	0.03	0.04	0.05	0.06
0.09	0.09	0.08	0.08	0.07	0.07	0.07	0.08	0.06	0.08
2.16	2.16	2.18	2.16	2.18	2.19	2.19	2.19	2.19	2.15
0.06	0.05	0.07	0.06	0.06	0.06	0.07	0.07	0.05	0.06
2.92	2.93	2.94	2.93	2.92	2.92	2.93	2.93	2.93	2.93
0.02	0.02	0.03	0.02	0.03	0.02	0.03	0.02	0.03	0.03
1.00	0.99	1.01	0.97	1.02	0.99	1.01	1.00	0.99	1.00
1.02	1.01	1.04	1.00	1.05	1.02	1.03	1.02	1.02	1.03
0.04	0.04	0.04	0.04	0.03	0.03	0.03	0.03	0.03	0.03

Análises de química mineral em biotita (cont.)

MSM AFS MS398 44 Annite	MSM AFS MS398 46 Annite	EM NMD EVES12 C1_2 Phlogopite	EM NMD EVES12 C1_3 Phlogopite	EM NMD EVES12 C1_4 Phlogopite	EM NMD EVES12 C3_3 Phlogopite	EM NMD EVES12 C3_4 Phlogopite	EM NMD EVES12 C3_5 Phlogopite	EM NMD EVES12 C3_6 Phlogopite
31.47	31.98	35.30	35.46	35.97	36.17	35.93	35.38	35.41
0.67	0.75	2.50	2.15	2.01	2.83	2.67	2.86	3.36
20.45	20.47	13.88	14.62	14.40	15.02	13.80	13.43	13.29
31.63	31.17	17.48	17.29	17.81	17.59	17.25	18.06	18.17
0.75	0.87	0.47	0.16	0.16	0.28	0.21	0.25	0.31
0.57	0.69	12.56	12.54	13.05	12.12	12.62	12.42	12.43
0.11	0.18	0.14	0.32	0.18	0.21	0.09	0.05	0.15
9.50	9.35	8.93	9.21	8.96	8.54	8.87	9.14	9.09
0.50	0.42	1.89	1.71	1.74	1.74	1.89	1.86	1.86
95.66	95.88	93.17	93.47	94.30	94.50	93.35	93.44	94.08
0.13	0.11	0.48	0.43	0.44	0.44	0.48	0.48	0.47
1.87	1.89	1.52	1.57	1.56	1.56	1.52	1.52	1.53
2.00	2.00	2.00	2.00	2.00	2.00	2.00	2.00	2.00
2.59	2.61	2.86	2.85	2.87	2.86	2.90	2.87	2.86
1.41	1.39	1.14	1.15	1.13	1.14	1.10	1.13	1.14
4.00	4.00	4.00	4.00	4.00	4.00	4.00	4.00	4.00
0.58	0.59	0.19	0.24	0.22	0.26	0.21	0.15	0.12
0.04	0.05	0.15	0.13	0.12	0.17	0.16	0.17	0.20
0.07	0.08	1.52	1.50	1.55	1.43	1.52	1.50	1.49
2.18	2.13	1.19	1.16	1.19	1.16	1.16	1.23	1.23
0.05	0.06	0.03	0.01	0.01	0.02	0.01	0.02	0.02
2.93	2.91	3.08	3.04	3.08	3.04	3.06	3.07	3.06
0.02	0.03	0.02	0.05	0.03	0.03	0.01	0.01	0.02
1.00	0.97	0.92	0.94	0.91	0.86	0.91	0.95	0.93
1.02	1.00	0.95	1.00	0.94	0.89	0.93	0.95	0.96
0.03	0.04	0.55	0.56	0.56	0.55	0.56	0.55	0.55

Análises de química mineral em biotita (cont.)

EM NMD EVES12 C3_7 Phlogopite	EM NMD EVES12 C3_8 Phlogopite	EM NMD EVES12 C3_1 (inc) Phlogopite	EM NMS EVES05 1 Siderophy.	EM NMS EVES05 4 Siderophy.	EM NMS EVES05 5 Siderophy.	EM NMS EVES05 8 Siderophy.	EM NMS EVES05 10 Siderophy.
35.85	36.12	36.06	34.73	34.16	35.00	34.71	35.02
3.22	3.09	2.76	0.56	0.70	0.50	0.46	0.23
13.82	14.53	15.10	20.07	21.06	20.93	20.84	21.36
17.90	18.05	17.39	20.58	21.64	21.87	21.40	22.28
0.12	0.24	0.21	0.33	0.18	0.23	0.34	0.35
12.76	11.93	11.84	7.21	6.28	6.37	6.59	5.51
0.19	0.17	0.23	0.20	0.13	0.16	0.12	0.17
9.09	9.21	8.87	9.91	10.09	10.09	10.10	9.98
1.79	1.58	1.71	0.78	0.47	0.38	0.46	0.21
94.73	94.91	94.17	94.38	94.71	95.53	95.02	95.09
0.45	0.40	0.43	0.19	0.12	0.09	0.11	0.05
1.55	1.60	1.57	1.81	1.88	1.91	1.89	1.95
2.00	2.00	2.00	2.00	2.00	2.00	2.00	2.00
2.85	2.85	2.86	2.74	2.68	2.72	2.71	2.72
1.15	1.15	1.14	1.26	1.32	1.28	1.29	1.28
4.00	4.00	4.00	4.00	4.00	4.00	4.00	4.00
0.15	0.21	0.28	0.61	0.63	0.63	0.63	0.68
0.19	0.18	0.16	0.03	0.04	0.03	0.03	0.01
1.51	1.40	1.40	0.85	0.74	0.74	0.77	0.64
1.19	1.19	1.16	1.36	1.42	1.42	1.40	1.45
0.01	0.02	0.01	0.02	0.01	0.01	0.02	0.02
3.06	3.00	3.01	2.87	2.84	2.83	2.85	2.80
0.03	0.03	0.04	0.03	0.02	0.02	0.02	0.03
0.92	0.93	0.90	1.00	1.01	1.00	1.01	0.99
0.95	0.95	0.93	1.03	1.03	1.02	1.02	1.02
0.56	0.54	0.55	0.38	0.34	0.34	0.35	0.30

Análises de química mineral em biotita (cont.)

EM	EM	EM	EM	EM	EM	EM	EM
NMS	NMS	NMS	NMS	NMS	NMS	NMS	NMS
EVES6B3	EVES6B3	EVES6B3	EVES6B3	EVES6B3	EVES6B3	EVES6B3	EVES6B3
3	4	5	6	7	8	9	10
Sideroph.	Sideroph.	Sideroph.	Sideroph.	Sideroph.	Sideroph.	Sideroph.	Sideroph.
33.63	32.23	32.16	32.33	31.30	31.41	32.49	31.91
0.63	0.56	0.56	0.56	0.83	0.55	0.77	0.45
22.89	21.68	22.02	21.59	23.06	23.53	22.09	21.90
25.68	25.71	26.16	26.46	25.97	26.07	26.21	26.57
0.72	0.83	0.60	0.73	0.89	0.94	0.75	0.69
3.57	2.94	3.14	3.19	2.75	2.67	3.22	2.87
0.21	0.15	0.20	0.25	0.13	0.18	0.21	0.20
9.47	9.74	9.74	9.81	9.83	9.70	9.57	9.84
1.45	1.22	1.15	1.18	1.11	1.07	1.30	0.99
98.24	95.06	95.71	96.09	95.86	96.11	96.61	95.41
0.36	0.31	0.29	0.30	0.28	0.27	0.33	0.26
1.64	1.69	1.71	1.70	1.72	1.73	1.67	1.74
2.00	2.00	2.00	2.00	2.00	2.00	2.00	2.00
2.64	2.63	2.61	2.62	2.53	2.53	2.61	2.60
1.36	1.37	1.39	1.38	1.47	1.47	1.39	1.40
4.00	4.00	4.00	4.00	4.00	4.00	4.00	4.00
0.76	0.72	0.71	0.68	0.74	0.77	0.71	0.70
0.04	0.03	0.03	0.03	0.05	0.03	0.05	0.03
0.42	0.36	0.38	0.39	0.33	0.32	0.39	0.35
1.69	1.76	1.77	1.79	1.76	1.76	1.76	1.81
0.05	0.06	0.04	0.05	0.06	0.06	0.05	0.05
2.95	2.93	2.94	2.94	2.94	2.94	2.95	2.93
0.03	0.02	0.03	0.04	0.02	0.03	0.03	0.03
0.95	1.02	1.01	1.01	1.02	1.00	0.98	1.02
0.98	1.04	1.04	1.05	1.04	1.03	1.01	1.05
0.19	0.16	0.17	0.17	0.15	0.15	0.18	0.16

Análises de química mineral em biotita (cont.)

EM NMS EVES6B3 11 Sideroph.	EM NMS EVES6B3 12 Sideroph.	EM NMS EVES6B3 13 Sideroph.	EM NMS EVES6B3 14 Sideroph.	EM NMS EVES6B3 15 Sideroph.	EM NMS EVES6B3 16 Sideroph.	EM NMS EVES6B3 17 Sideroph.	EM NMS EVES6B3 20 Sideroph.
31.88	31.79	32.51	32.34	32.18	31.52	32.26	31.74
0.44	0.65	0.32	0.63	0.41	0.34	0.70	0.53
22.16	22.84	21.58	22.05	22.46	21.82	22.53	21.99
26.43	26.84	26.59	26.25	25.89	26.41	25.32	25.93
0.56	0.97	0.89	0.96	0.66	0.69	0.91	0.92
2.89	2.86	3.33	3.26	3.36	3.04	3.00	3.02
0.29	0.19	0.18	0.20	0.19	0.21	0.14	0.15
9.68	9.65	9.94	9.56	9.86	9.81	9.91	9.75
1.02	1.17	1.31	1.35	1.22	1.26	1.19	1.14
95.34	96.97	96.65	96.59	96.22	95.09	95.96	95.16
0.26	0.30	0.34	0.34	0.31	0.33	0.30	0.29
1.74	1.70	1.66	1.66	1.69	1.67	1.70	1.71
2.00	2.00	2.00	2.00	2.00	2.00	2.00	2.00
2.59	2.55	2.63	2.61	2.59	2.59	2.60	2.59
1.41	1.45	1.37	1.39	1.41	1.41	1.40	1.41
4.00	4.00	4.00	4.00	4.00	4.00	4.00	4.00
0.71	0.71	0.68	0.70	0.73	0.71	0.74	0.71
0.03	0.04	0.02	0.04	0.02	0.02	0.04	0.03
0.35	0.34	0.40	0.39	0.40	0.37	0.36	0.37
1.80	1.80	1.80	1.77	1.75	1.82	1.71	1.77
0.04	0.07	0.06	0.07	0.04	0.05	0.06	0.06
2.93	2.97	2.96	2.97	2.95	2.96	2.92	2.94
0.05	0.03	0.03	0.03	0.03	0.03	0.02	0.02
1.00	0.99	1.03	0.98	1.01	1.03	1.02	1.02
1.05	1.02	1.05	1.01	1.04	1.06	1.04	1.04
0.16	0.16	0.18	0.18	0.18	0.17	0.17	0.17

Análises de química mineral em biotita (cont.)

EM NS EVES6B1 C2_3 Annite	EM NS EVES6B1 C2_4 Annite	EM NS EVES6B1 C2_5 Annite	EM NS EVES6B1 C2_7 Annite	EM NS EVES6B1 9 Annite	EM NS EVES6B1 11 Annite	EM NS EVES6B1 13 Annite	EM NS EVES6B1 16 Annite	EM NS EVES6B1 17 Annite
31.69	32.45	32.37	32.61	32.97	32.35	33.41	32.35	32.10
1.87	0.58	1.16	0.93	3.82	1.34	1.66	1.02	1.28
19.31	19.27	19.59	19.42	19.50	18.43	20.08	19.52	20.02
29.77	30.27	30.53	29.56	26.13	31.17	28.42	29.49	29.22
2.01	1.84	1.62	1.69	3.47	1.72	1.65	1.62	1.80
0.41	0.33	0.39	0.34	0.37	0.37	0.32	0.36	0.29
0.08	0.13	0.18	0.24	0.13	0.14	0.18	0.12	0.18
9.25	9.47	9.48	9.41	9.72	9.46	9.68	9.61	9.31
0.43	0.65	0.69	0.72	0.42	0.69	0.77	0.80	0.68
94.81	94.99	96.00	94.91	96.51	95.67	96.18	94.89	94.87
0.11	0.17	0.18	0.19	0.11	0.18	0.20	0.21	0.18
1.89	1.83	1.82	1.81	1.89	1.82	1.80	1.79	1.82
2.00	2.00	2.00	2.00	2.00	2.00	2.00	2.00	2.00
2.62	2.70	2.66	2.70	2.64	2.69	2.71	2.69	2.66
1.38	1.30	1.34	1.30	1.36	1.31	1.29	1.31	1.34
4.00	4.00	4.00	4.00	4.00	4.00	4.00	4.00	4.00
0.51	0.58	0.56	0.60	0.49	0.49	0.63	0.60	0.61
0.12	0.04	0.07	0.06	0.23	0.08	0.10	0.06	0.08
0.05	0.04	0.05	0.04	0.04	0.05	0.04	0.04	0.04
2.06	2.10	2.10	2.05	1.75	2.16	1.93	2.05	2.02
0.14	0.13	0.11	0.12	0.24	0.12	0.11	0.11	0.13
2.88	2.90	2.89	2.87	2.75	2.91	2.81	2.88	2.87
0.01	0.02	0.03	0.04	0.02	0.02	0.03	0.02	0.03
0.98	1.00	0.99	0.99	0.99	1.00	1.00	1.02	0.98
0.99	1.03	1.02	1.03	1.01	1.02	1.03	1.04	1.01
0.02	0.02	0.02	0.02	0.02	0.02	0.02	0.02	0.02

Análises de química mineral em biotita (cont.)

EM NS EVES6B1 19 Annite	EM NS EVES6B1 20 Annite	EM NS EVES6B2 10 Annite	EM NS EVES6B2 11 Annite	EM NS EVES6B2 12 Annite	EM NS EVES6B2 14 Annite	EM NS EVES6B2 15 Annite	EM NS EVES14 7 Annite	EM NS EVES14 8 Annite
31.88	32.01	33.07	31.88	31.47	32.27	32.24	32.72	33.45
1.82	1.46	1.96	3.49	2.69	1.33	1.82	1.05	0.89
20.40	19.62	19.39	19.57	18.97	19.60	19.98	17.34	17.34
28.30	31.36	28.23	27.91	28.06	29.40	28.08	31.33	31.42
1.84	1.86	2.08	2.28	2.91	1.84	1.80	1.86	2.04
0.39	0.38	0.35	0.35	0.25	0.37	0.44	0.53	0.64
0.17	0.11	0.21	0.16	0.16	0.20	0.19	0.21	0.19
9.71	9.45	9.43	9.34	9.50	9.27	9.50	9.40	9.29
0.80	0.48	0.76	0.52	0.66	0.66	0.62	0.44	0.63
95.30	96.72	95.46	95.49	94.67	94.93	94.66	94.88	95.87
0.21	0.12	0.20	0.13	0.17	0.17	0.16	0.12	0.16
1.79	1.88	1.80	1.87	1.83	1.83	1.84	1.88	1.84
2.00	2.00	2.00	2.00	2.00	2.00	2.00	2.00	2.00
2.63	2.62	2.71	2.60	2.62	2.67	2.66	2.73	2.77
1.37	1.38	1.29	1.40	1.38	1.33	1.34	1.27	1.23
4.00	4.00	4.00	4.00	4.00	4.00	4.00	4.00	4.00
0.61	0.50	0.58	0.49	0.49	0.58	0.60	0.44	0.46
0.11	0.09	0.12	0.21	0.17	0.08	0.11	0.07	0.06
0.05	0.05	0.04	0.04	0.03	0.05	0.05	0.07	0.08
1.95	2.14	1.93	1.91	1.96	2.03	1.94	2.19	2.17
0.13	0.13	0.14	0.16	0.21	0.13	0.13	0.13	0.14
2.85	2.91	2.82	2.81	2.85	2.87	2.83	2.89	2.91
0.03	0.02	0.03	0.03	0.03	0.03	0.03	0.03	0.03
1.02	0.98	0.99	0.97	1.01	0.98	1.00	1.00	0.98
1.05	1.00	1.02	1.00	1.04	1.01	1.03	1.04	1.01
0.02	0.02	0.02	0.02	0.01	0.02	0.03	0.03	0.03

Análises de química mineral em biotita (cont.)

EM NS EVES149 Annite	EM NS EVES1412 Annite	EM NS EVES1416 Annite	EM NS EVES1420 Annite	EM NS EVES371 Annite	EM NS EVES373 Annite	EM NS EVES374 Annite	EM NS EVES3711 Annite	EM NS EVES447 Annite
33.00	32.60	32.51	32.40	32.78	33.04	33.35	32.97	32.95
1.40	0.75	0.84	1.15	1.28	1.01	0.87	1.50	0.83
15.91	16.52	16.15	16.90	15.98	15.87	15.52	15.32	15.10
32.67	32.90	32.56	31.74	28.89	30.06	30.62	31.38	30.61
2.02	2.06	2.03	2.00	2.77	2.10	1.92	2.03	2.05
0.66	0.57	0.66	0.57	2.80	2.55	2.43	1.88	3.12
0.16	0.14	0.14	0.10	0.11	0.13	0.10	0.10	0.19
9.25	9.71	9.44	9.19	9.62	9.36	9.33	9.29	9.05
0.49	0.48	0.37	0.64	0.25	0.47	0.46	0.15	0.70
95.55	95.72	94.69	94.70	94.46	94.60	94.59	94.61	94.60
0.13	0.13	0.10	0.17	0.06	0.12	0.12	0.04	0.19
1.87	1.87	1.90	1.83	1.94	1.88	1.88	1.96	1.81
2.00	2.00	2.00	2.00	2.00	2.00	2.00	2.00	2.00
2.76	2.73	2.74	2.73	2.73	2.76	2.79	2.75	2.77
1.24	1.27	1.26	1.27	1.27	1.24	1.21	1.25	1.23
4.00	4.00	4.00	4.00	4.00	4.00	4.00	4.00	4.00
0.33	0.37	0.35	0.41	0.29	0.32	0.32	0.26	0.27
0.09	0.05	0.05	0.07	0.08	0.06	0.05	0.09	0.05
0.08	0.07	0.08	0.07	0.35	0.32	0.30	0.23	0.39
2.29	2.31	2.30	2.24	2.01	2.10	2.14	2.19	2.16
0.14	0.15	0.14	0.14	0.20	0.15	0.14	0.14	0.15
2.93	2.94	2.93	2.94	2.92	2.95	2.95	2.92	3.02
0.03	0.02	0.02	0.02	0.02	0.02	0.02	0.02	0.03
0.99	1.04	1.02	0.99	1.02	1.00	0.99	0.99	0.97
1.01	1.06	1.04	1.00	1.04	1.02	1.01	1.00	1.00
0.03	0.03	0.03	0.03	0.14	0.12	0.12	0.09	0.15

Análises de química mineral em biotita (cont.)

EM NS EVES44 10 Annite	EM NS EVES44 16 Annite	EM NS EVES44 17 Annite	EM NS EVES44 18 Annite	EM NS EVES50 C2_7 Annite	EM NS EVES50 C2_8 Sideroph.	EM NS EVES50 C3_1 Annite	EM NS EVES50 C3_2 Annite	EM NS EVES50 C3_3 Annite
33.37	33.34	31.91	33.78	30.46	31.10	30.72	30.58	30.56
1.69	0.98	0.63	0.67	0.37	0.04	0.00	0.28	0.47
15.10	14.92	17.12	14.90	22.42	21.97	22.30	21.87	22.36
28.01	31.32	30.73	30.84	30.99	30.14	30.90	31.54	31.19
2.91	2.15	1.86	2.18	0.89	0.73	0.90	0.73	0.83
3.68	2.82	2.44	2.99	0.78	0.83	0.46	0.50	0.42
0.18	0.11	0.08	0.14	0.18	0.15	0.14	0.19	0.16
9.48	9.23	9.38	9.42	9.66	9.70	9.43	9.53	9.47
0.56	0.56	0.53	0.71	1.16	1.20	1.17	1.11	1.07
94.98	95.43	94.68	95.63	96.91	95.85	96.02	96.33	96.52
0.15	0.15	0.14	0.19	0.30	0.32	0.31	0.29	0.28
1.85	1.85	1.86	1.81	1.70	1.68	1.69	1.71	1.72
2.00	2.00	2.00	2.00	2.00	2.00	2.00	2.00	2.00
2.77	2.78	2.68	2.81	2.51	2.58	2.55	2.54	2.52
1.23	1.22	1.32	1.19	1.49	1.42	1.45	1.46	1.48
4.00	4.00	4.00	4.00	4.00	4.00	4.00	4.00	4.00
0.24	0.25	0.37	0.28	0.69	0.73	0.73	0.68	0.70
0.11	0.06	0.04	0.04	0.02	0.00	0.00	0.02	0.03
0.45	0.35	0.30	0.37	0.10	0.10	0.06	0.06	0.05
1.94	2.19	2.16	2.15	2.14	2.09	2.15	2.19	2.15
0.20	0.15	0.13	0.15	0.06	0.05	0.06	0.05	0.06
2.95	3.00	3.00	2.99	3.01	2.98	3.00	3.00	2.99
0.03	0.02	0.01	0.02	0.03	0.02	0.02	0.03	0.03
1.00	0.98	1.00	1.00	1.02	1.03	1.00	1.01	1.00
1.03	1.00	1.02	1.02	1.04	1.05	1.02	1.04	1.02
0.17	0.13	0.12	0.14	0.04	0.05	0.03	0.03	0.02

Análises de química mineral em biotita (cont.)

EM NS EVES50 C3_5 Annite	EM NS EVES50 C3_6 Annite	EM NS EVES50 C4_1(rad) Sideroph.	EM NS EVES50 C4_2(rad) Sideroph.	EM NS EVES50 C4_3(rad) Sideroph.	EM NS EVES50 C4_4(rad) Sideroph.	EM NS EVES50 C4_5(rad) Sideroph.	EM NS EVES50 C5_1 Sideroph.
30.98	31.16	30.88	30.43	29.51	30.61	30.42	30.74
0.34	0.36	0.30	0.25	0.00	0.08	0.39	0.17
21.75	21.20	21.85	22.96	23.02	22.86	22.61	23.50
30.50	31.37	31.13	31.33	31.18	30.70	30.63	29.98
0.67	0.73	0.80	0.45	0.68	0.61	0.66	0.53
0.75	0.54	0.31	0.38	0.31	0.39	0.36	0.15
0.16	0.11	0.26	0.19	0.11	0.12	0.13	0.13
9.31	9.51	9.60	9.45	9.47	9.50	9.56	9.53
1.11	1.04	1.04	1.05	0.88	1.03	1.01	0.88
95.59	96.01	96.16	96.49	95.15	95.88	95.77	95.61
0.29	0.27	0.27	0.27	0.23	0.27	0.27	0.23
1.71	1.73	1.73	1.73	1.77	1.73	1.73	1.77
2.00	2.00	2.00	2.00	2.00	2.00	2.00	2.00
2.57	2.59	2.56	2.51	2.47	2.53	2.52	2.53
1.43	1.41	1.44	1.49	1.53	1.47	1.48	1.47
4.00	4.00	4.00	4.00	4.00	4.00	4.00	4.00
0.70	0.66	0.69	0.74	0.73	0.76	0.73	0.80
0.02	0.02	0.02	0.02	0.00	0.01	0.02	0.01
0.09	0.07	0.04	0.05	0.04	0.05	0.04	0.02
2.12	2.18	2.16	2.16	2.18	2.12	2.12	2.06
0.05	0.05	0.06	0.03	0.05	0.04	0.05	0.04
2.98	2.98	2.96	2.99	3.00	2.98	2.97	2.93
0.03	0.02	0.04	0.03	0.02	0.02	0.02	0.02
0.99	1.01	1.01	0.99	1.01	1.00	1.01	1.00
1.01	1.02	1.06	1.02	1.03	1.02	1.03	1.02
0.04	0.03	0.02	0.02	0.02	0.02	0.02	0.01

Análises de química mineral em biotita (cont.)

EM NS EVES50 C5_3 Sideroph.	EM NS EVES50 C5_4 Sideroph.	EM NS EVES50 9 Annite	EM NS EVES50 10 Annite	EM NS EVES50 11 Annite	EM NS EVES50 13 Annite	EM NS EVES50 14 Annite	EM NS EVES50 15 Sideroph.	EM NS EVES50 16 Sideroph.
30.34	31.36	29.81	31.57	31.21	30.88	31.11	31.29	32.08
0.24	0.36	0.10	0.48	0.26	0.21	0.33	0.25	0.27
23.45	23.52	22.71	21.11	22.22	21.89	21.48	22.11	23.66
29.01	29.48	31.06	31.51	30.69	30.77	30.99	29.96	28.72
0.58	0.61	0.81	0.76	0.79	1.01	0.83	0.87	0.64
0.18	0.23	0.66	0.67	0.64	0.97	0.81	0.60	0.69
0.28	0.23	0.14	0.11	0.23	0.21	0.23	0.16	0.35
9.77	9.54	9.52	9.60	9.50	9.61	9.42	9.64	9.55
1.02	1.15	1.19	1.09	1.11	1.06	1.17	1.12	1.03
94.88	96.47	96.01	96.91	96.63	96.61	96.38	95.99	96.98
0.27	0.30	0.31	0.28	0.29	0.28	0.31	0.29	0.26
1.73	1.70	1.69	1.72	1.71	1.72	1.69	1.71	1.74
2.00	2.00	2.00	2.00	2.00	2.00	2.00	2.00	2.00
2.52	2.56	2.49	2.60	2.56	2.54	2.57	2.58	2.58
1.48	1.44	1.51	1.40	1.44	1.46	1.43	1.42	1.42
4.00	4.00	4.00	4.00	4.00	4.00	4.00	4.00	4.00
0.82	0.82	0.72	0.64	0.72	0.67	0.67	0.73	0.82
0.02	0.02	0.01	0.03	0.02	0.01	0.02	0.02	0.02
0.02	0.03	0.08	0.08	0.08	0.12	0.10	0.07	0.08
2.02	2.01	2.17	2.17	2.11	2.12	2.15	2.07	1.93
0.04	0.04	0.06	0.05	0.05	0.07	0.06	0.06	0.04
2.91	2.92	3.03	2.98	2.97	2.99	2.99	2.95	2.90
0.05	0.04	0.02	0.02	0.04	0.03	0.04	0.03	0.06
1.04	0.99	1.01	1.01	1.00	1.01	0.99	1.02	0.98
1.08	1.03	1.04	1.03	1.03	1.04	1.03	1.04	1.03
0.01	0.01	0.04	0.04	0.03	0.05	0.04	0.03	0.04

Análises de química mineral em biotita (cont.)

EM NS EVES50 17 Sideroph.	EM NS EVES50 18 Annite	EM NS EVES50 19 Annite	EM NS EVES50 20 Annite	EM NS EVES50 21 Annite	EM NS EVES50 22 Sideroph.	EM NS EVES50 23 Sideroph.	EM NS EVES50 24 Sideroph.	EM NS EVES50 25 Sideroph.
31.15	31.19	30.51	30.11	31.03	31.41	31.30	31.77	31.40
0.21	0.27	0.23	0.22	0.26	0.32	0.26	0.26	0.05
22.45	21.85	22.19	21.88	22.32	21.76	22.05	22.65	21.63
30.25	30.53	30.80	30.89	30.67	29.51	28.59	29.57	29.89
0.64	0.78	0.60	0.52	0.75	0.89	0.89	0.70	0.54
0.73	0.85	0.79	0.64	0.75	0.80	1.22	1.08	0.79
0.22	0.17	0.22	0.18	0.19	0.19	0.18	0.22	0.21
9.25	9.50	9.48	9.41	9.47	9.39	9.41	9.39	9.65
1.27	1.02	1.06	1.10	1.10	1.07	1.17	1.25	1.25
96.15	96.17	95.86	94.94	96.55	95.33	95.07	96.89	95.41
0.33	0.27	0.28	0.29	0.29	0.28	0.31	0.32	0.33
1.67	1.73	1.72	1.71	1.71	1.72	1.69	1.68	1.67
2.00	2.00	2.00	2.00	2.00	2.00	2.00	2.00	2.00
2.57	2.57	2.53	2.53	2.55	2.60	2.59	2.59	2.61
1.43	1.43	1.47	1.47	1.45	1.40	1.41	1.41	1.39
4.00	4.00	4.00	4.00	4.00	4.00	4.00	4.00	4.00
0.75	0.69	0.70	0.70	0.71	0.72	0.75	0.76	0.74
0.01	0.02	0.01	0.01	0.02	0.02	0.02	0.02	0.00
0.09	0.10	0.10	0.08	0.09	0.10	0.15	0.13	0.10
2.09	2.10	2.14	2.17	2.11	2.04	1.98	2.01	2.08
0.04	0.05	0.04	0.04	0.05	0.06	0.06	0.05	0.04
2.99	2.97	2.99	3.00	2.98	2.95	2.96	2.97	2.96
0.04	0.03	0.03	0.03	0.03	0.03	0.03	0.03	0.03
0.97	1.00	1.00	1.01	0.99	0.99	0.99	0.97	1.02
1.01	1.03	1.04	1.04	1.02	1.02	1.02	1.01	1.06
0.04	0.05	0.04	0.04	0.04	0.04	0.07	0.06	0.04

Análises de química mineral em biotita (cont.)

EM AFS EVES4B C1_1 Annite	EM AFS EVES4B C1_2 Annite	EM AFS EVES4B C1_3 Annite	EM AFS EVES4B C1_4 Annite	EM AFS EVES4B C1_5 Annite	EM AFS EVES4B C2_1(inc) Annite	EM AFS EVES4B C2_2(inc) Annite	EM AFS EVES4B C4_1(inc) Annite	EM AFS EVES4B C4_2(inc) Annite
34.62	32.11	31.84	31.20	32.20	31.18	31.11	31.81	31.00
1.97	2.20	2.12	1.69	1.98	1.68	1.72	2.26	1.77
18.78	16.00	15.37	15.54	15.07	14.75	15.05	16.10	16.50
30.82	31.16	32.06	31.53	32.26	32.31	31.73	32.42	31.24
0.97	0.84	0.83	1.17	0.97	0.90	1.06	0.81	0.75
1.55	2.05	1.89	2.06	2.05	1.76	2.08	1.74	1.80
0.29	0.13	0.13	0.13	0.18	0.12	0.19	0.16	0.13
8.89	8.98	8.51	8.49	8.67	8.49	8.40	8.51	8.46
0.11	0.47	0.42	0.74	0.69	0.66	0.58	0.58	0.50
98.00	93.94	93.17	92.54	94.08	91.84	91.91	94.39	92.13
0.03	0.12	0.11	0.20	0.19	0.18	0.16	0.15	0.13
1.97	1.88	1.89	1.80	1.81	1.82	1.84	1.85	1.87
2.00	2.00	2.00	2.00	2.00	2.00	2.00	2.00	2.00
2.72	2.70	2.71	2.70	2.74	2.72	2.70	2.68	2.66
1.28	1.30	1.29	1.30	1.26	1.28	1.30	1.32	1.34
4.00	4.00	4.00	4.00	4.00	4.00	4.00	4.00	4.00
0.46	0.29	0.25	0.28	0.24	0.24	0.25	0.28	0.33
0.12	0.14	0.14	0.11	0.13	0.11	0.11	0.14	0.11
0.18	0.26	0.24	0.27	0.26	0.23	0.27	0.22	0.23
2.02	2.19	2.28	2.28	2.29	2.36	2.31	2.28	2.24
0.06	0.06	0.06	0.09	0.07	0.07	0.08	0.06	0.05
2.84	2.94	2.97	3.02	2.99	3.01	3.01	2.98	2.98
0.04	0.02	0.02	0.02	0.03	0.02	0.03	0.03	0.02
0.89	0.96	0.92	0.94	0.94	0.95	0.93	0.91	0.93
0.94	0.98	0.95	0.96	0.97	0.97	0.96	0.94	0.95
0.08	0.10	0.09	0.10	0.10	0.09	0.10	0.09	0.09

Análises de química mineral em biotita (cont.)

EM	EM	EM	EM	EM	EM	EM	EM	EM
AFS	AFS	AFS	AFS	AFS	AFS	AFS	AFS	AFS
EVES4B	EVES4B	EVES4B	EVES4B	EVES06A	EVES06A	EVES06A	EVES06A	EVES06A
C4_3(inc)	C4_4(inc)	C4_5(inc)	C4_6(inc)	1	2	3	4	5
Annite	Annite	Annite	Annite	Annite	Annite	Annite	Annite	Annite
31.33	32.00	31.69	31.82	33.96	34.28	33.32	33.54	33.22
2.31	2.27	2.45	1.93	2.78	2.87	2.02	3.10	2.71
16.20	16.22	15.79	16.02	13.95	14.09	14.22	13.61	13.46
30.99	31.32	31.80	31.81	32.14	31.23	32.52	32.15	31.84
0.77	0.98	0.94	0.94	0.77	0.72	0.97	0.99	0.82
2.01	1.89	1.77	1.76	2.46	2.73	2.50	2.94	2.83
0.14	0.12	0.14	0.12	0.14	0.18	0.15	0.14	0.19
8.62	8.62	8.57	8.77	9.50	9.42	9.20	9.39	9.33
0.63	0.51	0.46	0.47	0.72	0.70	0.62	0.74	0.74
92.98	93.92	93.60	93.64	96.41	96.21	95.52	96.59	95.16
0.17	0.14	0.12	0.13	0.19	0.18	0.16	0.19	0.20
1.83	1.86	1.88	1.87	1.81	1.82	1.84	1.81	1.80
2.00	2.00	2.00	2.00	2.00	2.00	2.00	2.00	2.00
2.67	2.69	2.68	2.70	2.81	2.82	2.79	2.78	2.79
1.33	1.31	1.32	1.30	1.19	1.18	1.21	1.22	1.21
4.00	4.00	4.00	4.00	4.00	4.00	4.00	4.00	4.00
0.30	0.30	0.26	0.29	0.17	0.19	0.19	0.10	0.13
0.15	0.14	0.16	0.12	0.17	0.18	0.13	0.19	0.17
0.26	0.24	0.22	0.22	0.30	0.33	0.31	0.36	0.36
2.21	2.20	2.25	2.25	2.22	2.15	2.27	2.23	2.24
0.06	0.07	0.07	0.07	0.05	0.05	0.07	0.07	0.06
2.97	2.95	2.96	2.96	2.92	2.90	2.97	2.96	2.95
0.02	0.02	0.02	0.02	0.02	0.03	0.02	0.02	0.03
0.94	0.92	0.93	0.95	1.00	0.99	0.98	0.99	1.00
0.96	0.94	0.95	0.97	1.02	1.02	1.01	1.01	1.03
0.10	0.09	0.09	0.09	0.12	0.13	0.12	0.14	0.13

Análises de química mineral em biotita (cont.)

EM	EM	EM	EM	EM	EM	EM	EM	EM
AFS	AFS	AFS	AFS	AFS	AFS	AFS	AFS	AFS
EVES06A	EVES06A	EVES06A	EVES06A	EVES06A	EVES06A	EVES06A	EVES06A	EVES06A
6	7	8	9	10	11	12	13	15
Annite	Annite	Annite	Annite	Annite	Annite	Annite	Annite	Annite
33.61	33.33	33.13	33.66	33.51	33.08	33.58	33.57	32.96
3.10	3.04	2.62	2.71	3.01	2.99	2.76	3.07	2.28
13.65	13.61	13.71	14.11	13.61	13.27	13.76	13.69	14.18
32.09	32.13	32.76	32.53	31.89	32.10	32.34	31.46	31.86
0.70	0.77	0.91	0.70	0.86	0.84	0.80	0.90	0.91
2.55	2.57	2.50	2.57	2.58	2.74	2.76	2.52	2.43
0.10	0.20	0.15	0.18	0.19	0.20	0.11	0.12	0.03
9.38	9.26	9.00	9.17	9.07	9.38	9.19	9.43	9.40
0.60	0.83	0.72	0.67	0.67	0.75	0.70	0.69	0.60
95.77	95.74	95.50	96.30	95.39	95.35	95.99	95.45	94.65
0.16	0.22	0.19	0.18	0.18	0.20	0.18	0.18	0.16
1.84	1.78	1.81	1.82	1.82	1.80	1.82	1.82	1.84
2.00	2.00	2.00	2.00	2.00	2.00	2.00	2.00	2.00
2.79	2.79	2.78	2.78	2.80	2.78	2.79	2.80	2.78
1.21	1.21	1.22	1.22	1.20	1.22	1.21	1.20	1.22
4.00	4.00	4.00	4.00	4.00	4.00	4.00	4.00	4.00
0.13	0.13	0.14	0.16	0.14	0.10	0.14	0.15	0.19
0.19	0.19	0.17	0.17	0.19	0.19	0.17	0.19	0.14
0.32	0.32	0.31	0.32	0.32	0.34	0.34	0.31	0.31
2.23	2.25	2.30	2.25	2.23	2.26	2.25	2.20	2.24
0.05	0.05	0.06	0.05	0.06	0.06	0.06	0.06	0.06
2.92	2.95	2.98	2.95	2.93	2.95	2.96	2.91	2.95
0.02	0.03	0.02	0.03	0.03	0.03	0.02	0.02	0.01
0.99	0.99	0.96	0.97	0.97	1.01	0.97	1.00	1.01
1.01	1.02	0.99	1.00	1.00	1.04	0.99	1.02	1.02
0.12	0.12	0.12	0.12	0.12	0.13	0.13	0.12	0.12

Análises de química mineral em biotita (cont.)

EM	EM	EM	EM	EM	EM	EM	EM	EM
AFS	AFS	AFS	AFS	AFS	AFS	AFS	AFS	AFS
EVES06A	EVES06A	EVES06A	EVES06A	EVES06A	EVES06A	EVES06A	EVES06A	EVES06A
16	17	18	20	22	23	24	25	26
Annite	Annite	Annite	Annite	Annite	Annite	Annite	Annite	Annite
33.56	33.65	33.63	33.82	33.79	34.16	33.13	33.35	33.52
2.63	2.54	3.01	2.83	1.96	1.96	2.73	2.45	3.01
13.92	13.52	13.98	13.28	13.24	13.51	13.48	13.64	13.80
31.35	31.81	31.27	30.87	32.06	32.69	31.93	31.91	32.56
0.87	0.99	0.81	0.88	0.84	0.89	0.79	0.91	1.01
2.66	2.66	2.75	2.76	2.60	2.84	2.67	2.59	2.65
0.11	0.16	0.16	0.14	0.19	0.15	0.15	0.15	0.13
9.27	9.24	9.27	9.33	9.55	9.35	9.38	9.12	9.13
0.65	0.68	0.51	0.65	0.61	0.73	0.66	0.55	0.68
95.02	95.24	95.38	94.55	94.84	96.27	94.90	94.67	96.49
0.17	0.18	0.13	0.17	0.16	0.19	0.17	0.15	0.18
1.83	1.82	1.87	1.83	1.84	1.81	1.83	1.85	1.82
2.00	2.00	2.00	2.00	2.00	2.00	2.00	2.00	2.00
2.81	2.82	2.79	2.84	2.85	2.84	2.79	2.80	2.78
1.19	1.18	1.21	1.16	1.15	1.16	1.21	1.20	1.22
4.00	4.00	4.00	4.00	4.00	4.00	4.00	4.00	4.00
0.18	0.15	0.15	0.15	0.16	0.16	0.13	0.15	0.12
0.17	0.16	0.19	0.18	0.12	0.12	0.17	0.16	0.19
0.33	0.33	0.34	0.34	0.33	0.35	0.34	0.32	0.33
2.19	2.23	2.17	2.17	2.26	2.27	2.25	2.24	2.25
0.06	0.07	0.06	0.06	0.06	0.06	0.06	0.06	0.07
2.93	2.94	2.91	2.90	2.93	2.97	2.94	2.94	2.96
0.02	0.03	0.03	0.02	0.03	0.02	0.02	0.02	0.02
0.99	0.99	0.98	1.00	1.03	0.99	1.01	0.98	0.96
1.01	1.01	1.01	1.02	1.06	1.01	1.03	1.00	0.98
0.13	0.13	0.13	0.13	0.12	0.13	0.13	0.12	0.12

Análises de química mineral em biotita (cont.)

EM AFS EVES06A 27 Annite	EM AFS EVES06A 28 Annite	EM AFS EVES06A 29 Annite	EM AFS EVES06A 30 Annite	EM AFS EVES06A 31 Annite	EM AFS EVES06A 32 Annite	EM AFS EVES06A 33 Annite	EM AFS EVES06A 34 Annite	EM AFS EVES06A 35 Annite
34.06	33.38	32.88	34.35	34.61	33.74	33.56	33.62	33.25
2.64	2.45	3.16	3.21	2.62	2.23	2.92	3.00	2.82
13.86	14.01	14.03	13.79	14.23	13.76	13.73	13.57	13.84
32.02	32.40	32.22	31.98	29.94	31.72	32.18	31.96	31.43
0.97	0.99	0.91	0.66	0.81	0.74	0.88	0.78	0.91
2.74	2.74	2.42	2.62	3.13	2.75	2.72	2.70	2.73
0.08	0.12	0.07	0.16	0.15	0.09	0.17	0.08	0.17
9.53	9.31	9.54	9.51	9.44	9.53	9.33	9.34	9.12
0.77	0.60	0.58	0.82	0.58	0.76	0.69	0.71	0.63
96.67	96.00	95.80	97.09	95.50	95.33	96.17	95.76	94.90
0.20	0.16	0.15	0.21	0.15	0.20	0.18	0.19	0.17
1.80	1.84	1.85	1.79	1.85	1.80	1.82	1.81	1.83
2.00	2.00	2.00	2.00	2.00	2.00	2.00	2.00	2.00
2.81	2.77	2.74	2.82	2.84	2.82	2.79	2.80	2.79
1.19	1.23	1.26	1.18	1.16	1.18	1.21	1.20	1.21
4.00	4.00	4.00	4.00	4.00	4.00	4.00	4.00	4.00
0.16	0.15	0.12	0.15	0.22	0.18	0.13	0.13	0.15
0.16	0.15	0.20	0.20	0.16	0.14	0.18	0.19	0.18
0.34	0.34	0.30	0.32	0.38	0.34	0.34	0.34	0.34
2.21	2.25	2.25	2.20	2.06	2.22	2.23	2.23	2.20
0.07	0.07	0.06	0.05	0.06	0.05	0.06	0.06	0.06
2.94	2.96	2.93	2.91	2.88	2.94	2.94	2.94	2.94
0.01	0.02	0.01	0.03	0.02	0.01	0.03	0.01	0.03
1.00	0.99	1.02	1.00	0.99	1.02	0.99	0.99	0.97
1.02	1.01	1.03	1.02	1.01	1.03	1.01	1.00	1.00
0.13	0.13	0.12	0.13	0.15	0.13	0.13	0.13	0.13

Massif	MSM	MSM	MSM	MSM	MSM	MSM	MSM
Rock Type	NS	NS	NS	NS	NS	NS	NS
Sample	MS22	MS22	MS22	MS344A	MS344A	MS344A	MS344A
Spot no.	C3_12	C3_13	C3_16	C1_1	C1_3	C1_10	C1_16
Classification	Taramite	Taramite	Taramite	Taramite	Taramite	Taramite	Taramite
SiO_2	37.43	37.41	36.90	36.61	35.78	36.84	36.83
TiO_2	0.54	0.38	0.28	0.30	0.25	0.28	0.16
Al_2O_3	12.72	12.73	13.05	12.38	12.59	12.34	12.50
$Fe_2O_3^{calc.}$	14.73	14.38	14.58	13.93	12.99	13.29	13.11
$FeO^{calc.}$	11.38	12.27	11.05	18.80	19.75	19.15	18.91
MnO	3.29	3.45	3.69	2.04	1.95	1.84	1.84
MgO	3.40	3.35	3.78	0.36	0.33	0.36	0.46
CaO	6.22	6.40	6.51	5.99	6.56	5.74	6.32
Na_2O	4.58	4.44	4.30	4.61	4.37	4.85	4.16
K_2O	2.43	2.62	2.72	2.65	2.72	2.63	2.57
F	0.64	0.38	0.32	0.31	0.20	0.34	0.29
Total	97.35	97.82	97.17	97.97	97.47	97.66	97.15
Formula based in 22 oxygen atoms and average estimation of Fe^{3+}							
OH	1.68	1.81	1.84	1.84	1.89	1.83	1.85
F	0.32	0.19	0.16	0.16	0.11	0.17	0.15
ΣOH	2.00	2.00	2.00	2.00	2.00	2.00	2.00
Si	5.99	5.95	5.89	5.95	5.85	5.99	6.02
ΣT	8.00	8.00	8.00	8.00	8.00	8.00	8.00
Al	0.39	0.34	0.34	0.32	0.28	0.36	0.43
Ti	0.06	0.05	0.03	0.04	0.03	0.03	0.02
Fe3+	1.75	1.71	1.75	1.77	1.76	1.75	1.55
Mg	0.81	0.79	0.90	0.09	0.08	0.09	0.11
Fe2+	1.55	1.64	1.48	2.49	2.54	2.49	2.65
Mn	0.44	0.46	0.50	0.28	0.27	0.25	0.24
ΣC	5.00	5.00	5.00	4.98	4.96	4.97	5.00
Mn	0.01	0.00	0.00	0.00	0.00	0.00	0.02
Fe2+	0.00	0.00	0.00	0.00	0.00	0.00	0.00
Ca	1.07	1.09	1.11	1.04	1.15	1.00	1.11
Na	0.93	0.91	0.89	0.96	0.85	1.00	0.88
ΣB	2.00	2.00	2.00	2.00	2.00	2.00	2.00
Na	0.50	0.46	0.44	0.49	0.53	0.53	0.44
K	0.50	0.53	0.55	0.55	0.57	0.55	0.54
ΣA	0.99	1.00	1.00	1.04	1.10	1.08	0.98
$Mg/(Mg+Fe^{2+}+Mn)$	0.29	0.27	0.31	0.03	0.03	0.03	0.04

MSM NS MS344A C1_19 Taramite	MSM NS MS344A C1_28 Taramite	MSM NS MS344A C1_39 Taramite	MSM NS MS344A C1_42 Taramite	MSM AFS MS319C C2_1 Taramite	MSM AFS MS319C C2_2 Taramite	MSM AFS MS319C C2_2 Taramite	MSM AFS MS319C C2_2 Taramite	MSM AFS MS319C C2_3 Taramite
37.30	37.03	36.51	36.94	37.58	37.77	38.17	37.58	37.82
0.34	0.34	0.11	0.07	0.59	0.65	0.88	0.56	0.57
12.22	12.01	12.42	12.29	12.89	12.71	12.29	12.59	12.81
11.97	12.90	13.22	13.69	11.70	12.80	10.82	12.12	12.06
19.59	19.39	19.05	18.50	17.53	16.72	18.00	17.00	17.71
1.83	1.68	1.77	1.82	1.68	1.39	1.48	1.58	1.48
0.45	0.50	0.50	0.48	1.86	2.06	1.98	1.99	1.87
5.77	5.86	6.13	5.82	6.53	6.46	6.63	6.54	6.63
4.71	4.67	4.74	4.69	4.38	4.15	3.95	4.20	4.22
2.60	2.67	2.52	2.42	2.76	2.82	2.82	2.66	2.67
0.29	0.34	0.39	0.35	0.51	0.58	0.50	0.53	0.45
97.07	97.39	97.37	97.07	98.01	98.11	97.51	97.34	98.27
1.85	1.83	1.80	1.82	1.74	1.71	1.75	1.73	1.77
0.15	0.17	0.20	0.18	0.26	0.29	0.25	0.27	0.23
2.00	2.00	2.00	2.00	2.00	2.00	2.00	2.00	2.00
6.09	6.04	5.96	6.04	6.03	6.06	6.16	6.07	6.05
8.00	8.00	8.00	8.00	8.00	8.00	8.00	8.00	8.00
0.44	0.35	0.35	0.41	0.47	0.46	0.49	0.47	0.47
0.04	0.04	0.01	0.01	0.07	0.08	0.11	0.07	0.07
1.53	1.67	1.78	1.70	1.49	1.51	1.25	1.46	1.44
0.11	0.12	0.12	0.12	0.44	0.49	0.48	0.48	0.44
2.61	2.56	2.45	2.52	2.27	2.28	2.49	2.31	2.39
0.25	0.23	0.24	0.25	0.23	0.18	0.19	0.21	0.20
4.98	4.98	4.96	5.00	4.98	5.00	5.00	5.00	5.00
0.00	0.00	0.00	0.00	0.00	0.01	0.02	0.00	0.00
0.00	0.00	0.00	0.00	0.00	0.00	0.00	0.00	0.00
1.01	1.02	1.07	1.02	1.12	1.11	1.15	1.13	1.14
0.99	0.98	0.93	0.98	0.88	0.88	0.84	0.87	0.86
2.00	2.00	2.00	2.00	2.00	2.00	2.00	2.00	2.00
0.50	0.50	0.57	0.50	0.48	0.41	0.40	0.45	0.45
0.54	0.56	0.53	0.50	0.57	0.58	0.58	0.55	0.55
1.04	1.05	1.10	1.01	1.05	0.99	0.98	1.00	0.99
0.04	0.04	0.04	0.04	0.15	0.17	0.15	0.16	0.15

MSM AFS MS319C C2_3 Taramite	MSM AFS MS319C C2_3 Taramite	MSM AFS MS319C C2_4 Taramite	MSM AFS MS319C C2_5 Taramite	MSM AFS MS319C C2_5 Taramite	MSM AFS MS319C C2_6 Taramite	MSM AFS MS319C C2_7 Taramite	MSM AFS MS319C C2_7 Taramite	MSM AFS MS319C C2_8 Taramite
38.15	37.35	37.67	36.99	37.23	37.72	38.10	37.23	37.42
0.87	0.73	0.62	0.63	0.59	0.71	0.59	0.52	0.83
12.72	12.55	12.68	12.42	12.63	12.38	12.47	12.39	12.41
11.75	11.87	11.61	12.94	12.96	10.30	12.26	12.41	12.07
17.75	17.51	17.91	16.80	16.89	19.07	17.64	17.57	17.17
1.58	1.58	1.42	1.50	1.54	1.40	1.61	1.34	1.51
1.90	1.92	1.95	2.01	2.04	1.99	1.97	1.99	2.11
6.61	6.59	6.63	6.61	6.69	6.87	6.66	6.53	6.56
4.27	4.23	4.44	4.21	4.15	4.55	4.16	4.57	4.25
2.62	2.69	2.75	2.63	2.63	2.61	2.69	2.52	2.63
0.51	0.47	0.57	0.53	0.46	0.50	0.42	0.51	0.50
98.73	97.47	98.25	97.26	97.81	98.10	98.58	97.57	97.45
1.75	1.76	1.71	1.73	1.77	1.74	1.79	1.74	1.75
0.25	0.24	0.29	0.27	0.23	0.26	0.21	0.26	0.25
2.00	2.00	2.00	2.00	2.00	2.00	2.00	2.00	2.00
6.08	6.03	6.04	6.00	5.99	6.05	6.08	6.01	6.04
8.00	8.00	8.00	8.00	8.00	8.00	8.00	8.00	8.00
0.47	0.42	0.43	0.37	0.39	0.39	0.43	0.36	0.40
0.10	0.09	0.08	0.08	0.07	0.09	0.07	0.06	0.10
1.38	1.47	1.52	1.60	1.56	1.45	1.43	1.63	1.48
0.45	0.46	0.47	0.48	0.49	0.48	0.47	0.48	0.51
2.40	2.34	2.28	2.25	2.29	2.35	2.40	2.25	2.31
0.20	0.22	0.19	0.21	0.21	0.19	0.20	0.18	0.21
5.00	4.99	4.96	4.99	5.00	4.94	5.00	4.97	5.00
0.01	0.00	0.00	0.00	0.00	0.00	0.01	0.00	0.00
0.00	0.00	0.00	0.00	0.00	0.00	0.00	0.00	0.00
1.13	1.14	1.14	1.15	1.15	1.18	1.14	1.13	1.13
0.86	0.86	0.86	0.85	0.84	0.82	0.85	0.87	0.87
2.00	2.00	2.00	2.00	2.00	2.00	2.00	2.00	2.00
0.46	0.46	0.52	0.47	0.45	0.60	0.44	0.56	0.46
0.53	0.55	0.56	0.54	0.54	0.53	0.55	0.52	0.54
0.99	1.02	1.08	1.02	0.99	1.13	0.98	1.08	1.01
0.15	0.15	0.16	0.16	0.16	0.16	0.15	0.16	0.17

MSM AFS MS319C C2_8 Taramite	MSM AFS MS319C C2_10 Taramite	MSM AFS MS319C C2_12 Taramite	MSM AFS MS319C C2_14 Taramite	MSM AFS MS319C C2_15 Taramite	MSM AFS MS319C C2_16 Taramite	MSM AFS MS319C C2_17 Taramite	MSM AFS MS319C C2_18 Taramite	MSM AFS MS319C C2_20 Taramite
37.52	37.52	37.43	37.45	37.83	37.41	37.83	37.67	37.20
1.15	1.03	0.56	0.58	0.72	0.77	0.61	0.80	0.72
12.19	12.55	12.51	12.55	12.35	12.53	12.45	12.71	12.63
12.48	11.38	12.51	11.79	11.43	11.07	12.72	12.26	10.73
17.20	18.23	17.15	17.54	17.41	18.18	17.48	17.32	18.20
1.65	1.41	1.43	1.59	1.57	1.55	1.62	1.62	1.51
2.04	1.99	2.03	1.94	1.95	1.96	2.01	1.97	1.95
6.64	6.74	6.72	6.74	6.46	6.60	6.73	6.72	6.76
4.26	4.29	4.06	4.21	4.43	4.34	4.24	4.16	4.31
2.62	2.62	2.71	2.64	2.44	2.65	2.75	2.69	2.76
0.57	0.42	0.51	0.52	0.59	0.36	0.49	0.51	0.49
98.31	98.17	97.65	97.55	97.18	97.42	98.93	98.40	97.24
1.71	1.79	1.74	1.73	1.70	1.82	1.75	1.74	1.75
0.29	0.21	0.26	0.27	0.30	0.18	0.25	0.26	0.25
2.00	2.00	2.00	2.00	2.00	2.00	2.00	2.00	2.00
6.02	6.01	6.04	6.05	6.12	6.03	6.03	6.03	6.02
8.00	8.00	8.00	8.00	8.00	8.00	8.00	8.00	8.00
0.33	0.38	0.42	0.43	0.48	0.41	0.37	0.43	0.43
0.14	0.12	0.07	0.07	0.09	0.09	0.07	0.10	0.09
1.52	1.41	1.51	1.48	1.41	1.41	1.55	1.46	1.45
0.49	0.48	0.49	0.47	0.47	0.47	0.48	0.47	0.47
2.30	2.40	2.33	2.32	2.34	2.39	2.30	2.33	2.32
0.22	0.19	0.19	0.22	0.21	0.21	0.22	0.21	0.21
5.00	4.99	5.00	4.99	5.00	4.98	4.99	5.00	4.96
0.00	0.00	0.00	0.00	0.00	0.00	0.00	0.00	0.00
0.00	0.00	0.00	0.00	0.00	0.00	0.00	0.00	0.00
1.14	1.16	1.16	1.17	1.12	1.14	1.15	1.15	1.17
0.86	0.84	0.83	0.83	0.88	0.86	0.85	0.84	0.83
2.00	2.00	2.00	2.00	2.00	2.00	2.00	2.00	2.00
0.47	0.49	0.44	0.48	0.51	0.50	0.46	0.45	0.52
0.54	0.53	0.56	0.54	0.50	0.54	0.56	0.55	0.57
1.01	1.02	1.00	1.03	1.01	1.04	1.02	0.99	1.09
0.16	0.15	0.16	0.16	0.16	0.15	0.16	0.16	0.16

MSM AFS MS319C C2_21 Taramite	EM NMD EVES12 C1_1 Hastingsite	EM NMD EVES12 C1_3 Hastingsite	EM NMD EVES12 C3_6 Hastingsite	EM NMD EVES12 C3_7 Hastingsite	EM NMD EVES12 C3_8 Hastingsite	EM NMD EVES12 C3_9 Hastingsite	EM NMD EVES12 C3_10 Hastingsite	EM NMD EVES12 C3_11 Hastingsite
37.06	40.12	40.08	39.72	39.89	39.64	38.79	39.57	40.09
0.91	1.04	1.31	1.22	0.81	0.88	0.73	0.79	1.16
12.50	13.34	13.11	13.40	13.39	13.19	15.46	14.14	13.82
11.77	5.44	5.31	5.84	6.54	5.06	7.21	6.42	5.18
17.30	12.08	11.73	11.74	11.17	11.86	10.33	10.10	11.97
1.67	0.12	0.21	0.29	0.26	0.30	0.41	0.26	0.34
2.00	8.67	8.76	8.38	8.48	8.79	8.05	8.33	8.53
6.59	10.71	10.53	10.52	10.43	10.74	10.41	10.07	10.71
4.23	2.82	2.71	2.62	2.58	2.88	2.81	2.45	2.66
2.67	1.92	1.93	1.93	1.94	1.97	1.99	1.84	1.91
0.45	1.10	1.05	1.03	1.00	1.11	1.07	1.04	1.01
97.15	97.36	96.72	96.68	96.47	96.43	97.28	94.99	97.39
1.77	1.46	1.48	1.49	1.51	1.45	1.47	1.48	1.50
0.23	0.54	0.52	0.51	0.49	0.55	0.53	0.52	0.50
2.00	2.00	2.00	2.00	2.00	2.00	2.00	2.00	2.00
6.00	6.21	6.24	6.20	6.23	6.19	6.01	6.25	6.19
8.00	8.00	8.00	8.00	8.00	8.00	8.00	8.00	8.00
0.39	0.64	0.64	0.67	0.69	0.62	0.83	0.88	0.71
0.11	0.12	0.15	0.14	0.09	0.10	0.08	0.09	0.14
1.47	0.64	0.56	0.59	0.63	0.70	0.78	0.49	0.53
0.48	2.00	2.03	1.95	1.97	2.05	1.86	1.96	1.97
2.31	1.55	1.59	1.63	1.59	1.44	1.39	1.56	1.62
0.23	0.02	0.01	0.01	0.00	0.04	0.04	0.00	0.02
4.99	5.00	5.00	5.00	5.00	4.97	5.00	5.00	5.00
0.00	0.00	0.02	0.03	0.03	0.00	0.02	0.04	0.02
0.00	0.00	0.00	0.00	0.01	0.00	0.00	0.04	0.00
1.14	1.77	1.76	1.76	1.74	1.80	1.73	1.70	1.77
0.86	0.22	0.22	0.21	0.21	0.20	0.26	0.21	0.20
2.00	2.00	2.00	2.00	2.00	2.00	2.00	2.00	2.00
0.47	0.63	0.60	0.58	0.57	0.68	0.59	0.54	0.60
0.55	0.38	0.38	0.39	0.39	0.39	0.39	0.37	0.38
1.02	1.01	0.98	0.97	0.95	1.07	0.98	0.91	0.97
0.16	0.56	0.56	0.54	0.55	0.58	0.56	0.55	0.54

EM NS EVES37 C3_1 Taramite	EM NS EVES37 C3_2 Taramite	EM NS EVES37 C3_3 Taramite	EM NS EVES37 C3_5 Taramite	EM NS EVES37 C2_6 Taramite	EM NS EVES37 C2_7 Taramite	EM NS EVES37 C2_8 Taramite	EM NS EVES37 C2_9 Taramite	EM NS EVES37 C2_10 Taramite
34.99	36.34	37.38	35.79	37.09	37.37	37.49	37.06	37.03
0.34	0.23	0.57	0.72	0.41	0.25	0.23	0.53	0.29
12.57	12.99	12.56	12.70	13.00	12.57	12.76	12.72	12.66
13.50	9.50	8.64	10.91	10.61	11.36	9.41	10.41	9.65
16.19	19.34	20.19	18.20	18.51	18.02	19.41	19.02	18.71
2.49	2.40	2.22	2.34	2.34	2.37	2.20	2.41	2.46
1.05	1.06	1.20	1.29	1.24	1.40	1.48	1.30	1.40
7.12	7.64	7.39	7.71	7.36	7.26	7.58	7.54	7.48
3.10	3.69	4.26	3.61	4.10	4.22	4.06	3.96	4.06
2.73	2.45	2.27	2.44	2.30	2.30	2.33	2.38	2.34
0.35	0.31	0.43	0.47	0.52	0.62	0.42	0.40	0.52
94.43	95.94	97.10	96.19	97.49	97.74	97.37	97.75	96.58
1.81	1.84	1.78	1.75	1.73	1.68	1.79	1.79	1.73
0.19	0.16	0.22	0.25	0.27	0.32	0.21	0.21	0.27
2.00	2.00	2.00	2.00	2.00	2.00	2.00	2.00	2.00
5.90	5.99	6.08	5.91	6.02	6.05	6.07	6.00	6.06
8.00	8.00	8.00	8.00	8.00	8.00	8.00	8.00	8.00
0.39	0.51	0.49	0.38	0.50	0.45	0.51	0.43	0.50
0.04	0.03	0.07	0.09	0.05	0.03	0.03	0.06	0.04
1.53	1.25	1.22	1.41	1.36	1.48	1.26	1.34	1.32
0.26	0.26	0.29	0.32	0.30	0.34	0.36	0.31	0.34
2.46	2.60	2.58	2.46	2.44	2.34	2.52	2.51	2.42
0.30	0.33	0.31	0.33	0.32	0.33	0.30	0.33	0.34
5.00	4.98	4.95	4.98	4.98	4.97	4.97	4.98	4.96
0.05	0.00	0.00	0.00	0.00	0.00	0.00	0.00	0.00
0.00	0.00	0.00	0.00	0.00	0.00	0.00	0.00	0.00
1.29	1.35	1.29	1.36	1.28	1.26	1.32	1.31	1.31
0.66	0.65	0.71	0.64	0.72	0.74	0.68	0.69	0.69
2.00	2.00	2.00	2.00	2.00	2.00	2.00	2.00	2.00
0.35	0.53	0.63	0.52	0.57	0.59	0.59	0.55	0.60
0.59	0.51	0.47	0.51	0.47	0.48	0.48	0.49	0.49
0.94	1.04	1.10	1.03	1.04	1.06	1.07	1.04	1.09
0.09	0.08	0.09	0.10	0.10	0.11	0.11	0.10	0.11

EM NS EVES39 1 Taramite	EM NS EVES39 2 Taramite	EM NS EVES39 3 Taramite	EM NS EVES39 4 Taramite	EM NS EVES39 4 Taramite	EM NS EVES39 5 Taramite	EM NS EVES39 5 Taramite	EM NS EVES39 6 Taramite	EM NS EVES39 6 Taramite
36.77	36.74	36.92	36.65	36.12	35.81	36.51	37.12	37.11
0.11	0.19	0.22	0.02	0.11	0.07	0.23	0.17	0.22
12.55	12.60	12.66	12.78	12.72	12.46	12.73	13.08	12.85
7.78	9.11	7.14	7.28	10.44	9.78	10.01	8.05	9.36
22.38	22.03	23.02	23.04	21.66	21.53	21.43	22.99	21.99
2.05	2.06	2.29	1.91	2.17	2.21	2.19	1.93	2.01
0.10	0.12	0.12	0.13	0.14	0.16	0.14	0.19	0.10
8.36	8.39	8.39	8.70	8.56	8.45	8.42	8.54	8.12
3.21	3.09	3.52	3.22	3.34	3.35	3.19	3.28	3.49
2.31	2.35	2.38	2.35	2.34	2.25	2.37	2.43	2.40
0.41	0.31	0.37	0.41	0.38	0.38	0.41	0.27	0.42
96.02	96.99	97.04	96.48	97.97	96.45	97.65	98.06	98.07
1.79	1.84	1.81	1.78	1.80	1.80	1.79	1.86	1.78
0.21	0.16	0.19	0.22	0.20	0.20	0.21	0.14	0.22
2.00	2.00	2.00	2.00	2.00	2.00	2.00	2.00	2.00
6.12	6.06	6.07	6.07	5.92	5.95	5.99	6.04	6.05
8.00	8.00	8.00	8.00	8.00	8.00	8.00	8.00	8.00
0.58	0.51	0.53	0.57	0.37	0.40	0.46	0.54	0.52
0.01	0.02	0.03	0.00	0.01	0.01	0.03	0.02	0.03
1.00	1.07	1.05	1.02	1.37	1.32	1.23	1.03	1.18
0.02	0.03	0.03	0.03	0.03	0.04	0.04	0.05	0.02
3.09	3.10	3.01	3.08	2.89	2.90	2.95	3.08	2.97
0.29	0.27	0.32	0.27	0.30	0.31	0.30	0.27	0.28
4.99	5.00	4.95	4.97	4.98	4.97	5.00	4.99	4.99
0.00	0.02	0.00	0.00	0.00	0.00	0.00	0.00	0.00
0.00	0.00	0.00	0.00	0.00	0.00	0.00	0.00	0.00
1.49	1.48	1.48	1.54	1.50	1.50	1.48	1.49	1.42
0.51	0.50	0.52	0.46	0.50	0.50	0.52	0.51	0.58
2.00	2.00	2.00	2.00	2.00	2.00	2.00	2.00	2.00
0.53	0.49	0.60	0.58	0.56	0.58	0.50	0.52	0.52
0.49	0.49	0.50	0.50	0.49	0.48	0.50	0.50	0.50
1.02	0.98	1.10	1.07	1.05	1.06	1.00	1.03	1.02
0.01	0.01	0.01	0.01	0.01	0.01	0.01	0.01	0.01

EM NS EVES397 Taramite	EM NS EVES398 Taramite	EM NS EVES3911 Taramite	EM NS EVES44C2_8 Taramite	EM NS EVES44C2_9 Taramite	EM NS EVES44C2_10 Taramite	EM NS EVES44C2_11 Taramite	EM NS EVES44C3_1 Taramite	EM NS EVES44C3_2 Taramite	EM NS EVES44C3_3 Taramite
37.27	37.10	36.73	36.36	38.40	37.41	37.24	37.98	38.47	37.67
0.00	0.14	0.29	0.38	0.09	0.23	0.54	0.17	0.15	0.22
12.64	12.34	13.00	12.09	12.26	12.44	12.02	11.71	12.71	12.14
8.00	8.02	7.68	13.66	10.99	10.60	10.91	9.89	10.49	10.44
22.68	22.72	22.64	16.46	18.12	18.37	17.80	19.04	18.36	18.61
2.21	2.08	2.12	2.03	2.19	2.05	1.99	1.72	2.05	1.81
0.20	0.16	0.11	1.72	1.75	1.65	1.78	1.72	1.80	1.91
8.46	8.30	8.46	7.11	7.10	7.65	7.28	7.40	7.44	7.53
3.46	3.45	3.20	4.10	4.35	3.89	3.90	4.03	4.13	4.23
2.29	2.35	2.45	2.23	2.24	2.29	2.26	2.29	2.18	2.14
0.37	0.40	0.32	0.62	0.58	0.61	0.57	0.66	0.57	0.61
97.58	97.05	97.00	96.77	98.08	97.20	96.28	96.61	98.36	97.31
1.81	1.79	1.84	1.68	1.70	1.69	1.71	1.66	1.71	1.69
0.19	0.21	0.16	0.32	0.30	0.31	0.29	0.34	0.29	0.31
2.00	2.00	2.00	2.00	2.00	2.00	2.00	2.00	2.00	2.00
6.10	6.11	6.04	5.96	6.17	6.09	6.11	6.22	6.16	6.11
8.00	8.00	8.00	8.00	8.00	8.00	8.00	8.00	8.00	8.00
0.53	0.50	0.56	0.30	0.49	0.47	0.43	0.47	0.55	0.43
0.00	0.02	0.04	0.05	0.01	0.03	0.07	0.02	0.02	0.03
1.08	1.09	0.99	1.72	1.39	1.36	1.34	1.31	1.27	1.40
0.05	0.04	0.03	0.42	0.42	0.40	0.43	0.42	0.43	0.46
3.01	3.04	3.08	2.23	2.38	2.44	2.45	2.52	2.45	2.39
0.31	0.29	0.29	0.28	0.30	0.28	0.27	0.24	0.28	0.25
4.97	4.97	4.99	4.99	4.98	4.98	5.00	4.98	5.00	4.96
0.00	0.00	0.00	0.00	0.00	0.00	0.00	0.00	0.00	0.00
0.00	0.00	0.00	0.00	0.00	0.00	0.00	0.00	0.00	0.00
1.48	1.47	1.49	1.25	1.22	1.33	1.28	1.30	1.28	1.31
0.52	0.53	0.51	0.75	0.78	0.67	0.72	0.70	0.72	0.69
2.00	2.00	2.00	2.00	2.00	2.00	2.00	2.00	2.00	2.00
0.58	0.57	0.51	0.55	0.58	0.56	0.52	0.58	0.56	0.64
0.48	0.49	0.51	0.47	0.46	0.48	0.47	0.48	0.45	0.44
1.06	1.06	1.02	1.02	1.04	1.04	1.00	1.06	1.00	1.08
0.01	0.01	0.01	0.14	0.14	0.13	0.14	0.13	0.14	0.15

EM NS EVES44 C3_4 Taramite	EM NS EVES44 C3_5 Taramite	EM NS EVES44 C3_6 Taramite	EM NS EVES44 C3_7 Taramite	EM NS EVES44 4 Taramite	EM NS EVES44 9 Taramite	EM NS EVES44 12 Taramite	EM NS EVES44 13 Taramite	EM NS EVES44 14 Taramite	EM NS EVES44 15 Taramite
37.30	38.18	37.58	37.49	38.02	37.04	37.61	37.45	37.18	37.52
0.11	0.33	0.14	0.04	0.25	0.37	0.04	0.20	0.18	0.11
12.29	12.14	12.16	12.43	12.34	12.20	11.96	12.36	12.37	12.45
12.33	9.76	11.94	12.48	9.73	12.15	12.81	13.33	11.53	12.31
16.87	19.00	17.07	16.96	18.63	17.85	16.65	17.08	17.92	17.11
2.08	1.90	2.05	2.18	2.03	2.08	2.00	2.10	2.11	2.02
1.97	2.00	1.91	1.85	1.74	1.70	1.99	1.92	1.59	1.76
7.19	7.43	7.34	7.29	7.33	7.46	7.21	7.40	7.17	7.27
4.36	4.45	4.17	4.28	4.11	4.09	4.09	4.29	4.09	4.09
2.24	2.23	2.10	2.19	2.16	2.16	2.25	2.21	2.44	2.26
0.71	0.62	0.73	0.68	0.54	0.52	0.71	0.63	0.52	0.69
97.46	98.03	97.18	97.88	96.88	97.62	97.31	98.96	97.11	97.59
1.64	1.69	1.62	1.65	1.72	1.73	1.63	1.68	1.73	1.65
0.36	0.31	0.38	0.35	0.28	0.27	0.37	0.32	0.27	0.35
2.00	2.00	2.00	2.00	2.00	2.00	2.00	2.00	2.00	2.00
6.05	6.14	6.11	6.05	6.18	6.01	6.11	5.99	6.05	6.08
8.00	8.00	8.00	8.00	8.00	8.00	8.00	8.00	8.00	8.00
0.40	0.43	0.44	0.42	0.54	0.34	0.40	0.32	0.43	0.46
0.01	0.04	0.02	0.00	0.03	0.05	0.00	0.02	0.02	0.01
1.64	1.37	1.51	1.60	1.22	1.53	1.58	1.68	1.49	1.52
0.48	0.48	0.46	0.45	0.42	0.41	0.48	0.46	0.39	0.42
2.15	2.36	2.28	2.21	2.50	2.37	2.25	2.20	2.37	2.30
0.29	0.26	0.28	0.30	0.28	0.29	0.28	0.28	0.29	0.28
4.96	4.95	4.99	4.98	4.99	4.99	5.00	4.98	4.98	4.99
0.00	0.00	0.00	0.00	0.00	0.00	0.00	0.00	0.00	0.00
0.00	0.00	0.00	0.00	0.00	0.00	0.00	0.00	0.00	0.00
1.25	1.28	1.28	1.26	1.28	1.30	1.26	1.27	1.25	1.26
0.75	0.72	0.72	0.74	0.72	0.70	0.74	0.73	0.75	0.74
2.00	2.00	2.00	2.00	2.00	2.00	2.00	2.00	2.00	2.00
0.62	0.67	0.59	0.60	0.57	0.58	0.54	0.60	0.54	0.55
0.46	0.46	0.44	0.45	0.45	0.45	0.47	0.45	0.51	0.47
1.08	1.12	1.03	1.05	1.02	1.03	1.01	1.05	1.05	1.01
0.16	0.15	0.15	0.15	0.13	0.13	0.16	0.16	0.13	0.14

EM NS EVES44 19 Taramite	EM AFS EVES02 C1_1 Taramite	EM AFS EVES02 C1_2 Taramite	EM AFS EVES02 C1_3 Taramite	EM AFS EVES02 C1_4 Taramite	EM AFS EVES02 C2_5 Taramite	EM AFS EVES02 C2_6 Taramite	EM AFS EVES02 C4_7 Taramite	EM AFS EVES02 C5_9 Taramite
39.50	37.48	37.13	37.79	37.16	37.29	37.81	37.41	37.03
0.20	0.78	0.69	0.92	0.82	0.50	0.89	1.09	0.81
13.06	10.27	11.12	10.53	10.43	10.86	10.50	10.47	10.73
11.12	12.90	13.39	12.49	13.29	14.02	11.73	14.08	12.85
18.14	18.55	18.81	18.54	18.48	17.41	18.71	17.31	18.53
2.06	1.07	1.15	1.27	1.05	1.08	1.41	1.18	1.25
1.78	1.56	1.46	1.66	1.40	1.75	1.71	1.85	1.59
7.40	6.21	6.61	6.34	6.28	6.55	6.37	6.26	6.50
4.19	4.64	4.56	4.60	4.51	4.20	4.53	4.54	4.53
2.47	1.92	2.13	2.10	2.00	2.10	1.94	1.96	2.17
0.80	0.55	0.48	0.60	0.59	0.58	0.46	0.62	0.55
100.72	95.94	97.52	96.84	96.00	96.35	96.05	96.76	96.52
1.60	1.71	1.75	1.69	1.69	1.70	1.76	1.68	1.71
0.40	0.29	0.25	0.31	0.31	0.30	0.24	0.32	0.29
2.00	2.00	2.00	2.00	2.00	2.00	2.00	2.00	2.00
6.19	6.20	6.04	6.18	6.15	6.14	6.22	6.13	6.09
8.00	8.00	8.00	8.00	8.00	8.00	8.00	8.00	8.00
0.60	0.20	0.17	0.21	0.19	0.25	0.25	0.16	0.16
0.02	0.10	0.08	0.11	0.10	0.06	0.11	0.13	0.10
1.32	1.59	1.69	1.55	1.64	1.64	1.42	1.66	1.67
0.41	0.38	0.36	0.40	0.34	0.43	0.42	0.45	0.39
2.36	2.58	2.51	2.52	2.58	2.50	2.61	2.45	2.47
0.27	0.15	0.16	0.18	0.14	0.12	0.19	0.14	0.17
5.00	5.00	4.99	5.00	5.00	5.00	5.00	5.00	4.98
0.00	0.00	0.00	0.00	0.01	0.03	0.01	0.02	0.00
0.00	0.00	0.00	0.00	0.00	0.00	0.00	0.00	0.00
1.24	1.10	1.15	1.11	1.12	1.16	1.12	1.10	1.14
0.76	0.90	0.85	0.88	0.88	0.82	0.86	0.88	0.85
2.00	2.00	2.00	2.00	2.00	2.00	2.00	2.00	2.00
0.52	0.59	0.59	0.57	0.57	0.52	0.58	0.56	0.59
0.49	0.41	0.44	0.44	0.42	0.44	0.41	0.41	0.45
1.01	1.00	1.03	1.01	0.99	0.97	0.99	0.97	1.05
0.14	0.12	0.12	0.13	0.11	0.14	0.13	0.15	0.13

EM AFS EVES02 C5_10 Taramite	EM AFS EVES02 C5_11 Taramite	EM AFS EVES03A C8_1 Taramite	EM AFS EVES03A C10_1 Taramite	EM AFS EVES03A C10_2 Taramite	EM AFS EVES03A C10_3 Taramite	EM AFS EVES03A C10_4 Taramite	EM AFS EVES03A C10_6 Taramite	EM AFS EVES03A C10_10 Taramite
37.19	37.16	36.34	37.39	36.73	36.52	38.29	37.04	37.00
0.71	0.42	1.10	1.40	0.77	0.98	1.02	1.53	1.00
10.25	10.60	10.77	10.22	10.35	10.24	11.68	10.17	10.21
14.91	13.70	11.69	10.50	13.17	12.78	8.61	11.35	11.98
16.80	17.74	20.37	21.00	19.57	19.43	21.35	19.09	18.94
1.35	1.15	1.08	1.07	1.30	1.41	1.15	1.31	1.22
1.62	1.65	0.83	1.02	1.05	0.90	0.82	1.33	1.33
6.11	6.45	7.19	6.84	6.83	6.72	6.55	6.57	6.46
4.33	4.47	3.73	4.10	4.21	4.05	4.37	3.74	4.12
1.98	2.06	2.07	1.96	1.97	2.02	1.83	1.92	1.87
0.57	0.64	0.43	0.44	0.43	0.47	0.36	0.32	0.41
95.81	96.05	95.60	95.94	96.37	95.52	96.03	94.37	94.54
1.70	1.66	1.77	1.77	1.77	1.75	1.81	1.83	1.78
0.30	0.34	0.23	0.23	0.23	0.25	0.19	0.17	0.22
2.00	2.00	2.00	2.00	2.00	2.00	2.00	2.00	2.00
6.17	6.15	6.08	6.21	6.09	6.12	6.29	6.23	6.22
8.00	8.00	8.00	8.00	8.00	8.00	8.00	8.00	8.00
0.17	0.21	0.21	0.21	0.11	0.14	0.54	0.24	0.24
0.09	0.05	0.14	0.17	0.10	0.12	0.13	0.19	0.13
1.70	1.73	1.38	1.24	1.62	1.54	0.95	1.14	1.36
0.40	0.41	0.21	0.25	0.26	0.22	0.20	0.33	0.33
2.50	2.43	2.94	2.99	2.74	2.79	3.05	2.98	2.81
0.14	0.16	0.13	0.13	0.18	0.18	0.13	0.10	0.13
5.00	4.99	5.00	5.00	5.00	5.00	5.00	5.00	5.00
0.05	0.00	0.03	0.02	0.01	0.02	0.03	0.08	0.04
0.00	0.00	0.00	0.00	0.00	0.00	0.00	0.00	0.00
1.09	1.14	1.29	1.22	1.21	1.21	1.15	1.18	1.16
0.87	0.86	0.68	0.76	0.78	0.77	0.81	0.73	0.80
2.00	2.00	2.00	2.00	2.00	2.00	2.00	2.00	2.00
0.52	0.58	0.53	0.56	0.58	0.55	0.58	0.49	0.55
0.42	0.43	0.44	0.42	0.42	0.43	0.38	0.41	0.40
0.94	1.01	0.97	0.98	0.99	0.98	0.96	0.90	0.95
0.13	0.14	0.06	0.07	0.08	0.07	0.06	0.10	0.10

Análises de química mineral em clinopiroxênio

Massif	MSM	MSM	MSM	MSM	MSM	MSM	MSM	MSM
Rock Type	NS	NS	NS	NS	NS	NS	NS	NS
Sample	MS22	MS22	MS22	MS22	MS22	MS22	MS22	MS22
Spot no.	C3_1	C3_1	C3_3	C3_4	C3_5	C3_8	C3_9	C3_10
Classification	Aegirine	Aegirine	Aegirine	Aegirine	Aegirine	Aegirine	Aegirine	Aegirine
SiO_2	53.36	52.59	53.35	53.01	53.09	51.98	52.90	52.24
TiO_2	0.11	0.15	0.09	0.00	0.06	0.19	0.00	0.00
Al_2O_3	5.63	5.54	5.42	5.28	5.58	5.08	5.07	5.29
Fe_2O_3	26.19	24.70	22.67	23.66	22.25	23.01	25.28	23.89
FeO	0.00	1.30	3.19	2.14	3.36	2.38	1.32	1.81
MnO	0.52	0.30	0.52	0.63	0.51	0.44	0.17	0.69
MgO	0.23	0.16	0.19	0.26	0.22	1.03	0.52	0.67
CaO	1.78	1.65	1.73	2.05	1.71	3.25	1.04	2.81
Na_2O	13.16	12.73	12.42	12.41	12.31	11.54	12.83	11.90
Total	100.99	99.11	99.58	99.43	99.09	98.90	99.12	99.29
Formula based in 6 oxygen atoms								
Si	1.98	1.99	2.01	2.00	2.01	1.98	2.00	1.98
Al	0.02	0.01	0.00	0.00	0.00	0.02	0.00	0.02
ΣT	2.00	2.00	2.01	2.00	2.01	2.00	2.00	2.00
Al	0.22	0.23	0.24	0.23	0.25	0.20	0.22	0.21
Fe3+	0.73	0.70	0.64	0.67	0.63	0.66	0.72	0.68
Ti	0.00	0.00	0.00	0.00	0.00	0.01	0.00	0.00
Mg	0.01	0.01	0.01	0.01	0.01	0.06	0.03	0.04
Fe2+	0.00	0.04	0.10	0.07	0.10	0.07	0.03	0.06
Mn	0.02	0.01	0.00	0.01	0.00	0.00	0.00	0.01
ΣM1	0.98	1.00	1.00	1.00	1.00	1.00	1.00	1.00
Fe2+	0.00	0.00	0.00	0.00	0.00	0.00	0.01	0.00
Mn	0.00	0.00	0.01	0.01	0.02	0.01	0.01	0.01
Ca	0.07	0.07	0.07	0.08	0.07	0.13	0.04	0.11
Na	0.94	0.93	0.91	0.91	0.90	0.85	0.94	0.87
ΣM2	1.02	1.00	0.99	1.00	0.99	1.00	1.00	1.00
%Q	4.10	5.79	9.29	8.34	9.64	13.09	5.64	10.24
%Jd	24.17	24.47	24.71	23.74	25.50	22.31	22.55	23.12
%Ae	71.74	69.73	65.99	67.92	64.87	64.60	71.81	66.64
$Mg/(Mg+Fe^{2+}+Mn)$	0.44	0.15	0.08	0.14	0.09	0.39	0.38	0.32

Análises de química mineral em clinopiroxênio (cont.)

MSM NS MS22 C3_11 Aegirine	MSM NS MS22 C3_11 Aegirine	MSM NS MS22 C3_12 Aegirine	MSM NS MS22 C3_12 Aegirine	MSM NS MS22 C3_13 Aegirine	MSM NS MS22 C3_14 Aegirine	MSM NS MS22 C3_16 Aegirine	MSM NS MS22 C3_17 Aegirine	MSM NS MS22 C3_18 Aegirine	MSM NS MS22 C3_20 Aegirine
52.63	52.98	52.96	52.84	52.73	53.14	53.07	53.22	53.17	52.51
0.01	0.15	0.02	0.00	0.09	0.00	0.16	0.07	0.15	0.11
5.32	5.84	6.31	5.46	5.53	5.35	5.52	5.54	5.94	5.29
23.48	22.60	23.17	23.17	24.47	25.13	24.01	25.82	23.99	25.90
2.57	2.45	2.16	3.22	1.34	1.27	1.95	0.65	1.54	0.45
0.48	0.52	0.28	0.41	0.48	0.60	0.52	0.54	0.52	0.43
0.25	0.24	0.19	0.16	0.18	0.18	0.25	0.19	0.17	0.22
2.03	1.84	1.39	1.72	1.73	1.80	1.79	1.63	1.63	1.74
12.26	12.45	12.68	12.31	12.68	12.73	12.60	12.96	12.78	12.81
99.02	99.07	99.16	99.29	99.21	100.20	99.86	100.62	99.89	99.45
2.00	2.00	1.99	2.00	1.99	1.99	1.99	1.98	1.99	1.98
0.00	0.00	0.01	0.00	0.01	0.01	0.01	0.02	0.01	0.02
2.00	2.00	2.00	2.00	2.00	2.00	2.00	2.00	2.00	2.00
0.23	0.26	0.27	0.24	0.24	0.23	0.24	0.23	0.25	0.22
0.67	0.64	0.66	0.66	0.70	0.71	0.68	0.72	0.68	0.73
0.00	0.00	0.00	0.00	0.00	0.00	0.00	0.00	0.00	0.00
0.01	0.01	0.01	0.01	0.01	0.01	0.01	0.01	0.01	0.01
0.08	0.08	0.06	0.09	0.04	0.04	0.06	0.02	0.05	0.01
0.00	0.00	0.00	0.00	0.01	0.02	0.01	0.02	0.01	0.01
1.00	1.00	1.00	1.00	1.00	1.00	1.00	1.00	1.00	0.99
0.00	0.00	0.01	0.01	0.00	0.00	0.00	0.00	0.00	0.00
0.02	0.01	0.01	0.01	0.00	0.00	0.01	0.00	0.01	0.00
0.08	0.07	0.06	0.07	0.07	0.07	0.07	0.06	0.07	0.07
0.90	0.91	0.93	0.90	0.93	0.92	0.92	0.94	0.93	0.94
1.00	1.00	1.00	1.00	1.00	1.00	1.00	1.00	1.00	1.01
8.92	8.37	6.72	9.08	6.11	6.08	7.38	4.72	6.15	4.73
23.87	26.39	27.87	24.50	24.53	23.48	24.52	23.96	26.22	23.10
67.21	65.23	65.41	66.41	69.36	70.44	68.10	71.31	67.64	72.17
0.13	0.12	0.12	0.07	0.15	0.14	0.15	0.22	0.13	0.31

Análises de química mineral em clinopiroxênio (cont.)

MSM	MSM	MSM	MSM	MSM	MSM	EM	EM	EM
NS	NS	NS	NS	NS	NS	NMD	NMD	NMD
MS22	MS22	MS22	MS22	MS336B	MS336B	EVES12	EVES12	EVES12
C3_20	C3_22	C3_23	C3_24	C1_3	C1_4	C1_1	C1_4	C1_5
Aegirine	Aegirine	Aegirine	Aegirine	Aeg.-aug.	Aeg.-aug.	Omphacite	Omphacite	Omphacite
52.53	52.44	50.35	52.58	51.73	52.47	51.48	50.52	50.17
0.25	0.00	0.29	0.03	0.00	0.13	0.34	0.23	0.47
5.38	5.39	4.03	5.47	4.53	4.92	5.14	4.60	5.01
21.88	24.21	24.46	23.81	23.60	24.54	2.47	2.67	4.79
4.08	1.89	1.77	2.04	3.52	2.11	9.02	8.90	7.36
0.43	0.53	0.68	0.58	0.37	0.40	0.39	0.13	0.28
0.55	0.22	1.59	0.19	0.14	0.10	8.16	8.38	8.32
2.27	1.95	5.81	1.90	2.62	2.00	19.00	19.13	18.66
11.78	12.38	10.30	12.41	11.72	12.43	2.93	2.62	3.03
99.15	99.01	99.27	99.00	98.24	99.09	98.92	97.18	98.09
1.99	1.99	1.93	1.99	1.99	1.99	1.95	1.95	1.92
0.01	0.01	0.07	0.01	0.01	0.01	0.05	0.05	0.08
2.00	2.00	2.00	2.00	2.00	2.00	2.00	2.00	2.00
0.23	0.23	0.11	0.24	0.20	0.21	0.18	0.16	0.14
0.62	0.69	0.71	0.68	0.68	0.70	0.07	0.08	0.14
0.01	0.00	0.01	0.00	0.00	0.00	0.01	0.01	0.01
0.03	0.01	0.09	0.01	0.01	0.01	0.46	0.48	0.47
0.10	0.06	0.06	0.06	0.11	0.07	0.28	0.28	0.23
0.00	0.01	0.02	0.01	0.00	0.01	0.00	0.00	0.00
1.00	1.00	1.00	1.00	1.00	1.00	1.00	1.00	1.00
0.03	0.00	0.00	0.00	0.00	0.00	0.00	0.01	0.00
0.01	0.01	0.00	0.01	0.01	0.00	0.01	0.00	0.01
0.09	0.08	0.24	0.08	0.11	0.08	0.77	0.79	0.76
0.87	0.91	0.77	0.91	0.88	0.92	0.21	0.20	0.22
1.00	1.00	1.00	1.00	1.00	1.00	1.00	1.00	1.00
12.75	7.50	17.87	7.61	11.42	7.70	71.67	73.12	66.94
24.26	23.92	16.83	24.43	20.48	22.04	21.68	19.60	20.52
62.99	68.58	65.30	67.96	68.10	70.26	6.64	7.27	12.53
0.18	0.14	0.53	0.11	0.06	0.06	0.61	0.62	0.66

Análises de química mineral em clinopiroxênio (cont.)

EM	EM	EM	EM	EM	EM	EM	EM	EM
NMD	NMD	NMD	NMD	NMD	NMD	NMD	NMD	NMD
EVES12	EVES12	EVES12	EVES12	EVES12	EVES12	EVES12	EVES12	EVES12
C3_2	C3_5	C3_6	C3_7	C3_8	1	2	3	9
Omphacite	Omphacite	Omphacite	Omphacite	Omphacite	Omphacite	Omphacite	Omphacite	Omphacite
50.04	49.86	50.14	50.68	50.60	51.88	51.20	52.20	51.62
0.36	0.69	0.33	0.20	0.15	0.10	0.36	0.13	0.15
4.77	4.83	4.88	4.61	4.86	5.46	6.18	5.77	5.55
5.40	3.40	2.85	2.97	3.04	2.82	2.06	1.98	1.56
6.59	8.64	8.65	8.54	8.28	7.81	7.76	7.58	8.26
0.13	0.29	0.28	0.27	0.35	0.19	0.32	0.25	0.22
8.33	8.01	8.10	8.65	8.15	8.27	8.19	8.60	8.23
18.50	18.36	18.87	18.95	18.65	18.03	17.63	18.07	17.61
3.21	2.91	2.74	2.65	2.93	3.51	3.51	3.50	3.48
97.33	96.98	96.85	97.53	97.03	98.07	97.19	98.07	96.67
1.92	1.93	1.94	1.95	1.95	1.96	1.95	1.97	1.98
0.08	0.07	0.06	0.05	0.05	0.04	0.05	0.03	0.02
2.00	2.00	2.00	2.00	2.00	2.00	2.00	2.00	2.00
0.14	0.15	0.16	0.15	0.17	0.21	0.23	0.22	0.23
0.16	0.10	0.08	0.09	0.09	0.08	0.06	0.06	0.04
0.01	0.02	0.01	0.01	0.00	0.00	0.01	0.00	0.00
0.48	0.46	0.47	0.50	0.47	0.47	0.47	0.48	0.47
0.21	0.27	0.28	0.26	0.27	0.24	0.24	0.23	0.25
0.00	0.00	0.00	0.00	0.00	0.00	0.00	0.00	0.00
1.00	1.00	1.00	1.00	1.00	1.00	1.00	1.00	1.00
0.00	0.01	0.00	0.02	0.00	0.00	0.01	0.01	0.01
0.00	0.01	0.01	0.01	0.01	0.01	0.01	0.01	0.01
0.76	0.76	0.78	0.78	0.77	0.73	0.72	0.73	0.72
0.24	0.22	0.21	0.20	0.22	0.26	0.26	0.26	0.26
1.00	1.00	1.00	1.00	1.00	1.00	1.00	1.00	1.00
66.08	70.18	71.46	72.45	70.88	69.07	68.02	69.93	71.17
19.69	20.58	20.79	19.52	20.80	23.26	26.36	24.67	24.45
14.23	9.24	7.75	8.04	8.32	7.67	5.62	5.40	4.38
0.69	0.62	0.62	0.64	0.63	0.65	0.64	0.66	0.63

Análises de química mineral em clinopiroxênio (cont.)

EM	EM	EM	EM	EM	EM	EM	EM	EM
NMD	NMD	NMD	NMD	NMD	NMD	NMD	NMD	NS
EVES12	EVES12	EVES12	EVES12	EVES12	EVES12	EVES12	EVES12	EVES4C
13	14	20	23	30	32	33	36	C1_1
Omphacite	Omphacite	Omphacite	Omphacite	Omphacite	Omphacite	Omphacite	Omphacite	Aeg.-aug.
50.70	50.79	50.98	50.85	52.39	52.65	52.96	51.82	48.48
0.62	0.25	0.58	0.35	0.23	0.35	0.39	0.34	0.00
4.60	4.89	4.37	4.60	5.33	5.39	5.52	5.28	3.39
2.02	3.65	2.87	2.25	2.87	2.19	2.07	3.14	21.50
8.45	7.65	7.78	8.31	8.25	8.72	8.55	7.84	5.04
0.36	0.26	0.37	0.30	0.35	0.29	0.29	0.23	1.48
8.86	8.18	8.65	8.26	8.44	8.32	8.60	8.54	1.24
18.86	18.21	18.23	18.01	18.73	18.02	18.18	18.31	8.78
2.68	3.26	3.14	3.17	3.28	3.52	3.50	3.35	8.19
97.15	97.15	96.97	96.08	99.86	99.45	100.06	98.85	98.11
1.95	1.95	1.96	1.97	1.95	1.97	1.97	1.95	1.92
0.05	0.05	0.04	0.03	0.05	0.03	0.03	0.05	0.08
2.00	2.00	2.00	2.00	2.00	2.00	2.00	2.00	2.00
0.16	0.17	0.16	0.18	0.19	0.21	0.21	0.18	0.07
0.06	0.11	0.08	0.07	0.08	0.06	0.06	0.09	0.64
0.02	0.01	0.02	0.01	0.01	0.01	0.01	0.01	0.00
0.51	0.47	0.50	0.48	0.47	0.46	0.48	0.48	0.07
0.26	0.25	0.25	0.27	0.25	0.26	0.25	0.24	0.17
0.00	0.00	0.00	0.00	0.00	0.00	0.00	0.00	0.05
1.00	1.00	1.00	1.00	1.00	1.00	1.00	1.00	1.00
0.01	0.00	0.00	0.00	0.00	0.01	0.02	0.01	0.00
0.01	0.01	0.01	0.01	0.01	0.01	0.01	0.01	0.00
0.78	0.75	0.75	0.75	0.75	0.72	0.72	0.74	0.37
0.20	0.24	0.23	0.24	0.24	0.26	0.25	0.24	0.63
1.00	1.00	1.00	1.00	1.00	1.00	1.00	1.00	1.00
74.45	69.11	72.69	73.06	70.09	70.92	70.99	69.38	27.74
19.96	20.92	19.24	20.53	22.27	23.08	23.40	22.19	14.30
5.59	9.97	8.07	6.41	7.65	6.00	5.61	8.43	57.96
0.64	0.65	0.65	0.63	0.64	0.62	0.63	0.65	0.25

Análises de química mineral em clinopiroxênio (cont.)

EM	EM	EM	EM	EM	EM	EM	EM	EM	EM
NS	NS	NS	NS	NS	NS	NS	NS	NS	NS
EVES4C	EVES4C	EVES4C	EVES4C	EVES4C	EVES4C	EVES4C	EVES4C	EVES4C	EVES4C
C3_9	C3_10	C3_11	C3_12	C3_13	C6_2	C6_3	C6_4	C6_5	C6_6
Aeg.-aug.	Aeg.-aug.	Aeg.-aug.	Aeg.-aug.	Aeg.-aug.	Aeg.-aug.	Aeg.-aug.	Aeg.-aug.	Aeg.-aug.	Aeg.-aug.
51.47	51.00	51.20	50.74	50.61	51.29	50.83	50.33	51.25	50.66
0.16	0.00	0.09	0.21	0.08	0.00	0.17	0.11	0.00	0.13
3.49	3.39	3.56	3.35	3.38	3.24	3.46	3.41	3.28	3.26
19.06	17.27	17.98	17.85	18.45	17.88	20.12	19.45	17.13	19.54
5.46	6.80	6.14	7.68	7.13	6.38	4.95	5.74	7.64	5.12
1.18	1.17	1.48	1.28	1.42	1.48	1.10	1.44	1.27	1.46
1.94	1.87	1.93	0.92	1.10	1.81	1.62	1.28	1.83	1.93
9.31	9.10	9.38	8.64	8.46	8.90	9.11	8.98	9.22	9.37
8.55	8.20	8.24	8.45	8.46	8.37	8.69	8.47	8.04	8.34
100.62	98.79	100.00	99.12	99.10	99.36	100.05	99.21	99.67	99.80
1.96	1.98	1.96	1.97	1.97	1.98	1.95	1.95	1.98	1.95
0.04	0.02	0.04	0.03	0.03	0.02	0.05	0.05	0.02	0.05
2.00	2.00	2.00	2.00	2.00	2.00	2.00	2.00	2.00	2.00
0.12	0.13	0.12	0.13	0.12	0.13	0.11	0.11	0.13	0.10
0.55	0.50	0.52	0.52	0.54	0.52	0.58	0.57	0.50	0.57
0.00	0.00	0.00	0.01	0.00	0.00	0.00	0.00	0.00	0.00
0.11	0.11	0.11	0.05	0.06	0.10	0.09	0.07	0.11	0.11
0.17	0.22	0.20	0.25	0.23	0.21	0.16	0.19	0.25	0.16
0.04	0.03	0.05	0.04	0.04	0.04	0.04	0.05	0.02	0.05
0.99	1.00	1.00	1.00	1.00	1.00	0.98	0.99	1.00	0.99
0.00	0.00	0.00	0.00	0.00	0.00	0.00	0.00	0.00	0.00
0.00	0.01	0.00	0.00	0.01	0.01	0.00	0.00	0.02	0.00
0.38	0.38	0.39	0.36	0.35	0.37	0.37	0.37	0.38	0.39
0.63	0.62	0.61	0.64	0.64	0.63	0.65	0.64	0.60	0.62
1.01	1.00	1.00	1.00	1.00	1.00	1.02	1.01	1.00	1.01
32.09	34.91	33.75	32.91	31.80	33.72	29.81	30.45	36.18	31.68
15.14	15.30	15.69	15.24	15.21	14.66	14.88	14.97	14.74	14.14
52.77	49.80	50.55	51.85	52.99	51.62	55.31	54.59	49.08	54.18
0.34	0.29	0.31	0.15	0.19	0.29	0.32	0.24	0.27	0.34